

---

**Zapping the Retina -**  
*Understanding electrical responsiveness and electrical  
desensitization in mouse retinal ganglion cells*

---

Dissertation

zur Erlangung des Grades eines  
Doktors der Naturwissenschaften

der Mathematisch-Naturwissenschaftlichen Fakultät  
und  
der Medizinischen Fakultät  
der Eberhard-Karls-Universität Tübingen

vorgelegt

von

**Archana Jalligampala**

aus Cuttack, India

April- 2018

Tag der mündlichen Prüfung: 13.07.2018  
Dekan der Math.-Nat. Fakultät: Prof. Dr. W. Rosenstiel  
Dekan der Medizinischen Fakultät: Prof. Dr. I. B. Autenrieth

1. Berichterstatter: Prof. Dr. / PD Dr. / Dr. Eberhart Zrenner

2. Berichterstatter: Prof. Dr. / PD Dr. / Dr. Elke Guenther

Prüfungskommission:  
Prof. Dr. Eberhart Zrenner  
Prof. Dr. Elke Guenther  
Prof. Dr. François Paquet-Durand  
Dr. Guenther Zeck

## **Erklärung/ Declaration:**

Ich erkläre, dass ich die zur Promotion eingereichte Arbeit mit dem Titel:

*„Zapping the Retina- Understanding electrical responsiveness and electrical desensitization in mouse retinal ganglion cells“*

selbständig verfasst, nur die angegebenen Quellen und Hilfsmittel benutzt und wörtlich oder inhaltlich übernommene Stellen als solche gekennzeichnet habe. Ich versichere an Eides statt, dass diese Angaben wahr sind und dass ich nichts verschwiegen habe. Mir ist bekannt, dass die falsche Abgabe einer Versicherung an Eides statt mit Freiheitsstrafe bis zu drei Jahren oder mit Geldstrafe bestraft wird.

Tübingen, den

19.04.2018

Datum / Date

Unterschrift /Signature

## DEDICATION

*Dedicated to my Family for their constant support and love.*

*“Remember to look up at the stars and not down at your feet. Try to make sense of what you see and wonder about what makes the universe exist. Be curious. And however difficult life may seem, there is always something you can do and succeed at. It matters that you don't just give up.”- Stephen Hawking (1942-2018)*

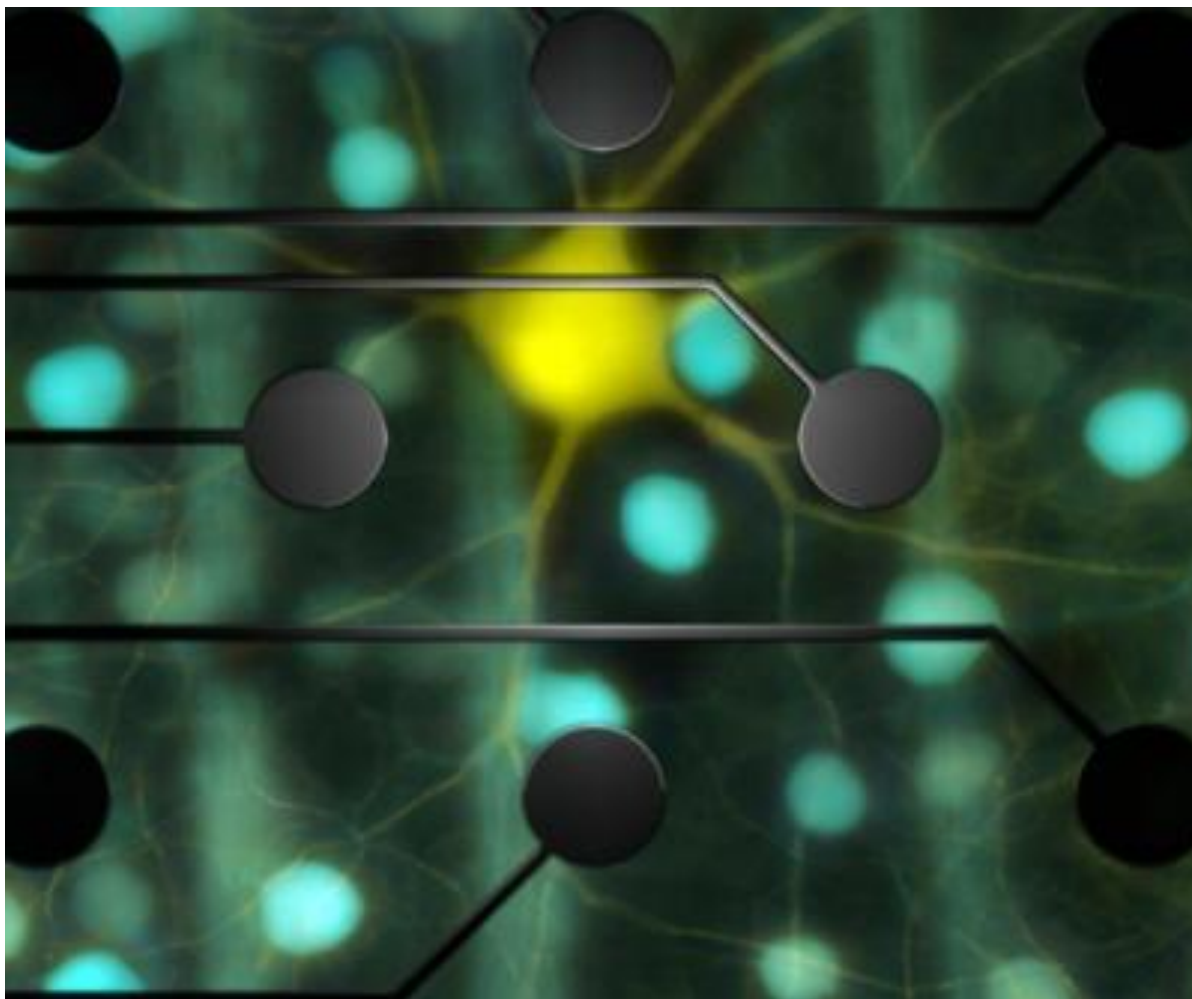


*Figure reprinted with permission- Chichilinsky lab from Cover Page of Journal of Neurophysiology, Volume 95 Number 1 2006*

# Table of Contents

ERKLÄRUNG / DECLARATION:.....	3
DEDICATION.....	4
TABLE OF CONTENTS.....	6
ACKNOWLEDGMENTS.....	9
PUBLICATIONS AND STATEMENT OF CONTRIBUTIONS.....	12
PUBLICATION 1. ....	12
PUBLICATION 2. ....	13
PUBLICATION 3. ....	13
ABSTRACT.....	16
CHAPTER 1.....	18
1.1 GENERAL INTRODUCTION .....	18
1.1.1 <i>Overview and dynamics of the nervous system</i> .....	19
1.1.2 <i>From light to perception- “What the eye tells the brain.”</i> .....	20
1.1.2.1 The human eye.....	20
1.1.2.2 Organization of the retina and visual perception .....	21
1.1.3 <i>Blindness and the effects on the visual system</i> .....	24
1.1.3.1 Epidemiology of blindness .....	24
1.1.3.2 Retinal degenerations -AMD and RP .....	24
1.1.4 <i>Current approaches to sight restoration</i> .....	26
1.1.4.1 Biological Approaches.....	26
1.1.4.2 Electronic visual prostheses.....	28
1.1.5 <i>Understanding responsiveness of RGCs to electrical stimulation</i> .....	35
1.1.6 <i>Scope of the thesis</i> .....	38
1.2 TECHNICAL ASPECTS OF THE THESIS.....	39
CHAPTER 2.....	47
PUBLICATION 1- OPTIMAL VOLTAGE STIMULATION PARAMETERS FOR WILD-TYPE AND <i>RD10</i> MOUSE RETINAL GANGLION CELLS. ....	47
2.1 SYNOPSIS AND FRAMEWORK OF THE STUDY: .....	47
2.2 CORRESPONDENCE OF ELECTRICAL RESPONSE PATTERNS TO VISUAL RESPONSE TYPES .....	69



<b>APPENDIX I –CHAPTER 3 /PUBLICATION 2 .....</b>	<b>102</b>
<b>APPENDIX II–CHAPTER 4 /PUBLICATION 3 .....</b>	<b>102</b>



## Acknowledgments

Writing the acknowledgments has been the most pleasant yet difficult part of the entire thesis. While the happiness of completing a project successfully is unmatched, there is a touch of sadness that I have to move on from a great lab. Many people have contributed towards this thesis in their special ways, and I am glad that I have an opportunity to thank them.

Words fail to describe my heartfelt gratitude to **Prof. Eberhart Zrenner**, who not only provided me the dream opportunity to work with him but also for being an excellent mentor in many ways. His knack for details, his curiosity, his drive for achievement and his humbleness are indeed few of the many qualities that I will carry forward with me for the rest of my life. His words “always be curious” has been my drive to succeed.

This body of work would not have been possible without the guidance, support, and encouragement of my co-supervisor **Dr. Daniel L. Rathbun**. While I dreamt of being a part of Zrenner lab during my master thesis, Daniel helped me realize my dream. I am incredibly thankful for his invaluable help during electrophysiology experiments and analysis. Being the first child of the experimental retinal prosthetics group, Daniel provided me the opportunity to set the lab from scratch, which was a gratifying process and I shall forever be grateful to him. Apart from lab opportunities, I was given the freedom to present my work at various national and international conferences and symposium, for which I will be forever grateful to both Daniel and Prof. Zrenner.

I would like to thank **Prof. Elke Guenther** who graciously accepted to be on my thesis committee and for being an evaluator of my thesis. Prof. Elke was the first person who

introduced me to the field of retinal prostheses during my master thesis, and I shall forever be grateful to her.

I would like to thank the lab members of the experimental retinal prosthetics group, especially **Sudarshan Sekhar**, who was not only a great colleague but also a great friend. The stimulating discussion about science and life is something I will miss going forward.

I would also like to thank **Klaudija, Norman, and Zohreh** for their help during the experiments.

I would like to thank the Pupillary group - **Prof. Barbara Wilhelm, Dr. Tobias Peters, Dr. Carina Klebsch, Dr. Krunoslav Stingl and Dr. Torsten Strasser** for not only providing me an opportunity to collaborate on such a fantastic project but also for being the best housemates during the ARVO conferences. ARVO for sure would not have been this fun without them.

I would like to thank the members of the Institute for Ophthalmic Research and CIN (Center for Integrative Neuroscience), especially **Prof. Thomas Euler** and his group, **Prof. Frank Schaeffel and Prof. Francois Paquet Durand** and his group for their guidance and sharing their wisdom on different aspects of visual neuroscience.

I would like to personally thank our international collaborators **Prof. Dr. Bryan Jones** and **Prof. Dr. Shelley Fried** for many helpful discussions and their unwavering enthusiasm for our research.

This acknowledgment would be incomplete without thanking the various funding organization who graciously supported this project. The doctoral stipend from ProRetina, Kerstan Stiftung, German Ophthalmology Society(DOG) and CIN helped accomplish the goals of my thesis.

Often while pursuing our professional dreams, we usually take our personal life for granted. This thesis provides me an opportunity to thank my biggest life support, my family, for their unconditional love and understanding. I would like to thank my parents, my brother, my in-laws, and my friends for their patience and faith in me.

Lastly, this journey is incomplete without mentioning one person who completes me, my husband, **Bharat**. He has been my best friend, my love, my rock and kept me sane during the most insane and infuriating periods of my doctoral thesis. He believed in me

when I did not believe in myself. You are everything to me, and I would not have come this far without you.

## **Publications and Statement of Contributions**

This thesis is composed of three manuscripts. The first manuscript (Chapter 2.) is published. The remaining two manuscripts (Chapter 3 and 4) are in preparation for submission. A part of Chapter 3 has been published as a conference proceeding (for doi. Refer to chapter 3). I have worked on other collaborative projects during my doctoral thesis which has been published (*refer to Curriculum Vitae*), but these three manuscripts are the core of my doctoral dissertation. The framework and synopsis of each publication are provided below under each chapter.

### **Publication 1.**

**Archana Jalligampala, Sudarshan Sekhar, Eberhart Zrenner and Daniel L. Rathbun. (published in Journal of Neural Engineering, 2017)**

**Title: “Optimal Voltage Stimulation Parameters for Wild-Type and rd10 Mouse Retinal Ganglion Cells.”**

My contribution: I planned, designed, collected the data for the experiments. I processed and analyzed the data. I drafted the manuscript and prepared the figures.

Co-author contribution: DLR was involved with the experimental design and analysis of the data. All authors edited the manuscript and provided critical feedback.

### **Publication 2.**

**Archana Jalligampala, Eberhart Zrenner , and Daniel L. Rathbun.**  
**(in preparation, see Appendix I)**

**Title: “Adaptation of visual responses in healthy and degenerating rd10 mice retinas during ongoing electrical stimulation.”**

My contribution: I planned, designed, collected the data for the experiments. I processed and analyzed the data. I drafted the manuscript and prepared the figures.

Co-author contribution: DLR was involved with the experimental design and analysis of the data. All authors provided critical feedback.

### **Publication 3.**

**Archana Jalligampala\*, Sudarshan Sekhar\*, Eberhart Zrenner and Daniel L. Rathbun.** (in preparation, see Appendix II)

\*equal contribution

**Title: “Spatiotemporal aspects of electrical desensitization in healthy mouse retinal ganglion cells (RGCs).”**

My contribution: I planned, designed, collected the data for the experiments. I processed and analyzed the data. I drafted the manuscript and prepared the figures.

Co-author contribution: SS, DLR was involved with the experimental design and analysis of the data. All authors provided critical feedback.



## Abstract

The field of science and technology has come a long way since the famous 70's science fiction series "The Six Million Dollar Man," where a disabled pilot was transformed into a bionic superhero after receiving artificial implants. What was indeed once a science fiction has now turned into a science fact with the development of various electronic devices interfacing the human neurons in the brain, retina, and limbs. One such advancement was the development of retinal implants.

Over the past two decades, the field of retinal prosthetics has made significant advancement in restoring functional vision in patients blinded by diseases such as *Retinitis pigmentosa* (RP) and Age-related macular degeneration (AMD). RP and AMD are the two leading cause of degenerative blindness. While there is still no definitive cure for either of these diseases, various treatment strategies are currently being explored. Of the various options, the most successful one has been the retinal implants. Retinal implants are small microelectrode or photodiode arrays, which are implanted in the eye of a patient, to stimulate the degenerating retina electrically. They are broadly classified into three types depending on the placement –epiretinal (close proximity to retinal ganglion cells, RGCs) , subretinal (close proximity to bipolar cells, BP) and suprachoroidal (close proximity to choroid). While the ongoing human trials have shown promising results, there remains a considerable variability among patients concerning the quality of visual percepts which limits the working potential of these implants. One such limitation often reported by the implanted patients is “**fading**” of visual percepts. Fading refers to the limited ability to elicit temporally stable visual percepts. While, this is not a primary concern for epiretinal implants , it is often observed in subretinal and suprachoroidal implants which use the remaining retinal network to control the temporal spiking pattern of the ganglion cells. The neural correlate of fading is often referred to as “electrical desensitization”, which is the reduction of ganglion cell responses to repetitive electrical stimulation .

While much is known about the temporal component of desensitization ( time constant,  $\tau$ ), the spatial aspects (space constant,  $\lambda$ ) has not been well characterized. Further, how both these aspects interact to generate spiking responses, remains poorly understood.



These crucial questions formed the critical components of my thesis. To address these questions, we stimulated the retinal network electrically, with voltage and current pulses and recorded the corresponding spiking activity using the microelectrode arrays (MEAs). While addressing the primary question of my thesis, we were able to address few idiosyncrasies which has currently stymied the field of retinal prosthetics.

At a conceptual level, we have developed an experimental and analysis framework by which one can identify the single stimulus that will activate the most ganglion cells (Chapter 2, Part 1). This stimulus is optimal for 'blind' experiments where the specific response properties of each cell are unknown. Furthermore, we attempted to understand the correspondence between the electrical response patterns and visual response types (Chapter 2, Part2). In Chapter 3, we sought to understand better how the visual responses parameters change during ongoing electrical stimulation. We demonstrated that apart from the adaptation occurring due to visual stimulation and *invitro* experimental conditions, the electrical stimulation alters the RGC visual responses, suggesting the requirement for stimulation-induced changes to be incorporated in the designing of stimulation paradigms for the implant. Finally addressing the primary question (Chapter 4) of my thesis with which we started, we were able to demonstrate, that the electrical desensitization requires the interaction of both time and distance and is not a global phenomenon of the retina. In the final chapter (Chapter 5) we summarize the results of the thesis, discuss the key outcomes and its relevance to the prosthetic field and other vision restoration strategies and the potential future directions of this research.

Therefore, in future, to improve the efficacy of retinal prostheses and patient outcomes, it is crucial to have an in-depth understanding of the responsiveness of the retinal circuitry to electrical stimulation.

# Chapter 1

## 1.1 General introduction

Man uses the various sensory modalities to understand and interpret the world around him. These sensory modalities are hearing, touch, taste, smell, and vision. Of these five senses, vision is by far the most dominant sensory modality used by humans to perceive the surroundings and can compensate for the loss of any other senses. For example, if a person has lost the sense of touch, he can use his vision to know if the object is harmful or not, before touching it. Similarly, if a person has lost his sense of taste, he can still function by interpreting the stimulus using his eyes. However, the reverse is not true. A person cannot smell a perfectly sunny day nor can he hear a beautiful scenery. No other sense can replicate or compensate for the loss of vision. Any form of visual impairment results in difficulty to perform simple day to day tasks. Currently, the leading causes of incurable blindness in developed countries are the retinal degenerative diseases retinitis pigmentosa (RP) and age-related macular degeneration (AMD). While there is no definitive cure for these diseases, several approaches are being undertaken worldwide to restore partial vision, of which the most promising approach is the visual prosthesis, often referred to as bionic eye in layman's term. This chapter of the thesis provides a general background of the nervous system, retina as a model system for encoding visual information and how electrical stimulation of the neuronal tissue can provide useful visual perception.

### 1.1.1 Overview and dynamics of the nervous system

Animals rely on their nervous system to communicate and transmit signals between different parts of the body. The nervous system at the cellular level is a complex collection of nerves and special type of cells called *neurons*.

The neurons also known as nerve cells are excitable cells which transmit information via electrical and chemical signals. Typically, the neuron is composed of a cell body or soma, one or more dendrites, a single axon and one or more axon terminals. The *dendrites* primarily receive signals from other neurons. Further, the soma transmits these input signals to a thin and long cable -the *axon* which relays the processed signal one or more *axon terminals*. These axon terminals otherwise known as presynaptic terminals relay the information to other neurons in the nervous system by forming synapses (both chemical and electrical).

In an animal body, nearly all the cell membranes are electrically polarized, i.e., there exists a voltage difference between the intracellular and extracellular medium of the cell. This voltage difference is known as the *membrane potential*. The cell membrane is a lipid bilayer with large protein molecules embedded in it. These large protein molecules are ion pumps, and special type of ion channels called voltage-gated ion channels and ligand-gated channels. In resting or steady state when these channels are closed the cell has a potential of -70mV. However, with the arrival of a neural signal, these channels rapidly open causing influx and efflux of various ionic species of sodium, potassium, and calcium. This, in turn, affects the membrane potential to rise rapidly and fall in a short time interval. At the cellular level, the dynamics of the ion channels is controlled by ligands known as neurotransmitters. The excitatory neurotransmitters increase the cell membrane potential, in other words, depolarizes the cell membrane with respect to the extracellular medium and inhibitory neurotransmitters decrease the membrane potential or hyperpolarize the membrane potential. This rapid rise and fall in membrane potential are known as an *action potential*, also known as a *spike*. Alan Lloyd Hodgkin and Andrew Huxley were the first to explain the ionic mechanisms underlying these rapid changes in the membrane voltage of neurons (*Hodgkin & Huxley, 1952*). Unlike graded potential which depends on the intensity of the stimulus, the action potential is an “all-or-none” event which requires the membrane potential to exceed a certain threshold and is independent of the stimulus intensity. The action potential is initiated at the axon hillock and propagates along the axon. On reaching

the axon terminals the action potential effects the release of neurotransmitters thereby passing on information to the adjacent neurons in the neural network.

In signal transduction, an external signal (light) results in fluctuations of membrane potential by opening and closing different ion channels. These changes in voltages result in depolarization of the axon hillock which initiates an action potential. However, not all the neurons convert their external signals into action potentials. Instead, they may convert the signal to graded potentials by modulating the release of a neurotransmitter, which may stimulate downstream neuron(s) into firing an action potential. One such classic example is the retina. In the retina, the photoreceptors on receiving light signal cause a graded potential (by releasing glutamate) in downstream neurons like bipolar cells and horizontal cells which in turn generates an action potential in the ganglion cells and some displaced amacrine cells which then propagates information to the brain via the optic nerve.

## **1.1.2 From light to perception- “What the eye tells the brain<sup>1</sup>.”**

### **1.1.2.1 The human eye**

The visual system is a complex yet remarkable piece of evolution, which demonstrates the architectural wonder of the entire anatomy of the species. The first point of entry of light signals is the eye. The functionality of an eye is in similar lines to a camera (Figure 1.1A). Just as a camera requires a lens and a film to produce an image of the outer world, the eyes function as a natural camera to capture and refract light enabling us to perceive our worldly surroundings. The light first enters the eye via a thin membrane in front of the eyeball known as the cornea. The cornea performs a dual purpose role of protecting the eye and refracting the light as it enters the eye. Further, the iris and the lens in the eye work like the aperture and objective of the camera respectively, limiting the amount of light entering the eye. Apart from controlling the amount of light entering the eye, the lens also serves an additional purpose. Unlike the camera lens which is fixed in shape, the lens of the eye can change its shape and size. The lens is attached to the ciliary muscles. These muscles can relax and contract thereby changing the shape of the lens. Therefore, by carefully adjusting the lens shape, the ciliary muscles assist in producing a fine-tuned image to the back of the eyeball. The image is projected onto the retina, lining the back of the eyeball, which is equivalent to

---

<sup>1</sup> “What the frog’s eye tells the frog’s brain”- *Lettvin et al.* (1959)

the film of a camera. The retina captures the image by registering tiny photons of light and converting them to electrical signals to be interpreted by higher-order parts of the brain (Figure 1.1B).

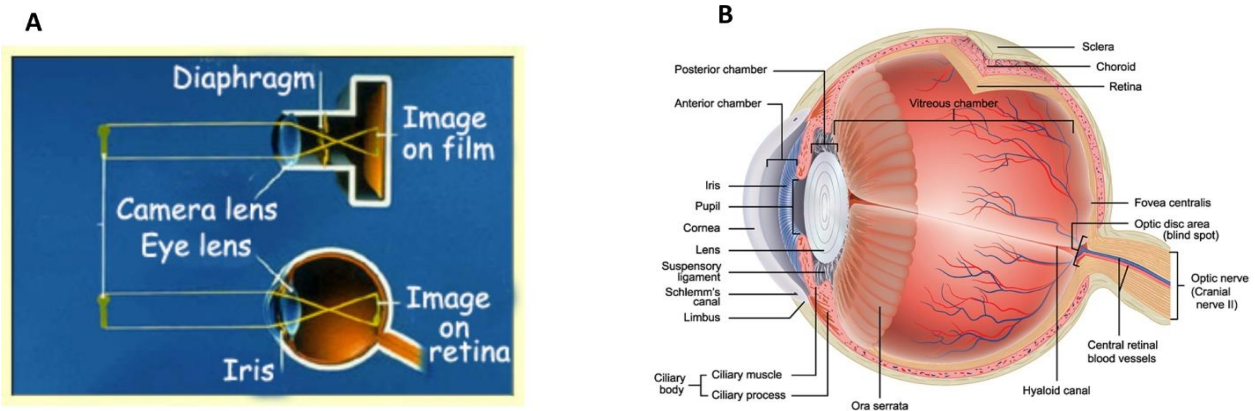


**Fig 1.1: Schematic of human eye and similarity with the camera. A)** functional similarity between the camera and the eye. Just as the film of the camera captures the image and is developed to generate a processed image, the retina acts as a film and captures the outside world image and sends the processed signal to the brain for further interpretation. **B)** The light signal enters the eye via the cornea and iris and is focused onto the retina by the lens. (Image in A is a “copyleft” image from -The brain from top to bottom site written and maintained by Bruno Dubuc. The image in B from American Optometric Association, Copyright Peter Junaidy, Image ID- 24992479)

### 1.1.2.2 Organization of the retina and visual perception

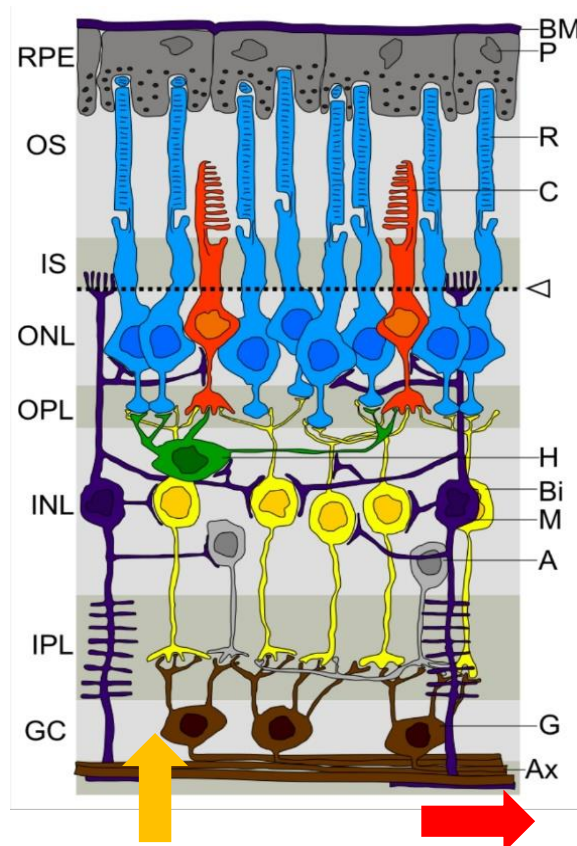
Although the visual pathway begins at the surface of the cornea, the retina is where the first step of visual information processing occurs leading to visual perception.

Since the 19<sup>th</sup> Century, the retina has been extensively studied both anatomically and functionally. One of the pioneers who tried elucidating the structural organization of the retina was Santiago Ramon y Cajal in 1900 using the Golgi staining method (Piccolino 1988). One of the main reason retina was an exemplary model for investigation was due to its development from the central nervous system. Because of this, it shares structural and functional similarities to the brain, making it a suitable model to investigate various cortical aspects like blood-brain barrier, laminar organization, immune response to injury and so on (London et al., 2013).

The retina is a thin, transparent tissue which lines the back of the eyeball. It is highly organized and is structured in distinct layers with over 50 different types of cells (Figure 1.2).

These cells can be divided into five main cell types: photoreceptors, bipolar cells, horizontal cells, amacrine cells and ganglion cells (Masland 2001). As the mammalian retina is inverted, with the photoreceptors layer entirely at the back of the eye and ganglion cell layer facing the vitreous humor, the incident light propagates through all the retinal neurons before it is transduced into neural signals.

The tiny photons of light, upon hitting the retina, are detected by the photoreceptors (PR)- rods (in peripheral vision) and cones (in central vision) which form the outer segment (OS) and inner segment (IS). The retinal pigment epithelium (RPE) provides nutrition to the photoreceptors and helps to recycle the OS of the photoreceptors. The nucleus of the PR forms the outer nuclear layer (ONL) and the nuclei of bipolar cells (Bi), horizontal cells (H) and amacrine cells (A) form the inner nuclear layer (INL). Dividing these nuclear layers are the two synaptic layers where synaptic connection occurs, i.e. the outer plexiform layer (OPL) and the inner plexiform layer (IPL). The OPL is where the photoreceptors synapse onto the dendrites of the bipolar cells. At this synapse, there is lateral integration and feedback to the PR from the broad dendrites of horizontal cells (Thoreson *et al.* 2008). The IPL consists of



synapses from multiple, parallel bipolar cell axons on to the ganglion cells (G) which form the ganglion cell layer (GC). Furthermore, there are synapses from amacrine cells which mediate lateral interactions and modulate the functional input to the GCL (Rodieck 1998). The ganglion cell generates action potentials which relay the visual information to the brain via its axons (Ax) which constitute the optic nerve (Dacey 2004).

**Fig 1.2: Laminar organization of the mammalian retina:** The incident light (in yellow arrow) is transduced at the photoreceptors. The transduced signal is processed by the various neurons of the retinal layers. The preprocessed visual signal is digitized and sent to the brain via axons of the ganglion cell (red arrow) which form the optic nerve.

See texts for an explanation of initials. (<https://commons.wikimedia.org/wiki/File:Retina.jpg>,

*Adapted from Peter Hartmann, Wikipedia image, Retina Layers, 2007, GNU Free Documentation License)*

Each eye carries a different perspective of the visual field, thus sending different information via its optic nerve. In the optic chiasm, some axons undergo decussation, i.e. cross over to provide information of the opposite visual field while some axons do not cross, and together these axons proceed via the optic tract and project to the lateral geniculate nucleus (LGN) in the thalamus (Dacey *et al.*, 2003). The visual information is then relayed further to the primary visual cortex, V1 in the occipital lobe via projections know as optic radiations. This pathway of visual information is also known as the **geniculostriate pathway** and is primarily responsible for conscious visual perception (Figure 1.3). The V1 further relays information to other parts of the brain responsible for complex visual processing (Koch 2004).

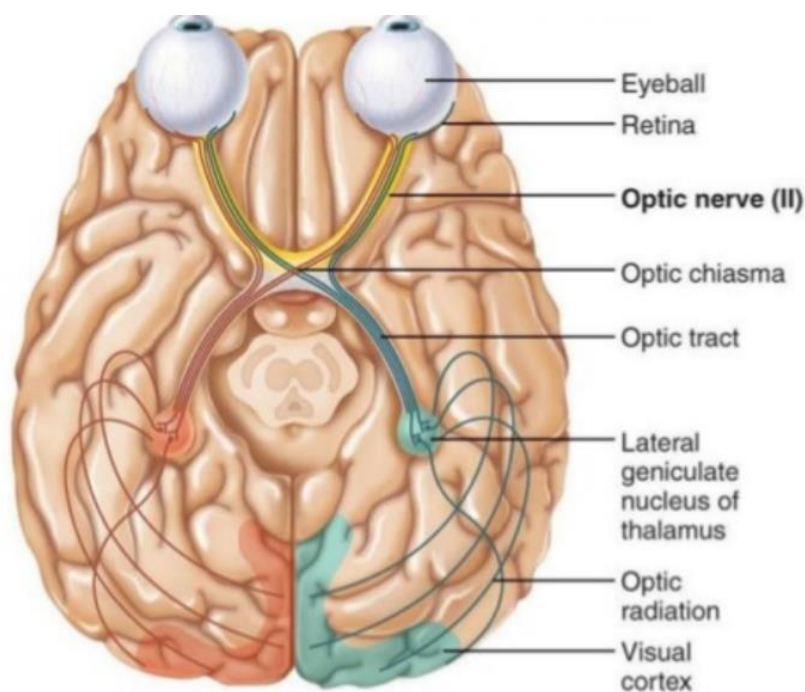


**Fig1.3: Schematic representation of visual pathway for conscious visual perception:** *The information from each eye is relayed to the lateral geniculate nucleus (LGN) where the signals are correlated in space and time. Further, these signals are relayed to the visual cortex, V1 which performs higher order processing of the visual signals.*

*(Image source- antranik.org, Function of*

*the optic nerve. <http://antranik.org/peripheral-nervous-system-cranial-nerves/>).*

### 1.1.3 Blindness and the effects on the visual system

#### 1.1.3.1 Epidemiology of blindness

According to the World health organization (WHO), a worldwide estimation of visually impaired people is around 285 million. Of these visually impaired people, 39 million people are blind while the remaining 246 million people suffer from low-vision impairment( *Lorach et al., 2013; Mariotti S., 2012*) Of the 39 million people suffering from blindness, cataract accounts for 51% of it (Figure 1.4). Although, there are effective treatments for cataracts, due to the sizeable socio-economic barrier in the underdeveloped countries the access to treatment is very limited. The remaining causes of blindness are glaucoma and diabetic retinopathy accounting for a total of 9% and additional 9% is accounted for diseases with retinal degenerations such age-related macular degeneration (AMD) and retinitis pigmentosa (RP).

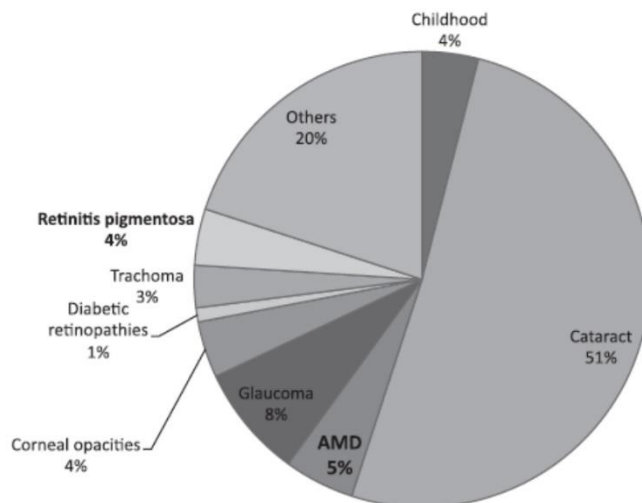


**Fig 1.4: Global causes of blindness:** The pie chart represents the various diseases accounting for the 39 million people suffering from blindness. Retinal degeneration diseases like AMD and RP account for 9% of the blindness cases. Data provided by WHO. (Image source- *Lorach et al. 2013*, reprinted with permission)

#### 1.1.3.2 Retinal degenerations -AMD and RP

The leading cause of incurable blindness in developed nations today is a broad category of inherited retinal degenerations [Goetz 2016]. Two of the primary diseases in this category are retinitis pigmentosa (RP) and few forms of age-related macular degeneration (AMD). Around four million people suffer from these blinding diseases, with estimated worldwide prevalence rates of 1 in 4000 each for AMD and RP (*Hamel, 2006; Hartong et al., 2006; Resnikoff et al., 2004; Mariotti S. 2012*). In these diseases, retinal photoreceptors cease to transform incident light into neural signals eventually leading to blindness. However, the cellular layering of inner retinal neurons is still preserved with moderate physiological and morphological changes until very late stages in the degeneration process (*Gargini et al.,*



2007; Jones *et al.*, 2016; Mazzoni *et al.*, 2008). This remaining inner retinal circuitry makes them prime target candidates for retinal prosthetics.

### **Age-Related Macular Degeneration (AMD)**

Age-related macular degeneration (AMD) is a medical condition which affects older patients typically after the age of 60. AMD primarily affects the central area of the visual field called the macula, leaving the peripheral vision relatively intact (Figure 1.5B). The macula predominantly contains cones which assist in high visual acuity. Therefore, people suffering from AMD have difficulties with tasks which require high visual acuity such as reading, facial recognition, and color vision. However, with the use of peripheral vision, they can navigate without the use of mobility aids. With the progression of AMD, there is an accumulation of cellular debris, called drusen, in the macula, between the retinal pigment epithelium (RPE) and the choroid which grows over a given time. AMD can be broadly classified into Dry and Wet AMD. Dry AMD accounts for most of the AMD cases. In dry AMD, the central visual field begins to atrophy with thinning and depigmentation of RPE. This condition is known as Geographic Atrophy and results in scotoma (Ambati & Fowler 2012).

In the wet form of AMD, the vision loss occurs due to neovascularization of the choroid through the Bruch's membrane into the retina. Currently, there exists treatment for wet AMD, in which the anti-angiogenic drugs like *ranibizumab*, can block the signaling pathway of the Vascular Endothelial Growth Factor (VEGF) and thereby prevent the formation of the choroidal neovascularization (Brown *et al.*, 2006). The dry form of AMD which accounts for the majority of AMD cases has no available treatment options. However, recently a retinal prosthetic group from California –Second Sight, implanted Argus (II) epiretinal system in a clinical trial of five patients with advanced dry AMD. Although, theoretically the prosthetic vision could take advantage of the slow progression of disease after the loss of central vision, it is yet to be demonstrated that the prosthetic system could significantly increase the quality of vision.

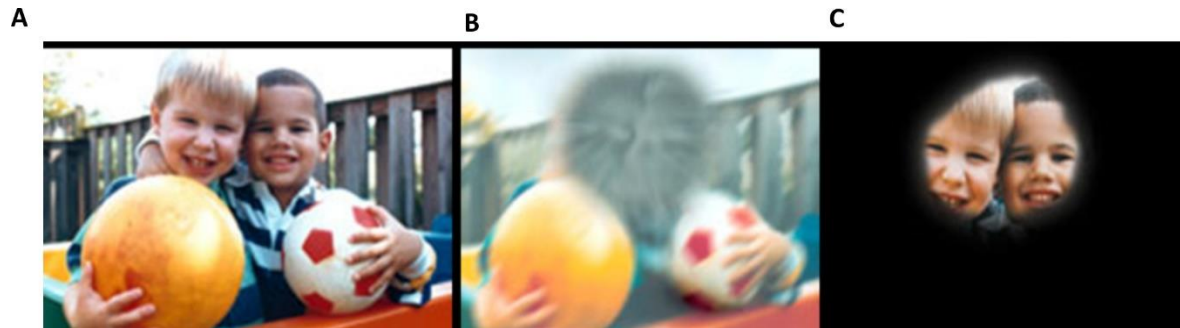


**Fig 1.5: Illustration of visual field loss during retinal degeneration: A)** Original scene as seen by people with normal vision. **B)** The same scene seen by an AMD patient with loss of central vision. **C)** The same scene seen by patients with late stage RP with complete loss of peripheral vision - tunnel vision. (Image source- NEI, NIH public image can be reused)

## Retinitis pigmentosa

*Retinitis pigmentosa* is an inherited degenerative disease which is characterized by progressive loss of photoreceptors. Unlike, AMD manifestation of RP is independent of age and can be diagnosed anywhere from childhood to late adulthood. One of the peculiarities of RP is that, as many as 50 genetic mutations can cause the RP phenotype, thereby limiting the treatment options (Wang *et al.*, 2005). RP primarily begins with the death of rod photoreceptors in the periphery followed by the loss of cone photoreceptors. With disease progression, the patients initially suffer from tunnel vision (Figure 1.5C) and nyctalopia- commonly known as night blindness. Later, vision loss progresses to the central visual field with the loss of cone photoreceptors ultimately leading to complete blindness.

### 1.1.4 Current approaches to sight restoration

The intact inner retinal circuitry provides a therapeutic window for multiple strategies for vision restoration in patients suffering from retinal degenerative diseases. These approaches range from electronic visual prostheses to various biological approaches like gene therapy, stem cells, neuroprotection, and optogenetics.

#### 1.1.4.1 Biological Approaches

##### Neuroprotection:

It has been demonstrated in preclinical studies that electrical stimulation using corneal electrodes like DTL (Dawson Trick Litzkow) can slow the progression of retinal

degeneration. These electrodes, when stimulated at high frequencies for a relatively extended period, release endogenous growth factors like ciliary neurotrophic factor (CNTF) and brain-derived neurotrophic factor (BDNF) (*Tao et al., 2016*). These growth factors have been shown to slow down photoreceptor loss and promote their cellular function. In studies from RP patients, such corneal electrostimulation once a week has shown a significant increase in the size of the visual field (*Schatz et al., 2011*). Although these devices have received regulatory approval, further studies are required to gauge the success of this method.

### **Gene therapy:**

Gene therapy is a technique of transferring a therapeutic gene in place of a mutated gene, responsible for encoding a specific type of protein using viral or non-viral vectors (*Bennett 2013*). This process of gene therapy is also known as gene augmentation. In syndromic and non-syndromic RP like Leber's congenital amaurosis (LCA) and Usher syndrome respectively, gene therapy techniques have been shown to deliver genes encoding proteins like RPE65 that are mutated in retinal degeneration into the subretinal space of the eye (*Bennett et al., 2016*). The primary goal is to restore the normal functioning of the protein, thereby slowing or halting the process of degeneration. After successful preclinical studies in a dog model of LCA (*Acland et al., 2005*). Gene therapy has shown promising results in patients with LCA2 mutation (*Grob et al., 2016*). Although with the phenomenal success achieved with LCA patients, gene therapy can trigger an unwanted immune reaction, infection from virus injections and in some cases cause tumors, therefore subjecting it to intense regulatory scrutiny (*Maguire et al., 2008*).

### **Stem cell therapy**

Stem cell therapy aims at differentiating embryonic stem cells (ESCs) into new photoreceptors cells when introduced into the subretinal space (*Schwartz et al., 2015*). These differentiated cells have been shown to restore some light sensitivity in blind mice and in some mice, have shown an increased visual acuity. Furthermore, these transplanted photoreceptors have demonstrated the possibility of treating scotomas (*MacLaren et al., 2006*).

## Optogenetics

Optogenetics is a technique in which light-sensitive ion channel of the opsin family is delivered to the neurons like bipolar cells (*Lagali et al., 2008*), ganglion cells (Nirenberg & Pandarinath 2012) and in some cases surviving photoreceptor somas (*Busskamp et al., 2010*) by gene therapy. Further, these light-sensitive ions are activated by an external light source, resulting in the switching on of the neuron.

Although there exists convincing proof of principle for this technique, the amount of light required to activate these probed neurons is very high and can result in cytotoxicity of remaining neurons. Since this technology relies on irreversible genetic modification – in similar lines to gene therapy, it is subject to intense regulatory scrutiny.

While optogenetics, gene therapy, and stem cells hold promising treatment for restoring vision in blind patients in the future, the systems currently being used in clinics, rely on extracellular electrical stimulation of the visual system to produce visual percepts. The following section briefly describes the various visual prostheses presently being developed, with a primary focus on three retinal implant designs which are currently in clinical trials.

### 1.1.4.2 Electronic visual prostheses

Visual prostheses aim at restoring vision in blind patients by attempting to recreate healthy light-driven neural activity in the remaining portions of the visual system. In 1755, Charles Le Roy was the first to apply electrical stimulation to produce visual sensations (phosphenes) in the eye of a blind man (LeRoy 1755). From that point onwards, various strategies of electrical stimulation have been investigated to restore visual perception. The visual system can be electrically stimulated at different locations in the visual pathway (Figure 1.6). The first point in the visual system, the *retina* can be stimulated when most of the inner retinal circuitry is preserved to transfer relevant information to the brain via optic nerve (*Ayton et al., 2014; da Cruz et al., 2013b; Zrenner et al., 2011*). The second stimulation location is the *optic nerve* which is a bundle of dense nerve fibers (*Brelén et al., 2005; Delbeke et al., 2003; Veraart et al., 2003, 1998*). And finally, it is possible to directly stimulate the higher order machinery such as the *lateral geniculate nucleus (LGN)* (*Bourkiza et al., 2013; Pezaris and Eskandar, 2009; Pezaris and Reid, 2007*) and the *visual cortex* (*Dobelle, 1994; Dobelle et al., 1974; Fernández et al., 2002; Maynard et al., 1997; Srivastava et al., 2009*). These locations

are preferable when there is significant trauma to the retina or the optic nerve. To allow for a degree of focus, the following section will only elaborate the various locations of the retinal implant, its advantages and disadvantages and the critical commercial players undergoing clinical trials.

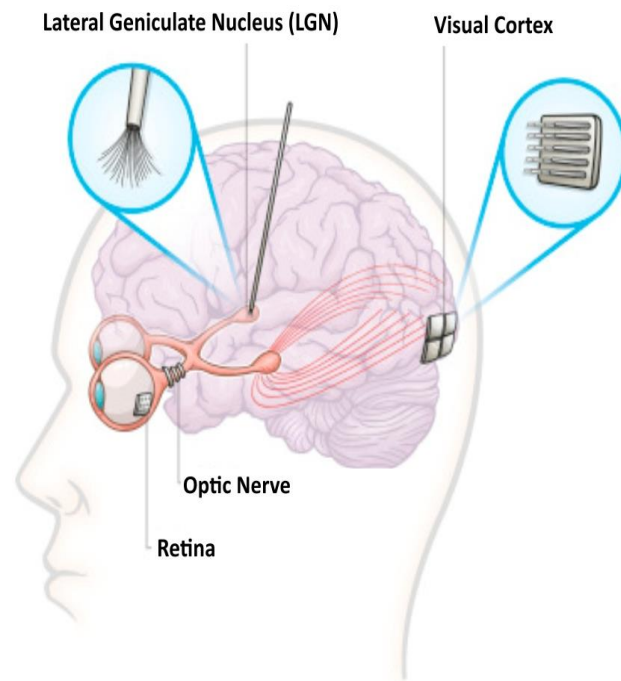


**Fig 1.6: Schematic representation of electrical stimulation targets in the visual pathway:** Small array of electrodes can be implanted in the retina to stimulate the remaining retinal circuitry (RGCs) to elicit visual percepts (phosphenes). The dense axons of the RGCs which form the optic nerve can be stimulated using “cuff” electrodes and in some cases penetrating electrodes. The LGN can be stimulated using deep brain stimulation electrodes or “tufts” of microelectrodes. Lastly, the visual cortex can be stimulated using surface electrode or penetrating microelectrodes as shown. (Image adapted from (Lewis et al., 2015) with reprint permission)

## Retinal Implants

The first ever retinal prosthesis for the blind was proposed by Tassicker in 1956. It consisted of a light-sensitive photodiode cell placed in between the choroid and the retina to treat patients with large central scotomas (Tassicker, 1956). Within the retina, multiple electrode configurations have been investigated and can be broadly classified into three categories depending on where in the patient’s eye they are implanted – *epiretinal*, *subretinal* and *suprachoroidal*.

### Epiretinal

The epiretinal approach targets the retinal ganglion cells (RGCs) primarily. In the epiretinal implant, the electrode array is placed in between the vitreous humor and the retina, primarily on top of the axons of the RGCs (Figure 1.7). In such devices, typically the glasses-mounted camera collects light signals and passes them to a microchip either within the glasses or carried by the user. Further, the processed signal from the microchip is transmitted

to the array which in turn stimulates the RGCs (*Dagnelie et al., 2006; Humayun et al., 2012, 2003*).

Due to its proximity to the vitreous, the heat dissipation due to electrical stimulation is relatively better in comparison to subretinal implants (*Fernandes et al., 2012*). Another advantage of epiretinal implants is that the signals are pre-processed before they reach the implant. This allows optimization of the signal's quality, which may lead to improved visual perception. However, the above point can act as a disadvantage as this increases the demand for sophisticated algorithms for image processing which requires complete knowledge of the retinal code which is not yet well understood. Further, due to the proximity to the axons, electrically stimulating the array, could potentially distort the retinotopy of the visual percepts (*Behrend et al., 2011; Eckhorn et al., 2006*).

### **Subretinal**

The subretinal approach to retinal prosthetics targets the retinal network, primarily the inner nuclear layer of the retina (surviving bipolar cells). In subretinal implants, the array of electrodes is inserted in the subretinal space, where the photoreceptors are lost (Figure 1.7). While the epiretinal implants aim at reintroducing the natural visual code into the RGCs, subretinal implants instead deliver input to non-spiking inner retinal neurons and rely on the conversion of these signal into spiking of the ganglion cells via synaptic transmission of the retinal neural network. The current subretinal prostheses use hundreds to thousands of microphotodiodes attached to microelectrodes. When light enters the retinas, these photodiodes are stimulated, resulting in an electrical pulse which excites the retinal cells (*Loudin et al., 2007; Zrenner, 2013, 2012; Zrenner et al., 2011*). Most of the subretinal implants do not require the external electrical source to generate electrical pulses. However, the incident light on the photodiodes being insufficient for stimulation, external handheld power supply (*Zrenner et al., 2011*) or an intense light source (*Adekunle et al., 2015; Mathieson et al., 2012*) is an additional requirement for these implants.

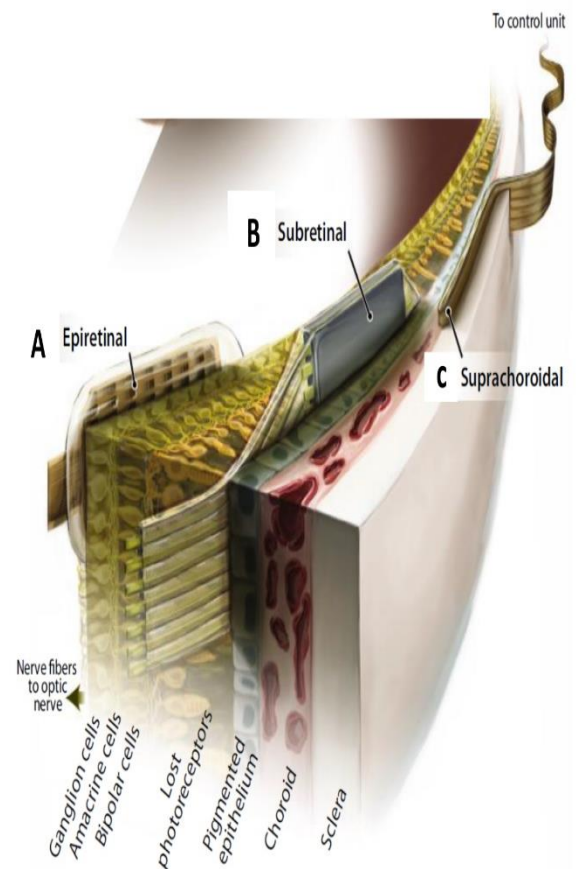
There are multiple advantages of this approach. First, the good contact between the electrodes and the bipolar cells facilitates long-term implant stability (*Palanker et al., 2004*). Second, as the electrode to neuron distance is much better controlled for subretinal implants, they tend to have lower thresholds and reduced current spread which in turn allows for a greater spatial resolution. Third, as they rely on the inner retinal neurons to transfer neural

signals to the ganglion cells, they could preferentially activate the ON and OFF pathways. Considering that the ON and OFF bipolar cells have different stratification depth in the inner plexiform layer (IPL) (Gerhardt *et al.*, 2010) and different calcium channel subtypes (Freeman *et al.*, 2011a), variable parameters like electrode diameter, stimulation frequency and duration could be employed for selective activation. The main disadvantage of this approach is that as the retina degenerates, it undergoes significant reorganization and since these implants rely on the remaining retinal network to relay visual information, it will be necessary to account for such remodeling (Marc *et al.* 2003) which is extremely challenging.

### Suprachoroidal

In the suprachoroidal approach, the implant is placed between the choroid and the sclera (Figure 1.7). One of the major advantages of this approach in comparison to epi- or subretinal prostheses (Fujikado *et al.*, 2011; Sakaguchi *et al.*, 2004; Shivdasani *et al.*, 2014), is that with this location the surgical placement is less technically challenging and does not pose any major risk to the retina. Further, the percepts from such implants also have shown to be retinotopically aligned. However, due to the considerable distance between stimulating electrodes and the retinal neurons (250-400 $\mu$ m away), the spatial resolution could be potentially compromised. Further, the large distance, could increase the stimulation threshold which might pose problems for long-term safety (Nayagam *et al.*, 2014; Shivdasani *et al.*, 2014).

**Fig 1.7: Schematic representation of location of different retinal implants: (A) Epiretinal (B) Subretinal (C) Suprachoroidal.** In epiretinal implants, an external camera sends a signal to the array placed on the nerve fibers of the RGCs. In subretinal implant, the photodiodes are positioned in the subretinal space, where photoreceptors are lost. They are stimulated with incident light which transfers signal to the electrode for stimulating the retinal neurons. The suprachoroidal



implant is placed in between the sclera and choroid. (Image source-Zrenner E. 2013, reprint with permission)

## Implants undergoing clinical trails

### *The Argus II epiretinal implant system*

The Argus II, was developed by Second Sight Medical Products (Sylmar, California, USA) and is currently the most advanced among the various epiretinal prosthetic system available to blind patients with retinitis pigmentosa (RP) and age-related macular degeneration (AMD). Argus II received European approval (CE mark) in 2011 for commercial use in Europe. It is the only prosthetic device which is currently approved for commercial use by the FDA (received in the year 2013).

It consists of a camera mounted spectacle frame which captures the external visual scenes and sends it to the video processing unit (VPU) for image processing. The processed image is sent to a radio frequency (RF) antenna that transmits the processed data wirelessly to an intraocular implant coil—which has a receiving antenna (Figure 1.8). The delivered signals are decoded and processed inside the implant or capsule, before being distributed over the 60 stimulating electrodes by means of an intraocular cable (*Humayun et al., 2012*). The stimulating electrodes are positioned above the nerve fibers of the retinal ganglion cells by means of a tack, and directly activate the ganglion cells to elicits phosphene in patients.

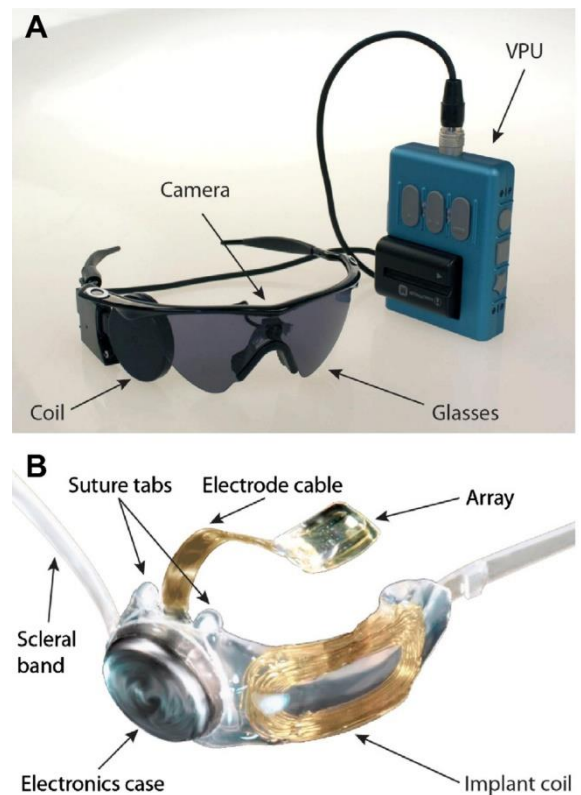


**Fig 1.8: Argus II epiretinal implant: A)** External image of the Argus II implant consisting of a camera mounted on a spectacle frame, a RF coil and a video processing unit (VPU) with rechargeable battery **(B)** Implanted portion includes 60 electrodes, an electronic case or capsule for receiver electronics and implant coil to receive the processing signal. (Image source-Humayun et al 2012, reprint with permission)



*Clinical outcome* -The Argus II has now been implanted in over 100 patients worldwide, with a best reported visual acuity of only 20/1260 (Ahuja et al., 2011; da Cruz et al., 2013a; Humayun et al., 2012; Yue et al., 2015). As stated above, the presence of nerve fiber layer (axons of the RGCs) distorts the retinotopy of the visual percepts due to axonal stimulation, in turn affecting the visual acuity and the thresholds (Ahuja et al., 2013). Additionally, in the Argus II system, the visual information sent to the implant is unrelated to the eye position. Therefore, unlike subretinal implants, which use their natural eye movements to scan a visual scene, epiretinal implant patients rely on head movements to scan and refresh images.

### ***The Alpha IMS Implant***

In parallel to Second Sight, the subretinal implant, Alpha-IMS system (Rothermel et al., 2009) was initiated in Germany by Retina Implant AG (Reutlingen, Germany). The Alpha IMS was originally developed by a consortium at the Universities of Tübingen and Stuttgart. The stimulation electrodes of the subretinal implant are placed in the subretinal space, where the entire photoreceptor layer is lost and are in proximity to the bipolar cells of the inner retina (Zrenner et al., 2011). The implant contains a 3.0 X 3.0 mm<sup>2</sup> CMOS-chip with 1500, 72 X 72 μm<sup>2</sup> stimulating pixels. Each pixel is made up of a 30 X 15 μm<sup>2</sup> photodiode and a titanium nitride electrode (50 x 50 μm<sup>2</sup>). The return electrode is common to all the electrodes in the implant and is located far from the stimulating electrodes. The electronic circuits in the chip are powered by a subdermal receiver placed behind the ear. This receiver receives power and control signals wirelessly via a transmitter antenna which is held in place via a subdermal magnet. The power and control signals are generated by a handheld box which is carried by the patients. The signals from the subdermal receiver box is sent via a subdermal cable leading to the eyeball, ending in a thin subretinal foil carrying the implant chip (Figure 1.9). The signal (image) is analyzed, amplified and is forwarded to the bipolar cells of the inner retina. From there, the neuronal network of retinal ganglion cells processes the signal normally and forwards it to the visual cortex for interpretation.

*Clinical outcome*- The Alpha-IMS chip received CE mark in 2013 for commercial use in Europe and is currently under review for FDA approval. Clinical trials of the implant have demonstrated to date the best visual acuity of 50/550 in a single patient. The rest of the patients have visual acuities worse than 20/1000 which is currently the best among all the

existing prosthetic devices. The patients with this system could identify, discriminate, and localize objects and some could also read large fonts (*Stingl et al., 2015, 2013a, 2013b, 2013c; Stingl and Zrenner, 2013; Wilke et al., 2016; Zrenner et al., 2011*). Currently, the next generation implant Alpha AMS is being implanted in the patients. The device is CE certified and has improvements in hardware from the previous Alpha IMS implant (*Stingl et al. 2017*).

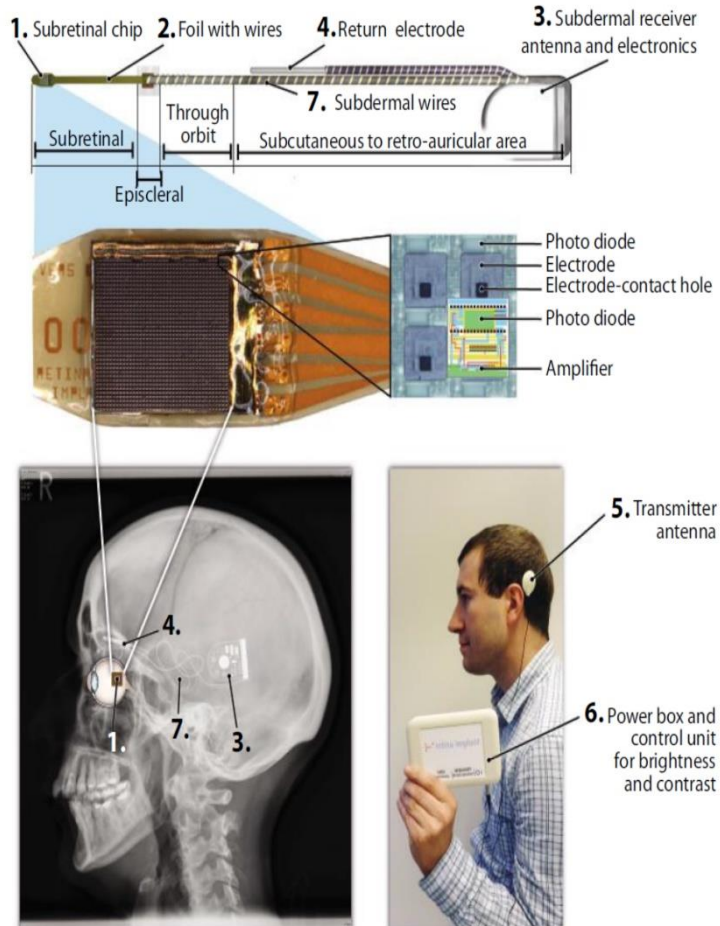


**Fig 1.9: Alpha IMS subretinal implant:** The upper panel shows the entire implanted electronic component starting from the chip in the eye to the subdermal electronics placed behind the ear. The middle panel is a magnified image of the implant chip containing 1500 light-sensitive photodiodes, amplifiers, and electrodes that are placed in the region of the retina where photoreceptors have been lost. The lower left panel shows the relative placement of the electronic implant seen under an X-ray. The lower right panel shows the patient holding the handheld device which controls the power and signal which is transmitted via an antenna to the receiver wirelessly. (Image source-Zrenner *E 2013*, reprint with permission)

### ***Bionic Vision Australia and the suprachoroidal approach***

The suprachoroidal implant is spearheaded by Bionic Vision Australia. It consists of an intra-ocular array of 33 platinum stimulating electrodes (30 X 600  $\mu\text{m}$  and 3 X 400  $\mu\text{m}$ ) and three return electrodes. Of these 33 electrodes, 20 electrodes could be stimulated individually and remaining 13 electrodes in the outer ring could be used for hexagonal stimulation (*Abramian et al., 2011*).

*Clinical outcome* - to date this device has been implanted in three patients (*Ayton et al., 2014; Leung et al., 2015*). All three patients reported perceiving phosphenes, and the electrodes

remained functional over the 12-months trial. However, the visual acuity ranged from 20/4,000 to 20/20,000 which was well in the region of ultra-low vision.

### 1.1.5 Understanding responsiveness of RGCs to electrical stimulation

To develop effective modes of electrical stimulation, it is necessary to have an in-depth understanding of the responses of the RGCs to the existing electrical stimulation strategies. Currently, two types of stimulation principles are possible with the retinal implant (both epiretinal and subretinal)- *direct* and *indirect* activation of the ganglion cells.

#### Direct activation of RGCs.

When the electrical stimulus acts directly on the ganglion cell, without stimulating the retinal network, such activation is known as direct activation of RGC. Typically, direct activation elicits a single action potential for a single electrical pulse, i.e., one spike per pulse (*Ralph J Jensen et al., 2005; Jepson et al., 2013; Sekirnjak et al., 2006*). It is common for an epiretinal implant to elicit direct RGC spike, however it was surprising to see that the RGC spikes could be evoked subretinally (*Tsai et al., 2012*), given that, the distance between the stimulating electrode and the RGCs was around 300  $\mu\text{m}$ , which is equivalent to the entire retinal thickness (*Grover et al., 2010*). These direct responses can be characterized by various parameters. Below, few of them have been described:

1. **Threshold-** The region of the ganglion cell which is most sensitive to direct activation is the initial segment of the axon (*Sekirnjak et al., 2006*). It has been shown that the threshold for stimulating spike in this region (axon initial segment, AIS) is the lowest (*Fried et al., 2009, 2006; Jepson et al., 2013*). Considering, that the direct RGC spikes arise from this segment, the threshold (stimulus amplitude) to activate the RGCs will be low (*Jeng et al., 2011*). Furthermore, these spikes have a higher sensitivity to shorter stimulus duration (i.e., chronaxie 0.1-0.4 ms, (*Jensen et al., 2003; Ralph J Jensen et al., 2005; Sekirnjak et al., 2006*). It has been shown from other studies that the chronaxies for the axons are comparatively shorter than soma (*Tehovnik et al., 2006*), suggesting that this short integration time found in RGC is likely the result of spikes being initiated at the AIS and not the soma.

**2. Polarity-** When stimulated epiretinally, the thresholds for direct activation are lower for a cathodic pulse and higher for anodic, whereas it is vice-versa for subretinal stimulation. This could be due to the higher concentration of Na channels (“sodium band” over the region of RGCs near the axonal initial segment (*Boinagrov et al., 2014; Fried et al., 2009; Jeng et al., 2011; Ralph J Jensen et al., 2005*)).

**3. Latency-** In response to electrical stimulation the direct RGC spikes have a shorter latency (< 2ms, *Sekirnjak, et al 2006*).

**4. Temporal resolution-** One of the most significant advantages of direct activation is that the elicited spikes can follow very high frequencies (50-500Hz). (*Fried et al., 2006; Sekirnjak et al., 2006*) and in some cases few kilohertz (*Cai et al., 2013; Freeman et al., 2010; Twyford et al., 2014*) Thus, direct RGC spikes can achieve a very high temporal resolution.

**5. Spatial resolution-** The activation of the passing axons of the RGCs increases the threshold in comparison to the threshold of axon initial segment (*Freeman et al. 2010*). Further, the passing axons also distort spatial resolution which is often reported by patients with epiretinal implant (*Humayan et al. 2003, 2012*).

## Indirect activation of RGCs.

Indirect activation of ganglion cells otherwise known as network-mediated activation arises through activation of neurons presynaptic to the ganglion cell. On electrical stimulation, these presynaptic neurons modulate their levels of synaptic release (neurotransmitter) which elicits spiking in the RGC. Unlike direct activation, where a single spike is elicited in response to a single pulse, the response to indirect activation of RGC consists of bursts of spikes (*Fried et al. 2006*). The above parameters used for characterizing the direct RGC spikes can also be used to describe the responses from indirect activation of the RGC.

**1. Threshold-** The strength-duration relationship of the indirect responses yields a significantly longer chronaxie (10-15 ms) in comparison to the direct RGC response (0.1-0.4 ms) (*Jensen et al., 2005*). This implies that to elicit network mediated RGC spikes; the stimulus pulse should be longer (1 – 4 ms) (*Im & Fried 2016; Im & Fried 2015*) to lower the threshold for stimulation (stimulus amplitude).

**2. Polarity-** When stimulated subretinally, the thresholds are lower for anodic pulse than cathodic. Whereas for epiretinal stimulation, the thresholds for network

mediated stimulation are lower for cathodic pulse than anodic. One probable reason for such preference could be due to the higher density of ion channels in the bipolar cell axons (activated during depolarization) (Boinagrov *et al.*, 2014; Lorach *et al.*, 2015).

**3. Latency-** In response to electrical stimulation, indirect responses have a latency ranging from 5ms - 50ms, arising from the inner nuclear layer. In some cases, the indirect RGC spikes could result from photoreceptors stimulation, which has a longer latency (>50ms) (Boinagrov *et al.* 2014, Mandel *et al.*, 2013).

**4. Temporal resolution-** Unlike direct RGC spikes which can follow high-frequency stimulation, the responses from indirect activation of RGC tend to desensitize (Freeman and Fried, 2011; Jensen and Rizzo, 2007; Ryu *et al.*, 2009a; Yue *et al.*, 2016). This limited temporal resolution has been reported in patients, where under continuous stimulation of the implant the visual percept tends to fade.

**5. Spatial resolution-** Due to the stimulation of the bipolar cells (primary target of the indirect activation), the spatial resolution of these indirect RGC spikes are comparatively better than the direct RGC spikes. As the bipolar cells serve as a vertical antenna with no lateral projecting axons, the spatial resolution is more confined (Freeman *et al.*, 2011b).

### 1.1.6 Scope of the thesis

The primary goals of the thesis were to gain a better understanding of the electrical responsiveness of the RGCs (in healthy and degenerating retinas) to epiretinal network stimulation and to explore the spatial-temporal interaction of electrical desensitization in mouse RGCs (primarily the healthy retina—used as a standard). For the study, an *in vitro* preparation of a living patch of the mouse retina, was used as a model and placed on a dense array of electrodes with ganglion cell side facing the electrodes. This configuration allowed us to inject various pattern of voltage and current pulses and simultaneously measure the responses from hundreds of RGCs.

Working towards understanding the electrical responsiveness of RGCs, the first aim of this thesis was to establish the optimal stimuli that can activate a majority of RGCs in both healthy and degenerating retinas. The optimal stimuli are determined, taking into account the variability of RGCs (morphology and heterogeneity of responses), which is often undermined while developing suitable stimulation paradigms. The second part of this study was to establish the electrical response types and correspond these response types to their visual response types, to identify hallmarks for pathway-specific stimulation.

The second aim of understanding the RGC responsiveness to electrical stimulation was to examine the adaptation of visual responses (again in healthy and degenerating retinas) to ongoing electrical stimulation and to identify the stimulation-induced changes. These stimulation-induced changes if present is crucial and needs to be taken into account while designing the stimulation paradigms.

To realize the final goal of electrical desensitization, we examined the RGC responses to electrical stimulation (by delivering current pulses) at different frequencies (ranging from low to high frequency) in healthy mouse retinas. Additionally, to inspect the spatiotemporal interaction we injected current pulses with varying interpulse intervals across multiple electrodes. Knowledge of such interaction would help in designing arrays (especially dense electrodes arrays), which would ameliorate fading of visual percepts to a large extent without compromising a lot on the spatial resolution.

## 1.2 Technical aspects of the thesis

To have an in-depth understanding of the various biological questions addressed in this thesis, it is crucial to comprehend the various technical aspects used to answer these questions efficiently. This segment gives an overview of the various technical complexities of high-throughput data, and the various measures are taken to address them efficiently. In other words, one could treat this section as a troubleshooting guide to achieve good large-scale data from the retina.

### I- Large-scale data collection using microelectrode array (MEA):

Over the past two decades, with the development of MEA, it has become possible to understand the various information processing at the level of the neural circuit. MEA consists of few tens to hundreds of electrodes which allow recording of neural activity from several neurons (like retinal ganglion cells, RGCs) in parallel (*Meister et al., 1994*). One of the advantages MEA has over other high-throughput data collection techniques like calcium imaging is that it can record neural activity which is in the order of several Hertz (kilo- Hertz to MegaHertz) which often get filtered during the process of calcium imaging. Currently, many groups use MEA to study the activity of RGCs to complex visual and electrical stimulation(*Eickenscheidt et al., 2012; Eickenscheidt and Zeck, 2014; Gerwig et al., 2012; Goo et al., 2011a*). In this thesis, I have used planar MEAs (Titanium nitride (TiN) electrodes, circular shape, diameters: 30 $\mu$ m on a glass substrate in an 8X8 square-type grid layout (MCS, Reutlingen, Germany) which record mouse RGC spikes from 59 electrodes simultaneously. Further specifications of the MEA system is described in detail in **Publication 1**.

During the process of data collection, various factors were needed to be considered to get reliable RGC responses to both visual and electrical stimulation. They were as follows:

**Retinal dissection & mounting of the retina on MEA:** To obtain good neural activity from the RGCs, it was extremely crucial that the process of retinal dissection was done efficiently within a short time interval and with the least damage to the retina. Care was taken to gently remove all the vitreous to facilitate a better contact to the planar electrode array (Figure 1.10). Furthermore, during the process of dissection fresh carbogenated (95% O<sub>2</sub> and 5% CO<sub>2</sub>) artificial cerebrospinal fluid (ACSF) was regularly provided to maintain the vitality of the retina. During the mounting process, two miniature paintbrushes were used to orient and flatten the retina on the MEA reducing the risk of damaging the retina and the electrodes of the MEA. In some cases, forceps could also be used instead of brushes for mounting the retina. Therefore, a good retinal preparation and mounting forms the basis for obtaining high-throughput RGC responses.

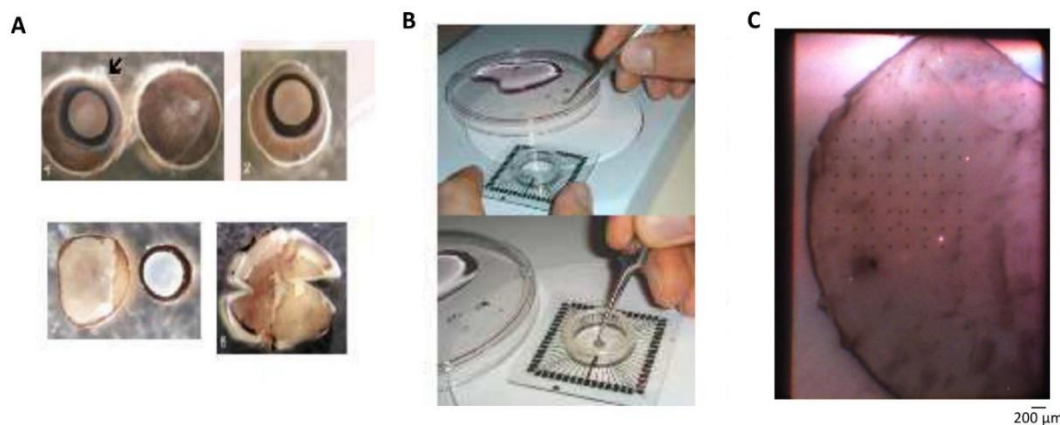


**Figure 1.10: Retina preparation and mounting.** The figure depicts the invitro acute retina preparation and mounting over planar MEA for recording. In **A)** the eyeball was enucleated, and the cornea, ora serrata, lens and vitreous body were removed, the retina was detached from the pigment epithelium, and the optic nerve was cut at the base of the retina. **B)** mounting of the retina over MEA. **C)** shows the mounted retina over a Planar MEA (8x8 array) seen from an inverted microscope. (Figure: (a & b)-courtesy of Prof. Dr. Elke Guenther, NMI, Reutlingen).

### 1. Selection of the retina area for stimulation:

From previous work (Dhande and Huberman, 2014; Dräger and Olsen, 1981; Jeon et al., 1998) it has been shown that the ganglion cell densities across various species vary as a function of retinal eccentricity. In mouse retina, the RGC exhibit a modest four-fold decrease in density from the central (near the optic disk) to the periphery.



For my experiments, I use retinal halves instead of the whole retina. This decision was solely based on sampling more data from the RGCs with minimal usage of animals. The retinal halves were cut along the naso-temporal axis into dorsal and ventral halves. For most of my recording, I used mid-periphery area of the retina for recording the RGC responses to visual as well as electrical stimulation. Therefore, I estimated that the area in contact with the electrodes had ganglion cell densities of approximately 1000-3000 cells/mm<sup>2</sup>. Furthermore, the selection of an electrode to deliver electrical stimulation to the retina was based on the proximity to electrodes with robust spontaneous neural signals and visual responses to ensure a maximum number of recorded neurons (**Publication 1**).

## 2. Stability of RGC responses:

Over long duration *invitro* experiments with MEA, it is observed that the physiological health of the retina deteriorates. Such deterioration could significantly change the characteristic responses of the RGCs to visual and electrical stimulation. These changes in the retina could stem from factors like change in temperature and pH. Therefore, to ensure the responses of the RGC were stable during the entire course of the experiment the temperature of the heating plate below the MEA (with the mounted retina) was maintained at 33°C. Further, the bottle containing ACSF was maintained at a similar temperature to the heating plate to prevent any form of instability in responses due to temperature variations.

The pH of the ACSF solution was also maintained with constant carbogenation (95% O<sub>2</sub> and 5% CO<sub>2</sub>). Controlling these factors ensured a continuous supply of nutrient and oxygen thereby enabling stable RGC responses during the entire duration of the recording. For my studies, in this thesis, only cells which had stable responsiveness during the entire duration of the experiment (2-3 hours) and showed no signs of rundown, were included for further analysis. The stability criteria were indeed crucial for isolating good RGC responses and will be further discussed below in the *Processing of Large-Scale Data* section.

## 3. Signal to Noise Ratio:

While recording responses with planar MEA one of the rate-limiting step is obtaining a good signal to noise ratio from the RGCs. It is observed that the signals from the RGCs are masked due to fragile vitreous humor attached to the retina and dead cells

resulting from the process of retinal dissection, thereby resulting in a weak signal to noise ratio. Therefore, for overcoming this issue, it was essential to make a tight contact between the retina and electrodes to prevent any leaky current resulting in poor RGC signals. Once the retina was mounted, with the RGC down on the electrodes it was essential to adhere the retina securely on the electrodes during the entire course of the experiment. My preliminary standardization experiments with closely spaced nylon mesh grids to secure the retina on the electrode yielded a weak signal to noise ratio. Therefore, I used a dialysis membrane mounted on a custom Teflon ring to press the retina on the MEA (Figure 1.11). Due to the relatively high flow rate (4-6ml/min) of ACSF during the experiment the dialysis membrane not only ensured a better contact of the retina to the electrodes but also due to its semi-permeability helped in maintaining the retinal vitality. Furthermore, the risk of damaging the retina was minimal with the membrane in comparison to the nylon mesh grid. Cases where there is noise due to electrical lines (50/60Hz oscillations) or due to the perfusion system an additional grounding (preferably with spring clips) could provide a better solution.

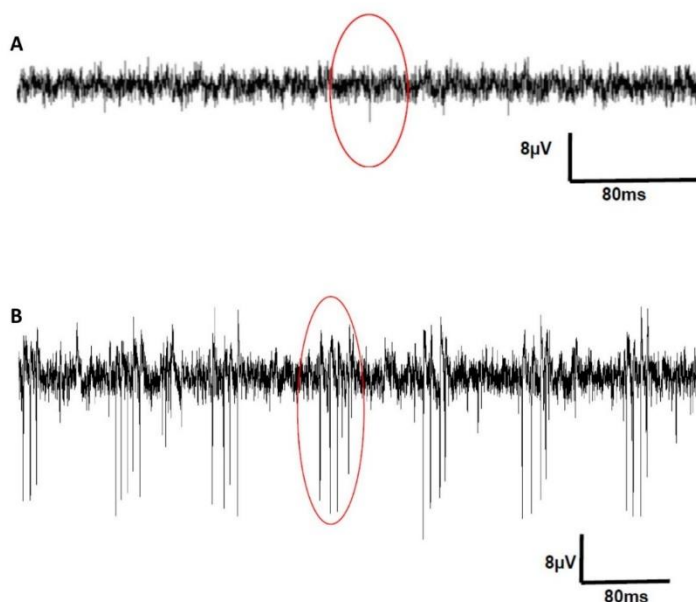


**Figure 1.11: Signal to Noise Ratio.** **A)** Raw voltage traces showing weak signal to noise ratio obtained from RGCs with retina pressed on a planar MEA (30µm electrode diameter, 200µm inter-electrode distance) with the nylon mesh platinum grid. **B)** Raw traces showing good signal to noise ratio obtained from the RGCs with the retina pressed on the same planar

MEA with dialysis membrane mounted on a Teflon ring. Post optimization with dialysis membrane mounted Teflon Ring enabled a good contact of the retina with the MEA electrodes yielding an excellent signal to noise ratio. The red circles encircle RGC activity.

## II-Processing the large-scale data:

### Identification of RGC responses

One of the difficult tasks of collecting such high-throughput data is the requirement for developing a stable and semi-automated process for identifying the RGC responses. Before analyzing and characterizing these responses, it is extremely crucial to identify each ganglion cell response reliably. The output of a ganglion cell is a spike (action potential). Each electrode of a MEA can record responses from multiple ganglion cells simultaneously. Therefore, it is necessary to develop a robust method which could isolate individual ganglion cell responses (often referred as a ‘unit’) from a single electrode. This method is often referred to as **Spike Sorting**.

In my thesis, I helped establish a robust semi-automated process of isolating individual RGC response. Further, I developed a protocol for manually validating these responses based on different parameters to classify them as ‘good’ isolated RGC cell response which was included in further analysis or ‘bad’ unit which was excluded from the analysis. This process of classification was termed as **Manual Cell Validation**.

### *Semi-Automated Data Processing:*

The semi-automated data processing primarily involved two steps.

1. Filtering and Detection- The stored raw data were processed using a commercial spike sorting software (Offline Sorter, Plexon Inc, Texas, USA). To process the raw data, the voltage traces (*refer to Figure 1.11*) were first filtered with a 12-pole Bessel low pass filter with a cut-off frequency of 51 Hz. The Bessel filter was selected due to its uniform phase response as a function of frequency and its negligible property to overshoot and ring. For fine-tuning the filtering ability, a higher pole of 12 was selected. A cut-off frequency of 51Hz was chosen to exclude low-frequency local field potentials (LFPs) and electrical line noise. Following this, the action potential events (spikes) whose filtered amplitude was greater than four standard deviations from the mean were detected.
2. Sorting- The filtered and detected events (spikes) were sorted into clusters with an automated spike sorting algorithm – T-Distribution Expectation Maximization. This sorting algorithm could assign noise events as well as spikes from up to 5 cells recorded

on each electrode to their own separate ‘units’ (Jalligampala *et al.* 2017, Sekhar *et al.* 2016). The rationale for choosing this algorithm was that it provides flexible degrees of freedoms and due to wider tails, could efficiently handle outliers.

***Manual Cell Validation or Data inclusion criteria:***

As a quality control for the automated sorted units, each electrode channel ‘units’ were manually inspected and modified as and when necessary. This was so done to minimize Type I and Type II errors, i.e. rejecting a true spiking event (false positive) as a noise/artifact and retaining an artifact/noise or spike from a different cell as a true spiking event, respectively.

For a unit (spike train) to be included in the analysis the following criteria need to be met:

1. The presence of a lock-out or absolute refractory period of 0.8 -1ms (Figure 1.12 #1, #2) in the interspike interval (ISI) distribution and auto correlogram, indicating spike train is from a single cell and not lumped from multiple cells
2. The absence of a peak in cross-correlogram with other cells. The presence of the peak is an indication of the splitting of the single cell into multiple cells, thereby addressing Type II error (Figure 1.12 #2).
3. A biphasic waveform whose shape is typical of a classic extracellular action potential (Figure 1.12 #2).
4. Stability of the RGC responses (in terms of spike shape and spiking frequency across all stimuli) over the entire course of an experiment (Figure 1.12 #2).
5. Each of these parameters was rated from 1 to 5 (1 being worst and 5 being best), and a weighted average (ISI lock out weighted at par with the average of cross-correlogram, stability, and waveform) was calculated (Figure 1.12 #3). Apart from objective classification, there was an additional subjective criterion (as per the person’s gestalt impression, independent of the objective ranking) of “keep 0/1” where 0 is rejecting the unit and 1 keeping the unit. Most of the times the subjective and objective criterion were coordinated.
6. These evaluated scores distribution was plotted as histograms (good unit and bad unit) using a custom script written in MATLAB. Looking at the histogram

distributions, one could decide the threshold for the cells to be included in further analysis.

- Following the process of cell validation, the cells to be analyzed tend to have a well-isolated cluster in their principal component (PCA) space.

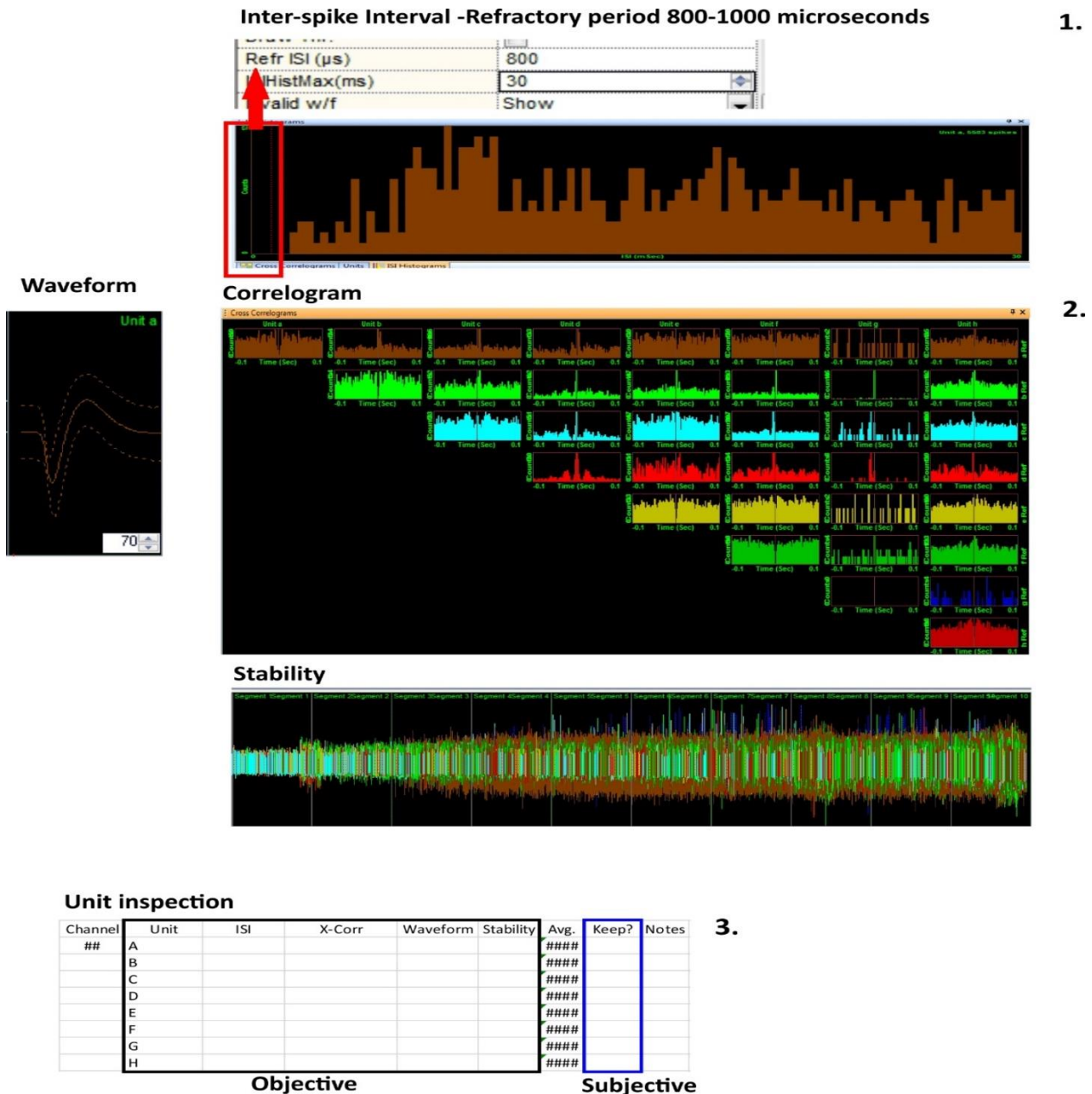


**Figure 1.12: Cell Validation protocol.** 1) The presence of a refractory period (0.8-1ms) in the ISI distribution. 2) A well-isolated waveform (in brown), lockout in auto correlogram (unit a with unit a), no peaks in cross-correlogram and stability of responses as gauged by the spike

*shape, count and frequency during the entire course of the experiment.3) Rating the above parameters from 1 to 5 (1-worst 5-best) to obtain a weighted average. Independent of these rankings, the gestalt impression was also given.*

Following the cell validation, the time stamps of these spiking units were collected with the Neuroexplorer software (Plexon, TX, USA) and exported to MATLAB for further complex analysis.

## Chapter 2

### Publication 1- Optimal voltage stimulation parameters for wild-type and *rd10* mouse retinal ganglion cells.

#### 2.1 Synopsis and framework of the study:

Many studies have investigated electrical responsiveness and electrical desensitization in response to current stimulation, however, only a handful have examined this effect via voltage stimulation of the retinal network (Goo *et al.*, 2011b; Stett *et al.*, 2007, 2000). Therefore, as a preliminary step to understand the aspects of electrical desensitization via voltage stimulation, we designed an initial set of paired-pulse stimuli established from earlier studies to probe desensitization. Unexpectedly, this attempt to verify previous results of others was unsuccessful and revealed significantly more complexity in determining single cell response thresholds. Furthermore, earlier studies from both our group and others were inconclusive regarding the appropriate voltage-duration combination for a square-wave voltage pulse to generate reliable responses from most ganglion cells. Therefore we set aside our attempt to validate desensitization (via voltage stimulation) and embarked upon a stimulus standardization study in order to identify an optimal stimulus that would elicit responses in a maximal number of RGCs.

Considering results from earlier stimulus standardization studies, one would expect that responsivity must plateau after a saturation point has been reached (*Ryu et al.*, 2009, *Goo et al.* 2011, *Stett et al.* 2000). However, we realized that many cells in our study demonstrated decreased responses at higher voltages. This would suggest that some RGCs are

nonmonotonic - having stimulus-response functions that do not monotonically increase. However, realizing that such reduced responses could also result from neural fatigue or recording instabilities and our choice of a sequential block paradigm (going from low to higher voltages sequentially), we randomized the voltage presentation order. It was seen that although stimulus randomization ameliorated fatigue, it unmasked both electrical adaptation and nonmonotonicity. Given the reality of nonmonotonicity, it became apparent that a stimulus that is just above the threshold for one neuron may be suppressed for a different neuron. This conclusion, combined with the weak influence of duration on firing rate finally led us to design an experiment to explore the full range of voltage-duration using sequential blocks of increasing voltage within which pulse durations were randomized.

To identify a small set of stimuli capable of driving a majority of neurons within their dynamic range, we generated a set of stimuli that sampled the entire duration-voltage space ranging from below threshold to just below safe charge injection limits (to exclude the possibility of electrolysis and electrode degradation).

Our primary goal with the present chapter was to systematically investigate the effects of multiple waveform parameters on network-mediated responses of the RGC population. Although many groups (*Boinagrov et al., 2014; Hadjinicolaou et al., 2014*) have studied the effects of electrical waveform parameters on stimulation efficacy for RGCs, the influence of these parameters at the population level remains unclear. Furthermore, while investigating the influence of such parameters, we found that the variability of the RGC population (due to different morphological cell classes and heterogeneity of electrical response patterns) has not been well accounted for and in most cases has been excluded from the study (*Ryu et al., 2010, 2009b*). Such exclusions introduce selection bias, which could oversimplify the diversity of the RGC population. Therefore, considering such variability, we have developed a novel conceptual framework for identifying the optimal stimulus parameters that will activate a majority of the RGCs across a multiparametric space. Furthermore, in this chapter, we have attempted to clarify some of the conventional conceptual notions of electrical thresholds in the current field of retinal prostheses.



# Optimal voltage stimulation parameters for network-mediated responses in wild type and *rd10* mouse retinal ganglion cells

Archana Jalligampala<sup>1,2,3</sup>, Sudarshan Sekhar<sup>1,2,3,4</sup>, Eberhart Zrenner<sup>1,2,4</sup> and Daniel L Rathbun<sup>1,2,4</sup>

<sup>1</sup> Institute for Ophthalmic Research, Eberhard Karls University, D-72076 Tübingen, Germany

<sup>2</sup> Werner Reichardt Centre for Integrative Neuroscience (CIN), D-72076 Tübingen, Germany

<sup>3</sup> Graduate Training Center of Neuroscience/International Max Planck Research School, D-72074 Tübingen, Germany

<sup>4</sup> Bernstein Center for Computational Neuroscience Tübingen, D-72076 Tübingen, Germany

E-mail: [daniel.rathbun@uni-tuebingen.de](mailto:daniel.rathbun@uni-tuebingen.de) (Daniel L Rathbun) and [archana.jalligampala09@gmail.com](mailto:archana.jalligampala09@gmail.com) (Archana Jalligampala)

Received 14 July 2016, revised 27 October 2016

Accepted for publication 8 November 2016

Published 3 February 2017



CrossMark

## Abstract


To further improve the quality of visual percepts elicited by microelectronic retinal prosthetics, substantial efforts have been made to understand how retinal neurons respond to electrical stimulation. It is generally assumed that a sufficiently strong stimulus will recruit most retinal neurons. However, recent evidence has shown that the responses of some retinal neurons decrease with excessively strong stimuli (a non-monotonic response function). Therefore, it is necessary to identify stimuli that can be used to activate the majority of retinal neurons even when such non-monotonic cells are part of the neuronal population. Taking these non-monotonic responses into consideration, we establish the optimal voltage stimulation parameters (amplitude, duration, and polarity) for epiretinal stimulation of network-mediated (indirect) ganglion cell responses.

We recorded responses from 3958 mouse retinal ganglion cells (RGCs) in both healthy (wild type, WT) and a degenerating (*rd10*) mouse model of retinitis pigmentosa—using flat-mounted retina on a microelectrode array. Rectangular monophasic voltage-controlled pulses were presented with varying voltage, duration, and polarity.

We found that in 4–5 weeks old *rd10* mice the RGC thresholds were comparable to those of WT. There was a marked response variability among mouse RGCs. To account for this variability, we interpolated the percentage of RGCs activated at each point in the voltage-polarity-duration stimulus space, thus identifying the optimal voltage-controlled pulse (−2.4 V, 0.88 ms).

The identified optimal voltage pulse can activate at least 65% of potentially responsive RGCs in both mouse strains. Furthermore, this pulse is well within the range of stimuli demonstrated to be safe and effective for retinal implant patients. Such optimized stimuli and the underlying method used to identify them support a high yield of responsive RGCs and will serve as an effective guideline for future *in vitro* investigations of retinal electrostimulation by establishing standard stimuli for each unique experimental condition.

Keywords: electrical stimulation, response surface, non-monotonic response function, variability, threshold

 Supplementary material for this article is available [online](#)

(Some figures may appear in colour only in the online journal)

## 1. Introduction

Around four million people suffer from the blinding diseases of retinitis pigmentosa (RP) or age-related macular degeneration (AMD), with estimated worldwide prevalence rates of 1 in 4000 each for AMD and RP (Resnikoff *et al* 2004, Hamel 2006, Hartong *et al* 2006, Pascolini and Mariotti 2012). In both cases, while retinal photoreceptors cease to transform incident light into neural signals, the cellular layering of inner retinal neurons is still preserved with moderate physiological and morphological changes until very late in the degeneration process (Gargini *et al* 2007, Mazzoni *et al* 2008, Jones *et al* 2016). This remaining inner retinal circuitry provides a potential substrate for sight restoration. Over the years various approaches have been explored for restoring meaningful vision in blind patients via electrical retinal prostheses, optogenetics (Busskamp and Roska 2011, Reutsky-Gefen *et al* 2013), gene therapy (Bennett *et al* 2016) and stem cell-based therapy (Schraermeyer *et al* 2001, Schwartz *et al* 2015). Of these, the greatest progress has been achieved in the field of retinal prostheses with many ongoing clinical trials and commercialization of two separate devices in USA and Europe over the last decade (Ahuja *et al* 2011, Weiland and Humayun 2014, Stingl *et al* 2015). Patients in these clinical trials have reported reliable perception of visual patterns as well as retinotopically aligned phosphenes upon stimulation (Zrenner *et al* 2011). An appreciable subset of these patients also report successful performance of simple day-to-day tasks like discriminating dark and light objects, identifying objects, and reading simple words (Ahuja *et al* 2011, Zrenner *et al* 2011, da Cruz *et al* 2013, Stingl *et al* 2015).

For any retinal implant, the ultimate goal is to generate neuronal signals in the population of retinal ganglion cells (RGCs) which convey information from the retina to the brain. Two primary mechanisms of RGC activation are possible: direct and indirect stimulation (Stett *et al* 2000, Jensen *et al* 2005, Fried *et al* 2006, Tsai *et al* 2009, Margalit *et al* 2011). Direct stimulation is best achieved with short pulses (typically <1ms, Fried *et al* 2006, Sekirnjak *et al* 2006) whereas indirect ganglion cell stimulation is achieved via activation of the underlying retinal network, typically using longer pulses (1–10ms, Lee *et al* 2013, Boinagrov *et al* 2014, Im and Fried 2015b). Stimulation thresholds for direct RGC stimulation are lowest for epiretinal electrode placement (Boinagrov *et al* 2014). In contrast, indirect RGC stimulation has similar thresholds in both epiretinal and subretinal configurations (Eickenscheidt *et al* 2012, Boinagrov *et al* 2014, Im and Fried 2015a). Here we examined indirect RGC responses using the epiretinal configuration so that stimulation and recording could be achieved simultaneously with a single

microelectrode array. Considering, the similarity between indirect ganglion cell response thresholds in subretinal and epiretinal configurations, it is expected that our results are also valid for subretinal stimulation.

In most human RP patients, degeneration manifests in adulthood after full development of the retinal circuitry. In contrast, the most extensively characterized animal model for human RP has been the *rd1* mouse in which degeneration begins before eye opening while retinal development remains incomplete (Caley *et al* 1972, Marquardt and Gruss 2002). The more recently discovered *rd10* mouse model of RP, has a relatively delayed onset and slower progression of retinal degeneration (Pennesi *et al* 2012) and is quickly becoming the preferred model for *in vitro* electrical stimulation experiments (Toychiev *et al* 2013, Park *et al* 2015, Cho *et al* 2016). Multiple studies have examined electrical stimulation during late-stage degeneration. Few, however, have examined the intermediate period, after the beginning of degeneration but before complete vision loss. Analogous to cochlear implant therapy for deafness, earlier implantation of retinal prostheses may prove to be more effective (Sharma *et al* 2002). Therefore, we chose to compare the electrically stimulated responses of WT and *rd10* retinas at the intermediate age of 4–5 weeks postnatal.

Our main goal was to identify a subset of pulse parameters (voltage amplitude, duration, and polarity) within the large range of possible combinations that can activate a maximal number of RGCs in both healthy and degenerating mouse retina. For each RGC, we generated a response surface that summarized how variations in the duration, polarity, and amplitude of rectangular-wave voltage pulses influence that cell's spiking response. Our data was in close agreement with previous studies, including the observation of a variety of response surface shapes across the RGC population (Ryu *et al* 2009). However, these variable response patterns have not been explored in-depth in previous multiparametric studies, particularly with regard to how such variability influences the determination of optimal stimulus parameters (Gerhardt *et al* 2011, Hadjinicolaou *et al* 2015). Therefore, to identify a generic electrical stimulus that will activate the majority of RGCs without customization, (1) we eliminated the simplifying assumption that RGC responses always increase with increases in the stimulus amplitude or duration, (2) we took special care to minimize sampling bias so that all electrically responsive RGCs were included in our analysis, (3) from the individual cell response surfaces, we determined the percentage of the RGC population that was activated at each point in voltage-polarity-duration space, and (4) we identified the optimal voltage-controlled pulse for retinal stimulation as the peak percentage in this parameter space.

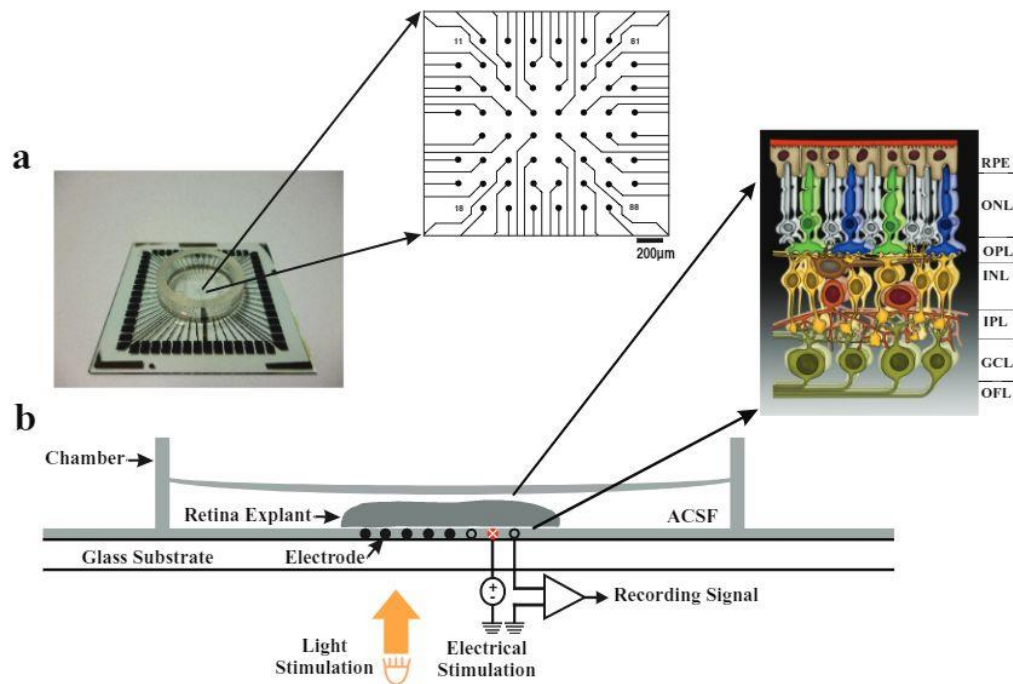


**Figure 1.** Experimental configuration. (a) Planar microelectrode array (MEA, 30  $\mu\text{m}$  electrode diameter, 200  $\mu\text{m}$  interelectrode distance, Multichannel Systems GmbH, Reutlingen, Germany) with electrode field enlarged (*expansion*). (b) Schematic representation of *in vitro* experimental configuration. Retinal explant with pigment epithelium removed was perfused with carbogenated ACSF and placed in the MEA chamber, ganglion cell layer down (*expansion*) covering all electrodes. Electrical stimulation was provided epi-retinally through one electrode (*white cross*) while remaining electrodes recorded ganglion cell action potentials extracellularly. The neighboring 8 electrodes were used for most analyses (*open circles*). Full-field flash stimulation was provided from below the transparent MEA. Abbreviations: RPE retinal pigment epithelium, PRL photoreceptor layer, ONL outer nuclear layer, OPL outer plexiform layer, INL inner nuclear layer, IPL inner plexiform layer, GCL ganglion cell layer, OFL optic fiber layer, ACSF artificial cerebrospinal fluid.

## 2. Methods

### 2.1. Animals

Animals were housed under standard white cyclic lighting, mimicking regular daily rhythms. They had free access to food and water. One litter each of adult wild type (WT) C57Bl/6J (The Jackson Laboratory, Bar Harbor, ME, USA) and *rd10* (on a C57Bl/6J background, The Jackson Laboratory) strains were used, with age ranging from post-natal day 28–37 for both strains. For each strain, 3 male and 2 female mice were used. All procedures were approved by state authorities (Regierungspraesidium, Tuebingen) and conducted under the supervision of the Tuebingen University Clinics facility for animal welfare (Einrichtung für Tierschutz, Tierärztlichen Dienst und Labortierkunde) in accordance with the Association for Research in Vision and Ophthalmology (ARVO) statement for the use of animals in ophthalmic and visual research. All efforts were made to minimize the number of animals used and their suffering.

### 2.2. Retinal preparation

For retinal dissection, mice were anesthetized by  $\text{CO}_2$  inhalation, checked for absence of withdrawal reflex to a pinch of the between-toe tissue, and then euthanized by cervical

dislocation. Under normal room lighting, the eyes were removed to carbogenated (95%  $\text{O}_2$  and 5%  $\text{CO}_2$ ) artificial cerebrospinal fluid (ACSF) solution containing the following (in mM): 125 NaCl, 2.5 KCl, 2  $\text{CaCl}_2$ , 1  $\text{MgCl}_2$ , 1.25  $\text{NaH}_2\text{PO}_4$ , 26  $\text{NaHCO}_3$  and 20 Glucose, pH 7.4. Under dim light conditions for each eye, the cornea, ora serrata, lens and vitreous body were removed, the retina was detached from the pigment epithelium, and the optic nerve was cut at the base of the retina. Special care was taken to remove all traces of vitreous material from the inner surface of the retina to optimize contact between the nerve fiber layer and recording electrodes. Retinas were maintained in carbogenated ACSF until needed. For recording, a retinal half was mounted with the ganglion cell layer down on a planar microelectrode array (MEA, figure 1). Two miniature paint brushes were used to orient and flatten the retinal half without risking damage to the MEA and the retina, and a dialysis membrane (CelluSep, Membrane Filtration Products Inc., Seguin, Texas, USA) mounted on a custom Teflon ring was lowered onto the retina to press it into closer contact with the MEA (Meister *et al* 1994). After securing the MEA under the preamplifier, the retina was continuously superfused with carbogenated ACSF ( $\sim 6 \text{ ml min}^{-1}$ ) maintained at 33  $^\circ\text{C}$  using both a heating plate and a heated perfusion cannula (HE-Inv-8, PH01, Multi Channel Systems, Reutlingen, Germany). A stabilization time of  $>30 \text{ min}$  was provided prior to recording the data.

### 2.3. Microelectrode array and data acquisition

For recording the spiking responses from RGCs, a planar MEA (figure 1), containing 59 circular titanium nitride electrodes (diameter: 30  $\mu\text{m}$ , interelectrode spacing: 200  $\mu\text{m}$ , 60MEA200/30iR-ITO, Multi Channel Systems, Reutlingen, Germany) arrayed in an  $8 \times 8$  rectilinear grid layout, with indium tin oxide (ITO) electrode tracks insulated by silicon nitride ( $\text{Si}_3\text{N}_4$ ) on a glass substrate was used. Electrodes were absent from the four corners of the grid and one electrode was substituted with a large reference electrode. The impedances of the electrodes in saline were measured to be approximately 200–250 k $\Omega$  at 1 kHz using a NanoZ impedance tester (Plexon Inc., TX, USA). The MEA60 system (MCS, Reutlingen, Germany) was used for data acquisition including: the RS-232 interface, a 60 channel preamplifier with integrated filters and a blanking circuit (MEA 1060-Inv-BC) controlled by MEA\_Select software to reduce recording noise by grounding any defective electrodes and to assign electrical stimulation waveforms to the selected electrode. Data was collected using the MC\_Rack program on a personal computer running Windows XP and fitted with MC\_Card data acquisition hardware and an analog input card to record stimulus trigger signals. The raw data were recorded at a rate of 50 kHz/channel with a filter bandwidth ranging from 1 Hz–3 kHz and amplification gain of 1100.

### 2.4. Stimulation

Stimulus pulses were generated using a stimulus generator (STG 2008, Multi Channel Systems, Reutlingen, Germany) in the MC\_Stim software program and delivered from the ganglion cell side of the retina (epiretinally) via one of the 59 electrodes—which was always an interior electrode and chosen based on proximity to electrodes with robust spontaneous neural signals and visual responses to ensure a maximum number of recorded neurons. Although subretinal implants deliver electrical stimulation from the photoreceptor side of the retina to activate the retinal network, it is well established that the desired network stimulation can be achieved by stimulating from either side of the retina by reversing the polarity of stimulation (Eickenscheidt *et al* 2012, Boinagrov *et al* 2014, Im and Fried 2015b). Therefore, electrodes of the MEA were used to simultaneously stimulate and record from the ganglion cell (epiretinal) side of the flat-mounted retina.

The stimulus (figure 2) consisted of monophasic rectangular voltage pulses, each with one of the following amplitudes (0.3, 0.5, 1.0, 1.5, 2.0, 2.5 V) and durations (60, 100, 200, 300, 500, 1000, 2000, 3000, 5000  $\mu\text{s}$ ). In order to reduce the possibility of electrolysis and electrode degradation only voltage/duration combinations that fell within safety limits were delivered (Gekeler *et al* 2004, Patan *et al* 2006, Microelectrode Array (MEA) Manual 2010). During presentation of the highest voltage-duration combinations, careful observations were made to ensure that there was no bubble formation due to hydrolysis of water. Additionally, to explore any selective preference of the cells to pulse polarity, we included both cathodic ( $-V$ ) and anodic ( $+V$ ) stimuli. Because

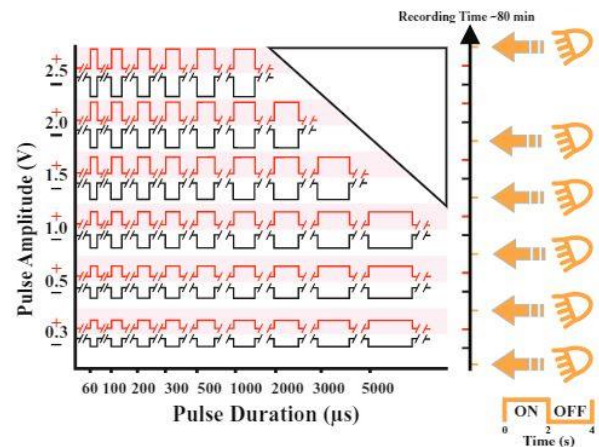


**Figure 2.** Schematic representation of experimental protocol. Electrical stimuli were presented over a range of voltage/duration pairs. Each constant-voltage stimulus block consisted of 5 repetitions of each duration. For higher voltages, the longest durations were excluded to avoid electrode damage (*open triangle*). Within each repetition, durations were randomized and pulses were separated by 5 s. The first voltage block was chosen randomly to be either positive (*shaded background*) or negative (*white background*) for each experiment with subsequent blocks alternating polarity throughout the experiment. Blocks of full-field flashing visual stimulation (20 repetitions of 2 s ON, 2 s OFF, *icons at right*) were interleaved between selected voltage blocks to monitor recording stability throughout each experiment. Timeline at right with tick marks indicates the order of the respective stimulus blocks. Stimulus blocks were separated by at least 120 s.

high-amplitude stimuli were observed to alter responses to low amplitude stimuli in preliminary experiments, pulses were presented in 12 constant-voltage blocks proceeding in the order of lowest to highest amplitude over the course of the experiment. For each experiment, the beginning polarity was randomly chosen and alternated with subsequent blocks thereafter. Prior to and after each stimulation block, spontaneous activity was recorded for  $\sim 30$  s. Within each voltage block, the durations were presented in 5 sequential, uniquely randomized sets, for a total of 5 repetitions for each voltage/duration combination, with an interval of 5 s after each pulse to allow the recovery of RGC responsiveness. A post-time of 100  $\mu\text{s}$  was set in MC\_Stim to facilitate discharge of the stimulating electrode. Additionally, a wait time of 1 ms was set in the MEA\_Select software to extend the blanking period before recording was resumed—thus minimizing stimulation artifacts. Voltage blocks were always separated by at least 120 s including a 30 s recording of spontaneous activity before and after each voltage block.

It is often observed that over the course of long-term *in vitro* recordings the physiological health of tissue deteriorates. In the retina, such deterioration can lead to instability in visual and electrical responses. Such changes can result from change in nutrient and oxygen supply, pH and temperature. Therefore, to monitor the stability of RGC responses over the duration of the experiment, 6 visual stimulus blocks were interleaved before, after, and within each electrical stimulation experiment that spanned  $\sim 80$  min of recording time, including

the first and last flash blocks (Carcieri *et al* 2003). Each visual stimulus block consisted of a full-field ‘flash’ stimulus of 2 s maximum brightness (ON, ~40 klx) followed by 2 s minimum brightness (OFF, ~20 lx), cycled 20 times without pause (mean illuminance ~20 klx), covering a wide range of intensities occurring in the natural environment (Rodieck 1998). Only the RGCs that had stable responsiveness over the course of the entire experiment and showed no sign of rundown were included for further analysis. For the current study, we pooled the results from all RGCs and did not distinguish them into physiological cell types.

### 2.5. Data processing

The stored raw data were processed using commercial spike sorting software (Offline Sorter, Plexon Inc., TX, USA). Raw voltage traces were first filtered (low-cut, 12 point Bessel filter at 51 Hz) to exclude line noise, then putative events were detected using a threshold crossing method (4 standard deviations below the mean of the amplitude histogram). These events were sorted into clusters with an automated routine (T-distribution Expectation Maximization) to assign noise events as well as spiking events to separate ‘units’. Finally, as a quality control step, multiple sorting solutions were manually inspected to identify the best solution and to occasionally modify this solution in order to minimize Type I and Type II errors in attribution of events to different sources (Sekhar *et al* 2016). Only units that met the following criteria were considered to be well-isolated single-cell spike trains and included in the analysis presented here: (1) a distinct waveform that was stable during the entire course of the experiment, (2) an interspike interval lock-out period indicating a refractory period, and (3) cross-correlograms with other units that disproved splitting of a single cell into multiple units or lumping of multiple cells into a single unit. Special care was taken to minimize sampling bias by including every possible RGC, even if its spike waveform was small or difficult to isolate. Due to electrical stimulation artifacts, spike trains could not be reliably isolated from the stimulating electrode. Time stamps assigned to the detection threshold crossing of these sorted spikes were collected with NeuroExplorer (Plexon Inc., TX, USA) and exported to MATLAB for further analysis. Accordingly, a total of 2078 WT cells (16 retinal halves) and 1880 *rd10* cells (9 retinal halves) were included in our dataset. Of these, the majority responded to visual stimulation (2076 WT, 1763 *rd10*).

### 2.6. Data analysis

For each cell, the responses to electrical stimulation were derandomized and collated. The spiking response was integrated over the interval spanning 10–100 ms after pulse onset, and averaged across the 5 repetitions of each of the 96 unique stimuli (figure 2). Likewise, a spontaneous rate, chosen to best characterize the baseline firing rate within the context of ongoing electrical stimulation, was calculated from the 1 s of recording time before each pulse and averaged across all 480

**Table 1.** Retinal ganglion cell (RGC) counts for WT and *rd10*. ‘Distances’ are recording distances relative to the stimulating electrode. For the definition of ‘responsive’ see methods—data analysis.

		WT	<i>rd10</i>
All distances	Total	2078	1880
	Electrically responsive	354	1188
200–283 $\mu\text{m}$	Total	216	232
	Electrically responsive	68	174

responses. The response integration window of 10–100 ms was chosen to exclude spikes generated by either direct RGC stimulation which have a latency <10 ms (Jensen *et al* 2005, Fried *et al* 2006, Sekirnjak *et al* 2006) or indirect RGC stimulation through residual photoreceptors which tend to have latencies >100 ms (Margalit 2011, Boinagrov *et al* 2014).

**2.6.1. Responsive RGC inclusion criteria.** For the present analysis, a cell was considered to be electrically responsive if (1) at least three of the 96 responses was greater than two standard deviations (SD) above the average spontaneous rate (*threshold*) and (2) such responses were equivalent to a firing rate of at least 8.89 Hz (at least 4 spikes within the  $5 \times 90$  ms integration windows of that stimulus). These criteria represent an acceptable compromise in rejecting false positives but not rejecting truly responsive cells with high thresholds and/or high variability. The number of electrically responsive cells was 354 for WT and 1188 for *rd10* retinas (table 1). This same response threshold of spontaneous  $+2 * \text{SD}$  was used to determine threshold voltages and durations for each cell. For the present analysis, it was necessary to add additional inclusion criteria to the data set. Because electrical field strength falls with distance from the stimulating electrode, it would be inappropriate to group cells recorded at vastly different distances (Stett *et al* 2007, Ryu *et al* 2009, Eickenscheidt *et al* 2012). Therefore, for most analyses, we only examined cells recorded on the 8 electrodes neighboring the stimulating electrode—a stimulation distance of either 200 or 283  $\mu\text{m}$  (see figure 1).

**2.6.2. Response activation surface.** To plot each cell’s electrical response surface, responses were normalized to the range from minimum response to maximum response and then cubic spline interpolated at a sampling resolution of 100 mV and 20  $\mu\text{s}$ . To determine the optimal stimulus, the percentage of RGCs activated at each point in this interpolated space was examined. A cell was considered activated at all points where its interpolated response exceeded the response threshold defined above.

**2.6.3. Threshold curves.** Threshold voltage was identified separately for each cell and each constant-duration, voltage response curve. It was defined as the lowest voltage whose response exceeded the threshold as defined above. Threshold durations were identified in a similar manner from constant-voltage, threshold response curves. For plots of voltage threshold versus duration and duration threshold versus

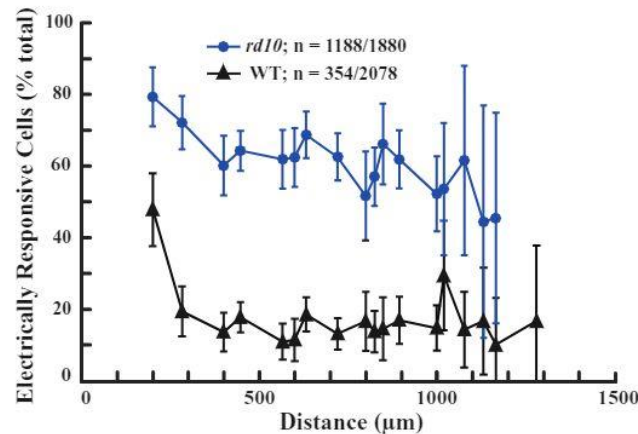


**Figure 3.** Percent of RGCs responding to electrical stimulation at each interelectrode distance between stimulating electrode and recording electrode ('responsiveness' is defined in methods section 2.6). Further analysis was limited to only cells recorded at distances of 200 or 283  $\mu\text{m}$ . Error bars are binomial confidence intervals. Population numbers are  $n = \text{number of electrically responsive cells}/\text{total number of cells}$ , summed across all distances.

voltage, only single cell curves with no more than 3 missing threshold measurements were included in the population curve. Few cells had suprathreshold responses at all voltages (or durations)—as assessed across the complementary parameter range (duration or voltage, respectively). In part, this was because safe charge injection limited the voltage at higher durations. Because the inclusion of a large number of cells with only a few responses artificially raised thresholds at intermediate voltages (or durations) we found that allowing up to 3 missing data points per curve achieved a compromise between population curve distortion and dataset reduction.

### 3. Results

#### 3.1. Responsiveness decreases with increasing distance

To assess the responsiveness of RGCs across the various distances we plotted the percent of cells which were electrically responsive (see section 2.6, table 1) at each distance from the stimulating electrode (figure 3). As predicted from earlier studies responsiveness decreased with increasing interelectrode distance for both WT and *rd10* cells (Stett *et al* 2007, Ryu *et al* 2009, Eickenscheidt *et al* 2012). For WT cells responsiveness decreased rapidly from 200  $\mu\text{m}$  to 283  $\mu\text{m}$  and did not vary much for distances up to 1000  $\mu\text{m}$ . For the *rd10* cells responsiveness also decreased from 200  $\mu\text{m}$  to 283  $\mu\text{m}$ , however after 283  $\mu\text{m}$  the decrease continued more gradually up to a distance of 1000  $\mu\text{m}$ . This gradual decrease could be attributed to the increased excitability of *rd10* due to degeneration as reflected by increased spontaneous rates (Stasheff *et al* 2011, Goo *et al* 2016). Since the minimum interelectrode spacing of the array is 200  $\mu\text{m}$ , we were unable to sample responses with shorter distances from the stimulating electrode. Based on these results, only cells recorded at distances of 200 and 283  $\mu\text{m}$  were included in further analysis in order to minimize the variability in electrical stimulation effectiveness due to stimulation distance.

#### 3.2. Diversity of RGC responses

The responses of an example cell recorded on an electrode 200  $\mu\text{m}$  from the stimulating electrode are shown in figure 4. As was typical for our data, a few spikes were detected within the first 10ms post-stimulus (figures 4(a) and (b)). As these spikes could not be discriminated from those resulting from direct RGC stimulation and were often obscured by stimulus artifacts (lasting for a few ms post stimulation), they were excluded from our analysis. Similarly, a longer response window (>100ms) would not be advisable because the signal-to-noise ratio would be decreased in evaluating responses due to progressively larger contributions from spontaneous spikes as the response window is increased. This exclusion of long latency spikes also minimizes the contribution of photoreceptor-mediated spikes, which is appropriate since such spikes are expected to be absent in degenerated retina. Since the mouse retina under healthy conditions has a higher spontaneous rate in comparison to retinas of other species like rabbit or chick, and such spontaneity of responses increases with progressive degeneration (Yee *et al* 2012, Goo *et al* 2016), it was necessary to set 100ms as the upper range of the integration window. Therefore, only spikes within the latency range of 10–100ms were included in our analysis, and were considered to represent mostly the effects of indirect RGC stimulation through the activation of presynaptic neurons—primarily bipolar cells. An examination of the average responses to each of the 96 unique pulses confirms that pulse amplitude and duration interact to activate each neuron such that longer pulses require lower amplitudes and shorter pulses require higher amplitudes figures 4(c)–(f). Each of these parameters has a threshold that limits this interaction such that neither very short durations nor very low amplitudes can activate the cell. For example, in this cell the minimum cathodic voltage and duration for activation are around  $-0.5\text{ V}$  and 0.1 ms. Note that the data points plotted in figures 4(c) and (d) are merely replotted in figures 4(e) and (f) to facilitate

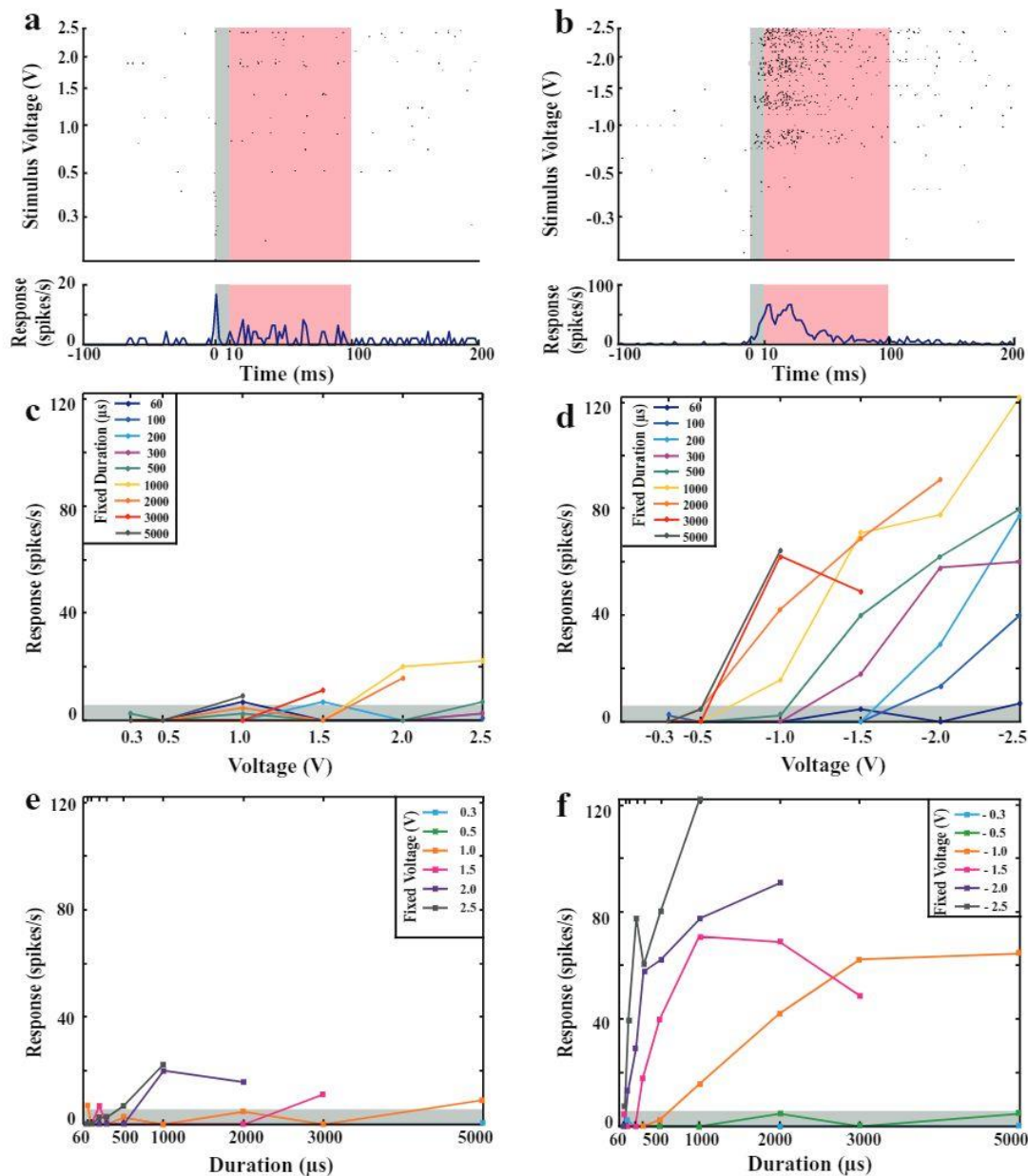


**Figure 4.** Electrical response profile for example monotonic, WT RGC. Panels in the left column are positive voltage pulse responses and right column panels are negative voltage responses. (a) and (b) (*top*) Spike train dot rastergram showing responses sorted into labeled voltage blocks with pulse duration sorted low to high from bottom to top of each block (480 rows in total). (*bottom*) Peristimulus time histogram (PSTH) from all 480 responses binned at 1 ms intervals with shaded 10 ms spike exclusion (*grey*) and 90 ms response integration (*pink*) periods indicated. (c) and (d) Constant-duration, voltage response curves calculated from the responses in (a) and (b). (e) and (f) Constant-voltage, duration response curves. Thin grey bars at the bottom of panels (c)–(f) indicate the threshold. Error bars were omitted for clarity.

examination of the separate effects of duration and amplitude on RGC response.

A confound in identifying the optimal electrical stimulus for RGCs is that many different RGC types exist with significantly variable morphology, circuitry, and physiology (Masland 2011, Maturana *et al* 2014, Seung and Sümbül 2014, Sümbül *et al* 2014, Baden *et al* 2016). Accordingly, the electrical responses of RGCs also vary greatly. Notably,

many RGCs appear to violate the expectation that their spiking responses invariably increase and eventually saturate as either pulse amplitude or duration is increased. Such non-monotonic cells are often excluded from population analyses to determine the best stimulus for RGC activation (Ryu *et al* 2009, Goo *et al* 2011). To illustrate this point, we show the electrical response surfaces of monotonic and non-monotonic example cells for both WT and *rd10* in figure 5. For each

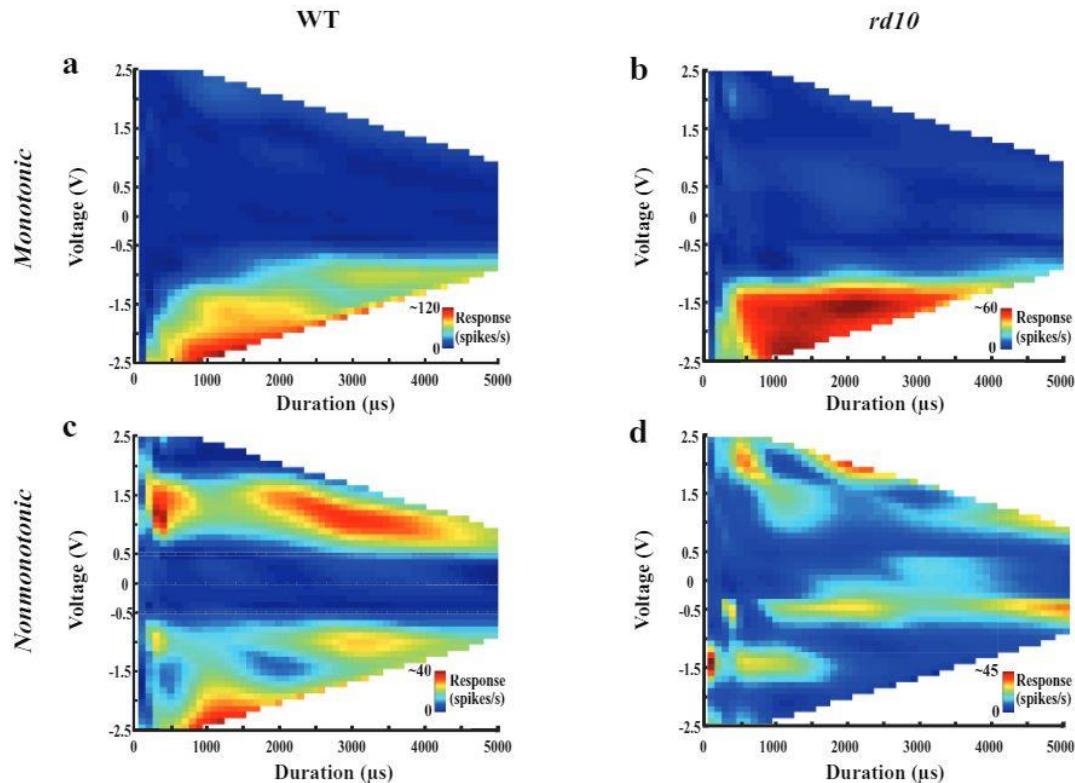


**Figure 5.** Voltage-polarity-duration response surfaces. Four example cells depict monotonically increasing (*top row*, a and b) and non-monotonic responses surfaces (*bottom row*, c and d) for both WT and *rd10* (left and right columns, respectively). Colorbars range from minimum to maximum response for each cell. The two non-monotonic cells shown also responded well to anodic pulses. Data in (a) are from the same cell as figure 4.

surface, response curve data points as in figures 4(c) and (d) were minimum response-subtracted, peak normalized, and interpolated. In addition to monotonic response surfaces, both cells in figures 5(a) and (b) demonstrated markedly stronger responses to negative (cathodic) voltage pulses in comparison to positive voltages.

Non-monotonic cells tended to respond to both cathodic and anodic voltage pulses as represented by the example cells of figures 5(c) and (d), which were specifically chosen to illustrate this point. There may be a modest correlation between the monotonic response pattern and a preference for cathodic pulses, however this weak correlation was not examined in depth. Notably, all cells which exhibited strong responses to anodic pulses had equally strong cathodic responses—we observed no purely anodic cells. Both non-monotonic responses and cathodic-anodic responses were more common in *rd10* than WT (supplement, S1 ([stacks.iop.org/JNE/14/026004/mmedia](http://stacks.iop.org/JNE/14/026004/mmedia))). Another example of rastergrams and response curves (as in figure 4) is provided in the supplement (S2) for the cell shown in figure 5(d).

### 3.3. Response thresholds

To facilitate comparison of the present dataset with previous research, we examined the threshold voltage for each pulse duration figures 6(a) and (c). As is typical, we found that

threshold voltage (both anodic and cathodic) tends to decrease in amplitude with increasing pulse duration for both WT and *rd10* RGCs, however, this trend did not hold for the shortest durations (below 300  $\mu$ s). This deviation is because, as short duration increases (from 60 to 300  $\mu$ s), high-threshold cells that were previously not activated at shorter durations become activated due to increased charge delivery, thereby contributing high voltage thresholds to the population average. This effect is reflected in the number of cells contributing to each data point in figures 6(a) and (c) (see supplement S3). We reduced this effect by limiting our examination of threshold to cells with suprathreshold responses for at least six durations (see methods). We found that there was no significant difference in thresholds for positive voltage pulses compared to negative voltage pulses for either mouse strain. Comparing duration-matched voltage thresholds between WT and *rd10* cells, we also found no significant differences. Significance of threshold comparisons was evaluated using the non-parametric Kruskal-Wallis test for whether multiple samples originate from the same distribution (*kruskalwallis*, MATLAB) and visualized with MATLAB's *multcompare* function to examine specific pairwise comparisons while controlling for the effect of multiple comparisons ( $p < 0.05$ ). All pairwise comparisons are presented in matrix table form in the supplement S3.

To facilitate comparison with other studies we estimated charge densities from these voltages based on the geometric



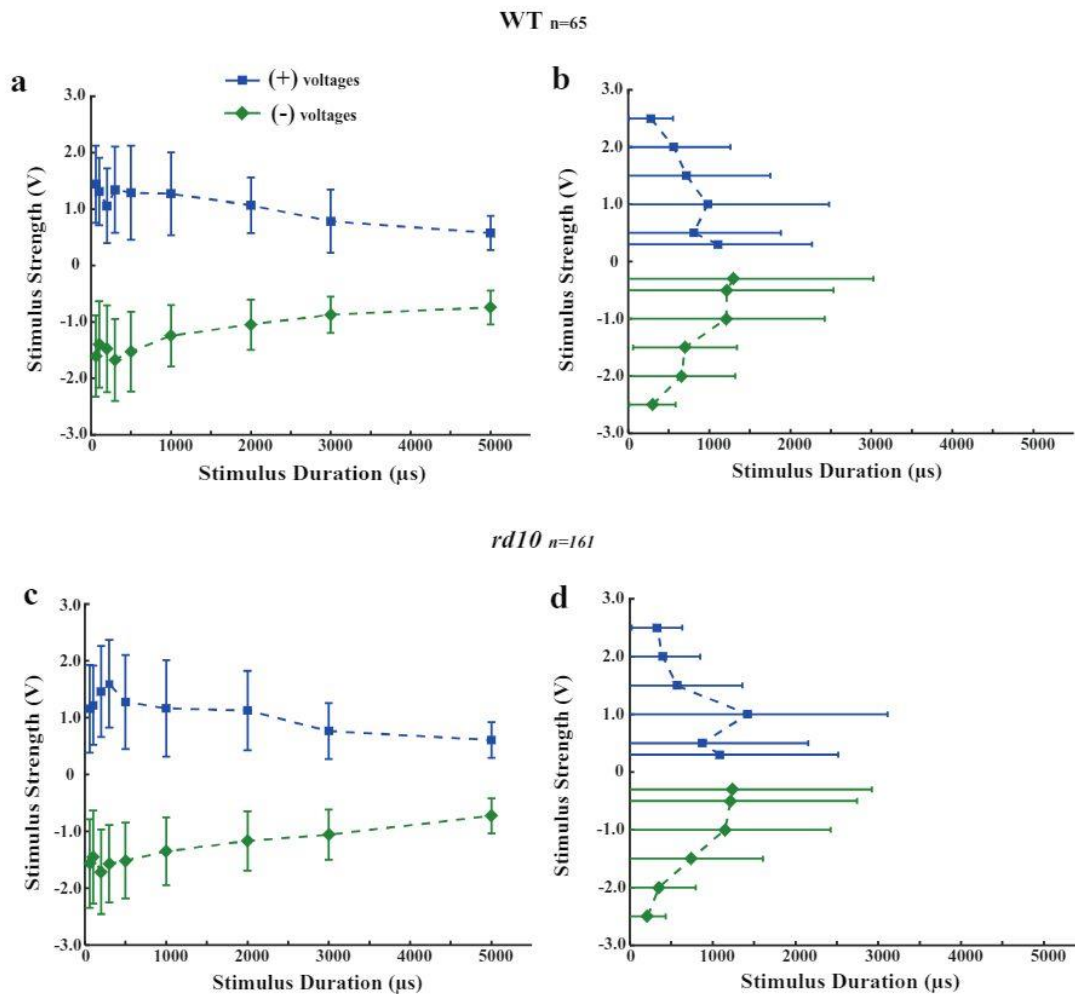


**Figure 6.** Electrical response thresholds. (a) and (c) Constant-duration, voltage thresholds for WT and *rd10*, respectively. (b) and (d) Constant-voltage, duration thresholds for WT and *rd10*, respectively. Threshold was spontaneous rate + 2 \* SD. The  $n$  above each row indicates the number of RGCs that met response criteria for inclusion (see methods—threshold curves) and therefore contribute to the two panels in that row. For  $n$  pertaining to the 8 individual curves and each separate data point see supplement S3.

**Table 2.** Thresholds of WT and *rd10* RGC populations for 0.5 ms, rectangular, voltage-controlled pulses.

	Voltage (V)		Charge density ( $\text{mC cm}^{-2}$ )	
	WT	<i>rd10</i>	WT	<i>rd10</i>
Anodic	$1.29 \pm 0.83$	$1.28 \pm 0.83$	$0.37 \pm 0.24$	$0.36 \pm 0.23$
Cathodic	$-1.53 \pm 0.71$	$-1.52 \pm 0.67$	$-0.43 \pm 0.20$	$-0.43 \pm 0.19$

surface area of our 30  $\mu\text{m}$  diameter electrodes ( $707 \mu\text{m}^2$ ). Although we did not record the actual current waveform during stimulation, we can estimate the current with Ohm's law based on impedances that we measured from our electrode arrays which ranged around  $\sim 250 \text{k}\Omega$ . Because these impedances were measured at a frequency of 1 kHz, it is most appropriate to calculate the charge density from a 500  $\mu\text{s}$  voltage pulse. This duration is also the most useful for comparisons with other studies. Our 500  $\mu\text{s}$  pulses yielded mean voltage thresholds in the range of 1.25–1.55 V (table 2). These

voltage thresholds correspond to mean charge density thresholds in the range of 0.35–0.45  $\text{mC cm}^{-2}$ .

Because we explored a large stimulus space rather than examining a single pulse duration, it was also possible to examine threshold durations for fixed voltages figures 6(b) and (d). In agreement with the voltage thresholds figures 6(a) and (c), threshold duration decreased with increasing voltage amplitude, however, the shape of these threshold curves was noticeably different from the voltage threshold curves. This accentuates the fact that the method used to compute a strength-duration threshold curve from a discretized response surface critically influences the curve shape. It is notable that the number of cells with robust response curves (see inclusion criterion in methods) is much larger for negative voltages than positive voltages (see supplement S3). It is generally assumed that anodic pulse thresholds for epiretinal configuration, network-mediated responses are much higher than cathodic, therefore, only the cells with the lowest cathodic thresholds should also be able to respond to anodic stimulation

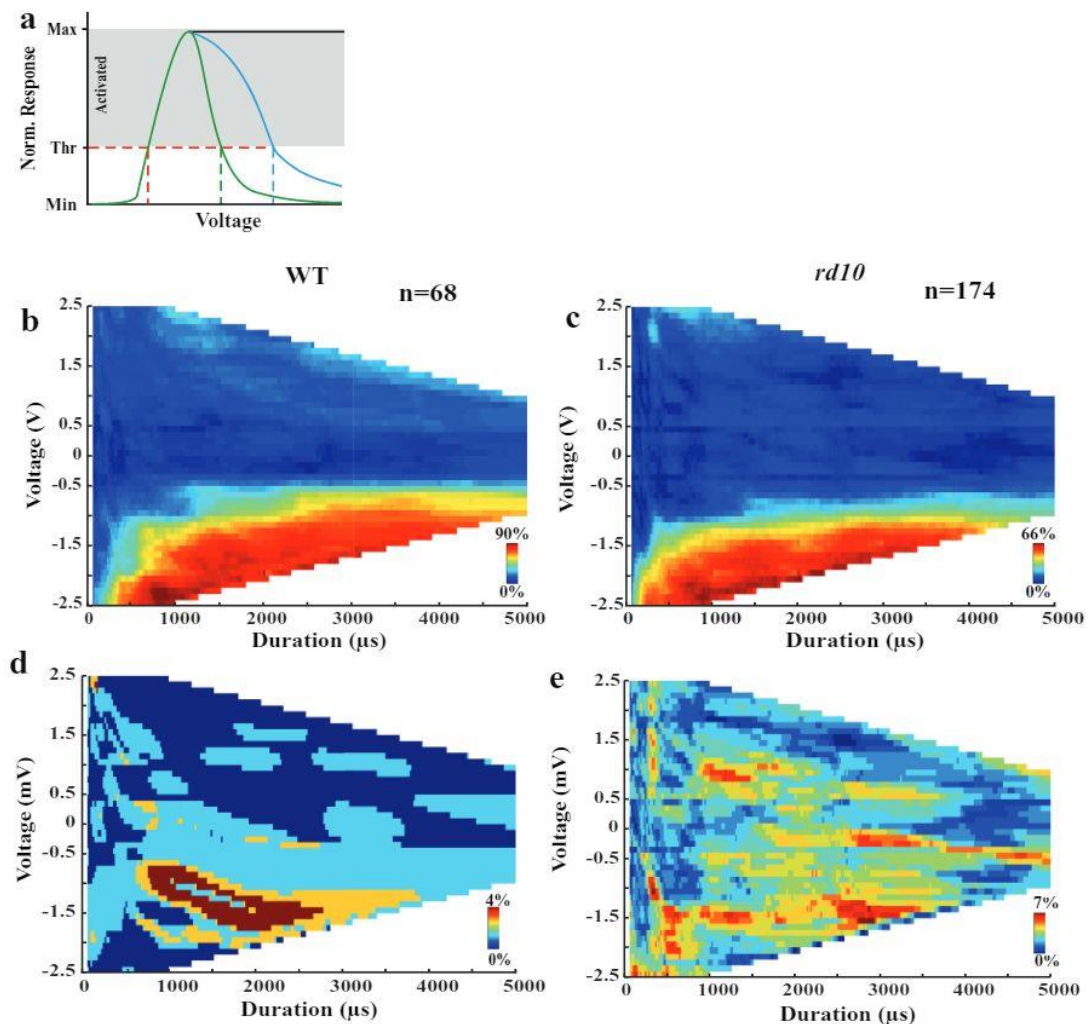


**Figure 7.** Identifying the optimal stimulus with population activation surfaces. (a) Schematic illustrating how non-monotonic RGCs (green and blue curves) may have subthreshold responses at high stimulus values (above the green and blue dotted lines, respectively)—a potential flaw in threshold measurements. Red lines indicate threshold and threshold voltage, black is a monotonic cell. For this figure, cells were judged to be activated (grey bar) by a given stimulus if the average response to that stimulus was above threshold (spontaneous + 2 \* SD). (b) and (c) Population activation surface for WT and *rd10*, respectively. In contrast to figure 5, the color bars were scaled to the maximum percentage of RGCs responding above threshold for each plot. Surfaces were interpolated from the 96 unique voltage-polarity-duration pulses that were tested (figure 2). (d) and (e) Population response surface for all cells that were not activated by the maxima in (b) and (c), respectively. Color bars correspond to percent of the original 68 and 174 cells, for WT and *rd10*, respectively.

at the voltages presented. This would cause average anodic thresholds to be higher than cathodic thresholds. In contrast, cathodic thresholds tended to be higher for our study (although not statistically significant). We attribute this similarity to the high variability in single cell thresholds which has often been reported in earlier studies (Jensen *et al* 2005, Boinagrov *et al* 2014). A likely explanation is that different RGC subtype responses vary in their relative anodic and cathodic thresholds.

#### 3.4. Determining the optimal stimulus

The existence of cells with non-monotonic response functions indicates that some cells become nonresponsive at sufficiently high stimulus amplitudes or durations. For such cells,

a sufficiently high ‘suprathreshold’ stimulus might be unable to actually activate a robust response figure 7(a). Therefore, we sought to identify voltage-polarity-duration combinations that would activate the maximal percentage of the RGC population. By plotting the percentage of RGCs activated as a function of the voltage-polarity-duration stimulus space, we found that 90% of electrically responsive WT RGCs are activated at the maximum of the population activation surface (figure 7(b), table 3, 1st Max). Likewise, a very similar stimulus activates 66% of *rd10* cells figure 7(c). Setting aside these cells that can be activated by the optimal stimulus for each population, we found that an additional 4% of WT cells and 7% *rd10* cells, can be activated by a secondary stimulus (figures 7(d) and (e), table 3, 2nd Max). From this sequential maxima process it is

**Table 3.** Comparison of optimal stimulus to activation surface maxima. Right two columns list the number of electrically responsive RGCs activated by the stimulus identified in each row.

		Amplitude (V)	Duration (ms)	Charge density (mC cm <sup>-2</sup> )	WT	<i>rd10</i>
WT	1st Max	-2.4	0.76	1.03	61	106
	2nd Max	-1.8	1.78	1.81	57	98
<i>rd10</i>	1st Max	-2.1	2.00	2.37	55	114
	2nd Max	-1.6	2.74	2.48	50	98
	Optimal	-2.4	0.88	1.19	61	113

evident that the consideration of additional stimuli beyond the optimal stimulus yields quickly diminishing returns in terms of additional activated RGCs.

The similarity of these population activation surfaces for WT and *rd10* retina suggest that a single pulse could activate near-maximal percentages of both populations. Therefore, we summed the activation surfaces of the two strains to identify a single pulse that is optimal for joint experiments where both WT and *rd10* are examined. The pulse at the maximum of this combined surface had an amplitude of -2.4 V and a duration of 0.88 ms, activating 90% and 65% of electrically responsive RGCs for WT and *rd10*, respectively.

The methods used to identify this optimal stimulus can also be used for populations that are not strongly correlated in their activation surfaces. In this case one should apply the sequential maxima process described above to the summed activation surface. For alternative experimental configurations (e.g. different electrodes, subretinal stimulation, current-controlled pulses, different mouse strains, or different stages of degeneration) the empirical methods presented here can serve as effective tools to determine the optimal pulse or set of pulses.

#### 4. Discussion

In the present study, we have investigated the optimal rectangular-wave voltage-controlled pulses to yield the highest probability of activating an RGC in healthy mice and in the intermediate stage of a slowly degenerating model of retinitis pigmentosa (*rd10*). Our main findings were as follows: (1) The effectiveness of electrical stimulation strongly depends on distance from the stimulating electrode. To reduce response variability, only responses from a narrow range of distances should be pooled for analysis. (2) There exists a heterogeneity of RGC responses to electrical stimulation. Monotonic cells, whose response continuously increases with stimulus strength, are a majority in both WT and *rd10* retina. However, non-monotonic responses were more common in *rd10* retina than in WT (supplement S1). WT responses were evenly divided between RGCs which responded to only cathodic pulses and RGCs which responded to both cathodic and anodic pulses. In *rd10* retina RGCs which responded to both cathodic and anodic pulses were four times more common than cathodic responding RGCs. No RGCs in either mouse strain responded exclusively to anodic pulses. (3) In accordance, to earlier threshold studies, voltage thresholds decrease with increasing

pulse duration in both mouse strains. These thresholds do not differ between mouse strains, nor do they differ between anodic and cathodic pulses in either strain. (supplement S3). (4) By combining the full voltage-polarity-duration response surfaces of all electrically responsive RGCs we found that a maximum percentage of these cells could be activated by a pulse of -2.4 V and 0.88 ms in both WT and *rd10*. The process used to identify this pulse can easily be generalized to other experimental configurations.

##### 4.1. Comparison to previous data

It has been demonstrated that the current waveform for a voltage-controlled pulse is different from a current-controlled pulse, with an initial sharp rise in capacitive current that then decays down to the steady-state current necessary to maintain the voltage (Stett *et al* 2000). For a rectangular-wave, monophasic voltage pulse, this onset spike in current is mirrored by an offset spike, the pair of which are similar to a biphasic current pulse. Still, the difference in waveforms means that the instantaneous current, and charge vary much more for voltage-controlled pulses than for current pulses. Therefore, it is most useful to compare our threshold values to previous experiments which used voltage-controlled pulses.

Our voltage thresholds of 1.3–1.5 V for a 500  $\mu$ s pulse were well within the range of previous studies of network-mediated RGC stimulation (0.55–2.5 V, Zrenner *et al* 1999, Stett *et al* 2000, Schwahn *et al* 2001, Gekeler *et al* 2004, Jin *et al* 2005, Goo *et al* 2011, Rathbun *et al* 2015, Samba *et al* 2015). Although no single measure (voltage, current, charge, current density, charge density, voltage curvature, etc) is adequate to fully capture the threshold of an RGC under all conditions, most investigators find it useful to compare current and charge density between disparate studies. Such comparisons account for differences in electrode impedance due to size and materials. As with threshold voltages, our corresponding charge density thresholds of <0.5 mC cm<sup>-2</sup> were also within the range of previous studies (0.05–13 mC cm<sup>-2</sup>, Zrenner *et al* 1999, Stett *et al* 2000, Schwahn *et al* 2001, Gekeler *et al* 2004, Jin *et al* 2005, Goo *et al* 2011, Samba *et al* 2015). Likewise, the optimal stimulus we identified of -2.4 V for 0.88 ms had a charge density of 1.19 mC cm<sup>-2</sup> that is well within the range of optimal or standardized stimuli used previously by other groups (0.04–2.12 mC cm<sup>-2</sup>, Jin *et al* 2005, Goo *et al* 2011, Yang *et al* 2011).

**4.1.1. Comparable thresholds for WT and *rd10* RGCs.** There are many studies comparing the thresholds of *rd1* retinas with WT retinas (Suzuki *et al* 2004, O’Hearn *et al* 2006, Ye and Goo 2007, Ye *et al* 2008, Jensen and Rizzo 2008, Goo *et al* 2011, Margalit *et al* 2011). The general consensus from these studies is that stimulation thresholds for *rd1* retinas are higher than for WT retinas. It has been well documented morphologically and functionally, that the *rd1* mouse model is a fast progressing model of RP, in comparison to the slower *rd10* mouse model which better mimics the process of degeneration in humans (Gargini *et al* 2007, Stasheff *et al* 2011). Although many studies have characterized the *rd10* model structurally and morphologically (Chang *et al* 2002, Gargini *et al* 2007, Chang *et al* 2007, Barhoum *et al* 2008, Mazzoni *et al* 2008, Phillips *et al* 2010, Chrenek *et al* 2012, Pennesi *et al* 2012, Roesch *et al* 2012, Rösch *et al* 2014, Hasegawa *et al* 2016, Krishnamoorthy *et al* 2016) as well as functionally (Puthussery *et al* 2009, Stasheff *et al* 2011, Biswas *et al* 2014, Menzler *et al* 2014), only a handful have investigated the activation thresholds for *rd10* retinas (Gerhardt *et al* 2011, Toychiev *et al* 2013, Park *et al* 2015, Cho *et al* 2016). The most recent of these studies (Cho *et al* 2016) has shown that the activation thresholds of WT and *rd10* retinas in response to current stimulation are comparable, but that *rd10* thresholds have a much broader range (113 mA cm<sup>-2</sup>–1811 mA cm<sup>-2</sup>). This finding is in agreement with our results of comparable thresholds between the two strains via voltage stimulation. Furthermore, Cho *et al* 2016 found that WT and *rd10* thresholds are most similar when considering *rd10* cells with high spontaneous activity (which peaks around the age of our mice). These high spontaneous activities are lost as degeneration progresses which may result in higher thresholds for older *rd10* mouse retinas. Such observations suggest that it may be beneficial to implant patients shortly after useful vision is lost rather than waiting for very late-stage degeneration.

**4.1.2. Preference for cathodic voltage pulses.** In our study, we found that for both WT and *rd10* retinas, only a small subset of electrically responsive cells responded to anodic (positive) voltages whereas all electrically responsive cells responded to cathodic (negative) voltages. This finding is consistent with earlier studies using current-controlled pulses to elicit retinal network-mediated responses via epiretinal stimulation. These studies found higher thresholds for anodic stimulation (Jensen *et al* 2003, Jensen *et al* 2005, Boinagrov *et al* 2014). However, in our study, we found no significant differences in threshold for cathodic or anodic pulses for the nearby cells in both WT and *rd10* mice. Given our safety limit of 2.5 V or less depending on duration, and the high variability of thresholds, it is not surprising that anodic and cathodic thresholds did not differ significantly. In addition to the role of response variability of different RGC subtypes affecting the relative anodic and cathodic thresholds (as stated above), it is possible that if higher voltages had been presented, more cells could have responded to positive voltages resulting in significantly higher anodic population thresholds.

## 4.2. Variability

**4.2.1. Cell-to-cell variability.** There is a growing body of literature illuminating the wide array of RGC types found in the mammalian retina. While this variability is most evident in the morphology of RGCs (Masland 2011, Sumbul *et al* 2014), it can also be seen in the circuitry feeding into the various RGCs (Seung and Sumbul 2014, Maturana *et al* 2014) and consequently their varied physiological responses (Baden *et al* 2016). This diversity in the RGC population strongly suggests that the sensitivity of RGCs to various electrical stimuli as well as their patterns of response to such stimuli could vary greatly. Accordingly, recent investigators have attempted to address this variability in responses to electrical stimulation (Jensen *et al* 2005, Jensen and Rizzo 2006, Jensen and Rizzo 2008, Cai *et al* 2011, Jepson *et al* 2013, Im and Fried 2016). In the present study, we consider it highly likely that the variability of response surface shapes and thresholds observed owe at least as much to the diversity of the RGC population as it does to the variability of such biological measurements. We anticipate that cell type identification similar to that of Baden *et al* 2016 coupled with MEA-based electrical stimulation experiments will shed much light on how different RGC types vary in their electrical responses. Moreover, such variability could form the basis for selective stimulation of the different pathways of visual information that correspond to each RGC type.

Another source of population variability could be the distance from the stimulation electrode that is assigned to each cell based on the electrode on which it is recorded. While we know the location of each recording electrode, we do not know the exact location of each cell recorded on that electrode. We do know that cells are never recorded on neighboring electrodes (spaced 200  $\mu$ m apart) based on careful comparison of neighboring spike trains during data processing. This means that the electrodes cannot detect a cell more than 100  $\mu$ m away, otherwise more than one electrode would be able to record from the same cell. Thus, some cells assigned a distance of 200  $\mu$ m could be 100  $\mu$ m away from the stimulating electrode while others could be 300  $\mu$ m away. This results in great variability in the effective stimulus strength, and thus the cell’s estimated threshold value.

**4.2.2. Single cell reliability.** Apart from cell-to-cell variability, there was also high variability within individual cells for repetitions of the same stimulus. Notably, this variability in mouse RGCs seems to contrast with the high reliability and low noise level demonstrated in rabbit RGCs (Lee *et al* 2013, Im and Fried 2015, 2016). We suspect that this response variability could be a prime factor in the large error bars of our threshold versus voltage and threshold versus duration curves. At this time, it remains uncertain how much of the non-monotonicity discussed here may reflect such response variability and how much of it truly reflects irregularity in the sensitivity of cells over the voltage-duration parameter space.

**4.2.3. Variability of voltage-controlled stimulation.** In addition to neural variability and uncertainty in stimulation distance, the use of voltage-controlled pulses resulted in variability in

the delivered charge from one electrode to the next. Unlike most threshold studies which use current-controlled pulses for determining the thresholds of RGCs, we chose to use voltage-controlled pulses. This selection was made primarily to match the operational paradigm of the Tuebingen retinal implant (Alpha IMS). Voltage-controlled pulses have been well advocated in earlier studies (Stett *et al* 2000, Stett *et al* 2007, Goo *et al* 2011). Briefly, the advantages are that (1) voltage-controlled pulses provide easy control over electrode polarization such that electrochemical reactions can be easily avoided, (2) voltage-controlled stimulation is more efficient, and (3) such pulses are easy to implement in CMOS chips. However, a caveat with voltage-controlled pulses is that the actual charge injected into the tissue depends on the tissue resistance and the capacity at the tissue/electrode interface and must be measured separately for each experiment. In contrast, it is very easy to calculate precise charge densities using current-controlled pulses. Nevertheless, in consideration of limiting electrochemical interactions and efficient charge injection, voltage-controlled pulses seemed more appropriate when this study was initiated.

#### 4.3. Thresholds and the optimal stimulus

There is disagreement in how to define response threshold for electrical stimulation of the retina. Collectively, such studies have aimed at identifying an average threshold across the population of RGCs. Presumably, one goal of estimating the population threshold is to determine a stimulus level that can be used to activate most RGCs while remaining within the various constraints of the implant system. Accordingly, most investigators will choose a multiple of this average threshold as a standardized stimulus to be used when specific thresholds are not known. One threshold determination method (most commonly used for extracellular patch electrode recordings) is to increase a sub-threshold current, charge, or voltage during the ongoing presentation of stimuli until 50% (Jensen *et al* 2003, Freeman and Fried 2011, Yang *et al* 2011, Cloherty *et al* 2012, Sim *et al* 2014, Samba *et al* 2015), 66% (Suzuki *et al* 2004), 80% (Eickenscheidt *et al* 2012) of the stimuli at a single amplitude elicit an action potential or burst of action potentials. Others use the criteria of the minimum amount of current, charge, or voltage required to elicit an average response rate of 0.5 (Goo *et al* 2011, Boinagrov *et al* 2012) or 0.66 (Fried *et al* 2009) spikes per stimulus using a sigmoid fit to the response curve. Such measures serve well for cells showing a well-modulated response with increasing amplitude (monotonic). While this might hold true for a majority of RGCs, there is a sizable fraction of cells that show a trend of non-monotonicity with increasing amplitude. Such non-monotonic response patterns have only been addressed recently (Boinagrov *et al* 2010, Boinagrov *et al* 2012). It was shown that there is an upper threshold of stimulation due to crossing of the reversal potential for depolarizing ion channels. While this theoretical and experimental work was developed for direct stimulation of RGCs, it could be equally applicable to bipolar cells in which voltage-gated sodium and calcium channels play an important role in neurotransmitter release

onto RGCs. In the presence of significant non-monotonicity the assumption that RGCs remain active at all stimulus amplitudes above threshold could lead to an overestimation of the number of RGCs activated by a suprathreshold stimulus.

The method presented in our study to identify the optimal stimulus, free from any strong assumptions about the strength-duration response surface, provides a useful alternative to traditional population threshold approaches. Interestingly, despite our careful consideration of individual non-monotonic cells, the population activation surfaces for both WT and *rd10* retina were still essentially monotonic over the voltage-duration range examined. This means that any monotonic cells which are suppressed at high stimulus levels are more than compensated for by the addition of other, higher-threshold RGCs. We conclude that the optimal single stimulus for activation of the maximal number of RGCs is also among the strongest stimuli allowed by safety limits. However, if more than one stimulus is allowed, stronger stimuli can be used to preferentially activate monotonic cells whereas weaker stimuli can be used to preferentially activate non-monotonic cells.

The optimal stimulus we identified in our study was comparable to those of previous studies, thus, validating the use of these stimuli, even in the presence of non-monotonic cells. However, although their influence is modest, non-monotonic cells should not be dismissed when considering appropriate stimuli for prosthetic applications, especially when subtypes of the cell population are targeted.

#### 4.4. Limitations

Owing to the large interelectrode distance (200–300  $\mu\text{m}$ ) used in this study, it should be recalled that, although the identified optimal stimulus can activate a substantial fraction of the electrically responsive cells (90% for WT and 65% for *rd10*), this stimulus is expected to activate only 28% of the total (both electrically responsive and nonresponsive WT RGC population and 49% of the total *rd10* RGC population (61/216 and 113/232, respectively; tables 1 and 3). Based on figure 3 and the work of others (Stett *et al* 2007, Eickenscheidt *et al* 2012) we expect these percentages to increase significantly for measurements closer to the stimulation electrode.

## 5. Conclusions

To date, this study is the most complete comparison of WT and *rd10* ganglion cell responses to rectangular, voltage-controlled pulses, examining the responses of 68 WT and 174 *rd10* cells. We have further developed a conceptual framework to identify an optimal stimulus based on the percentage of activated RGCs. Our approach is well-suited to the broad diversity of RGC response types. Finally, we have identified a single voltage-controlled pulse that can be expected to activate a large fraction of RGCs in both WT and *rd10* retinas

#### 5.1. Implications to retinal prosthesis

The current field of retinal prostheses is somewhat stymied by a few systematic idiosyncrasies, one of which is the assumed

homogeneity of the RGC population. Many studies estimate stimulation thresholds and standardized stimuli based on this assumption, potentially disadvantaging non-standard RGCs. A careful examination of recent studies, demonstrates that the broad variability amongst different RGC types continues to complicate simple attempts to characterize RGC responses to electrical stimulation. Therefore, we propose that the great diversity of RGCs must be accounted for in the design of future experiments if our field is to make acceptable progress in understanding retinal electrostimulation.

A second limiting assumption of our field is that retinal responses are a monotonically increasing function of stimulus strength. While this may be the dominant behavior, ignoring non-monotonicity can lead to faulty conclusions about optimal stimulation, as well as obscure promising opportunities for RGC type-specific stimulation. In many experiments such as the present study, response thresholds are not immediately available for the personalization of the stimulus to each cell or even each retina. To better identify optimal stimuli that can be used under such *in vitro* conditions, we have shown how the full strength-duration-polarity assessment of a population that goes beyond simple threshold measurements can be used to identify one or more stimuli that will best activate the RGC populations.

### 5.2. Future work

In a follow-up study from our group we will assess the correlation of non-monotonic and anodic-cathodic response patterns to specific mouse RGC types. We hope to determine whether such responses signify distinct RGC types. Additionally, it would be instructive to determine how the occurrence of such responses changes over the course of retinal degeneration. It may be possible to classify the physiological type of RGCs based on these response patterns even at later stages of degeneration, when visual responses are completely lost. Apart from investigating the cell type specificity for these responses, understanding the underlying mechanisms contributing to such non-monotonic responses would be worth exploring.

### Funding and acknowledgments

This study was supported by the Werner Reichardt Centre for Integrative Neuroscience (CIN) at the Eberhard-Karls University of Tübingen. The CIN is an Excellence Cluster funded by the Deutsche Forschungsgemeinschaft (DFG) within the framework of the Excellence Initiative (EXC307, including the senior professorship of Prof. Eberhart Zrenner and PP 2011-07 and 2013-04 to DLR). This study is also part of the research program of the Bernstein Center for Computational Neuroscience, Tuebingen, funded by the German Federal Ministry of Education and Research (BMBF, 01GQ1002 and 031A308). Additional funding was provided by the Tistou and Charlotte Kerstan Foundation (to AJ and DLR), the German Ophthalmology Society (DOG, to AJ), and PRO RETINA Germany foundation for prevention of blindness (to AJ and SS).

The authors would especially like to thank Professor Thomas Euler and his laboratory for their guidance and

support. We thank Mrs. Regina Ebenhoch for expert graphics support. In particular, DLR thanks Prof Euler for his selfless mentorship, Dr Tobias Breuninger for his work in setting up the optical pathway used in these experiments, and Dr Haq Wadood for an introduction to MEA recording techniques. Finally, we thank Professor Shelley Fried for many helpful discussions and his unwavering enthusiasm for this research.

### Author contributions

AJ and DLR designed the experiments. AJ performed the experiments. AJ and DLR performed the analysis. AJ and DLR prepared the draft of the manuscript. AJ, SS, EZ and DLR edited and finalized the manuscript.

### References

- Ahuja A K et al 2011 Blind subjects implanted with the Argus II retinal prosthesis are able to improve performance in a spatial-motor task *Br. J. Ophthalmol.* **95** 539–43
- Baden T, Berens P, Franke K, Román Rosón M, Bethge M and Euler T 2016 The functional diversity of retinal ganglion cells in the mouse *Nature* **529** 345–50
- Barhoum R, Martínez-Navarrete G, Corrochano S, Germain F, Fernandez-Sanchez L, de la Rosa E J, de la Villa P and Cuenca N 2008 Functional and structural modifications during retinal degeneration in the *rd10* mouse *Neuroscience* **155** 698–713
- Bennett J et al 2016 Safety and durability of effect of contralateral-eye administration of AAV2 gene therapy in patients with childhood-onset blindness caused by RPE65 mutations: a follow-on phase 1 trial *Lancet* **388** 661–72
- Biswas S, Haselier C, Mataruga A, Thumann G, Walter P and Mueller F 2014 Pharmacological analysis of intrinsic neuronal oscillations in *rd10* retina *PLoS One* **9** e99075
- Boinagrov D, Loudin J and Palanker D 2010 Strength-duration relationship for extracellular neural stimulation: numerical and analytical models *J. Neurophysiol.* **104** 2236–48
- Boinagrov D, Pangratz-Fuehrer S, Goetz G and Palanker D 2014 Selectivity of direct and network-mediated stimulation of the retinal ganglion cells with epi-, sub- and intraretinal electrodes *J. Neural Eng.* **11** 26008
- Boinagrov D, Pangratz-Fuehrer S, Suh B, Mathieson K, Naik N and Palanker D 2012 Upper threshold of extracellular neural stimulation *J. Neurophysiol.* **108** 3233–8
- Busskamp V and Roska B 2011 Optogenetic approaches to restoring visual function in retinitis pigmentosa *Curr. Opin. Neurobiol.* **21** 942–6
- Cai C, Ren Q, Desai N J, Rizzo J F and Fried S I 2011 Response variability to high rates of electric stimulation in retinal ganglion cells *J. Neurophysiol.* **106** 153–62
- Caley D W, Johnson C and Liebelt R A 1972 The postnatal development of the retina in the normal and rodless CBA mouse: a light and electron microscopic study *Am. J. Anat.* **133** 179–211
- Carcieri S M, Jacobs A L and Nirenberg S 2003 Classification of retinal ganglion cells: a statistical approach *J. Neurophysiol.* **90** 1704–13
- Chang B, Hawes N L, Hurd R E, Davisson M T, Nusinowitz S and Heckenlively J R 2002 Retinal degeneration mutants in the mouse *Vis. Res.* **42** 517–25
- Chang B et al 2007 Two mouse retinal degenerations caused by missense mutations in the beta-subunit of rod cGMP phosphodiesterase gene *Vis. Res.* **47** 624–33

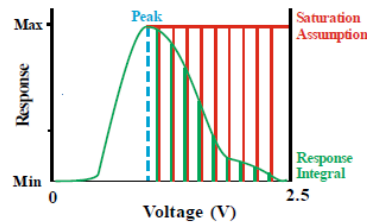
- Cho A, Ratliff C, Sampath A and Weiland J 2016 Changes in ganglion cell physiology during retinal degeneration influence excitability by prosthetic electrodes *J. Neural Eng.* **13** 25001
- Chrenek M A, Dalal N, Gardner C, Grossniklaus H, Jiang Y, Boatright J H and Nickerson J M 2012 Analysis of the RPE sheet in the *rd10* retinal degeneration model *Adv. Exp. Med. Biol.* **723** 641–7
- Cloherly S L, Wong R C S, Hadjinicolaou A E, Meffin H, Ibbotson M R and O'Brien B J 2012 Epiretinal electrical stimulation and the inner limiting membrane in rat retina *Conf. Proc., IEEE Engineering in Medicine and Biology Society (San Diego, CA)* pp 2989–92
- da Cruz L et al 2013 The Argus II epiretinal prosthesis system allows letter and word reading and long-term function in patients with profound vision loss *Br. J. Ophthalmol.* **97** 632–6
- Eickenscheidt M, Jenkner M, Thewes R, Fromherz P and Zeck G 2012 Electrical stimulation of retinal neurons in epiretinal and subretinal configuration using a multicapacitor array *J. Neurophysiol.* **107** 2742–55
- Freeman D K and Fried S I 2011 Multiple components of ganglion cell desensitization in response to prosthetic stimulation *J. Neural Eng.* **8** 16008
- Fried S I, Hsueh H A and Werblin F S 2006 A method for generating precise temporal patterns of retinal spiking using prosthetic stimulation *J. Neurophysiol.* **95** 970–8
- Fried S I, Lasker A C W, Desai N J, Eddington D K and Rizzo J F 2009 Axonal sodium-channel bands shape the response to electric stimulation in retinal ganglion cells *J. Neurophysiol.* **101** 1972–87
- Gargini C, Terzibasi E, Mazzoni F and Strettoi E 2007 Retinal organization in the retinal degeneration 10 (*rd10*) mutant mouse: a morphological and ERG study *J. Comput. Neurol.* **500** 222–38
- Gekeler F, Kobuch K, Schwahn H N, Stett A, Shinoda K and Zrenner E 2004 Subretinal electrical stimulation of the rabbit retina with acutely implanted electrode arrays *Graefes Arch. Clin. Exp. Ophthalmol.* **242** 587–96
- Gerhardt M, Proeger G and MacCarthy N 2011 Monopolar versus bipolar subretinal stimulation—an *in vitro* study *J. Neurosci. Methods* **199** 26–34
- Goo Y S, Park D J, Ahn J R and Senok S S 2016 Spontaneous oscillatory rhythms in the degenerating mouse retina modulate retinal ganglion cell responses to electrical stimulation *Front. Cell. Neurosci.* **9** 1–8
- Goo Y S, Ye J H, Lee S, Nam Y, Ryu S B and Kim K H 2011 Retinal ganglion cell responses to voltage and current stimulation in wild-type and *rd1* mouse retinas *J. Neural Eng.* **8** 35003
- Hadjinicolaou A, Savage C, Apollo N, Garrett D, Cloherly S, Ibbotson M and O'Brien B 2015 Optimizing the electrical stimulation of retinal ganglion cells *IEEE Trans. Neural Syst. Rehabil. Eng.* **23** 169–78
- Hamel C 2006 Retinitis pigmentosa *Orphanet J. Rare Dis.* **1** 40
- Hartong D T, Berson E L and Dryja T P 2006 Retinitis pigmentosa *Lancet* **368** 1795–809
- Hasegawa T, Ikeda H O, Nakano N, Muraoka Y, Tsuruyama T, Okamoto-Furuta K, Kohda H and Yoshimura N 2016 Changes in morphology and visual function over time in mouse models of retinal degeneration: an SD-OCT, histology, and electroretinography study *Japan. J. Ophthalmol.* **60** 111–25
- Im M and Fried S I 2015a Spatial properties of network-mediated response of retinal ganglion cells to electric stimulation *7th Int. IEEE EMBS Neural Engineering Conf.—NER (Montpellier, France)* pp 256–9
- Im M and Fried S I 2015b Indirect activation elicits strong correlations between light and electrical responses in ON but not OFF retinal ganglion cells *J. Physiol.* **593** 3577–96
- Im M and Fried S I 2016 Temporal properties of network-mediated responses to repetitive stimuli are dependent upon retinal ganglion cell type *J. Neural Eng.* **13** 25002
- Jensen R J and Rizzo J F 2006 Thresholds for activation of rabbit retinal ganglion cells with a subretinal electrode *Exp. Eye Res.* **83** 367–73
- Jensen R J and Rizzo J F 2008 Activation of retinal ganglion cells in wild-type and *rd1* mice through electrical stimulation of the retinal neural network *Vis. Res.* **48** 1562–8
- Jensen R J, Rizzo J F, Ziv O R, Grumet A and Wyatt J 2003 Thresholds for activation of rabbit retinal ganglion cells with an ultrafine, extracellular microelectrode *Investigative Ophthalmol. Vis. Sci.* **44** 3533–43
- Jensen R J, Ziv O R and Rizzo J F 2005 Responses of rabbit retinal ganglion cells to electrical stimulation with an epiretinal electrode *J. Neural Eng.* **2** S16–21
- Jepson L H, Hottowy P, Mathieson K, Gunning D E, Dabrowski W, Litke A M and Chichilnisky E J 2013 Focal electrical stimulation of major ganglion cell types in the primate retina for the design of visual prostheses *J. Neurosci.* **33** 7194–205
- Jin G-H, Ye J H, Lee T S and Goo Y S 2005 Electrical stimulation of isolated rabbit retina *Conf. Proc., IEEE Engineering in Medicine and Biology Society (Shanghai, China)* vol 6 pp 5967–70
- Jones B W, Pfeiffer R L, Ferrell W D, Watt C B, Marmor M and Marc R E 2016 Retinal remodeling in human retinitis pigmentosa *Exp. Eye Res.* **150** 149–65
- Krishnamoorthy V, Cherukuri P, Poria D, Goel M, Dagar S and Dhingra N K 2016 Retinal remodeling: concerns, emerging remedies and future prospects *Front. Cell. Neurosci.* **10** 1–9
- Lee S W, Eddington D K and Fried S I 2013 Responses to pulsatile subretinal electric stimulation: effects of amplitude and duration *J. Neurophysiol.* **109** 1954–68
- Margalit E, Babai N, Luo J and Thoreson W B 2011 Inner and outer retinal mechanisms engaged by epiretinal stimulation in normal and *rd* mice *Vis. Neurosci.* **28** 145–54
- Marquardt T and Gruss P 2002 Generating neuronal diversity in the retina: one for nearly all *Trends Neurosci.* **25** 32–8
- Masland R H 2011 Cell populations of the retina: the proctor lecture *Investig. Ophthalmol. Vis. Sci.* **52** 4581–91
- Maturana M I, Kameneva T, Burkitt A N, Meffin H and Grayden D B 2014 The effect of morphology upon electrophysiological responses of retinal ganglion cells: simulation results *J. Comput. Neurosci.* **36** 157–75
- Mazzoni F, Novelli E and Strettoi E 2008 Retinal ganglion cells survive and maintain normal dendritic morphology in a mouse model of inherited photoreceptor degeneration *J. Neurosci.* **28** 14282–92
- Meister M, Pine J and Baylor D A 1994 Multi-neuronal signals from the retina: acquisition and analysis *J. Neurosci. Methods* **51** 95–106
- Menzler J, Channappa L and Zeck G 2014 Rhythmic ganglion cell activity in bleached and blind adult mouse retinas *PLoS One* **9** 1–10
- Microelectrode Array (MEA) Manual 2010 *Multi Channel Systems MCS (Reutlingen: GmbH)*
- O'Hearn T M, Sada S R, Weiland J D, Maia M, Margalit E and Humayun M S 2006 Electrical stimulation in normal and retinal degeneration (*rd1*) isolated mouse retina *Vis. Res.* **46** 3198–204
- Park D J, Senok S S and Goo Y S 2015 Degeneration stage—specific response pattern of retinal ganglion cell spikes in *rd10* mouse retina *37th Annual Int. Conf. of the IEEE Engineering in Medicine and Biology Society (Milan, Italy)* pp 3351–4
- Pascolini D and Mariotti S P 2012 Global estimates of visual impairment: 2010 *British J. Ophthalmol.* **614**–8
- Patan M, Shah T and Sahin M 2006 Charge injection capacity of TiN electrodes for an extended voltage range *28th Annual Int. Conf. of the IEEE Engineering in Medicine and Biology, Proc. (New York)* pp 890–2

- Pennesi M E, Michaels K. V, Magee S S, Maricle A, Davin S P, Garg A K, Gale M J, Tu D C, Wen Y, Erker L R and Francis P J 2012 Long-term characterization of retinal degeneration in *rd1* and *rd10* mice using spectral domain optical coherence tomography. *Invest. Ophthalmol. Vis. Sci.* **53** 4644–56
- Phillips M J, Otteson D C and Sherry D M 2010 Progression of neuronal and synaptic remodeling in the *rd10* mouse model of retinitis pigmentosa *J. Comput. Neurol.* **518** 2071–89
- Puthussery T, Gayet-Primo J, Pandey S, Duvoisin R M and Taylor W R 2009 Differential loss and preservation of glutamate receptor function in bipolar cells in the *rd10* mouse model of retinitis pigmentosa *Eur. J. Neurosci.* **29** 1533–42
- Rathbun D L, Jalligampala A, Stingl K and Zrenner E 2015 To what extent can retinal prostheses restore vision? *7th Int. IEEE EMBS Neural Engineering Conf.—NER (Montpelier, France)* pp 244–7
- Resnikoff S, Pascolini D, Etya'ale D, Kocur I, Pararajasegaram R, Pokharel G P and Mariotti S P 2004 Global data on visual impairment in the year 2002 *Bull. World Health Organ.* **82** 844–51
- Reutsky-Gefen I, Golan L, Farah N, Schejter A, Tsur L, Brosh I and Shoham S 2013 Holographic optogenetic stimulation of patterned neuronal activity for vision restoration *Nat. Commun.* **4** 1509
- Rodieck R W 1998 *The First Steps in Seeing* 1st edn (Sunderland, MA: Sinauer Associates, Inc.)
- Roesch K, Stadler M B and Cepko C L 2012 Gene expression changes within Müller glial cells in retinitis pigmentosa *Mol. Vis.* **18** 1197–214
- Rösch S, Johnen S, Müller F, Pfarrer C and Walter P 2014 Correlations between ERG, OCT, and anatomical findings in the *rd10* mouse *J. Ophthalmol.* **2014** 874751
- Ryu S B, Ye J H, Lee J S, Goo Y S and Kim K H 2009 Characterization of retinal ganglion cell activities evoked by temporally patterned electrical stimulation for the development of stimulus encoding strategies for retinal implants *Brain Res.* **1275** 33–42
- Samba R, Herrmann T and Zeck G 2015 PEDOT-CNT coated electrodes stimulate retinal neurons at low voltage amplitudes and low charge densities *J. Neural Eng.* **12** 16014
- Schraermeyer U, Thumann G, Luther T and Kociok N 2001 Subretinally transplanted embryonic stem cells rescue photoreceptor cells from degeneration in the RCS rats *Cell Transplant.* **10** 673–80
- Schwahn H N, Gekeler F, Kohler K, Kobuch K, Sachs H G, Schulmeyer F, Jakob W, Gabel V P and Zrenner E 2001 Studies on the feasibility of a subretinal visual prosthesis: data from Yucatan micropig and rabbit *Graefes Arch. Clin. Exp. Ophthalmol.* **239** 961–7
- Schwartz S D, Hubschman J-P, Heilwell G, Franco-Cardenas V, Pan C K, Ostrick R M, Mickunas E, Gay R, Klimanskaya I and Lanza R 2015 Embryonic stem cell trials for macular degeneration: a preliminary report *Lancet* **379** 713–20
- Sekhar S, Jalligampala A, Zrenner E and Rathbun D L 2016 Tickling the retina: integration of subthreshold electrical pulses can activate retinal neurons *J. Neural Eng.* **13** 46004
- Sekirnjak C, Hottowy P, Sher A, Dabrowski W, Litke A M and Chichilnisky E J 2006 Electrical stimulation of mammalian retinal ganglion cells with multielectrode arrays *J. Neurophysiol.* **95** 3311–27
- Seung H S and Sümbül U 2014 Neuronal cell types and connectivity: lessons from the retina *Neuron* **83** 1262–72
- Sharma A, Dorman M F and Spahr A J 2002 A sensitive period for the development of the central auditory system in children with cochlear implants: implications for age of implantation *Ear Hearing* **23** 532–9
- Sim S L, Szalewski R J, Johnson L J, Akah L E, Shoemaker L E, Thoreson W B and Margalit E 2014 Simultaneous recording of mouse retinal ganglion cells during epiretinal or subretinal stimulation *Vis. Res.* **101** 41–50
- Stasheff S F, Shankar M and Andrews M P 2011 Developmental time course distinguishes changes in spontaneous and light-evoked retinal ganglion cell activity in *rd1* and *rd10* mice *J. Neurophysiol.* **105** 3002–9
- Stett A, Barth W, Weiss S, Haemmerle H and Zrenner E 2000 Electrical multisite stimulation of the isolated chicken retina *Vis. Res.* **40** 1785–95
- Stett A, Mai A and Herrmann T 2007 Retinal charge sensitivity and spatial discrimination obtainable by subretinal implants: key lessons learned from isolated chicken retina *J. Neural Eng.* **4** S7–16
- Stingl K et al 2015 Subretinal visual implant alpha IMS—clinical trial interim report *Vis. Res.* **111** 149–60
- Sümbül U, Song S, McCulloch K, Becker M, Lin B, Sanes J R, Masland R H and Seung H S 2014 A genetic and computational approach to structurally classify neuronal types *Nat. Commun.* **5** 3512
- Suzuki S, Humayun M S, Weiland J D, Chen S-J, Margalit E, Piyathaisere D V and de Juan E 2004 Comparison of electrical stimulation thresholds in normal and retinal degenerated mouse retina *Japan. J. Ophthalmol.* **48** 345–9
- Toychiev A H, Ivanova E, Yee C W and Sagdullaev B T 2013 Block of gap junctions eliminates aberrant activity and restores light responses during retinal degeneration *J. Neurosci.* **33** 13972–7
- Tsai D, Morley J W, Suaning G J and Lovell N H 2009 Direct activation and temporal response properties of rabbit retinal ganglion cells following subretinal stimulation *J. Neurophysiol.* **102** 2982–93
- Weiland J D and Humayun M S 2014 Retinal prosthesis *IEEE Trans. Biomed. Eng.* **61** 1412–24
- Yang Y T, Lin P K, Wan C, Yang W C, Lin L J, Wu C Y and Chiao C C 2011 Responses of rabbit retinal ganglion cells to subretinal electrical stimulation using a silicon-based microphotodiode array *Investigative Ophthalmol. Vis. Sci.* **52** 9353–61
- Ye J H and Goo Y S 2007 Comparison of voltage parameters for the stimulation of normal and degenerate retina *28th Annual Int. Conf. of the IEEE Engineering in Medicine and Biology, Proc. (Lyon)* pp 5782–5
- Ye J H, Kim K H and Goo Y S 2008 Comparison of electrically-evoked ganglion cell responses in normal and degenerate retina *30th Conf. Proc., IEEE Engineering in Medicine and Biology Society (Vancouver, BC)* pp 2465–8
- Yee C W, Toychiev A H and Sagdullaev B T 2012 Network deficiency exacerbates impairment in a mouse model of retinal degeneration *Front. Syst. Neurosci.* **6** 1–14
- Zrenner E et al 2011 Subretinal electronic chips allow blind patients to read letters and combine them to words *Proc. Biol. Sci.* **278** 1489–97
- Zrenner E, Stett A, Weiss S, Aramant R B, Guenther E, Kohler K, Miliczek K D, Seiler M J and Haemmerle H 1999 Can subretinal microphotodiodes successfully replace degenerated photoreceptors? *Vis. Res.* **39** 2555–67



## Supplementary Figures:

S1



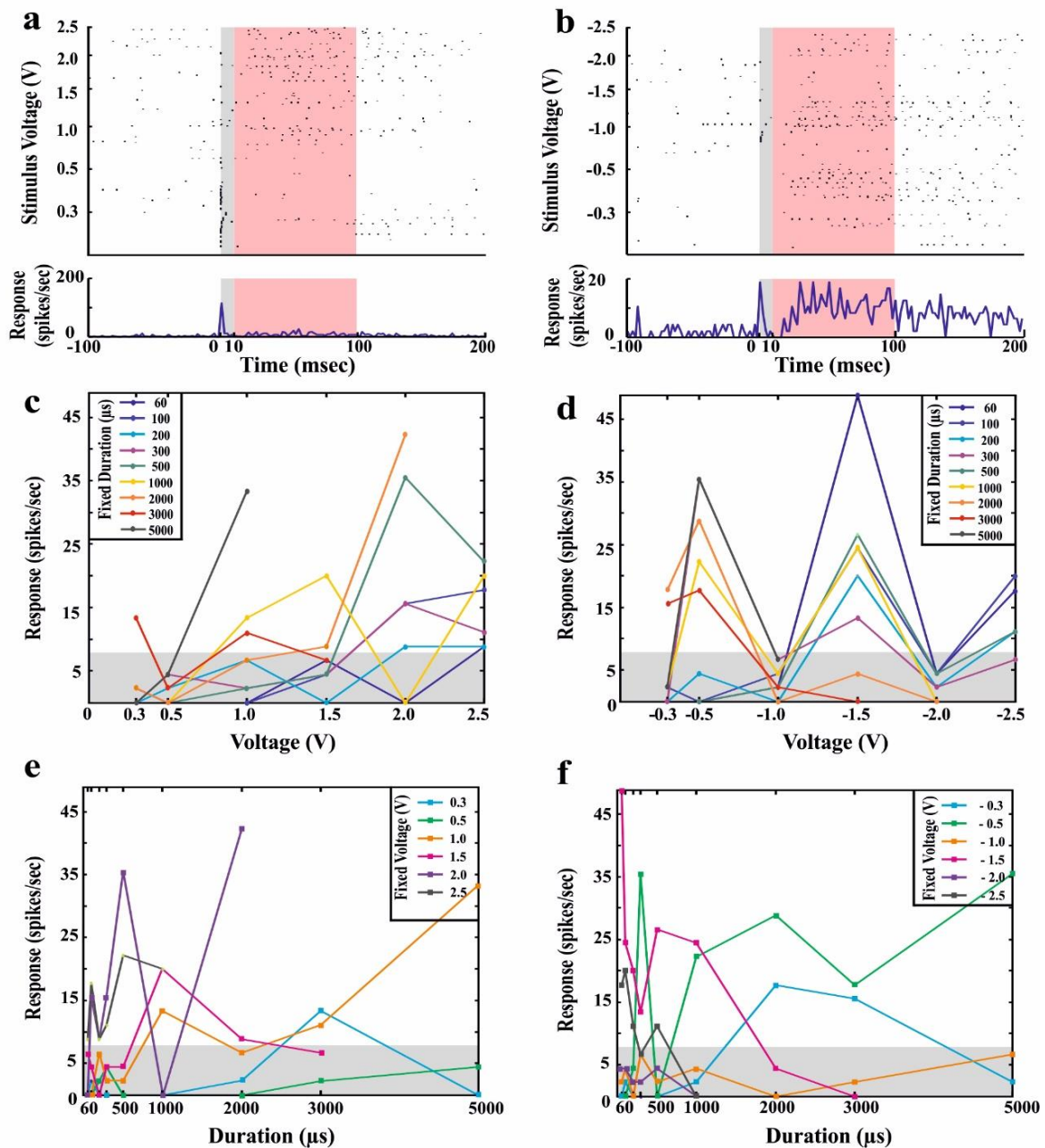
WT	Cathodic	Anodic	Cathodic-Anodic	Total
Monotonic	34	0	16	50
Nonmonotonic	2	0	16	18
Total	36	0	32	68

rd10	Cathodic	Anodic	Cathodic-Anodic	Total
Monotonic	28	0	74	102
Nonmonotonic	5	0	67	72
Total	33	0	141	174

**S1. Table of cell counts for electrically responsive retinal ganglion cell response types at 200-283 $\mu$ m distance from stimulation electrode.** Columns represent polarity types. Polarity categorization was calculated by separately summing all cathodic responses (C) and all anodic responses (A) using the normalized response surface. From these responses, a polarity index (PI) was calculated  $(A-C)/(A+C)$ . Cathodic cells responded predominately to negative voltage pulses ( $-1 \leq PI < -0.5$ ), whereas anodic cells responded predominately to positive voltage pulses ( $0.5 < PI \leq 1$ ). Cells that strong responses to both polarities were termed cathodic-anodic ( $-0.5 \leq PI \leq 0.5$ ). To quantify the degree to which responses continued to increase with increasing voltage a monotonicity index (MI) was calculated. The MI was calculated separately for each constant-duration,

voltage response curve and then averaged across the nine durations. For each curve, the peak response was identified, and the integral of responses above this peak was calculated. The MI was the ratio of this integral to an assumption of pure saturation in which each response above the peak is equal to the peak (see schematic). For a monotonic cell that either peak at the highest voltage or saturates, the MI would be 1. Non-monotonic were defined as cells with an  $MI < 0.75$  and  $MI \geq 0.75$  indicated a monotonic cell. All index boundaries were subjectively placed after examination of the index histograms. While clear modes were apparent in the distribution of PI, MI appeared to be a continuum.

S2



**S2 Electrical response profile, for example, non-monotonic, rd10 RGC shown in Fig. 5d.** (as in Fig. 4) Panels in the left column are positive voltage pulse responses, and right column panels are negative voltage responses. **(a,b)** (top) Spike train dot rastergram showing responses sorted into labeled voltage blocks with pulse duration sorted low to high from bottom to top of each block (480 rows in total). (bottom) Peristimulus time histogram (PSTH) from all 480 responses binned at 1 ms intervals with shaded 10 ms spike exclusion (grey) and 90 ms response integration (pink) periods indicated. **(c,d)** Fixed-duration, voltage response curves calculated from the responses in a and b. **(e,f)** Fixed-voltage, duration response curves. Thin grey bars at the bottom of panels c-f indicate the threshold. Error bars were omitted for clarity.

## S3

## CONSTANT DURATION

a

WT

		ANODIC (+)												
		48	12	9	14	14	14	15	16	14	13	16		
			60	100	200	300	500	1000	2000	3000	5000			
CATHODIC (-)	DURATION ( $\mu$ s)	(-)60											60	
	(-)100												100	
	(-)200												200	
	(-)300												300	
	(-)500												500	
	(-)1000												1000	
	(-)2000												2000	
	(-)3000												3000	
	(-)5000												5000	
			(-)60	(-)100	(-)200	(-)300	(-)500	(-)1000	(-)2000	(-)3000	(-)5000			
		47	22	25	37	41	46	47	47	47	38			
		CATHODIC (-)												

## CONSTANT VOLTAGE

b

WT

		ANODIC (+)									
		65	20	21	25	24	20	21	31		
			300	500	1000	1500	2000	2500			
CATHODIC (-)	VOLTAGE (mV)	-300								300	
	-500									500	
	-1000									1000	
	-1500									1500	
	-2000									2000	
	-2500									2500	
			-300	-500	-1000	-1500	-2000	-2500			
		64	62	64	60	53	28	20			
		CATHODIC (-)									

c

RD10

		ANODIC (+)												
		117	32	20	27	32	29	31	26	20	17	35		
			60	100	200	300	500	1000	2000	3000	5000			
CATHODIC (-)	DURATION ( $\mu$ s)	(-)60											60	
	(-)100												100	
	(-)200												200	
	(-)300												300	
	(-)500												500	
	(-)1000												1000	
	(-)2000												2000	
	(-)3000												3000	
	(-)5000												5000	
			(-)60	(-)100	(-)200	(-)300	(-)500	(-)1000	(-)2000	(-)3000	(-)5000			
		112	55	86	100	106	107	110	106	103	59			
		CATHODIC (-)												

d

RD10

		ANODIC (+)									
		161	60	69	76	72	74	76	108		
			300	500	1000	1500	2000	2500			
CATHODIC (-)	VOLTAGE (mV)	-300								300	
	-500									500	
	-1000									1000	
	-1500									1500	
	-2000									2000	
	-2500									2500	
			-300	-500	-1000	-1500	-2000	-2500			
		148	130	132	130	104	74	80			
		CATHODIC (-)									

**S3 Matrix tables of pairwise threshold comparisons and related number of RGCs used in Figure 6 (see Methods - Threshold Curves for inclusion criteria).** (a,c) Voltage threshold comparisons for WT and rd10. Cathodic (-) voltage thresholds (bottom-left half, blue) and anodic (+) voltage thresholds (upper-right half, orange) as well as anodic vs. cathodic voltage thresholds (central diagonal, grey) are compared for nine (60, 100, 200, 300, 500, 1000, 2000, 3000, 5000  $\mu$ s) constant-duration voltage response curves (see Fig. 6a, c). Significant pairwise comparisons ( $p < 0.05$ ) are shown in green with an arrow pointing to the duration with a higher voltage threshold relative to the other duration. All significant (green) comparisons support the hypothesis that voltage thresholds for shorter durations are higher than voltage thresholds for longer durations. For both WT & rd10, the numbers in the top and bottom rows of each table (black) indicate the number of RGCs included in each duration

of the response curve. **Red** numbers indicate the total number of RGCs included in the anodic (+) voltage threshold curve and **blue** numbers indicate the total number of RGCs included in the cathodic (-) voltage threshold curve. **Purple** numbers indicate the total number of RGCs included in all curves for that table (including both anodic and cathodic threshold curves). **(b,d)** Duration threshold comparisons for WT and rd10. Cathodic (-) duration thresholds (bottom-left half, **blue**) and anodic (+) duration thresholds (upper-right half, **orange**) as well as anodic vs. cathodic duration thresholds (central diagonal, **grey**) are compared for six (300, 500, 1000, 1500, 2000, 2500 mV) constant-voltage duration response curves (see **Fig. 6b,d**). Significant pairwise comparisons are shown in **green** with an arrow pointing to the voltage with a higher duration threshold relative to the other voltage. All significant (**green**) comparisons support the hypothesis that duration thresholds for lower voltages are higher than duration thresholds for higher voltages. As in **a** and **c**; **black**, **red**, **blue**, and **purple** numbers indicate the number of cells that were included in each curve. The absence of arrows in (**grey**) cells indicates that no anodic-cathodic threshold comparisons were significant.

## 2.2 Correspondence of electrical response patterns to visual response types

As a follow up to the above study, we wanted to assess the correspondence between the electrical response pattern types – depending upon the monotonicity index and the polarity index (monotonic and non-monotonic; cathodic, anodic, and cathodic & anodic respectively) and the visual response types (ON, OFF, ON-OFF). For characterizing the visual responses, we used full-field flash stimuli (2s ON followed by 2s OFF, without any pause for 80 seconds – 20 trials, refer to *Stimulation in the Methods* section). We interleaved six full-field flash stimuli blocks within the electrical stimulation blocks. Therefore, we provided in total 120 trials and characterized the response index across all trials (otherwise known as Bias index or ON-OFF index) based on *Carcieri et al.* 2003 i.e

$$\text{Bias Index} = (A_{\text{on}} - A_{\text{off}}) / (A_{\text{on}} + A_{\text{off}}),$$

where  $A_{\text{on}}$  and  $A_{\text{off}}$ , are peak responses of ON and OFF respectively, relative to the baseline. Based on the bias indices, an index of  $> 0.5$  to  $1$  was an ON response,  $< -0.5$  to  $1$  was an OFF response and an index  $\leq 0.5$  and  $\geq -0.5$  was designated as an ON-OFF response (*Carcieri et al., 2003*).

### 2.2.1 Distribution of visual response types for electrically responsive RGCs in wild-type(WT) and *rd10*

The number of electrically responsive cells (electrode distance 200-283  $\mu\text{m}$ ) for WT and *rd10* retinas was **68** and **174** cells respectively (Table 1 and S1). Of these, all the cells in WT retinas responded to full-field flash stimulus, however, in *rd10* retina **seven** cells of **174** cells could not be visually classified, thus resulting in a total of **167** cells which were responsive to the visual stimulus (**Table 2.1 and A**).

Table 2.1

Mouse Strains	ON	ON-OFF	OFF	ON%	ON-OFF %	OFF%
WT (n=68)	20	42	6	29%	62%	9%
<i>rd10</i> (n=167)	34	87	46	20%	52%	28%

A

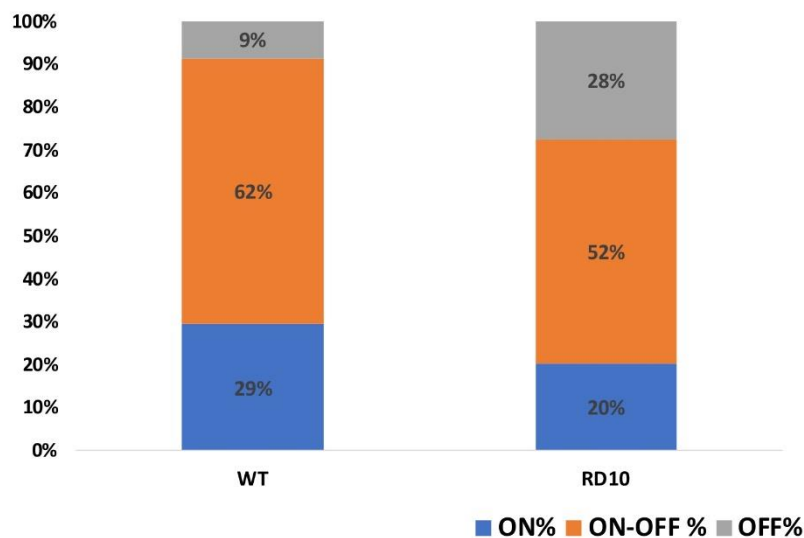


**Table 2.1 & Fig 2.1 A: Distribution of electrically responsive RGCs into different visual response types.** The table and stacked percentage bar chart represents the distribution of visual response types of RGCs which are electrically responsive at an inter-electrode distance of 200-283 $\mu$ m. Each percentage is calculated as (number of cells/total number of cells) \* 100.

The percentage of cells with ON-OFF responses were comparatively higher for both the mouse strains (62% for WT and 52% for *rd10*). This observation was in agreement with the previous studies in healthy mice retina (Kim *et al.*, 2010; Zhang *et al.*, 2012) and bullfrog retina (Xiao *et al.*, 2014). These studies showed that the majority of the RGC population function as feature detectors which respond transiently to both onset and offset of stimuli (i.e., ON-OFF response) receiving inputs from both ON and OFF bipolar cells. For the *rd10* retina, all our observations were conducted at intermediate

stages of degeneration (P28-P37), where the majority of the rods are lost but the cones are still viable. Considering, the visual stimulus operated in the range from higher mesopic (OFF) to higher photopic (ON) range, where the cones are predominantly active, it was not surprising that the percentage of cells with ON-OFF responses were comparable to the wild-type retinas.

For pure ON and OFF responses, it was observed that in the WT retina, the RGCs with pure ON responses were more receptive to electrical stimulation than cells with pure OFF responses (**Fig 2.1A**). Previous studies with *in vitro* and *in vivo* healthy mouse retinas (*Balkema et al., 1982; Nirenberg and Meister, 1997, Carciari et al. 2003*), have shown that in response to full field flash stimuli a large fraction of the RGC population was responsive to the onset of the flash stimuli (ON) than the offset (OFF). However, in *rd10* retinas, RGCs with pure ON and OFF responses were responsive to electrical stimulation, with slightly higher inclination towards RGCs with OFF responses. This slight shift towards OFF responses could be an indication that during the progression of the disease, the OFF responses are more preserved than the ON responses [as seen in the *rd1* model of aggressive degeneration] (*Stasheff, 2008; Stasheff et al., 2011*).

### **2.2.2 Correspondence of electrical response types with visual response types.**

From the above study, we could identify four different types of response patterns depending upon the polarity index (PI) and the monotonicity index (MI) as shown in **S1**. Briefly, as per the polarity index, we could classify the electrically responsive cells into cells which responded to only cathodic (-ve) monophasic stimulation and cells which responded to both monophasic cathodic (-ve) and monophasic anodic stimulation (+ve). None of the RGCs had a response to purely anodic stimulation. This is because during epiretinal stimulation, the RGCs have more preference for cathodic stimuli rather than anodic stimuli (*refer to section 4.1.2 Preference for cathodic voltage pulses*). As per the monotonicity index (MI) calculated from the constant duration voltage curves, the electrically responsive RGCs response patterns could be classified as monotonic response (response of RGCs increases with increasing amplitude and

saturates at higher amplitudes i.e. a strong correspondence between response and amplitude) and non-monotonic response (responses of RGCs fluctuates with increasing responses, i.e. weak correspondence between response and amplitude). In some cases, monotonic responses (only increasing responses) are differentiated from saturated responses (*Barriga-Rivera et al., 2017*), however, for our study, we categorize both these responses under one category, i.e. the monotonic response.

In order, to develop efficient stimulation paradigms for the retinal implants, it is not only necessary to identify these electrical response pattern types, but also to understand if such electrical response types could correspond to specific visual response types. In doing so, one could shed light on the potential hallmarks for preferential stimulation which is the final goal for an efficient retinal implant.

### 2.2.2.1 Heterogeneity of Visual Responses

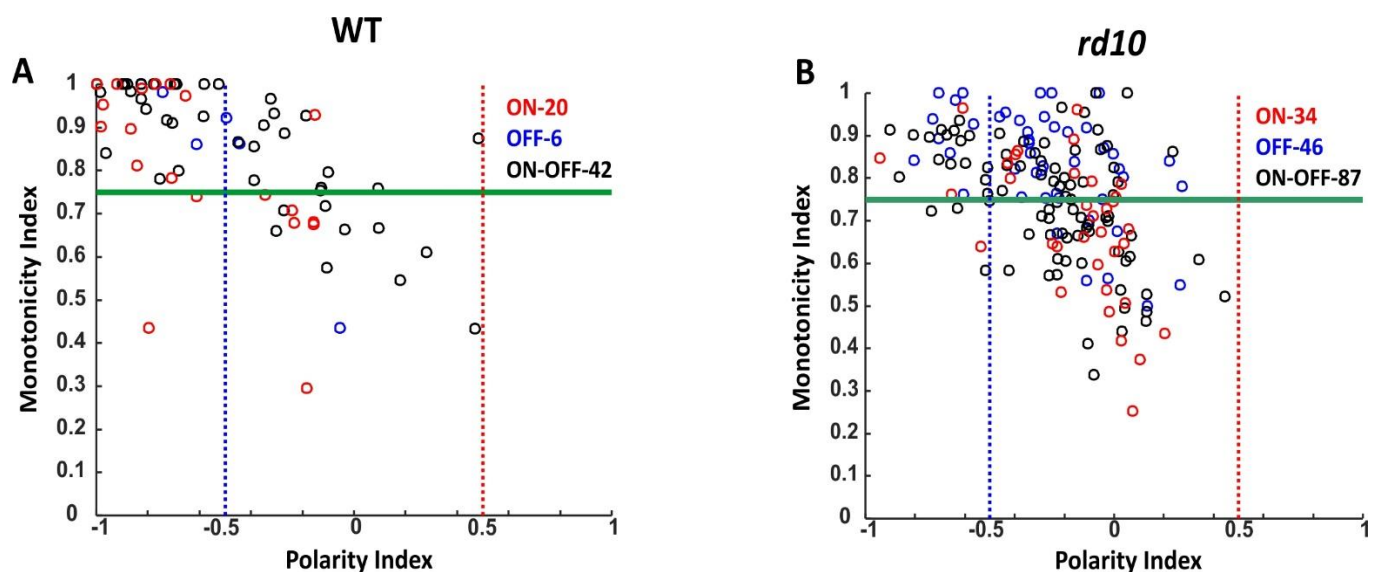


**Fig 2.2: Scatter plot showing the diversity of visual response types based on MI and PI.**

(A) & (B) Scatter plot exhibiting a diversity of visual responses based on the monotonicity and polarity indices in WT and rd10 retinas respectively. The open circles in red, blue, and black represent ON, OFF and ON-OFF visual responses respectively. The dashed lines in blue and red represent the cut-off index for purely cathodic and anodic response respectively as described above. The solid green line represents the cut-off for the monotonicity index (refer to S1 above). The scatter plot represents the diversity of visual responses in relation to electrical responses patterns in both the WT and rd10 retinas.



As stated earlier (*refer to Conclusions, Implications to Retinal Prosthesis*) the field of retinal prosthesis is currently stymied with an idiosyncrasy, which assumes the RGC population is homogenous. However, from the above scatter plot using a simple visual stimulus, like a flash there not only exist a diversity of responses among different RGC types but also within a given RGC type. In Fig 2.2 (A and B) based on the electrical response classification, the visual response types (ON, OFF, and ON-OFF) have a diversified response. Furthermore, within a group of visual response type, there is a significant spread which further validates the requirement for considering such variability while designing optimal stimulation paradigms. Therefore, using complex visual stimuli coupled with electrical response indices could potentially help in developing parameters for pathway-specific stimulation.

### **2.2.2.2 Distribution of visual response types based on monotonicity and polarity indices.**

#### **Monotonicity index**

In WT retinas, based on the monotonicity index, large fraction of all the visual response types, i.e. ON, OFF, and ON-OFF, showed a monotonic trend. Only a few cells in each visual category showed the non-monotonic trend as seen in Table 2.2 and Fig 2.3 (A). Unlike WT retinas, for the *rd10* retinas, a large fraction of RGCs with ON responses had non-monotonic response trend[Table 2.2] Further the ON-OFF responses had equivalent fractions of monotonic and non-monotonic responses. However, large fraction of RGCs with OFF responses had monotonic response patterns in comparison to non-monotonic responses (Table 2.2 and Fig 2.3C). Such transitions in ON and ON-OFF cells from monotonic to non-monotonic response patterns but not in OFF cells possibly could support the observations from earlier studies, that during the disease progression the OFF pathway is relatively preserved for a longer duration in comparison to ON pathway (*Stasheff 2008*).

**Table 2.2**

<b>WT</b>	Monotonic	Monotonic %	Non-monotonic	Non-monotonic%
ON	12	60%	8	40%
OFF	5	83%	1	17%
ON-OFF	33	79%	9	21%
<b>rd10</b>				
<b>rd10</b>	Monotonic	Monotonic %	Non-monotonic	Non-monotonic%
ON	13	38%	21	62%
OFF	39	85%	7	15%
ON-OFF	46	53%	41	47%

*Table 2.2: Classification of visual response types based on Monotonicity Index (MI) in WT and rd10 retinas. Distribution of visual response types (ON, OFF and ON-OFF) in monotonic (blue) and non-monotonic responses (orange). The column represents the number of cells and fraction of cells in percentage (number of cells / total number of cells with monotonic and non-monotonic response) for each visual type (in rows).*

### Polarity index

In WT retinas, based on the polarity index, a large fraction of ON RGCs responded to only monophasic cathodic stimulation. Whereas, both OFF and ON-OFF cells had comparable fractions responding to both only cathodic and cathodic-anodic stimulations (Table 2.3 and Fig 2.3B). However, in *rd10* retinas, all the visual responses types had a larger fraction of cells responding to cathodic and anodic stimulation (Figure 2.3D). As stated in the paper, cells which were responsive to anodic stimulation also had responses to cathodic stimulation. None of the cells had only anodic responses.

**Table 2.3**

<b>WT</b>	Cathodic	Cathodic %	Anodic	Anodic %	Cathodic/Anodic	Cathodic/Anodic %
ON	13	65%	0	0%	7	35%
OFF	3	50%	0	0%	3	50%
ON-OFF	20	48%	0	0%	22	52%
<b>rd10</b>						
<b>rd10</b>	Cathodic	Cathodic %	Anodic	Anodic %	Cathodic/Anodic	Cathodic/Anodic %
ON	4	12%	0	0%	30	88%
OFF	9	20%	0	0%	37	80%
ON-OFF	20	23%	0	0%	67	77%

**Table 2.3: Classification of visual response types based on Polarity Index (PI) in WT and rd10 retinas.** Distribution of visual response types (ON, OFF, and ON-OFF) in cathodic only (blue) anodic only (orange) and cathodic and anodic (grey). The column represents the number of cells and fraction of cells in percentage (number of cells/ total number of cells responding to only cathodic, only anodic, cathodic and anodic) for each visual type (in rows).

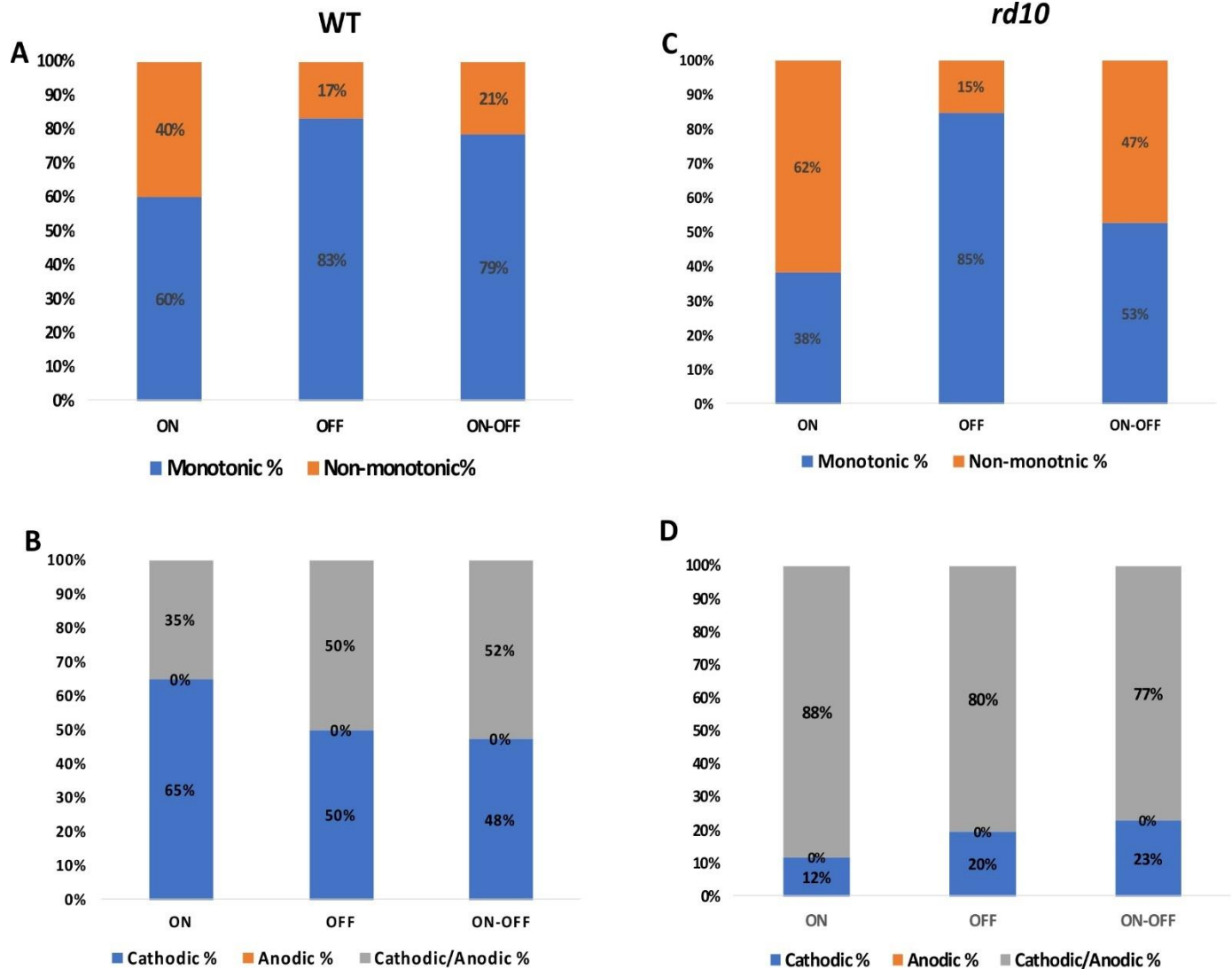


**Figure 2.3: Distribution of visual response types based on Monotonicity and Polarity Indices in WT and rd10 retinas.** (A and C) Stacked percentage bar showing fraction of monotonic (blue) and non-monotonic (orange) response patterns in each visual response types (ON, OFF and ON-OFF) for WT and rd10 respectively. (B and D) Stacked percentage bar showing fraction of RGCs in each visual response types (ON, OFF and ON-OFF) responding to cathodic only (blue) & cathodic and anodic (grey) monophasic stimulation in WT and rd10

respectively. The 0% in the stacked bar shows that no RGCs responded to only anodic stimulation.

### 2.2.2.3 Summary

Taking together, the RGCs classification based on both monotonicity and polarity indices, for each visual response types we observed that in both WT and *rd10*, a large fraction of ON, OFF and ON-OFF cells had monotonic response patterns when stimulated with only monophasic cathodic stimulation (Fig 2.4 A and Table 2.4). For ON cells which responded to both monophasic cathodic and anodic stimulation, a large fraction had non-monotonic response pattern. However, for OFF and ON-OFF cells the response pattern was more inclined towards monotonic (Fig 2.4C). Similar observations were seen in *rd10* retinas (Table 2.4 Fig 2.4B) with an exception that, for the ON-OFF cells which responded to both anodic and cathodic stimulation, the cell tend to display more non-monotonicity (Fig 2.4D).

**Table 2.4**

<b>WT</b>	Monotonic/cathodic	Monotonic/cathodic %	Non-monotonic/cathodic	Non-monotonic/cathodic%
ON	11	85%	2	15%
OFF	3	100%	0	0%
ON-OFF	20	100%	0	0%
	Monotonic/cathodic-Anodic	Monotonic/cathodic-Anodic%	Non-monotnic/cathodic-Anodic	Non-monotonic/cathodic-Anodic %
ON	1	14%	6	86%
OFF	2	67%	1	33%
ON-OFF	13	59%	9	41%
<hr/>				
<b><i>rd10</i></b>	Monotonic/cathodic	Monotonic/cathodic %	Non-monotonic/cathodic	Non-monotonic/cathodic%
ON	3	75%	1	25%
OFF	9	100%	0	0%
ON-OFF	16	80%	4	20%
	Monotonic/cathodic-Anodic	Monotonic/cathodic-Anodic%	Non-monotonic/cathodic-Anodic	Non-monotonic/cathodic-Anodic %
ON	10	33%	20	67%
OFF	30	81%	7	19%
ON-OFF	30	45%	37	55%

---

**Table 2.4: Classification of visual response types based on Monotonicity and Polarity Indices in WT and rd10 retinas.** Distribution of visual response types (ON, OFF and ON-OFF) based on monotonicity and polarity indices (considering both indices simultaneously). Monotonic (*blue*) and non-monotonic responses (*orange*) have been categorized into cathodic and cathodic-anodic based on polarity index. The column represents the number of cells and fraction of cells in percentage (number of cells/ total number of cells) for each visual type (in rows).

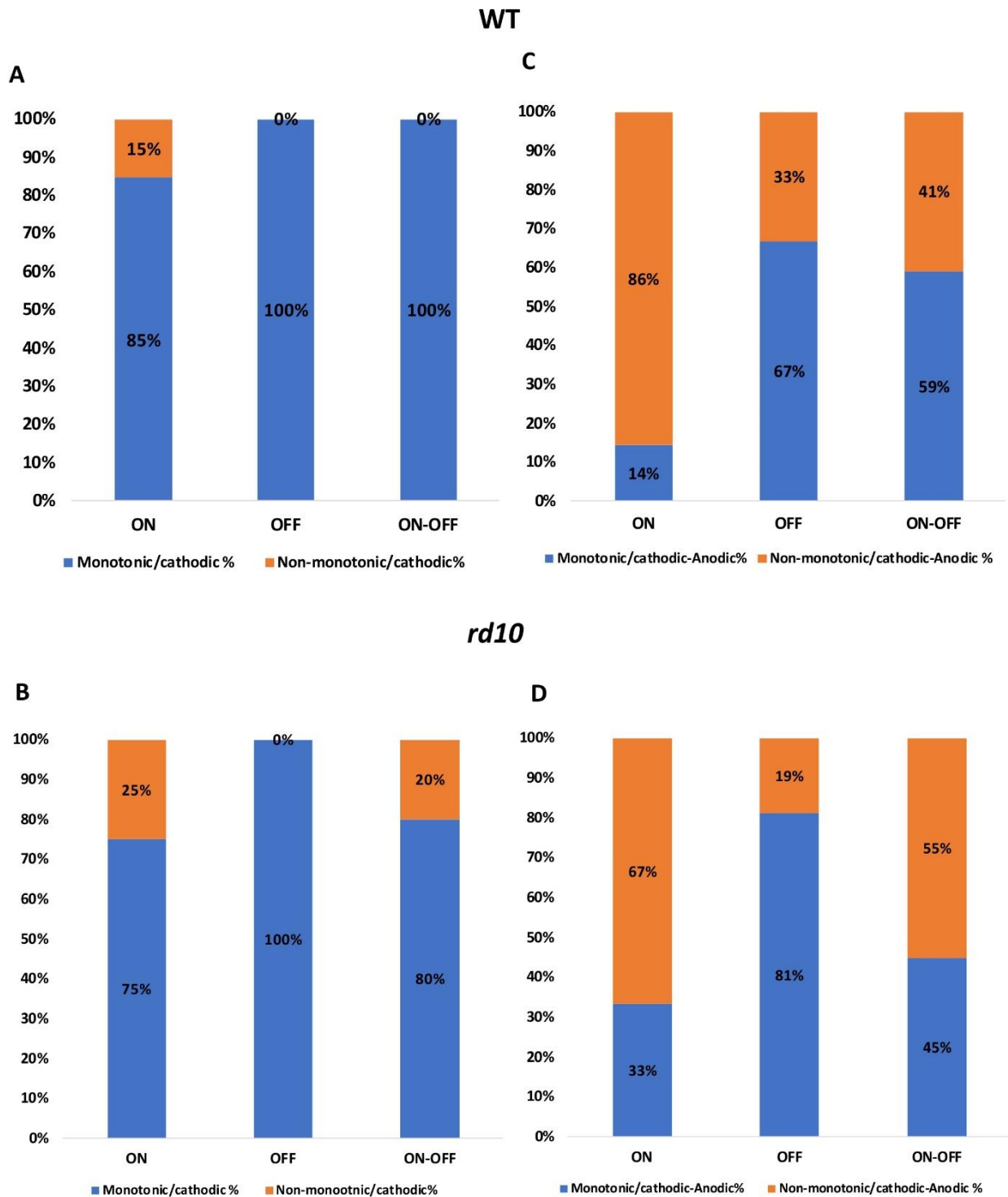


**Figure 2.3: Distribution of visual response types based on Monotonicity and Polarity Indices (considered simultaneously) in WT and rd10 retinas. (A and B) Stacked percentage bar showing fraction of monotonic (blue) and non-monotonic (orange) responses, in each visual response types (ON, OFF and ON-OFF) responding to only monophasic cathodic**

stimulation for WT and *rd10* respectively. **(C and D)** Stacked percentage bar showing fraction of monotonic (*blue*) and non-monotonic (*orange*) responses, in each visual response types (ON, OFF and ON-OFF) responding to both monophasic anodic and cathodic stimulation for WT and *rd10* respectively.

#### 2.2.2.4 Limitations

Although we could determine some subtle hallmarks (as shown above with the use of various indices like MI AND PI) which could lay the foundation of pathway-specific stimulation, there remains a potential confound. The above observations were made at an intermediate stage of degeneration where most of the cone photoreceptors are still viable. However, in patients with the retinal implant, most of the photoreceptors are gone, with little to no light perception. Such circumstances correlate to late stages of degeneration (in mice) where no visual responses exist, and the retina is heavily rewired. Therefore, it is indeed crucial to determine changes in electrical response patterns during late stages of degeneration. Considering, visual stimuli cannot be used to categorize the RGCs at late stages, different experimental setups like patch clamping or calcium imaging interfaced with MEA (microelectrode array) recording needs to be used. Visualization of the retinal cell layers / retinal cells will provide us information regarding the state of degeneration and the extent to which the retina has been rewired. By electrically stimulating the preserved and viable pathway at different stages of degeneration and understanding their responses, it would be feasible to design pathway-specific stimulus paradigms even at late stages of degeneration.

## Chapter 3

### **Publication 2 -Adaptation of visual responses in healthy and degenerating *rd10* mice retinas during ongoing electrical stimulation.**

#### **3.1 Synopsis and framework of the study:**

As a follow-up to the previous study (in Chapter 2, 2.1) we assessed the correspondence between the electrical response types (monotonic and non-monotonic responses; cathodic, anodic and cathodic & anodic responses) to the visual response types (ON, OFF, ON-OFF types; Chapter 2, 2.2). During the analysis, few observations that piqued our interest were that the visual response parameters in response to full-field flash stimulus (especially the amplitude/firing rate) increased (when compared to the visual response parameters without electrical stimulation) after electrical stimulation (Figure 2, *Jalligampala et al. 2017*). Furthermore, the relative weighting of ON and OFF response types changed following electrical stimulation. In classical neuroscience, a change in firing rate/ amplitude is often a measure to account for neural “adaptation.” Based on the first-hand observation we asked the following questions. (1) Does the increase in amplitude correspond to a phenomenon attributed to visual adaptation? (2) Does electrical stimulation alter the adaptation of visual



responses? (3) Are the adaptation effects due to *invitro* recordings?. To address these questions, we at first compared the test condition, i.e., the electrically responsive cells (*refer to Responsive RGC inclusion criteria*, Chapter 2, 2. 1) to an internal control condition from the same tissue, i.e. cells which were not electrically responsive. For the two conditions, we compared the changes in visual response parameters before and after electrical stimulation for both healthy and degenerating retinas. Additionally, as an appropriate control condition, we compared these changes between electrically responsive cells (test) and cells with only visual responses (i.e., the visual stimulation blocks were provided at the same time as provided for the cells in the test condition but without any electrical stimulation).

What surprised us is that, the increasing trend of amplitudes for ON and OFF responses, decreasing OFF latency responses and increasing ON and OFF durations were also observed for RGCs which were only visually responsive (i.e., without any electrical stimulation). However, when compared to the electrically responsive RGCs these changes were significant for the electrically responsive cells. This suggested us that although there are some ongoing changes attributed to visual adaptation and *invitro* changes, following electrical stimulation, this is further enhanced. What was also evident in most cells was that these changes were observed after delivering a lower voltage stimulation (300 millivolts) and were strengthened with increasing voltage values.

The novelty of the study lies in the fact that, many earlier studies have researched on visual adaptation and electrical adaptation by itself, however, this is the only study that investigates the visual adaptation during ongoing electrical stimulation, thereby providing an opportunity to understand the complex interaction between the two. This study has a crucial implication in the field of the retinal prosthesis. While most of the stimulation paradigms for clinical implementation are determined from *invitro* studies (pre-clinical), it is necessary that such ongoing electrical stimulation changes need to be accounted for while determining appropriate stimulation parameters for future retinal implants.

## Chapter 4

### **Publication 3- Spatio-temporal aspects of electrical desensitization in healthy mouse retinal ganglion cells (RGCs).**

#### **4.1 Synopsis and framework of the study:**

Retinitis pigmentosa (RP) patients with retinal implants perceive the sensation of light when stimulated. These sensations are known as “phosphenes.” To provide the blind patients with the ability to perform daily tasks such as reading or navigating a room will require complex temporal and spatial patterns of electrical stimulations. Further such complex patterns would require hundreds or thousands of electrodes. By stimulating these electrodes in an appropriate spatiotemporal sequence, one can take into consideration the visuotopic organization of the retina to convey the desired information to the higher orders of the visual system. While clinical trials have shown some promising results in providing useful visual cues, there remains inconsistency among implanted patients. Further, testing in human subjects has shown that the electrode interactions significantly affect the resultant visual percepts (Wilke *et al.* 2011). Therefore, it is necessary to have a thorough understanding of the interaction occurring between repetitive stimuli both at the single electrode (temporal) as well as spatiotemporal interaction occurring between different electrodes.

Various *invitro* studies have shown that the electrical responsiveness of RGCs decreases with repetitive stimulation (Freeman and Fried 2011, Jensen and Rizzo 2006) delivered at a single

electrode. Such reduction in RGC sensitivity is termed as “desensitization.” These findings may play an essential role in the fading of visual percepts as reported by implanted patients. Interestingly these subjects not only report losing the brightness of phosphene but also see marked changes in size, shape and even color (*Perez-Fornos et al. 2012*), which suggest that the phosphene fading is rather a complex phenomenon and employs both spatial and temporal interaction.

In this study, we investigated the temporal aspects of desensitization, by providing trains of biphasic current pulses (delivered at a single electrode) at different frequencies and recording the RGC spiking responses to electrical stimulation using MEA in the healthy mouse retina. Additionally, we provided paired pulses of biphasic current pulse simultaneously at different interelectrode distances to study the spatiotemporal interaction of the electrical desensitization.

We found a reduction of responses to continuous pulse trains, however in comparison to the previous studies this reduction was modest. Further, we found that for the shortest interelectrode distance the desensitization was most pronounced.

Therefore, it is necessary to consider such spatiotemporal interactions while designing high-resolution implants.

# Chapter 5

## 5.1 General Discussion

### 5.1.1. Restoring vision to the blind

The idea of restoring vision to the blind has long been thought to be fanciful. However, beginning as far back as the mid-1950s vision neuroscientists started to investigate the possibility of vision restoration to the blind by stimulating neurons of the visual pathway (Tassicker 1956; Brindley 1970). Most blindness occurring worldwide is caused by the defect in the eye. It can be caused, first by damage to the sensory membrane which lines the inner surface of the back of the eye. Second, it can be caused due to optical impediments such as cataracts and keratoconus. Today, it is possible to cure blindness occurring due to optical impediments. In many parts of the world, cataract surgery is carried routinely by removing the opaque lens and replacing it with an artificial lens. Also, corneal transplants with natural and artificial corneas have proved to be successful. However, it should be noted, that in those parts of the world where such procedures are not available, blindness due to optical impediments remains common.

The primary cause of untreatable blindness throughout the world today is a retinal degenerative disease. Most often these diseases are caused because of loss of photoreceptor cells, but also, in inner retinal neurons in case of glaucoma, where the loss of ganglion cells prevents the visual signals to be relayed ( via optic nerve) to higher visual centers like cortex. Because most retinal degenerative diseases are caused by loss of photoreceptors ( retinitis pigmentosa (RP) and age-related macular degeneration (AMD)), much emphasis is placed on the substitution for the loss of photoreceptor functions or restoration of the photoreceptive function in the blind eyes.

There is an enormous diversity of approaches which are currently underway to restore vision to the blind (*refer to Introduction section, Current approaches to sight restoration*). However, each of these approaches come with their own complexities and limitations. For example, approaches like optogenetics and gene therapy promise a targeted approach which could increase the vision resolution (spatial), however, the safety and efficacy of these approaches remain a concern for many clinicians. Likewise, stem cell therapy which introduces photoreceptors in the degenerated retina has not shown much success in restoring functional vision. Of the various approaches available currently, retinal prostheses have been clinically successful so far in restoring vision to blind patients. Although, being successful to restore light sensitivity and low-acuity vision in patients, there are some challenges which limit this approach. Some of the obstacles include reproducibility of phosphenes, limited stimulation frequencies, low spatial resolution, low contrast. Although, with success seen in patients, there is a lot we do not understand about the electrical stimulation at the retinal network level. Keeping this in our mind, this thesis aimed at unraveling facets of some of these challenges *in vitro* at the retinal network level. Additionally, we proposed some measures which would help to address some of these challenges, to develop a better and improved implant for the blind.

## **5.1.2. Key take-home messages of the thesis**

### **5.1.2.1 Acknowledging Variability**

Up until recently, the field of retinal prosthesis considers the retinal ganglion cell (RGC) population to be homogenous. Based on these assumptions, many studies (Goo *et al.* 2011b; Ryu, Ye, Lee, Goo & Kim 2009; Jensen *et al.* 2003; Jensen & Rizzo 2007) estimated the standardized or optimal stimulation paradigms for stimulating the retinal circuit. However, a careful examination of recent studies (Farrow & Masland 2011; Baden *et al.* 2016; Sumbul *et al.* 2014) has shown that there is a broad variability amongst different RGC types. This variability continues to complicate the simple characterization of the RGC responses to electrical stimulation. Therefore, to have a better understanding of the retinal electrostimulation for developing better implants, it is necessary to design stimulation paradigms that would acknowledge this variability. In our study, we went beyond the conventional threshold measurement method and developed an analytical framework that

assessed the full strength-duration-polarity of a population to identify the optimal stimuli for stimulation the retinal network ( Chapter 2, Publication 1).

### **5.1.2.1 Hallmark for pathway-specific stimulation**

Recent studies (Sekhar *et al.* 2017; Ho, Smith, *et al.* 2018) have shown that different RGC types have different electrical input filters, suggesting that stimulation of the specific pathway is a feasible option for the next-generation implants. However, the current implants stimulate all the RGCs simultaneously. Therefore, in our study ( section 2.1 and 2.2) when the RGC populations are being stimulated simultaneously, we identified different electrical response patterns ( monotonic and non-monotonic; cathodic and cathodic-anodic) which could correspond to different RGC types in healthy and degenerating retinas. It is necessary we identify such hallmarks, as with progression of the disease when these cell types cannot be visually classified; these electrical hallmarks would indicate the cell being stimulated and hence would help in developing cell-specific stimulation for the implants even when the neurons of the retina are extremely degenerated.

### **5.1.2.1 Adaptation effects**

The outcome of clinical studies primarily depends on the success of the preclinical studies *invitro* or *invivo*. Therefore, it is necessary to have a deeper understanding of the various aspects observed at the preclinical level. In our study, we examined, how the visual responses of the RGCs adapt during ongoing electrical stimulation (Chapter 3). We observed that post electrical stimulation the responses of the RGCs increased significantly. Such ongoing adaptation effects, could hint at the level of plasticity occurring in the retina and needs to be accounted for while determining stimulation paradigms.

### **5.1.2.1 Electrical desensitization**

Of the various challenges mentioned above, limited stimulation frequency and spatial resolution are the most important concerns for the prosthetic community. Patients with retinal implants (Zrenner *et al.* 2011; Stingl *et al.* 2017; Stingl *et al.* 2015) report the fading of visual percepts with repetitive stimulation ( high stimulation frequencies). This in *invitro* studies is referred to as desensitization (Freeman & Fried 2011; Jensen & Rizzo 2007; Im & Fried 2016). In our study, we investigated the spatial extent of desensitization and how the

spatial and the temporal component interaction have effects on the RGC response (Chapter 4). We found that the desensitization is a local phenomenon (local to the stimulating electrodes) rather than a global phenomenon. Additionally, we proposed that with the increasing demand for high-density arrays, which would improve the spatial resolution, it is necessary to account for the spatial component of desensitization to design an efficient implant with good spatiotemporal resolution.

### 5.1.3. Future directions

There are a number of potential extensions to the research presented in this thesis.

#### 5.1.3.1 Electrical stimulation at different stages of degeneration.

For this thesis, we used degenerating rd10 retina for studying the effects of electrical stimulation on the RGC responses. However, there was a caveat to the present study. The age at which the experiments were performed, the majority of the cones were still viable (all the rod photoreceptor are gone). However, the patients with retinal implants have a bare minimum light perception with loss of the majority of photoreceptors. Additionally, the inner retinal circuitry is heavily rewired (Jones *et al.* 2016). Previous studies have shown that with progressive degeneration there is hyperactivity of the RGC responses (Stasheff 2008). Furthermore, the spontaneous responses tend to be more oscillatory (Ryu, Ye, Lee, Goo, Kim, *et al.* 2009; Goo *et al.* 2016; Park *et al.* 2015; Cho *et al.* 2016; Biswas *et al.* 2014). Therefore, it is necessary that the above-mentioned experiments (Chapter 2-4) need to be performed at different stages of degeneration. Additionally, as most of the visual responses are gone towards the later stages of degeneration, interfacing techniques like calcium imaging and MEA recording would help in better understanding of the retinal rewiring.

Often hyperactivity and oscillatory responses are considered to mask the electrically driven responses. However, recent studies (Ho, Lorach, *et al.* 2018) have shown that on electrically stimulating the degenerated retina, a group of cells had a suppressive effect on electrical stimulation. It would be interesting, to develop stimulation paradigms that would enhance the electrically driven spikes by reducing such hyperactive responses.

### **5.1.3.2 Immunological staining to understand the impact of electrical stimulation**

Many studies (Cohen 2009; Eleftheriou *et al.* 2017) have shown that on electrical stimulation there is an increase in glial scarring measured by the release of Glial Fibrillary Acidic Protein (GFAP). This protein helps in evaluating the integrity of the retinal tissue to electrical stimulation. As in our study, we use high stimulation frequencies to evaluate the RGC responses; it is necessary to visualize how such high pulse rates affect the retinal circuit at the morphological level. One such method is the computational molecular phenotyping (CMP), which profiles the micro-molecules at subcellular resolution (Jones *et al.* 2011; Jones *et al.* 2003). Such CMP profiles along with tracking the diseased state of the retina can also help in identifying the various changes different retinal neurons undergo during electrical stimulation. As our study employed both suprathreshold stimulation and high-frequency stimulation, it is necessary to visualize how such stimulations affect the retinal circuitry.

### **5.1.3.3 Developing a catalogue of electrical response profiles.**

For our study, we could identify only two broad categories of electrical response profiles based on the monotonicity index and the polarity index (Refer to 2.1). Further, using simple full-field flash stimulus, we were able to classify the cells into ON, OFF, and ON-OFF cells. However, a recent study by Baden *et al.* have shown that there are up to 32 different functional RGC types in the retina (Baden *et al.* 2016). Therefore, corresponding to such functional visual types, it is necessary to develop a catalog of electrical response types which would correspond to these visual types. There is a possibility that for electrical stimulations multiple RGC types could combine to give a single electrical output. However, such assumption can only be tested by developing complex electrical stimulus (combining various electrical stimulation parameters into one stimulus) that would target these functional RGC types.

### **5.1.3.4 High-density MEA recording.**

All our experiments were carried out on MEA which had an inter-electrode distance of 200  $\mu\text{m}$ . However, to achieve high resolution, it is necessary to repeat our experiments (primarily the desensitization experiments) on a high-density MEA with closely spaced inter-electrode distances. A previous study (Stett *et al.* 2007b) has shown that a minimum of 100  $\mu\text{m}$  of the inter-electrode is required to resolve between two points (using the electrical point



spread function). However, this study did not consider the aspect of spatial aspect of electrical desensitization, which plays a vital role in the stability of phosphene. Additionally, the study suggests that with increasing amplitudes the inter-electrode distance tend to increase, in order to resolve between two points. Thus, using high-density MEA ( hex-MEA) would shed more light on how close the electrodes can get before maximum desensitization is achieved.

### **5.1.3.5 Working towards cell-specific stimulation**

Considering, this study (thesis) reiterates the need to acknowledge the variability of RGC responses and cell types; it is necessary to develop stimulation paradigms that would selectively target specific RGC types. A recent study from Sekhar *et al.* showed that different visual RGC types have different electrical input filters and these input filters were primarily sinusoidal in shape (Sekhar *et al.* 2017). This knowledge is extremely crucial in designing electrical stimulation paradigm which is specific to a cell type. Furthermore, Twyford *et al.* showed that a specific cell type responds to a single phase of sinusoidal stimulus (Twyford & Fried 2015). Therefore, exploring such stimulation paradigms and perfecting them to interface with the hardware of the retinal implants would be extremely crucial.

## **5.1.4. Concluding remarks**

### **5.1.4.1 How much encoding is required? Brain plasticity and the neural code**

There is an ongoing debate in the field of retinal prosthetics, regarding the necessity to have a complete and accurate restoration of the visual code. Proponents of the subretinal implants argue that an implant providing high visual acuity with sufficient image contrast should be enough to deliver meaningful visual percepts to patients. They hope that as long as the retinotopic map is preserved, by supervised learning, the brain will be capable of adapting and learning the new prosthetic language. On the other hand, the proponents of epiretinal implants argue that for the optimal performance of the implants, complete knowledge of the visual code is necessary to deliver meaningful visual percepts. This debate is likely to continue until each type of implant is tested in patients, and the behavioral performance is carefully assessed.

### **5.1.4.2 Motivation from cochlear implants**

Currently, the field of retinal prosthetics bears a striking resemblance with the field of cochlear implants in the 1970s, during its developmental stage. The clinical performance of

the retinal implants today is at a subpar level and do not justify the broad adoption of the technology in the blind patients. Further, the visual percepts are crude and distorted, just as the percepts elicited by cochlear implants during the stages of development. Currently, the visual neuroscience community looks at the field of the retinal prosthesis with skepticism, and there is arguably no proof today that the retinal implants will elicit better visual percepts than crude phosphenes currently reported by patients. However, one can hope that through collaborative efforts from various research organizations and industry players the field will advance significantly within a few years and drastically improve the quality of life of implanted patients.

## Bibliography

- Abramian, M. *et al.*, 2011. Activation of retinal ganglion cells following epiretinal electrical stimulation with hexagonally arranged bipolar electrodes. *Journal of Neural Engineering*, 8(3), p.35004. Available at: <http://www.ncbi.nlm.nih.gov/pubmed/21593545> [Accessed May 11, 2017].
- Acland, G.M. *et al.*, 2005. Long-Term Restoration of Rod and Cone Vision by Single Dose rAAV-Mediated Gene Transfer to the Retina in a Canine Model of Childhood Blindness. *Molecular Therapy*, 12(6), pp.1072–1082. Available at: <http://www.ncbi.nlm.nih.gov/pubmed/16226919> [Accessed May 10, 2017].
- Adekunle, A.N. *et al.*, 2015. Integration of Perforated Subretinal Prostheses With Retinal Tissue. *Translational vision science & technology*, 4(4), p.5. Available at: <http://www.pubmedcentral.nih.gov/articlerender.fcgi?artid=4539203&tool=pmcentrez&rendertype=abstract>.
- Ahuja, A.K. *et al.*, 2011. Blind subjects implanted with the Argus II retinal prosthesis are able to improve performance in a spatial-motor task. *The British journal of ophthalmology*, 95(4), pp.539–43. Available at: <http://bj.o.bmj.com/cgi/content/abstract/95/4/539>.
- Ahuja, A.K. *et al.*, 2013. Factors Affecting Perceptual Threshold in Argus II Retinal Prosthesis Subjects. *Translational vision science & technology*, 2(4), p.1. Available at: <http://www.pubmedcentral.nih.gov/articlerender.fcgi?artid=3763895&tool=pmcentrez&rendertype=abstract>.
- Ambati, J. & Fowler, B.J., 2012. Mechanisms of age-related macular degeneration. *Neuron*, 75(1), pp.26–39.
- Ayton, L.N. *et al.*, 2014. First-in-human trial of a novel suprachoroidal retinal prosthesis. *PLoS ONE*, 9(12), pp.1–26.
- Baden, T. *et al.*, 2016. The functional diversity of mouse retinal ganglion cells. *Nature*, pp.1–21. Available at: <http://dx.doi.org/10.1038/nature16468>.
- Balkema, W., Pinto, H. & Lafayette, W., 1982. Electrophysiology of Retinal Ganglion Cells in the Mouse : a Study of a Normally Pigmented Mouse and a Congenic Hypopigmentation Mutant , Pearl. , 48(4), pp.17–19.
- Barriga-Rivera, A. *et al.*, 2017. High-amplitude electrical stimulation can reduce elicited neuronal activity in visual prosthesis. *Scientific Reports*, 7, p.42682. Available at: <http://www.ncbi.nlm.nih.gov/pubmed/28209965> [Accessed June 5, 2017].
- Behrend, M.R. *et al.*, 2011. Resolution of the Epiretinal Prosthesis is not Limited by Electrode Size. , 19(4), pp.436–442.
- Bennett, J. *et al.*, 2016. Safety and durability of effect of contralateral-eye administration of AAV2 gene therapy in patients with childhood-onset blindness caused by RPE65 mutations: a follow-on phase 1 trial. *Lancet (London, England)*, 388(10045), pp.661–672. Available at: <http://www.thelancet.com/article/S0140673616303713/fulltext> [Accessed July 12, 2016].
- Bennett, J. and M.A.M., 2013. Retina. In S. J. Ryan, ed. *Gene Therapy for Retinal DisuRetina*. London ;;New York: Saunders, pp. 652–668.
- Biswas, S. *et al.*, 2014. Pharmacological analysis of intrinsic neuronal oscillations in rd10 retina. *PLoS ONE*, 9(6), p.e99075.
- Boinagrov, D. *et al.*, 2014. Selectivity of direct and network-mediated stimulation of the retinal ganglion cells with epi-, sub- and intraretinal electrodes. *Journal of neural engineering*, 11(2), p.26008. Available at:

- 2552/11/i=2/a=026008.
- Bourkiza, B. *et al.*, 2013. Visual Acuity of Simulated Thalamic Visual Prostheses in Normally Sighted Humans. *PLoS ONE*, 8(9).
- Brelén, Må.E. *et al.*, 2005. Creating a meaningful visual perception in blind volunteers by optic nerve stimulation. *Journal of neural engineering*, 2(1), pp.S22-8. Available at: <http://www.ncbi.nlm.nih.gov/pubmed/15876651>.
- Brindley, G.S., 1970. Sensations produced by electrical stimulation of the occipital poles of the cerebral hemispheres, and their use in constructing visual prostheses. *Annals of the Royal College of Surgeons of England*, 47(2), pp.106–108.
- Brown, D.M. *et al.*, 2006. Ranibizumab versus Verteporfin for Neovascular Age-Related Macular Degeneration. *New England Journal of Medicine*, 355(14), pp.1432–1444. Available at: <http://www.ncbi.nlm.nih.gov/pubmed/17021319> [Accessed May 10, 2017].
- Busskamp, V. *et al.*, 2010. Genetic Reactivation of Cone Photoreceptors Restores Visual Responses in Retinitis Pigmentosa. *Science*, 329(5990), pp.413–417. Available at: <http://www.ncbi.nlm.nih.gov/pubmed/20576849> [Accessed May 10, 2017].
- Cai, C., Twyford, P. & Fried, S., 2013. The response of retinal neurons to high-frequency stimulation. *Journal of neural engineering*, 10(3), p.36009. Available at: <http://www.pubmedcentral.nih.gov/articlerender.fcgi?artid=3712762&tool=pmcentrez&rendertype=abstract>.
- Carcieri, S.M., Jacobs, A.L. & Nirenberg, S., 2003. Classification of retinal ganglion cells: a statistical approach. *Journal of neurophysiology*, 90, pp.1704–1713.
- Cho, A. *et al.*, 2016. Changes in ganglion cell physiology during retinal degeneration influence excitability by prosthetic electrodes. *Journal of Neural Engineering*, 13(2), p.25001. Available at: <http://stacks.iop.org/1741-2552/13/i=2/a=025001?key=crossref.48d47d637ce90afc6f51b356e2263961>.
- Cohen, E.D., 2009. Effects of high-level pulse train stimulation on retinal function. *Journal of neural engineering*, 6(3), p.35005.
- da Cruz, L., Coley, B.F., Dorn, J., Merlini, F., Filley, E., Christopher, P., Chen, F.K., Wuyyuru, V., Sahel, J., Stanga, P., Humayun, M., Greenberg, R.J., Dagnelie, G., *et al.*, 2013. The Argus II epiretinal prosthesis system allows letter and word reading and long-term function in patients with profound vision loss. *The British journal of ophthalmology*, 97(5), pp.632–6. Available at: <http://www.ncbi.nlm.nih.gov/pubmed/23426738> [Accessed July 9, 2016].
- da Cruz, L., Coley, B.F., Dorn, J., Merlini, F., Filley, E., Christopher, P., Chen, F.K., Wuyyuru, V., Sahel, J., Stanga, P., Humayun, M., Greenberg, R.J. & Dagnelie, G., 2013. The Argus II epiretinal prosthesis system allows letter and word reading and long-term function in patients with profound vision loss. *The British journal of ophthalmology*, 97(5), pp.632–6. Available at: <http://www.pubmedcentral.nih.gov/articlerender.fcgi?artid=3632967&tool=pmcentrez&rendertype=abstract>.
- Dacey, D., 2004. 20 Origins of Perception: Retinal Ganglion Cell Diversity and the Creation of Parallel Visual Pathways. In M. S. Gazzaniga, ed. *The Cognitive Neurosciences Iii*. MIT Press.
- Dacey, D.M. *et al.*, 2003. Fireworks in the Primate Retina. *Neuron*, 37(1), pp.15–27.
- Dagnelie, G. *et al.*, 2006. Paragraph text reading using a pixelized prosthetic vision simulator: Parameter dependence and task learning in free-viewing conditions. *Investigative Ophthalmology and Visual Science*, 47(3), pp.1241–1250.
- Delbeke, J., Oozeer, M. & Veraart, C., 2003. Position, size and luminosity of phosphenes

- generated by direct optic nerve stimulation. *Vision research*, 43(9), pp.1091–102. Available at: <http://www.ncbi.nlm.nih.gov/pubmed/12676250> [Accessed May 11, 2017].
- Dhande, O.S. & Huberman, A.D., 2014. Visual circuits: Mouse retina no longer a level playing field. *Current Biology*, 24(4), pp.7–11.
- Dobelle, W.H., 1994. Artificial vision for the blind. The summit may be closer than you think. *Asaio J*, 40(4), pp.919–922. Available at: [http://www.ncbi.nlm.nih.gov/entrez/query.fcgi?cmd=Retrieve&db=PubMed&dopt=Citation&list\\_uids=7858325](http://www.ncbi.nlm.nih.gov/entrez/query.fcgi?cmd=Retrieve&db=PubMed&dopt=Citation&list_uids=7858325).
- Dobelle, W.H., Mladejovsky, M.G. & Girvin, J.P., 1974. Artificial vision for the blind: electrical stimulation of visual cortex offers hope for a functional prosthesis. *Science (New York, N.Y.)*, 183(123), pp.440–444.
- Dräger, U.C. & Olsen, J.F., 1981. Ganglion cell distribution in the retina of the mouse. *Investigative ophthalmology & visual science*, 20(3), pp.285–93. Available at: <http://www.ncbi.nlm.nih.gov/pubmed/6162818> [Accessed May 11, 2017].
- Eckhorn, R. *et al.*, 2006. Visual resolution with retinal implants estimated from recordings in cat visual cortex. *Vision Research*, 46(17), pp.2675–2690.
- Eickenscheidt, M. *et al.*, 2012. Electrical stimulation of retinal neurons in epiretinal and subretinal configuration using a multicapacitor array. *Journal of Neurophysiology*, 107(10), pp.2742–2755.
- Eickenscheidt, M. & Zeck, G., 2014. Action potentials in retinal ganglion cells are initiated at the site of maximal curvature of the extracellular potential. *Journal of neural engineering*, 11(3), p.36006. Available at: <http://www.ncbi.nlm.nih.gov/pubmed/24762943>.
- Eleftheriou, C.G. *et al.*, 2017. Carbon nanotube electrodes for retinal implants: A study of structural and functional integration over time. *Biomaterials*, 112, pp.108–121. Available at: <http://www.ncbi.nlm.nih.gov/pubmed/27760395> [Accessed April 18, 2018].
- Farrow, K. & Masland, R.H., 2011. Physiological clustering of visual channels in the mouse retina. *Journal of neurophysiology*, 105(4), pp.1516–1530. Available at: [http://www.ncbi.nlm.nih.gov/entrez/query.fcgi?cmd=Retrieve&db=PubMed&dopt=Citation&list\\_uids=21273316](http://www.ncbi.nlm.nih.gov/entrez/query.fcgi?cmd=Retrieve&db=PubMed&dopt=Citation&list_uids=21273316).
- Fernandes, R.A.B. *et al.*, 2012. Artificial vision through neuronal stimulation. *Neuroscience Letters*, 519(2), pp.122–128. Available at: <http://dx.doi.org/10.1016/j.neulet.2012.01.063>.
- Fernández, E. *et al.*, 2002. Towards a Cortical Visual Neuroprosthesis for the Blind. *Brain*, 3(2), pp.17–18.
- Freeman, D.K., Jeng, J.S., *et al.*, 2011. Calcium channel dynamics limit synaptic release in response to prosthetic stimulation with sinusoidal waveforms. *Journal of neural engineering*, 8(4), p.46005.
- Freeman, D.K. *et al.*, 2010. Selective activation of neuronal targets with sinusoidal electric stimulation. *J Neurophysiol*, 104(5), pp.2778–2791. Available at: <http://www.pubmedcentral.nih.gov/articlerender.fcgi?artid=2997038&tool=pmcentrez&rendertype=abstract>.
- Freeman, D.K. & Fried, S.I., 2011. Multiple components of ganglion cell desensitization in response to prosthetic stimulation. *Journal of neural engineering*, 8, p.16008.
- Freeman, D.K., Rizzo, J.F. & Fried, S.I., 2011. Encoding visual information in retinal ganglion cells with prosthetic stimulation. *Journal of neural engineering*, 8(3), p.35005.
- Fried, S.I. *et al.*, 2009. Axonal sodium-channel bands shape the response to electric stimulation in retinal ganglion cells. *Journal of neurophysiology*, 101(February 2009), pp.1972–1987.

- Fried, S.I., Hsueh, H.A. & Werblin, F.S., 2006. Retinal Spiking Using Prosthetic Stimulation A Method for Generating Precise Temporal Patterns of A Method for Generating Precise Temporal Patterns of Retinal Spiking Using Prosthetic Stimulation. *Journal of Neurophysiology* by guest on. Available at: <http://jn.physiology.org/content/95/2/970.full#ref-list-1> [Accessed July 11, 2016].
- Fujikado, T. *et al.*, 2011. Testing of semichronically implanted retinal prosthesis by suprachoroidal-transretinal stimulation in patients with retinitis pigmentosa. *Investigative Ophthalmology and Visual Science*, 52(7), pp.4726–4733.
- Gargini, C. *et al.*, 2007. Retinal organization in the retinal degeneration 10 (rd10) mutant mouse: A morphological and ERG study. *Journal of Comparative Neurology*, 500(2), pp.222–238.
- Gerhardt, M., Alderman, J. & Stett, A., 2010. Electric Field Stimulation of Bipolar Cells in a Degenerated Retina - A Theoretical Study. *IEEE Trans Neural Syst Rehabil Eng*, p.Jan 12. [Epub ahead of print]. Available at: [http://www.ncbi.nlm.nih.gov/entrez/query.fcgi?cmd=Retrieve&db=PubMed&dopt=Citation&list\\_uids=20071281](http://www.ncbi.nlm.nih.gov/entrez/query.fcgi?cmd=Retrieve&db=PubMed&dopt=Citation&list_uids=20071281).
- Gerwig, R. *et al.*, 2012. PEDOT-CNT Composite Microelectrodes for Recording and Electrostimulation Applications: Fabrication, Morphology, and Electrical Properties. *Frontiers in neuroengineering*, 5(May), p.8. Available at: <http://www.pubmedcentral.nih.gov/articlerender.fcgi?artid=3343311&tool=pmcentrez&rendertype=abstract>.
- Goo, Y.S. *et al.*, 2011a. Retinal ganglion cell responses to voltage and current stimulation in wild-type and rd1 mouse retinas. *J Neural Eng*, 8(3), p.35003. Available at: [http://www.ncbi.nlm.nih.gov/entrez/query.fcgi?cmd=Retrieve&db=PubMed&dopt=Citation&list\\_uids=21593549](http://www.ncbi.nlm.nih.gov/entrez/query.fcgi?cmd=Retrieve&db=PubMed&dopt=Citation&list_uids=21593549) \n[http://iopscience.iop.org/1741-2552/8/3/035003/pdf/1741-2552\\_8\\_3\\_035003.pdf](http://iopscience.iop.org/1741-2552/8/3/035003/pdf/1741-2552_8_3_035003.pdf).
- Goo, Y.S. *et al.*, 2011b. Retinal ganglion cell responses to voltage and current stimulation in wild-type and rd1 mouse retinas. *J Neural Eng*, 8(3), p.35003. Available at: [http://www.ncbi.nlm.nih.gov/entrez/query.fcgi?cmd=Retrieve&db=PubMed&dopt=Citation&list\\_uids=21593549](http://www.ncbi.nlm.nih.gov/entrez/query.fcgi?cmd=Retrieve&db=PubMed&dopt=Citation&list_uids=21593549) \n[http://iopscience.iop.org/1741-2552/8/3/035003/pdf/1741-2552\\_8\\_3\\_035003.pdf](http://iopscience.iop.org/1741-2552/8/3/035003/pdf/1741-2552_8_3_035003.pdf).
- Goo, Y.S. *et al.*, 2016. Spontaneous Oscillatory Rhythms in the Degenerating Mouse Retina Modulate Retinal Ganglion Cell Responses to Electrical Stimulation. *Frontiers in Cellular Neuroscience*, 9(January), pp.1–8. Available at: <http://journal.frontiersin.org/Article/10.3389/fncel.2015.00512/abstract>.
- Grob, S.R. *et al.*, 2016. Clinical Trials in Retinal Dystrophies. *Middle East African journal of ophthalmology*, 23(1), pp.49–59. Available at: <http://www.ncbi.nlm.nih.gov/pubmed/26957839> [Accessed May 10, 2017].
- Grover, S. *et al.*, 2010. Comparison of Retinal Thickness in Normal Eyes Using Stratus and Spectralis Optical Coherence Tomography. *Investigative Ophthalmology & Visual Science*, 51(5), p.2644. Available at: <http://iovs.arvojournals.org/article.aspx?doi=10.1167/iovs.09-4774> [Accessed May 11, 2017].
- Hadjinicolaou, A. *et al.*, 2014. Optimizing the Electrical Stimulation of Retinal Ganglion Cells. *Neural Systems and Rehabilitation Engineering, IEEE Transactions on*, PP(99), p.1. Available at: <http://ieeexplore.ieee.org/ielx7/7333/4359219/06928461.pdf?tp=&arnumber=6928461&isnumber=4359219>.

- Hamel, C., 2006. Retinitis pigmentosa. *Orphanet journal of rare diseases*, 1, p.40. Available at: <http://www.pubmedcentral.nih.gov/articlerender.fcgi?artid=1621055&tool=pmcentrez&rendertype=abstract>.
- Hartong, D.T., Berson, E.L. & Dryja, T.P., 2006. Retinitis pigmentosa. *Lancet*, 368(9549), pp.1795–1809.
- Ho, E., Smith, R., *et al.*, 2018. Spatiotemporal characteristics of retinal response to network-mediated photovoltaic stimulation. *Journal of Neurophysiology*, 119(2), pp.389–400. Available at: <http://www.physiology.org/doi/10.1152/jn.00872.2016> [Accessed April 18, 2018].
- Ho, E., Lorach, H., *et al.*, 2018. Temporal structure in spiking patterns of ganglion cells defines perceptual thresholds in rodents with subretinal prosthesis. *Scientific Reports*, 8(1), p.3145. Available at: <http://www.nature.com/articles/s41598-018-21447-1> [Accessed April 18, 2018].
- Hodgkin, A.L. & Huxley, A.F., A QUANTITATIVE DESCRIPTION OF MEMBRANE CURRENT AND ITS APPLICATION TO CONDUCTION AND EXCITATION IN NERVE. *J. Physiol. (1952) I*, 7, pp.500–544. Available at: <https://www.ncbi.nlm.nih.gov/pmc/articles/PMC1392413/pdf/jphysiol01442-0106.pdf> [Accessed May 10, 2017].
- Humayun, M.S. *et al.*, 2012. Interim results from the international trial of second sight's visual prosthesis. *Ophthalmology*, 119(4), pp.779–788.
- Humayun, M.S. *et al.*, 2003. Visual perception in a blind subject with a chronic microelectronic retinal prosthesis. *Vision Research*, 43(24), pp.2573–2581.
- Im, M. & Fried, S.I., 2015. Indirect activation elicits strong correlations between light and electrical responses in ON but not OFF retinal ganglion cells. *The Journal of Physiology*, 593(16), pp.3577–3596. Available at: <http://doi.wiley.com/10.1113/JP270606>.
- Im, M. & Fried, S.I., 2016. Temporal properties of network-mediated responses to repetitive stimuli are dependent upon retinal ganglion cell type. *Journal of Neural Engineering*, 13(2), p.25002. Available at: <http://stacks.iop.org/1741-2552/13/i=2/a=025002?key=crossref.eee9c91228f81380402dc77a7dadc79c>.
- Jeng, J. *et al.*, 2011. The sodium channel band shapes the response to electric stimulation in retinal ganglion cells. *Journal of neural engineering*, 8(3), p.36022.
- Jensen, R.J. *et al.*, 2003. Thresholds for activation of rabbit retinal ganglion cells with an ultrafine, extracellular microelectrode. *Investigative Ophthalmology and Visual Science*, 44(8), pp.3533–3543.
- Jensen, R.J. & Rizzo, J.F., 2007. Responses of ganglion cells to repetitive electrical stimulation of the retina. *Journal of neural engineering*, 4(1), pp.S1–S6.
- Jensen, R.J., Ziv, O.R. & Rizzo, J.F., 2005. Responses of rabbit retinal ganglion cells to electrical stimulation with an epiretinal electrode. *Journal of neural engineering*, 2(1), pp.S16–S21.
- Jensen, R.J., Ziv, O.R. & Rizzo, J.F., 2005. Thresholds for activation of rabbit retinal ganglion cells with relatively large, extracellular microelectrodes. *Investigative Ophthalmology and Visual Science*, 46(4), pp.1486–1496.
- Jeon, C.J., Strettoi, E. & Masland, R.H., 1998. The major cell populations of the mouse retina. *The Journal of neuroscience : the official journal of the Society for Neuroscience*, 18(21), pp.8936–8946.
- Jepson, L.H. *et al.*, 2013. Focal electrical stimulation of major ganglion cell types in the primate retina for the design of visual prostheses. *The Journal of neuroscience : the*

- official journal of the Society for Neuroscience*, 33(17), pp.7194–7205. Available at: <http://www.ncbi.nlm.nih.gov/pubmed/23616529>.
- Jones, B.W. *et al.*, 2016. Retinal remodeling in human retinitis pigmentosa. *Experimental Eye Research*, 150, pp.149–165. Available at: <http://dx.doi.org/10.1016/j.exer.2016.03.018>.
- Jones, B.W. *et al.*, 2011. Retinal remodeling in the Tg P347L rabbit, a large-eye model of retinal degeneration. *Journal of Comparative Neurology*, 519(14), pp.2713–2733.
- Jones, B.W. *et al.*, 2003. Retinal remodeling triggered by photoreceptor degenerations. *Journal of Comparative Neurology*, 464(1), pp.1–16.
- Kim, I.-J. *et al.*, 2010. Laminar Restriction of Retinal Ganglion Cell Dendrites and Axons: Subtype-Specific Developmental Patterns Revealed with Transgenic Markers. *Journal of Neuroscience*, 30(4), pp.1452–1462. Available at: <http://www.jneurosci.org/cgi/doi/10.1523/JNEUROSCI.4779-09.2010>.
- Koch, C., 2004. *The Quest for Consciousness*, Denver, Colorado: h. Roberts & Publishers.
- Lagali, P.S. *et al.*, 2008. Light-activated channels targeted to ON bipolar cells restore visual function in retinal degeneration. *Nature neuroscience*, 11(6), pp.667–75. Available at: <http://www.ncbi.nlm.nih.gov/pubmed/18432197>.
- LeRoy, C., 1755. O lon rend compte de quelques tentatives que lon a faites pour gurir plusieurs maladies par llectricit. Hist Acad Roy Sciences (Paris). *Mmoire Math Phys*, 95, pp.60–87.
- Leung, R.T. *et al.*, 2015. Safety and efficacy of explanting or replacing suprachoroidal electrode arrays in a feline model. *Clinical and Experimental Ophthalmology*, 43(3), pp.247–258.
- Lewis, P.M. *et al.*, 2015. Restoration of vision in blind individuals using bionic devices: A review with a focus on cortical visual prostheses. *Brain Research*, 1595, pp.51–73. Available at: <http://dx.doi.org/10.1016/j.brainres.2014.11.020>.
- London, A., Benhar, I. & Schwartz, M., 2012. The retina as a window to the brain—from eye research to CNS disorders. *Nature Reviews Neurology*, 9(1), pp.44–53. Available at: <http://www.ncbi.nlm.nih.gov/pubmed/23165340> [Accessed May 10, 2017].
- Lorach, H. *et al.*, 2013. Neural stimulation for visual rehabilitation: Advances and challenges. *Journal of Physiology Paris*, 107(5), pp.421–431. Available at: <http://dx.doi.org/10.1016/j.jphysparis.2012.10.003>.
- Lorach, H. *et al.*, 2015. Performance of photovoltaic arrays in-vivo and characteristics of prosthetic vision in animals with retinal degeneration. *Vision Research*, 111, pp.142–148. Available at: <http://dx.doi.org/10.1016/j.visres.2014.09.007>.
- Loudin, J.D. *et al.*, 2007. Optoelectronic retinal prosthesis: system design and performance. *Journal of neural engineering*, 4(1), pp.S72-84. Available at: <http://iopscience.iop.org/article/10.1088/1741-2560/4/1/S09>.
- MacLaren, R.E. *et al.*, 2006. Retinal repair by transplantation of photoreceptor precursors. *Nature*, 444(7116), pp.203–7.
- Maguire, A.M. *et al.*, 2008. Safety and Efficacy of Gene Transfer for Leber’s Congenital Amaurosis. *New England Journal of Medicine*, 358(21), pp.2240–2248. Available at: <http://www.ncbi.nlm.nih.gov/pubmed/18441370> [Accessed May 10, 2017].
- Mandel, Y. *et al.*, 2013. Cortical responses elicited by photovoltaic subretinal prostheses exhibit similarities to visually evoked potentials. *Nature communications*, 4, p.1980. Available at: [http://www.nature.com/ncomms/2013/130618/ncomms2980/full/ncomms2980.html?WT.ec\\_id=NCOMMS-20130619](http://www.nature.com/ncomms/2013/130618/ncomms2980/full/ncomms2980.html?WT.ec_id=NCOMMS-20130619).



- Mariotti S., 2012. Global Data on Visual Impairments 2010. *World Health Organization*, 20. Available at: <http://>.
- Masland, R.H., 2001. The fundamental plan of the retina. *Nature neuroscience*, 4(9), pp.877–886.
- Mathieson, K. *et al.*, 2012. Photovoltaic retinal prosthesis with high pixel density. *Nature Photonics*, 6(6), pp.391–397.
- Maynard, E.M., Nordhausen, C.T. & Normann, R.A., 1997. The Utah Intracortical Electrode Array: A recording structure for potential brain-computer interfaces. *Electroencephalography and Clinical Neurophysiology*, 102(3), pp.228–239.
- Mazzoni, F., Novelli, E. & Strettoi, E., 2008. Retinal ganglion cells survive and maintain normal dendritic morphology in a mouse model of inherited photoreceptor degeneration. *J Neurosci*, 28(52), pp.14282–14292. Available at: <http://www.ncbi.nlm.nih.gov/pubmed/19109509>.
- Meister, M., Pine, J. & Baylor, D.A., 1994. Multi-neuronal signals from the retina: acquisition and analysis. *Journal of Neuroscience Methods*, 51(1), pp.95–106.
- Nayagam, D.A.X. *et al.*, 2014. Chronic electrical stimulation with a suprachoroidal retinal prosthesis: A preclinical safety and efficacy study. *PLoS ONE*, 9(5).
- Nirenberg, S. & Meister, M., 1997. The light response of retinal ganglion cells is truncated by a displaced amacrine circuit. *Neuron*, 18(4), pp.637–650.
- Nirenberg, S. & Pandarinath, C., 2012. Retinal prosthetic strategy with the capacity to restore normal vision. *Proceedings of the National Academy of Sciences of the United States of America*, 109(37), pp.15012–7. Available at: <http://www.pubmedcentral.nih.gov/articlerender.fcgi?artid=3443127&tool=pmcentrez&rendertype=abstract>.
- Palanker, D. *et al.*, 2004. Migration of retinal cells through a perforated membrane: Implications for a high-resolution prosthesis. *Investigative Ophthalmology and Visual Science*, 45(9), pp.3266–3270.
- Park, D.J., Senok, S.S. & Goo, Y.S., 2015. Degeneration Stage - specific Response Pattern of Retinal Ganglion Cell Spikes in rd10 Mouse Retina. *Annual International Conference of the IEEE Engineering in Medicine and Biology Society.*, 2015, pp.3351–4.
- Perez-Fornos, A. *et al.*, 2012. Temporal properties of visual perception on electrical stimulation of the retina. *Invest Ophthalmol Vis Sci*, 53(6), pp.2720–2731. Available at: <http://www.ncbi.nlm.nih.gov/pubmed/22447863>.
- Pezaris, J.S. & Eskandar, E.N., 2009. Getting signals into the brain: visual prosthetics through thalamic microstimulation. *Neurosurgical focus*, 27(1), p.E6. Available at: <http://www.pubmedcentral.nih.gov/articlerender.fcgi?artid=2848996&tool=pmcentrez&rendertype=abstract>.
- Pezaris, J.S. & Reid, R.C., 2007. Demonstration of artificial visual percepts generated through thalamic microstimulation. *Proceedings of the National Academy of Sciences of the United States of America*, 104(18), pp.7670–5. Available at: <http://www.pubmedcentral.nih.gov/articlerender.fcgi?artid=1863473&tool=pmcentrez&rendertype=abstract>.
- Piccolino, M., 1988. Cajal and the retina: a 100-year retrospective. *Trends in Neurosciences*, 11(12), pp.521–525. Available at: <http://www.sciencedirect.com/science/article/pii/0166223688901750> [Accessed May 10, 2017].
- Resnikoff, S. *et al.*, 2004. Policy and Practice. *Bulletin of the World Health Organization*, 82(11), pp.844–851. Available at:

<http://eutils.ncbi.nlm.nih.gov/entrez/eutils/elink.fcgi?dbfrom=pubmed&id=15640920&retmode=ref&cmd=prlinks\papers2://publication/uuid/BAA31E85-D8BD-4CD4-A484-651963213B14>.

- Rodieck, R.W., 1998. *The First Steps in Seeing First.*, Sunderland, Massachusetts: Sinauer Associates, Inc. Available at: <http://www.sinauer.com/the-first-steps-in-seeing.html>.
- Rothermel, A. *et al.*, 2009. A CMOS chip with active pixel array and specific test features for subretinal implantation. *IEEE Journal of Solid-State Circuits*, 44(1), pp.290–300.
- Ryu, S.B., Ye, J.H., Lee, J.S., Goo, Y.S. & Kim, K.H., 2009. Characterization of retinal ganglion cell activities evoked by temporally patterned electrical stimulation for the development of stimulus encoding strategies for retinal implants. *Brain Research*, 1275, pp.33–42. Available at: <http://dx.doi.org/10.1016/j.brainres.2009.03.064>.
- Ryu, S.B. *et al.*, 2010. Decoding of retinal ganglion cell spike trains evoked by temporally patterned electrical stimulation. *Brain Research*, 1348, pp.71–83. Available at: <http://dx.doi.org/10.1016/j.brainres.2010.06.044>.
- Ryu, S.B., Ye, J.H., Lee, J.S., Goo, Y.S., Kim, C.H., *et al.*, 2009. Electrically-evoked neural activities of rd1 mice retinal ganglion cells by repetitive pulse stimulation. *Korean Journal of Physiology and Pharmacology*, 13(6), pp.443–448.
- Sakaguchi, H. *et al.*, 2004. Transretinal electrical stimulation with a suprachoroidal multichannel electrode in rabbit eyes. *Japanese Journal of Ophthalmology*, 48(3), pp.256–261.
- Schatz, A. *et al.*, 2011. Transcorneal Electrical Stimulation for Patients with Retinitis Pigmentosa: A Prospective, Randomized, Sham-Controlled Exploratory Study. *Investigative Ophthalmology & Visual Science*, 52(7), p.4485. Available at: <http://iovs.arvojournals.org/article.aspx?doi=10.1167/iovs.10-6932>.
- Schwartz, S.D. *et al.*, 2015. Human embryonic stem cell-derived retinal pigment epithelium in patients with age-related macular degeneration and Stargardt's macular dystrophy: Follow-up of two open-label phase 1/2 studies. *The Lancet*, 385(9967), pp.509–516. Available at: [http://dx.doi.org/10.1016/S0140-6736\(14\)61376-3](http://dx.doi.org/10.1016/S0140-6736(14)61376-3).
- Sekhar, S. *et al.*, 2017. Correspondence between visual and electrical input filters of on and off mouse retinal ganglion cells. *Journal of Neural Engineering*, 14(4).
- Sekirnjak, C. *et al.*, 2006. Electrical stimulation of mammalian retinal ganglion cells with multielectrode arrays. *J Neurophysiol*, 95(6), pp.3311–3327. Available at: <http://www.ncbi.nlm.nih.gov/pubmed/16436479>.
- Shivdasani, M.N. *et al.*, 2014. Factors affecting perceptual thresholds in a suprachoroidal retinal prosthesis. *Investigative Ophthalmology and Visual Science*, 55(10), pp.6467–6481.
- Srivastava, N.R., Troyk, P.R. & Dagnelie, G., 2009. Detection, eye-hand coordination and virtual mobility performance in simulated vision for a cortical visual prosthesis device. *Journal of neural engineering*, 6(3), p.35008. Available at: <http://www.pubmedcentral.nih.gov/articlerender.fcgi?artid=3902177&tool=pmcentrez&rendertype=abstract>.
- Stasheff, S.F., 2008. Emergence of sustained spontaneous hyperactivity and temporary preservation of OFF responses in ganglion cells of the retinal degeneration (rd1) mouse. *Journal of neurophysiology*, 99(3), pp.1408–1421. Available at: <http://jn.physiology.org/content/99/3/1408\http://jn.physiology.org/cgi/doi/10.1152/jn.0144.2007>.
- Stasheff, S.F., Shankar, M. & Andrews, M.P., 2011. Developmental time course distinguishes changes in spontaneous and light-evoked retinal ganglion cell activity in rd1 and rd10

- mice. *Journal of neurophysiology*, 105(6), pp.3002–3009. Available at: <http://jn.physiology.org/content/105/6/3002.abstract>.
- Stett, A. *et al.*, 2000. Electrical multisite stimulation of the isolated chicken retina. *Vision Research*, 40(13), pp.1785–1795.
- Stett, A., Mai, A. & Herrmann, T., 2007a. Retinal charge sensitivity and spatial discrimination obtainable by subretinal implants: key lessons learned from isolated chicken retina. *Journal of neural engineering*, 4(March 2016), pp.S7–S16.
- Stett, A., Mai, A. & Herrmann, T., 2007b. Retinal charge sensitivity and spatial discrimination obtainable by subretinal implants: key lessons learned from isolated chicken retina. *Journal of neural engineering*, 4, pp.S7–S16.
- Stingl, K., Bartz-Schmidt, K.U., *et al.*, 2013. Artificial vision with wirelessly powered subretinal electronic implant alpha-IMS. *Proceedings. Biological sciences / The Royal Society*, 280(1757), p.20130077. Available at: <http://www.pubmedcentral.nih.gov/articlerender.fcgi?artid=3619489&tool=pmcentrez&rendertype=abstract>.
- Stingl, K., Bartz, K.U.S., *et al.*, 2013. Functional outcome in subretinal electronic implants depends on foveal eccentricity. *Investigative Ophthalmology and Visual Science*, 54(12), pp.7658–7665.
- Stingl, K. *et al.*, 2017. Interim Results of a Multicenter Trial with the New Electronic Subretinal Implant Alpha AMS in 15 Patients Blind from Inherited Retinal Degenerations. *Frontiers in Neuroscience*, 11, p.445. Available at: <http://www.ncbi.nlm.nih.gov/pubmed/28878616> [Accessed April 18, 2018].
- Stingl, K., Bach, M., *et al.*, 2013. Safety and efficacy of subretinal visual implants in humans: Methodological aspects. *Clinical and Experimental Optometry*, 96(1), pp.4–13.
- Stingl, K. *et al.*, 2015. Subretinal Visual Implant Alpha IMS - Clinical trial interim report. *Vision Research*, 111(March), pp.149–160. Available at: <http://dx.doi.org/10.1016/j.visres.2015.03.001>.
- Stingl, K. & Zrenner, E., 2013. Electronic approaches to reconstitute vision in patients with neurodegenerative diseases of the retina. *Ophthalmic Research*, 50(4), pp.215–220.
- Sümbül, U. *et al.*, 2014. A genetic and computational approach to structurally classify neuronal types. *Nature communications*, 5, p.3512. Available at: <http://www.nature.com/ncomms/2014/140324/ncomms4512/full/ncomms4512.html>.
- Tao, Y. *et al.*, 2016. The transcorneal electrical stimulation as a novel therapeutic strategy against retinal and optic neuropathy: a review of experimental and clinical trials. *International journal of ophthalmology*, 9(6), pp.914–9. Available at: <http://www.ncbi.nlm.nih.gov/pubmed/27366697> [Accessed May 10, 2017].
- TASSICKER, G.E., 1956. Preliminary report on a retinal stimulator. *The British journal of physiological optics*, 13(2), pp.102–5. Available at: <http://www.ncbi.nlm.nih.gov/pubmed/13315967> [Accessed May 11, 2017].
- Tehovnik, E.J. *et al.*, 2006. Direct and indirect activation of cortical neurons by electrical microstimulation. *Journal of neurophysiology*, 96(2), pp.512–21. Available at: <http://jn.physiology.org/content/96/2/512.abstract>.
- Thoreson, W.B., Babai, N. & Bartoletti, T.M., 2008. Feedback from horizontal cells to rod photoreceptors in vertebrate retina. *The Journal of neuroscience: the official journal of the Society for Neuroscience*, 28(22), pp.5691–5. Available at: <http://www.ncbi.nlm.nih.gov/pubmed/18509030> [Accessed May 10, 2017].
- Tsai, D. *et al.*, 2012. Responses of Retinal Ganglion Cells to Extracellular Electrical Stimulation, from Single Cell to Population: Model-Based Analysis S. Barnes, ed. *PLoS*

- ONE*, 7(12), p.e53357. Available at: <http://dx.plos.org/10.1371/journal.pone.0053357> [Accessed May 11, 2017].
- Twyford, P., Cai, C. & Fried, S., 2014. Differential responses to high-frequency electrical stimulation in ON and OFF retinal ganglion cells. *Journal of neural engineering*, 11(2), p.25001. Available at: <http://www.ncbi.nlm.nih.gov/pubmed/24556536>.
- Twyford, P. & Fried, S., 2015. The Retinal Response to Sinusoidal Electrical Stimulation. *IEEE Transactions on Neural Systems and Rehabilitation Engineering*, 4320(c), pp.1–1. Available at: <http://ieeexplore.ieee.org/lpdocs/epic03/wrapper.htm?arnumber=7078925>.
- Veraart, C. *et al.*, 2003. Pattern recognition with the optic nerve visual prosthesis. *Artificial organs*, 27(11), pp.996–1004. Available at: <http://www.ncbi.nlm.nih.gov/pubmed/14616518> [Accessed May 11, 2017].
- Veraart, C. *et al.*, 1998. Visual sensations produced by optic nerve stimulation using an implanted self-sizing spiral cuff electrode. *Brain research*, 813(1), pp.181–6. Available at: <http://www.ncbi.nlm.nih.gov/pubmed/9824694> [Accessed May 11, 2017].
- Wang, D.Y. *et al.*, 2005. Gene mutations in retinitis pigmentosa and their clinical implications. *Clinica Chimica Acta*, 351(1–2), pp.5–16. Available at: <http://www.ncbi.nlm.nih.gov/pubmed/15563868> [Accessed May 10, 2017].
- Wilke, R. *et al.*, 2016. Spatial Resolution and Perception of Patterns Mediated by a Subretinal 16-Electrode Array in Patients Blinded by Hereditary Retinal Dystrophies. , (1), pp.5995–6003.
- Wilke, R. *et al.*, 2011. Spatial resolution and perception of patterns mediated by a subretinal 16-electrode array in patients blinded by hereditary retinal dystrophies. *Investigative Ophthalmology and Visual Science*, 52(8), pp.5995–6003.
- Xiao, L. *et al.*, 2014. Effects of dopamine on response properties of ON-OFF RGCs in encoding stimulus durations. *Frontiers in Neural Circuits*, 8, p.72. Available at: <http://journal.frontiersin.org/article/10.3389/fncir.2014.00072/abstract> [Accessed March 21, 2018].
- Yue, L. *et al.*, 2016. Retinal stimulation strategies to restore vision: Fundamentals and systems. *Progress in Retinal and Eye Research*, 53, pp.21–47. Available at: <http://dx.doi.org/10.1016/j.preteyeres.2016.05.002>.
- Yue, L. *et al.*, 2015. Ten-year follow-up of a blind patient chronically implanted with epiretinal prosthesis argus i. *Ophthalmology*, 122(12), p.2545–2552e1. Available at: <http://dx.doi.org/10.1016/j.optha.2015.08.008>.
- Zhang, Y. *et al.*, 2012. PNAS Plus: The most numerous ganglion cell type of the mouse retina is a selective feature detector. *Proceedings of the National Academy of Sciences*, 109(36), pp.E2391–E2398.
- Zrenner, E., 2012. Artificial vision: Solar cells for the blind. *Nature Photonics*, 6(6), pp.344–345. Available at: <http://www.nature.com/doi/10.1038/nphoton.2012.114>.
- Zrenner, E., 2013. Fighting blindness with microelectronics. *Science translational medicine*, 5(210), p.210ps16. Available at: <http://www.ncbi.nlm.nih.gov/pubmed/24197733>.
- Zrenner, E. *et al.*, 2011. Subretinal electronic chips allow blind patients to read letters and combine them to words. *Proceedings. Biological sciences / The Royal Society*, 278(1711), pp.1489–97. Available at: <http://www.pubmedcentral.nih.gov/articlerender.fcgi?artid=3081743&tool=pmcentrez&rendertype=abstract>.



## **Appendix**

**Appendix I –Chapter 3 /Publication 2**

**Appendix II–Chapter 4 /Publication 3**

## **Appendix I- Chapter 3/ Publication 2**

# **TITLE: Adaptation of visual responses in degenerating and healthy mice retinas during ongoing electrical stimulation.**

**PREPARED FOR:** Neurosignals

**AUTHORS:** Archana Jalligampala<sup>1-3\*</sup>, Eberhart Zrenner<sup>1,2,4</sup>, Daniel L. Rathbun<sup>1,2,4\*</sup>

\*Corresponding Authors: Archana Jalligampala [archana.jalligampala09@gmail.com](mailto:archana.jalligampala09@gmail.com), Daniel L. Rathbun [daniel.rathbun@uni-tuebingen.de](mailto:daniel.rathbun@uni-tuebingen.de)

## **Affiliations:**

<sup>1</sup> Institute for Ophthalmic Research, Eberhard Karls University, D-72076 Tübingen, Germany

<sup>2</sup> Werner Reichardt Centre for Integrative Neuroscience [CIN], D-72076 Tübingen, Germany

<sup>3</sup> Graduate Training Center of Neuroscience/International Max Planck Research School, D-72074 Tübingen, Germany

<sup>4</sup> Bernstein Center for Computational Neuroscience Tübingen, D-72076 Tübingen, Germany

## **Funding & Acknowledgements:**

This study was supported by the Werner Reichardt Centre for Integrative Neuroscience [CIN] at the Eberhard-Karls University of Tübingen. The CIN is an Excellence Cluster funded by the Deutsche Forschungsgemeinschaft [DFG] within the framework of the Excellence Initiative [**EXC307**, including the senior professorship of Prof. Eberhart Zrenner and **PP 2011-07 & 2013-04** to DLR]. This study is also part of the research program of the Bernstein Center for Computational Neuroscience, Tuebingen, funded by the German Federal Ministry of Education and Research [BMBF, **01GQ1002 & 031A308**]. Additional funding was provided by the Tistou and Charlotte Kerstan Foundation [to AJ & DLR], the German Ophthalmology Society [DOG, to AJ], and PRO RETINA Germany foundation for prevention of blindness [to AJ].

The authors would especially like to thank Professor Thomas Euler and his laboratory for their guidance and support. We thank Mrs. Regina Ebenhoch for expert graphics



support The authors gratefully acknowledge the technical assistance of Kludija Masarini and Norman Rieger. In particular, DLR thanks Prof. Euler for his selfless mentorship, Dr. Tobias Breuninger for his work in setting up the optical pathway used in these experiments. Finally, we thank Professor Shelley Fried for many helpful discussions and his unwavering enthusiasm for this research.

**Competing Financial Interests:**

None

**Disclosure:**

A part of the finding reported in this article was initially presented at IEEE NER 2015 (April 20-24), Montpellier, France and has been published as a conference proceeding and is reused with permission, from. “Jalligampala A, Zrenner E, Rathbun DL. Electrical stimulation alters light responses of mouse retinal ganglion cells”*International Ieee/Embs Conference On Neural Engineering, Ner.* 2015: 675-678. DOI: 10.1109/NER.2015.7146713

**Author Contributions:**

AJ & DLR designed the experiments. AJ performed the experiments. AJ & DLR conducted the analysis. AJ prepared the draft of the manuscript. EZ & DLR provided critical feedback to the manuscript.

## Abstract

*Objective:* Over the years, the visual neuroscience community, has achieved a deeper understanding of the various aspects of visual adaptation and cell-classification. Recent studies have that there are up to 32 different types of functional retinal ganglion cell (RGC) types. Likewise, the field of a retinal prosthesis is increasing its understanding for electrical adaptation (like desensitization) and cell-specific stimulation. However, very little is known about the interaction of visual and electrical stimulation. As a first step to understanding such complex interaction, we evaluated the effect of electrical stimulation on the visual response parameters.

*Methods/Approach:* Using full-field flash visual stimulus, we characterized various visual response parameters using micro-electrode array (MEA) in healthy and degenerating *rd10* retinas, and evaluated the visual response changes to the monophasic voltage controlled pulses.

*Main Results:* Apart from the time invitro and the adaptation effects occurring due to visual stimulation, the electrical stimulation strengthens the visual responses.

*Significance:* Encoding of visual stimuli by retinal prosthetic devices may require the consideration of stimulation-induced changes in the retina.

**Keywords:** MEA, electrical stimulation, response changes, latency, duration, ON/OFF index.

## Introduction

The issue of characterizing the retinal ganglion cells (RGCs) based on their morphological types or the functional types has been a long-standing debate in the field of visual neuroscience. While the morphological types of RGCs are slowly being identified based on molecular markers[cite], there has been a growing body of literature to understand the various functional types of RGCs.

Over the past century, many luminaries like Ramón y Cajal, Hartline, Barlow, & Kuffler, Lettvin, Hubel, and Wiesel have collectively contributed to today's understanding of the information processing via the visual system (Kuffler 1953; Rodieck & Stone 1965; Hubel & Wiesel 1998; Hartline 1938; BARLOW 1953; Lettvin *et al.* 1959.) One such profound concept being the discovery of the visual receptive field (RF). The idea of RF was first introduced by Weber in 1846 in context of tactile stimulation (Weber 1846). Weber proposed a confined area known as sensory circles, a region over which the neuron was responsive to stimulation.

The history of visual RF can be traced back to 1938, from the works of Hartline, who found that by stimulating a small circular area in the retina one could elicit an excitatory response in the optic nerve fiber of the frog (Hartline 1938). He termed this area as the visual RF. Based on the responses, he classified the fibers as *on*, *on-off* and *off*, which corresponded to response to light on, the second to both light on and light off and third to light off. In 1953, Barlow and Kuffler established the lateral inhibition in the frog and cat eye's respectively, by discovering the antagonistic center-surround organization of the RF ( Barlow 1953, Kuffler 1953). Kuffler further classified the RF as *on-center RF* (center stimulated by light) and *off-center RF* (center stimulated by dark). Furthermore, they extended this work to classify these RF as *sustained* and *transient* based on the stimulus size and state of adaptation. Shortly after that, Lettvin and Hubel & Wiesel in their iconic work classified the visual RF selective to different complex features (such as—shape, size, orientation, the position of the stimulus relative to the background, movement, and ocularity; Letvinn 1959, Hubel & Wiesel 1959). A

recent study in mice retina by Baden and co-workers (Baden *et al.* 2016) have shown that there are at least 40 different physiological types of retinal output channels.

Recent studies (Sekhar *et al.* 2017; Ho *et al.* 2018) in the field of the retinal prosthesis have shown that different RGC types have different electrical input filters, suggesting the possibility for cell-specific stimulation.

Apart from cell classification, there is a growing body of literature illuminating the various visual adaptations occurring in the retina (Tikidji-Hamburyan *et al.* 2017; Tikidji-Hamburyan *et al.* 2015; Baccus & Meister 2002; Demb 2002). While many studies have investigated visual adaptation and electrical adaptation (Freeman & Fried 2011) independently, little is known about the complex interaction between the two mechanisms. A recent study (Kara *et al.* 2002) investigated the interaction of electrical stimulation and visual stimulation on the spatial receptive field in the thalamus. They observed that in comparison to the spatial receptive of visual stimulation, the spatial receptive field for electrical stimulation was elongated suggesting a complex interaction between the two.

In this study, using full-field flash stimulus, we characterize the cell's visual response parameters and evaluate how these responses change post electrical stimulation with voltage controlled pulses.

## Materials and Methods

### *Experimental Design*

In a previous study from our group (Jalligampala *et al.* 2017), we established an experimental and analysis framework, by which one could identify the optimal stimulus paradigms that will activate a majority of retinal neurons (RGCs) via epiretinal network stimulation. This stimulus was optimal for 'blind' experiments where the specific response properties for each cell was unknown. During the entire duration of the experiment, six visual stimulus blocks of full-field 'flash' stimulus were applied to monitor the stability of RGC responses. These visual blocks were interleaved before, after and within each electrical stimulation block spanning ~80 minutes of the entire

recording time **Fig. 1(a)**. Apart from monitoring the stability of the RGC responses, the visual stimulus provided us with an opportunity to classify the cells into different physiological cell types based on their response to the visual stimulus. In our previous study, we pooled all the RGCs and did not distinguish them into different physiological cell types. However, in this study, we attempted to classify them into different response types and understand how various visual response parameters (*refer to Data Analysis*) change during ongoing electrical stimulation. For this study, the primary dataset came from the previous study (*Jalligampala et al. 2017*). To test our hypothesis if ongoing electrical stimulation alters the visual response parameters in healthy and degenerating mouse retinas, we compared the visual response changes (*refer to Data Analysis, Visual response changes*) between the test and control conditions (*refer to Test and control conditions*). Details of the test and control conditions (their corresponding cell counts) and the test comparisons are described below.

### ***Test and control conditions***

*Test Condition-* The test condition was the visual response parameters obtained from RGCs which were responsive to electrical stimulation (see *Jalligampala et al. 2017. Data Analysis, Responsive RGC inclusion criteria*). Briefly, for a cell to be classified as electrically responsive, 1) at least three of the 96 responses (corresponding to the 96 unique electrical stimuli, **Fig. 1(a)**) was greater than two standard deviations (SD) above the average spontaneous rate (*threshold*). 2) such responses had a high enough firing rate equivalent to at least 8.89 Hz (at least four spikes within the 5 x 90 ms integration windows of that stimulus). An additional inclusion criterion was included for the data set. Because electrical field strength falls with increasing inter-electrode distance from the stimulating electrode—it was inappropriate for us to group the cells recorded at vastly different distances. Therefore only responses from cells recorded at the 8 electrodes surrounding the stimulating electrode (a distance of 200 $\mu$ m and 283 $\mu$ m) were included in the test condition. As these cells were near to the stimulating electrode (in red) **Fig. 1(b, left panel)** and were electrically responsive they were termed as nearby-responsive (NEARBY-R).

*Control Conditions-* We compared the test condition to two different control conditions.

- 1) Internal control condition- As an internal control condition, we considered cells which were electrically nonresponsive, i.e., cells which were not well-driven by the electrical stimulation in the same recording (tissue) and were at an inter-electrode distance  $>300\mu\text{m}$  from the stimulating electrode. The advantage of the internal control condition was that the responses from these cells were from the same tissue. Hence the factor of tissue variability is minimal. However, there is a caveat to this control condition. Although these cells did not have robust electrical responses, it is known the electrical responses can extend as far as  $800\mu\text{m}$  from the stimulating electrode (Eickenscheidt *et al.* 2012; Ryu *et al.* 2009; Stett *et al.* 2007, Jalligampala *et al.* 2017, Wilke *et al.* 2011), thereby providing a small chance to respond to electrical stimulation. As these cells included responses from a vastly different distance ( $>300\mu\text{m}$ ) and were electrically non-responsive hence they were termed as distant-non-responsive (DISTANT-NR, **Fig. 1(b) middle panel**)
- 2) External control condition- A more appropriate control condition to strengthen our hypothesis, was to stimulate the retinal tissue with only visual stimulus in the absence of any electrical stimulation. Further, the visual stimulus was provided at the same time point in the protocol (i.e., the same time point in the protocol which included both electrical and visual stimulation, **Fig. 1(a)**). Recording at the same time point would account for any *invitro* changes occurring during the recording. An advantage of this control condition was that the retinal tissue was not electrically stimulated, hence providing a better comparison to the test condition. However, a caveat to this condition is that there could be some inter-tissue variability. As these cells were only visually responsive and recorded from all 59 electrodes, they were termed as visual-only responsive (VISUAL-OR, **Fig. 1(b) right panel**)

Therefore, comparing the test condition to the above two control conditions can account for the potential caveats and can provide a more meaningful comparison.

### ***Animals***

The animals were housed under standard white cyclic lighting, mimicking regular daily rhythms. They had free and ample access to food and water. Adult wild-type C57Bl/6J (Jackson Laboratory, Bar Harbor, ME, USA) and *rd10* (on a C57Bl/6J background;

Jackson Laboratory) strains were used, with age ranging from post-natal day 28 to 35 for both strains. For each strain, three male and two female mice were used. For external control, condition age-matched mice were used for both strains. For each strain of the control mice, two male mice were used. All procedures were approved by the Tübingen University committee on animal protection (Einrichtung für Tierschutz, Tierärztlichen Dienst und Labortierkunde directed by Dr. Franz Iglauer) and performed by the Association for Research in Vision and Ophthalmology (ARVO) statement for the use of animals in ophthalmic and visual research. All efforts were made to minimize the suffering and usage of number of animals.

### ***Retinal preparation***

For dissecting the retina, the mice were anesthetized by CO<sub>2</sub> inhalation. Following CO<sub>2</sub> inhalation, the mice were checked for absence of withdrawal reflex by pinching the between-toe tissue and then euthanized by cervical dislocation. Under normal room lighting, the eyes were removed to carbogenated (95% O<sub>2</sub> and 5% CO<sub>2</sub>) artificial cerebrospinal fluid (ACSF) solution containing the following (in mM): 125 NaCl, 2.5 KCl, 2 CaCl<sub>2</sub>, 1 MgCl<sub>2</sub>, 1.25 NaH<sub>2</sub>PO<sub>4</sub>, 26 NaHCO<sub>3</sub> and 20 Glucose, pH 7.4. For each eye, the cornea, ora serrata, lens and vitreous body were removed, the retina was detached from the pigment epithelium, and the optic nerve was cut at the base of the retina. Special care was taken to remove all traces of vitreous material from the inner surface of the retina to optimize contact between the nerve fiber layer and recording electrodes. The retinas were maintained in carbogenated ACSF until needed. For recording, a retinal half was mounted with the ganglion cell layer down on a planar multielectrode array (MEA). Two small paint brushes were used to orient and flatten the retinal half without risking damage to the MEA. A dialysis membrane (Cellu Sep, Membrane Filtration Products Inc., Seguin, Texas, USA) mounted on a custom Teflon ring was lowered onto the retina to press it into closer contact with the MEA (Meister *et al.* 1994). After securing the MEA under the preamplifier, the retina was continuously superfused with carbogenated ACSF (~6 ml/min) maintained at 33° C using both a heating plate and a heated perfusion cannula (HE-Inv-8 & PH01; Multi Channel Systems, Reutlingen, Germany). A stabilization time of >30 minutes was provided prior to recording the data.

### ***Microelectrode array (MEA) and Data acquisition***

For recording the spiking responses from the RGCs, a planar MEA containing 59 circular titanium nitride electrodes (diameter: 30 $\mu$ m, interelectrode spacing: 200 $\mu$ m; Multi Channel Systems, Reutlingen, Germany) arrayed in an 8X8 rectilinear grid layout, and with Indium tin oxide (ITO) electrode tracks insulated by Silicon Nitride (Si<sub>3</sub>N<sub>4</sub>) on a glass substrate was used. Four electrodes were absent from the four corners of the grid, and one electrode was substituted with a large reference electrode. The impedances of the electrodes were approximately 200-250k $\Omega$  at 1 kHz, measured using a NanoZ impedance meter (Plexon Inc., TX, USA) in saline water. The MEA60 system (MCS, Reutlingen, Germany) was used for data acquisition including: the RS-232 interface, a 60 channel preamplifier with integrated filters and a blanking circuit (MEA 1060-Inv-BC) controlled by MEA\_Select software to reduce recording noise by grounding any defective electrodes and to assign electrical stimulation waveforms to the selected electrode. Data were collected using the MC\_Rack program on a personal computer running Windows XP and fitted with MC\_Card data acquisition hardware and an analog input card to record stimulus trigger signals. The raw data were recorded at a rate of 50 kHz/channel with a filter bandwidth ranging from 1 Hz - 3 kHz and amplification gain of 1100.

### ***Electrical Stimulation***

A detailed description of the electrical stimulation is provided in our previous study (*see Stimulation section, Material and Methods Jalligampala et al. 2017*). Briefly, the stimulus pulses were generated using a stimulus generator (STG 2008, Multi Channel Systems, Reutlingen, Germany) and delivered from the ganglion cell side of the retina (epiretinally) via one of the 59 electrodes – which was always an interior electrode and chosen based on proximity to electrodes with robust neural signals to ensure a maximum number of recorded neurons. As the retinal network can be activated from either side of the retina by reversing the polarity of stimulation (Im & Fried 2015; Boinagrov *et al.* 2014, Eickenscheidt *et al.* 2012), due the ease of accessing the retina, the electrodes of the MEA were used to simultaneously stimulate and record from the ganglion cell (epiretinal) side of the flat-mounted retina. The stimulus(**Fig. 1(a), left panel**) consisted of monophasic rectangular voltage pulses, each with one of the



following amplitudes (0.3, 0.5, 1.0, 1.5, 2.0, 2.5 V) and durations (60, 100, 200, 300, 500, 1000, 2000, 3000, 5000  $\mu$ s). To reduce the possibility of electrolysis and electrode degradation only voltage/duration combinations that fell within safety, limits were delivered (Microelectrode Array (MEA) Manual 2010). Additionally, to explore any particular preference of the cells to pulse polarity, we included both cathodic (-V) and anodic (+V) stimuli. Within each increasing voltage block, the durations were presented in 5 sequential, uniquely randomized sets, for a total of 5 repetitions for each voltage/duration combination, with an interval of 5 s after each pulse to allow the recovery of RGC responsiveness. Additionally, for each experiment, the beginning polarity was randomly chosen and alternated with subsequent blocks after that. Before and after each stimulation block, spontaneous activity was recorded for ~30 seconds.

### ***Visual stimulation***

Visual stimuli were presented to the retina from below through the transparent MEA by a commercially available DLP-based projector (K10; Acer Inc., San Jose, California, USA). The image was focused and centered onto the plane of the retina directly over the MEA with a custom-built series of optical components and manual microdrive with 3 degrees of freedom. Visual stimuli were controlled with custom software. Each visual stimulus block consisted of a full-field (~3 x 4 millimeters) 'flash' stimulus, cycling 2 seconds ON( 40 klx) followed by 2 seconds OFF (20 lux), 20 times without pause (mean illuminance = 20 klx, 99.9% Michelson contrast, **Fig. 1(a), right panel**). The brightness range chosen covered a wide range of intensities occurring in the natural environment (*Rodieck* 1998). The six visual stimulus blocks were interleaved before, after, and within an electrical stimulation experiment that spanned ~80 minutes of recording time, including the first and last flash blocks.

### ***Data processing and Inclusion criteria***

Commercial spike sorting software was used to process the raw data (Offline Sorter, Plexon Inc., TX, USA). Raw voltage traces (data from both electrical and visual stimulation) were first filtered (using low-cut, 12 point Bessel filter at 51 Hz to exclude line noise); then putative events were detected using a threshold crossing method (4

standard deviations below the mean of the amplitude histogram). These events were sorted into clusters with an automated routine (Standard Expectation Maximization) to assign noise events as well as spiking events from up to 10 cells recorded on each electrode to separate units. Finally, as a quality control step, multiple sorting solutions were manually inspected to identify the best solution and to occasionally modify this solution to minimize Type I and Type II errors in the attribution of events to different sources (Sekhar *et al.* 2016). Units were only judged to contain the spike train from a single RGC and considered for the analysis presented here if they: 1) had a clear lock-out period in the ISI histogram and autocorrelogram. 2) absence of a peak in the cross-correlogram between different cells which would indicate that a single cell had been incorrectly split into 2 or more units. 3) good separation in principal component space of a biphasic waveform whose shape is typical of extracellularly recorded action potentials, and 4) stability of the waveform shape and firing rate over the entire experiment. Time stamps of these sorted spikes were collected with NeuroExplorer (Plexon Inc, TX, USA) and exported to MATLAB for further analysis. Accordingly, a total of 2078 WT cells (16 retinal halves) and 1880 *rd10* cells (9 retinal halves) were included in our dataset (containing cells for test condition and internal control condition). For external control condition, a total of 366 WT cells (3 retinal halves) and 573 *rd10* cells (3 retinal halves) were included post data processing. A detailed description of the cell count for electrically responsive cells and visually responsive cells for the test and control conditions are provided in **Table 1**.

### ***Data Analysis***

***Determining the visual response parameters:*** For each visual block of 20 repetitions, the responses were quantified according to the methods of Carciari *et al.* (Carciari *et al.* 2003) **Fig 1. (c)**. Briefly, a mean post-stimulus time histogram (PSTH) was generated by aligning each of the 20, 4-s responses, at a ten-millisecond binning resolution and averaging firing rates across all 20 repetitions. The PSTH was smoothed with a Gaussian filter of  $\sigma = 50$  milliseconds. To compensate for cells with high firing rates, a baseline firing rate and corresponding SD were calculated for each cell by averaging the firing rates during the last 250 milliseconds of each response phase (ON

and OFF, 40 samples per 20-cycle stimulus block). The peak firing rate of each phase ( $A_1$  and  $A_2$ ) was identified to determine peak latency ( $Tp_1$  and  $Tp_2$ ) and amplitude ( $A_1$  and  $A_2$ ). The duration/ transience of each response phase ( $D_1$  and  $D_2$ ) was defined as the time over which the responses fall from peak firing rate ( $A$ ) to  $A/e$  over baseline (i.e.,  $A_1$  to  $A_1/e$  and  $A_2$  to  $A_2/e$ ). Amplitude, latency, and duration of response were excluded from analysis if the amplitude did not exceed baseline firing rate + 2SD. Additionally, care was taken to remove any nonsignificant peaks arising from noisy data or ‘false’ response peaks arising from sustained responses of one phase extending into the following phase and being detected as a peak. To classify the RGC according to their response polarity, an ON/OFF index was calculated from the amplitudes of ON ( $A_1$ ) and OFF ( $A_2$ ) responses according to the equation,  $(A_1 - A_2) / (A_1 + A_2)$ . Using the ON/OFF index we classified the cell into OFF (-1 to -0.5), ON-OFF (-0.5 to 0.5) and ON (0.5 to 1).

**Visual response changes:** For testing our hypothesis, we compared the changes in visual response parameters before and after electrical stimulation (for the test and two control conditions) **Fig 1. (d)**. At first, we compared the response parameters of the visual block before any electrical stimulation was delivered to the retina, to the response parameters of the visual block after the entire electrical stimulation protocol was over. The visual block prior to any electrical stimulation was termed as “**first**” block (in red). The visual block after ~80 minutes of electrical and visual stimulation was termed as “**last**” block (in green). However, for most cells, we observed that the visual response parameters changed after stimulating at lower voltages (0.3 and 0.1V, ~20minutes) as seen from the, and rastergram. Hence the visual block following 20 minutes post electrical stimulation (lower voltage stimulation) was termed as “**second**” block (in blue). It should be noted that although we provided 0.1 V (both cathodic and anodic pulses) due its uneven current waveform and inconsistent charge delivery (*Refer to 4.1 Comparison to previous data, Discussion section, Jalligampala et al. 2017*) was excluded from the analysis. For all the statistical comparisons, the non-parametric Wilcoxon’s *ranksum* test (MATLAB; The Mathworks, Natick, MA) was used with a significance threshold of 0.05.

## Results

### I. Overall distribution of response parameters

Using full-field flash stimulus, we evaluated the distribution of visual response parameters for multimodality. The response parameters measured were the latency of the response to flash on (light, ON) and flash off (dark, OFF), duration of the response to flash on (light, ON) and flash off (dark, OFF) and the relative amplitudes of the response to flash on (light, ON) and flash off (dark, OFF) (*refer methods Data Analysis for definition*). If each of the response parameters divided into more than one mode, it would indicate that the RGCs divided naturally into more than one class. The multimodality was examined for both the test (Nearby-R) and control conditions (Distant-NR and Visual-OR) and both the strains of the mice (i.e., WT and *rd10*).

#### Test Condition:

**Nearby-R: WT -Latency:** Both ON (**Fig. 2 Col 1, Row 1**) and OFF (**Fig. 2 Col 2, Row 1**) latencies had a unimodal distribution. Based on the multimodality boundaries for latencies described in Carcieri *et al.* (< 400 ms for short latencies and >400 ms for long latencies) majority of the cells had short latency response for both flashes of ON and OFF. **Duration/Transience:** The duration of ON response (**Fig. 2 Col 3, Row 1**) had a bimodal distribution whereas for the OFF responses (**Fig. 2 Col 4, Row 1**) the distribution was rather unimodal. Based on the multimodality boundaries for the duration of responses described in Carcieri *et al.* (<200 ms for transient cells and > 200 ms for sustained cells) the ON responses had both transient and sustained responses. Whereas, the OFF responses were primarily transient. **ON/OFF index:** Based on the relative amplitude of the response to flash ON and flash OFF a bias index was calculated (*refer to methods, Carcieri et al. 2003*). The distribution of the cells based on the bias index (termed as ON/OFF index for our study) was trimodal dividing the cells into purely ON (+1), purely OFF (-1) and ON-OFF (centered around 0) (**Fig. 2 Col 5, Row 1**). The cells which responded to the only flash on (light) were classified as purely ON cells. The cells which responded only to flash off (dark) were classified as purely OFF cells. Cells which responded to both flashes on (light) and off (dark) were classified as

ON-OFF cells. However, based on the distribution, the number of purely ON were higher in comparison to purely OFF cells.

**Nearby-R: *rd10* -Latency:** Both ON (**Fig. 2 Col 1, Row 2**) and OFF (**Fig. 2 Col 1, Row 2**) responses had latencies with multimodal distribution (primarily bimodal) with both short and long latencies. ***Duration/Transience:*** Duration of both ON (**Fig. 2 Col 3, Row 2**) and OFF (**Fig. 2 Col 4, Row 2**) responses had a bimodal distribution containing both sustained and transient responses. ***ON/OFF index:*** Similar to the WT retinas, based on the bias index the cells in the *rd10* retina had a trimodal distribution, classifying the cells into purely ON, purely OFF, and ON-OFF cells (**Fig. 2 Col 5, Row 2**). In contrast to WT retinas, the number of purely OFF cells were comparatively higher in comparison to purely ON cells.

#### **Control Conditions: (i) Internal Control**

**Distant-NR: WT -Latency:** Similar to the previous observation of the test condition (Nearby-R) both ON and OFF responses had latencies with unimodal distribution, predominantly the short latency response (< 400 ms, **Fig. 2 Col 1, 2, Row 3**). ***Duration/Transience:*** Although the duration of the ON responses had both transient and sustained responses, the distribution was rather unimodal with continuity from transient to sustained responses (< 200 ms transient cells, >200 ms sustained response, **Fig. 2 Col 3, Row 3**). However for the duration of OFF responses were transient with unimodal distribution (**Fig. 2 Col 4, Row 3**). ***ON/OFF index:*** Similar to the observation in Nearby-R WT cells the distribution based on the bias index was trimodal (**Fig. 2 Col 5, Row 3**), classifying the cells in purely ON, purely OFF and purely ON-OFF. Additionally, the number of purely OFF cells were substantially less in comparison to purely ON cells.

**Distant-NR: *rd10* -Latency:** Similar to the previous observation of the test condition (Nearby-R) both ON and OFF responses had latencies with multimodal distribution (bimodal) with both short and long latencies (< 400 ms, short and >400 ms long **Fig. 2. Col 1, 2, Row 4**). ***Duration/Transience:*** Duration of both ON and OFF responses had a multimodal distribution (bimodal) with both transient and sustained cells (**Fig. 2 Col**

**3,4 Row 4). *ON/OFF index*:** Based on the bias index the distribution of the cells was trimodal (purely ON, purely OFF, ON-OFF). However, unlike the test condition (Nearby-R) the number of purely OFF cells were comparatively lower in comparison to purely ON cells (**Fig. 2 Col 5, Row 4**).

#### **Control Conditions: (ii) External Control**

**Visual-OR: WT -Latency:** Similar to the test and internal control condition the latency distribution for both ON and OFF responses was unimodal with a short latency (< 400 ms **Fig. 2 Col 1,2, Row 5**) response. ***Duration/Transience:*** The distribution of duration of ON responses were bimodal with both transient and sustained responses (**Fig. 2 Col 3, Row 5**). For the duration of OFF responses, the distribution was unimodal with transient responses (**Fig. 2 Col 4, Row 5**). ***ON/OFF index:*** Similar to the observation for the test and internal control the distribution of the cells was trimodal (purely ON, purely OFF and ON-OFF) and the number of purely OFF cells were comparatively lower to purely ON cells (**Fig. 2 Col 5, Row 5**).

**Visual-OR: *rd10*-Latency:** Similar to previous observations in test and internal control condition the distribution of latencies for ON and OFF response was bimodal with both short and long latency response (**Fig.2 Col 1, 2 Row 6**). ***Duration/Transience:*** The distribution of duration of both ON and OFF responses was multimodal (bimodal) with both transient and sustained responses (**Fig. 2 Col 3,4 Row 6**). ***ON/OFF index:*** Similar to our previous observation in the internal control condition the distribution based on the bias index was trimodal (purely ON, purely OFF and ON-OFF). The number of purely OFF cells were comparatively lower than purely ON cells.

For the *rd10* retina, although the OFF responses had latencies with a bimodal distribution, the number of cells with short latencies (<400 ms) were comparatively higher than the long latency responses (>400 ms). Additionally, for the distribution of the duration of OFF responses, the number of transient cells (< 200 ms) were higher in comparison to sustained cells (> 200 ms).

It should be noted, that for the overall distribution of response parameters described above (Fig. 2) we could observe a discrepancy between the number of cells for latency,

duration, and the ON/OFF index (see the 'n' values for Figure. 2). As mentioned above (*refer Data Analysis*) while examining the visual response parameters (latency and duration) for flash ON and flash OFF we excluded any cell which had a response amplitude at latencies <100 ms (arising from responses extending from an earlier phase). Additionally, cells with non-significant amplitude peaks were also excluded while examining these response parameters. However, while determining the ON/OFF index of the cells, relative response amplitudes from both ON and OFF is considered. Hence for cells which had a response amplitude, either for ON or OFF were included in the cell count. Only cells which neither had a response for flash on or flash off were excluded from the cell count of ON/OFF index.

## II. Distribution of response parameters based on ON/OFF index

Next, we evaluated the distribution of visual response parameters (latency and duration) of the cells classified as ON (+0.5 to 1), OFF (-1 to -0.5) and ON-OFF (-0.5 to 0.5) cells based on the ON/OFF index (Carcieri *et al.* 2003, Sekhar *et al.* 2017). We evaluated the distribution for the test and control conditions and both the strains (WT and *rd10* retina).

**WT ON- latency:** For the test condition (Nearby-R) and the internal control condition (Distant-NR) the distribution of ON response latency was unimodal (**Fig. 3 Col 1, Row 1 & 3**) with short latency response (< 400 ms). However, for the external control condition (Visual-OR) the distribution of ON latency was bimodal with both short and long latency responses (>400 ms) (**Fig. 3 Col 1, Row 5**). **Duration/Transience:** For the test condition and the control conditions (both internal and external controls) the distribution of duration of ON responses was multimodal (primarily bimodal) (**Fig. 3 Col 1, Row 2, 4 and 6**) with both transient (< 200 ms) and sustained responses (> 200 ms).

**WT OFF-latency:** For the test and the control conditions (both internal and external control conditions) the distribution of OFF response latency was unimodal with short latency responses (**Fig. 3 Col 2, Row 1, 3 and 5**). For the internal control condition (Distant-NR) we did observe few long latency responses. However, most of the cells had a distribution which was primarily unimodal. It should be noted that we did observe a

cell count peak at 0. This peak corresponded to the really short latency response amplitudes (< 100 ms). To show the entire cell count distribution for OFF cells, we included these cells in the histogram. ***Duration/Transience***: For the test condition the distribution for the duration of OFF responses was unimodal with transient responses ( **Fig. 3 Col 2, Row 2**). However, for both the control conditions the distribution was multimodal (bimodal) with both transient and sustained responses (> 200 ms) (**Fig. 3 Col 2, Row 4 and 6**).

**WT ON-OFF-latency**: For both the test and control conditions the distribution of ON-OFF response latency was unimodal with short latency responses ( Fig. 3 Col 3, Row 1, 3 and 5). ***Duration/Transience***: For both test and control conditions the distribution was multimodal (bimodal) with both transient and sustained responses. (**Fig. 3 Col 3, Row 2, 4 and 6**).

**rd10 ON- latency**: For both the test and control conditions the distribution of the latency of ON responses was multimodal (bimodal) with both short and long latency responses ( **Fig. 3 Col 4, Row 1,3, and 5**). ***Duration/Transience***: Similar to the latency distribution, the distribution of the duration of ON responses was multimodal (primarily bimodal) with both transient and sustained responses (**Fig 3. Col 4, Row 2, 4 and 6**). For the control conditions, some of the cells had sustained responses lasting up to 2 seconds.

**rd10 OFF- latency and duration/transience**: For both the test and control conditions the distribution was rather obscure ( for both latency and duration) with a majority of cells peaked around zero ( response amplitude of latency < 100 ms). The remaining cells were distributed at various time scales and had no particular distribution. This suggests that the cells contributing to the overall distribution of OFF latency and OFF duration ( Fig. 2) were primarily the cells with ON-OFF responses ( **Fig 3. Col 5, Row 1-6**).

**rd10 ON-OFF -latency and duration/transience**: For both the test and control conditions the distribution of the ON-OFF response latency was multimodal ( primarily bimodal) with both short and long latency responses. For all the 3 conditions we did observe cells which had long latencies >1 second and in some cells a latency up to 2



seconds was observed (**Fig. 3 Col 6, Row 1, 3 and 5**). Likewise, the distribution of duration of ON-OFF responses was bimodal for both the test and control conditions with both transient and sustained responses, with few cells having a sustained response up to 2 seconds (**Fig. 3 Col 6, Row 2, 4 and 6**)

### **III- Diversity in alteration of visual responses to electrical stimulation**

To evaluate how electrical stimulation alters the visual response parameters, we plotted the rastergram and PSTH's of the cell's response to full-field flash stimulus (**Fig. 4**). These example cells were both electrically and visually responsive. The rastergram shows the visual response to all the six flash blocks presented before, after and within the electrical stimulation blocks. The PSTH (above) represents the average response (20 trails) of the 'first block,' i.e., before electrical stimulation. The PSTH (below) shows the average response (20 trails) of the 'last block,' i.e. after the entire electrical stimulation protocol was over.. We observed diversity in the alteration of the visual responses. For our study, our definition of neural adaptation was the change in the cell's firing rate/ amplitude. Therefore, to evaluate the effect of electrical stimulation, we observed how the cell's firing rate changed post electrical stimulation. Apart from the changes in firing rate/amplitude, observed in all the example cells (**Fig. 4 a-e**), we observed changes in other visual response parameters (latency, duration and ON/OFF index). For some cells, we observed that post electrical stimulation the latency of the responses became shorter (**Fig. 4. b and e**, ON responses). For some cells, we observed a change in the transiency of the responses, i.e., the cells which were transient before electrical stimulation became sustained post electrical stimulation (**Fig. 4. c and d**). Interestingly, we observed that for some cells, a change in polarity, i.e., before electrical stimulation the cell responded to a single phase of the flash stimulus, however after post electrical stimulation the cell responded to both the periods/phases of the flash stimulus (**Fig 4.e, ON to ON-OFF**). It should be noted, that such diversified responses were also observed during Visual-OR condition.

### **III- Quantifying the alteration in visual responses in response to electrical stimulation**

As described above our primary measure of alternation of visual responses (adaptation) in response to electrical stimulation was the change in the cell's relative firing rate/amplitude. Apart from measuring the changes in firing rate, we measured the changes in latency and duration of visual responses. We represented each of these response parameters in notched box-whisker plot (plotting the median and the quartiles) to show the variation across various comparisons. As mentioned above (refer to methods Fig 1. d, visual response changes, and experimental design) we started out with measuring the changes of the 'first block' to the 'last block.' However, from the rastergram (also see Fig. 4), we observed changes in visual response parameters were as early as ~20 minutes (second block) into the recording time (i.e., after the 2 electrical stimulation blocks of 0.1 and 0.3 V, subthreshold stimulus). Therefore, we measured the changes of visual response parameters from the 'first block' to the 'second block.' Finally, we measured the changes of the visual responses from the 'second block' to the 'last block' (~ 60 minutes time difference). We compared these changes for the test condition (Nearby-R) and control conditions (internal and external control). The statistical comparisons are presented in **Table 2**. The number of cells for each block (of the box plot) is presented in **Table 3**.

#### WT retinas:

- (1) **First Vs. Last Block (red vs. green): Amplitude-** For both ON and OFF response, there was a significant increase (across all quartiles) in the relative amplitude (firing rate) from the first block to the last block for all the three conditions (test and both the controls, **Fig. 5.1 a-c**). However, when comparing the magnitude of pre and post stimulation changes between the test (Nearby-R) and the control conditions ( Distant-NR and Visual-OR), we found the increase in ON and OFF amplitudes to be significantly greater for the test condition (or electrically responsive cells, *Table 2*, numbers in red). **Latency-** For the latency of ON responses we did not observe any statistical difference between the first and the last block for all the 3 conditions. The latency of OFF responses significantly decreased for all the 3 conditions. However, when comparing the magnitude of pre and post stimulation changes between the test and external

control condition (Visual-OR), we found the decrease in OFF response latency to be significantly greater for the test condition. There was no statistical difference in latency of OFF response between the Nearby-R and Distant-NR (**Fig 5.2. a-c**) ***Duration/Transience***: For all the 3 conditions, there was a significant increase in duration of ON responses, from the first to the last block. However, on comparing the test and control conditions, these changes were not significant (**Fig 5.3 a-c**). Likewise, for the duration of OFF responses, we saw a significant increase from the first to last block only for the control conditions ( Visual-OR and Distant-NR). When compared to the test condition there was no significant difference.

- (2) **First Vs. Second Block (red vs. blue): *Amplitude***- For both ON and OFF responses, there was a significant increase in the relative amplitude from the first to the second block for all the 3 conditions. However, when comparing the magnitude of pre and post stimulation changes between the test and control conditions, we found the increase in ON amplitudes to be significantly greater for the test conditions. However, the increase in OFF response amplitudes was significantly greater for the test condition in comparison to the internal control condition ( Distant-NR). There was no statistical difference between the test and external control condition (Visual-OR) (**Fig 5.1 a-c**). ***Latency***- Only for the internal control condition, the latency of the ON responses significantly decreased from the first to the second block. There was no significant decrease in the test and external control condition. Additionally, when the test and control conditions were compared, there was no significant difference (**Fig, 5.2 a-c**). For the OFF response latency, there was a significant decrease in latency from the first to the second block. On comparing the test and control conditions, the decrease in latency of OFF responses was significantly greater for the test condition. ***Duration/Transience***- Only for the internal control condition (Distant- NR) there was a significant increase in duration of the ON responses from the first to the second block. For the test condition, there was a significant decrease in duration of the OFF responses from the first to the second block. For the external control ( Visual-OR) there was a significant increase in duration of

the OFF responses from the first to the second block. There were no significant changes for the Distant-NR. On comparing the test to the Visual-OR, we found a significant difference (**Fig. 5.3 a-c**).

- (3) **Second Vs. Last Block (blue vs. green): *Amplitude***- Only for the Visual-OR condition there was an increase in ON response amplitude from the second to the last block. However, comparing the test and control conditions, there was no statistical significance. There was no increase in OFF response amplitude from the second to the last block for all the 3 conditions (**Fig. 5.1 a-c**). ***Latency***- Likewise, for both ON and OFF response latency we observed no statistical difference between the second and the last block for all the 3 conditions (**Fig. 5.2 a-c**). ***Duration/Transience***- There was a significant increase in duration of the ON responses for all the 3 conditions. However, comparing the test to the control conditions the magnitude of increase in ON response duration was significantly greater for the test condition (**Fig. 5.3 a-c**). For all the 3 conditions, there was no significant increase from the second to last block. However, we observed a statistical difference between the test and control conditions which could be due to the outliers ( supplement S1.3).

***rd10* retinas:**

- (1) **First Vs. Last Block (red vs. green): *Amplitude***- Only for the Visual-OR condition there was a significant increase in ON and OFF response amplitudes from the first to the last block. Comparing the test to control conditions there was no statistical difference between the test and control conditions for ON response amplitudes. However, comparing the test to the control conditions only for the OFF response amplitudes the magnitude of changes from the first to the last block was significantly higher for the control conditions (Visual-OR). Comparing the changes between the test and external control (Distant-NR) for the OFF response amplitudes, the magnitude of change was significantly greater for the test condition (possibly due to outliers, **Fig. 5.1 d-f**). ***Latency***- There was a significant increase in ON response latency from the first to last block for the test (Nearby-R) condition. However, compared to the control conditions, there was no statistical

difference. For both the control conditions, there was a significant decrease in OFF response latency, from the first to the last block. Comparing the test to control conditions, the magnitude of decrease was significantly higher for both the control conditions (**Fig. 5.2 d-f**). *Duration/Transience*- Only for the control conditions (both), there was a significant decrease in the duration of OFF responses from the first to the last block. However, compared to test condition there was a statistical difference. Likewise, there were no changes in duration of ON responses for all the 3 conditions.(**Fig. 5.3 d-f**).

- (2) **First Vs. second Block (red vs. blue): Amplitude**-Only for the Visual-OR there was a significant increase in response amplitude from the first to the second block. However, there was no statistical difference between the test and control conditions. (**Fig. 5.1 d-f**). *Latency and Duration* -Only for the Visual-OR, there was a significant decrease in the latency of OFF response, and for the duration of OFF responses from the first to the second block. This magnitude of decrease was significantly higher for the Visual-OR condition when compared to the test (Nearby-R) condition (**Fig, 5.2, 5.3 (d-f)**).
- (3) **Second Vs. Last Block (blue vs. green): Amplitude**- There was a significant increase in ON and OFF response amplitudes from the second to the last block for Visual-OR. There was no significant change from the second to the last block for the test and internal control condition. However comparing the test to both the control conditions, the magnitude of increase in ON response amplitude was higher for the Visual-OR than the test condition. Likewise, the magnitude of increase in OFF response amplitude was significantly higher for Visual-OR in comparison to test condition. In comparison to the Distant -NR, the magnitude of change for the test condition was significantly higher for the test condition (**Fig 5.1 d-f**). *Latency and Duration*- There was a decrease in ON latency from the second to last block for the Distant-NR. However, it was not significant. But in comparison to the test condition, the magnitude of the decrease was significantly higher for the Distant-NR condition. Although there was a significant decrease in latency and duration OFF responses for the control condition from the second to last block, there was no statistical

difference when compared to the test condition (**Fig 5.2, 5.3 d-f**). For details of outlier refer to the supplement (S1.1, S1.2, S1.3).

#### **IV- Change in the ON/OFF ratio**

In **Fig. 6** we compared the relative weighting of the ON and OFF response before and after electrical stimulation for the test and control conditions. For the WT retinas, we observed a change in ON/OFF ratio from the first to the second block for all the 3 conditions. This change in ratio was primarily the change from the purely ON (0.5 to 1) to ON-OFF (-0.5 to 0.5) responses. The change in ON/OFF ratio was substantially large for the visual-OR condition, suggesting that this weighting of the ON and OFF responses are primarily caused by adaptation of the retina to visual stimulus. Furthermore, such adaptation is rather fast as seen by the change from the first to the second block for all the conditions (**Fig. 6 a-c**). In comparison to the second block, there was no substantial change in the ON/OFF ratio for the last block, suggesting that these changes although, occurring early on remains consistent till the end of the experiment. There were no changes from purely OFF to ON-OFF cells for the WT retina. Interestingly, for the *rd10* retinas, the above observation (ON to ON-OFF) was true only for the external control condition (Visual- OR). For both the Nearby-R and the distant-NR we found no change in the ON/OFF ratio between the three visual blocks. This suggested that the electrical stimulation prevents the change in the ON/OFF ratio in the *rd10* retinas. Similar to the WT retinas there was no change from purely OFF response to ON-OFF response (**Fig. 6 d-f**). The number of cells contributing to each visual block for the test and control condition is presented in **Table 4**.

## **Discussion**

In the present study, we investigated the changes of visual response parameters (latency, duration, amplitude) before and after electrical stimulation. We demonstrated that, while the time invitro and visual adaptation increase the neuronal responsiveness by increasing the firing rate (amplitude) of the cell, electrical stimulation further strengthens these visual response changes.

## Multimodality - Cell Classification

To evaluate if our dataset could naturally divide into more than one class, we examined our dataset for multimodality. While for the majority of visual responses in WT retina we observed a unimodal distribution, for the *rd10* retina we observed a rather multimodal distribution. This was not surprising, as the age (P28-P40) of the degenerating *rd10* mouse considered in our study had a substantial amount of viable cone photoreceptors which would contribute to the long latency, sustained responses. However, what was intriguing is that for most of the visual responses for WT retinas the responses had a shorter latency and rather a transient response. As the photoreceptors (both rods and cones) are still intact, it was surprising that we did not observe a substantial amount of long latency response. Additionally, for our dataset which showed weak multimodality, the physiological response properties were rather a continuum (Carcieri *et al.* 2003, Rodieck 1998). One reason for this could be the use of full-field stimulus rather than a spot stimulus optimized to the receptive field center of each cell. Simplifying our stimulus, allowed us to gather an enormous amount of data. However, this simplification could significantly impair the ability to classify the visual responses of individual cells. Therefore, a set of visual stimuli addressing the spatial domain may be better to differentiate between the cell classes.

### ***rd10* changes predominant for OFF responses**

For our *rd10* dataset, we observed the majority of response changes for the OFF responses. Further, comparing the test to control conditions ( primarily the Visual-OR) these responses were most significant. Previous studies (Stasheff *et al.* 2011) have shown that with progressive degeneration, for *rd10* retinas both the ON and OFF responses are equally affected. However, for *rd1* retinas, which is an aggressive form of retinal degeneration (RP), the OFF pathway remain preserved for a longer time span in comparison to the ON pathway (Stasheff *et al.* 2011). Therefore, our observation could suggest that towards later stages of degeneration the OFF pathway would be preserved for a longer time span allowing the opportunity for cell-specific stimulation.

### **Role of *invitro* adaptation**

It is often observed that over the course of long-term *invitro* recordings the physiological properties of the tissue changes. Such changes can lead to changes in visual as well as electrical responses. Some of these changes could result from a change in pH, temperature, and oxygen supply. A recent study by Maturana *et al.* demonstrated that by changing the temperature, the electrical response properties of the ganglion cells were altered. They showed with increased temperature (34° C, similar to our temperature) the responses of the RGC to electrical stimulation were more stimulus-locked, with shorter latency and shortened duration (Maturana *et al.* 2015). While their observation was primarily for electrical responses, it could well be extended to the visual responses, suggesting that some of the changes in the visual responses could be attributed to the changes developed over time *invitro*. Therefore, to control for this adaptation, we used an external control condition (Visual -OR) which would also have an adaptation effect developed over time *invitro*, making it a suitable control condition to measure the real changes attributed to electrical stimulation.

### **Contribution from visual adaptation**

Work in human ERG (electroretinogram) from Peter Gouras and colleagues (Gouras & MacKay 1989) have shown a gradual increase in amplitude (of the a-wave and b-wave component) during light adaptation, over a period of approximately 20 minutes suggesting that the photoreceptors are involved in the rise in amplitudes. Additionally, this phenomenon occurred during suprathreshold light levels. This observation could explain the immediate response (~20 minutes) in the Visual-OR condition. Additionally, our flash ON stimulus was in the suprathreshold range which further supports our observation in Visual-OR condition. This increase in response is thought to reflect the redepolarization of the cones, after the initial hyperpolarization to an adaptation field. Such redepolarization also redepolarizes the horizontal cells. Therefore, apart from the *invitro* adaptation effect, the adaptation to visual stimulus also plays a role in the increased response in the test and the external control condition (Visual-OR).

### **Characterizing visual type before electrical stimulation**



As we have shown in this study, that the electrical stimulation can alter visual response parameters, it is strongly recommended that we characterize the visual responses for extracellular recording (like MEA) before any electrical stimulation. Such characterization is essential in healthy retinas or early degenerating retinas, as it is tough to classify the cells during the late stages of degeneration when the visual responses are completely lost. In earlier studies (Goo *et al.* 2011 , Ryu *et al.* 2009) it has been seen that the different RGCs are considered as one homogeneous population. In doing so, it becomes challenging to identify how electrical stimulation affects the visual pathways (ON and OFF) individually. It could be argued, that patch-clamp technique or calcium imaging could identify individual cell types morphologically and electrophysiologically. However, it is also crucial for these experimental setups that the identified cells need to be visually characterized first.

### **Providing a steady-state- electrical stimulation**

The observed increase in response amplitude is the result of alterations in cell physiology or network connectivity. In this case, this effect may also change how the retina responds to electrical stimulation. Such effect may have been overlooked in earlier studies as only a few investigators habituate the retina to ongoing electrical stimulation before examining its electrical responsiveness. An investigation of the cellular and network changes induced by ongoing electrical stimulation – particularly focusing on electrical responsiveness will shed light on this possibility. One way to investigate this would be, providing the retina with an electrical noise stimulation (Sekhar *et al.* 2017). This would influence the cellular and network responsiveness by bringing it to a steady state of electrical stimulation. Once the retina, is adapted to a steady state of electrical stimulation, it would be interesting to see how the electrical responsiveness would be affected with single pulses at threshold or supra-threshold electrical stimulation. Therefore, for future investigations of prosthetic stimulation it would be highly advisable to develop such electrical paradigms which would account for the ongoing network responsiveness.

## Changes in ON/OFF ratio

In our study, we observed a change in relative weighting for ON and OFF responses, with a shift of purely ON responses to ON-OFF. This shift was mostly observed for WT retinas for all the three conditions and the *rd10* retinas only for the Visual-OR condition. Such observations have been reported in a previous study in healthy retinas (Tikidji-Hamburyan *et al.* 2015). This study showed that on full-field stimulation, at some light levels the cell was classified as OFF and in other light levels some cells were classified as ON/OFF. This suggests that the changes in the weighting of ON and OFF responses are mostly occurring due to adaptation to visual stimulus. These changes primarily occurred from the first to the second block and remain constant till the last block. One possible reason for this observation is that the first visual stimulus is presented after 30 minutes of no light stimulation, i.e., adapted to dark condition. However, post electrical stimulation or *invitro* adaptation the retina was in a different adapted state. However, for *rd10* retina we did not observe changes in the test and internal control (Distant -NR). A possible reason for this observation is that the electrical stimulation prevents any modifications of the weighting of the ON and OFF responses. If this holds true, then post electrical stimulation, although with the rewiring the physiological properties of the pathway would be preserved for exploring pathway-specific stimulation. It would be worth exploring the change in ON/OFF ratio at different time points of degeneration.

## Limitations

For the current study, we simplified the full-field stimulus. While with this simplification we could gather responses from thousands of RGCs, the ability to categorize the visual response of individual cells is impaired. For example, if an ON cell has a strong enough OFF surround, it may be categorized as ON-OFF or OFF with the present stimulus. Similarly, response latencies and durations can be contaminated when a full-field stimulus is used. Therefore, using stimulation spots to elicit a response in the visual receptive field would help in classifying the cell's response accurately.

## Implications to the field of retinal prosthesis

The increase in response amplitude observed in this study is the result of alteration in the network connectivity and the cell physiology. In this case, this effect may also change how the retina responds to electrical stimulation. One reason that such an effect may have been overlooked in previous studies is that few investigators habituate the retina to ongoing electrical stimulation before examining its electrical responsiveness. An investigation of the cellular and network changes induced by ongoing electrical stimulation – particularly focusing on electrical responsiveness will shed light on this possibility. Given the likelihood that ongoing electrical stimulation will be shown to influence cellular and network responsiveness, it is advisable to develop paradigms of ongoing background electrical stimulation for future investigations of prosthetic retinal stimulation.

## Bibliography

- Multi Channel Systems, 2010. *Microelectrode array (MEA) manual*, Reutlingen: Multi Channel Systems MCS GmbH.
- Baccus, S.A. & Meister, M., 2002. Fast and Slow Contrast Adaptation in Retinal Circuitry. , 36, pp.909–919.
- Baden, T. *et al.*, 2016. The functional diversity of mouse retinal ganglion cells. *Nature*, pp.1–21. Available at: <http://dx.doi.org/10.1038/nature16468>.
- BARLOW, H.B., 1953. Summation and inhibition in the frog's retina. *The Journal of physiology*, 119(1), pp.69–88. Available at: <http://www.ncbi.nlm.nih.gov/pubmed/13035718> [Accessed April 19, 2018].
- Boinagrov, D. *et al.*, 2014. Selectivity of direct and network-mediated stimulation of the retinal ganglion cells with epi-, sub- and intraretinal electrodes. *Journal of neural engineering*, 11(2), p.26008. Available at: <http://stacks.iop.org/1741-2552/11/i=2/a=026008>.
- Carcieri, S.M., Jacobs, A.L. & Nirenberg, S., 2003. Classification of retinal ganglion cells: a statistical approach. *Journal of neurophysiology*, 90, pp.1704–1713.
- Demb, J.B., 2002. Multiple mechanisms for contrast adaptation in the retina. *Neuron*, 36(5), pp.781–783.
- Eickenscheidt, M. *et al.*, 2012. Electrical stimulation of retinal neurons in epiretinal and subretinal configuration using a multicapacitor array. *Journal of Neurophysiology*, 107(10), pp.2742–2755.

- Freeman, D.K. & Fried, S.I., 2011. Multiple components of ganglion cell desensitization in response to prosthetic stimulation. *Journal of neural engineering*, 8, p.16008.
- Gouras, P. & MacKay, C.J., 1989. Growth in amplitude of the human cone electroretinogram with light adaptation. *Investigative Ophthalmology and Visual Science*, 30(4), pp.625–630.
- Hartline, H.K., 1938. THE RESPONSE OF SINGLE OPTIC NERVE FIBERS OF THE VERTEBRATE EYE TO ILLUMINATION OF THE RETINA. *American Journal of Physiology-Legacy Content*, 121(2), pp.400–415. Available at: <http://www.physiology.org/doi/10.1152/ajplegacy.1938.121.2.400> [Accessed April 19, 2018].
- Ho, E. *et al.*, 2018. Spatiotemporal characteristics of retinal response to network-mediated photovoltaic stimulation. *Journal of Neurophysiology*, 119(2), pp.389–400. Available at: <http://www.physiology.org/doi/10.1152/jn.00872.2016> [Accessed April 18, 2018].
- Hubel, D.H. & Wiesel, T.N., 1998. Early exploration of the visual cortex. *Neuron*, 20(3), pp.401–412.
- HUBEL, D.H. & WIESEL, T.N., 1959. Receptive fields of single neurones in the cat's striate cortex. *The Journal of physiology*, 148(3), pp.574–91. Available at: <http://www.ncbi.nlm.nih.gov/pubmed/14403679> [Accessed April 19, 2018].
- Im, M. & Fried, S.I., 2015. Indirect activation elicits strong correlations between light and electrical responses in ON but not OFF retinal ganglion cells. *The Journal of Physiology*, 593(16), pp.3577–3596. Available at: <http://doi.wiley.com/10.1113/JP270606>.
- Jalligampala, A. *et al.*, 2017. Optimal voltage stimulation parameters for network-mediated responses in wild type and rd10 mouse retinal ganglion cells. *Journal of Neural Engineering*, 14(2).
- Kara, P. *et al.*, The spatial receptive field of thalamic inputs to single cortical simple cells revealed by the interaction of visual and electrical stimulation. Available at: <http://www.pnas.org/content/pnas/99/25/16261.full.pdf> [Accessed March 18, 2018].
- Kuffler, S.W., 1953. Discharge Patterns and Functional Organization of Mammalian Retina. *Journal of Neurophysiology*, 16(1), pp.37–68. Available at: [ftp://retina.anatomy.upenn.edu/pub/judy/visual neuroscience BBB 217/kuffler\\_53.pdf](ftp://retina.anatomy.upenn.edu/pub/judy/visual%20neuroscience%20BBB%20217/kuffler_53.pdf) \n<http://www.ncbi.nlm.nih.gov/pubmed/13035466>.
- Lettvint, J.Y. *et al.*, What the Frog's Eye Tells the Frog's Brain \*. Available at: [https://hearingbrain.org/docs/letvin\\_ieee\\_1959.pdf](https://hearingbrain.org/docs/letvin_ieee_1959.pdf) [Accessed April 19, 2018].
- Maturana, M.I. *et al.*, 2015. The effects of temperature changes on retinal ganglion cell responses to electrical stimulation. In *2015 37th Annual International Conference*

- of the *IEEE Engineering in Medicine and Biology Society (EMBC)*. IEEE, pp. 7506–7509. Available at: <http://www.ncbi.nlm.nih.gov/pubmed/26738028> [Accessed April 19, 2018].
- Meister, M., Pine, J. & Baylor, D.A., 1994. Multi-neuronal signals from the retina: acquisition and analysis. *Journal of Neuroscience Methods*, 51(1), pp.95–106.
- Rodieck, R.W., 1998. *The First Steps in Seeing First.*, Sunderland, Massachusetts: Sinauer Associates, Inc. Available at: <http://www.sinauer.com/the-first-steps-in-seeing.html>.
- Rodieck, R.W. & Stone, J., 1965. Analysis of Receptive Fields of Cat Retinal Ganglion Cells. *Journal of Physiology*, 28(5), pp.833–849.
- Ryu, S.B. *et al.*, 2009. Characterization of retinal ganglion cell activities evoked by temporally patterned electrical stimulation for the development of stimulus encoding strategies for retinal implants. *Brain Research*, 1275, pp.33–42. Available at: <http://dx.doi.org/10.1016/j.brainres.2009.03.064>.
- Sekhar, S. *et al.*, 2017. Correspondence between visual and electrical input filters of on and off mouse retinal ganglion cells. *Journal of Neural Engineering*, 14(4).
- Sekhar, S. *et al.*, 2016. Tickling the retina: Integration of subthreshold electrical pulses can activate retinal neurons. *Journal of Neural Engineering*, 13(4).
- Stasheff, S.F., Shankar, M. & Andrews, M.P., 2011. Developmental time course distinguishes changes in spontaneous and light-evoked retinal ganglion cell activity in rd1 and rd10 mice. *Journal of neurophysiology*, 105(6), pp.3002–3009. Available at: <http://jn.physiology.org/content/105/6/3002.abstract>.
- Stett, A., Mai, A. & Herrmann, T., 2007. Retinal charge sensitivity and spatial discrimination obtainable by subretinal implants: key lessons learned from isolated chicken retina. *Journal of neural engineering*, 4, pp.S7–S16.
- Tikidji-Hamburyan, A. *et al.*, 2015. Retinal output changes qualitatively with every change in ambient illuminance. *Nat Neurosci*, 18(1), pp.66–74. Available at: <http://www.ncbi.nlm.nih.gov/pubmed/25485757>.
- Tikidji-Hamburyan, A. *et al.*, 2017. Rods progressively escape saturation to drive visual responses in daylight conditions. *Nature Communications*, 8(1), p.1813. Available at: <http://www.nature.com/articles/s41467-017-01816-6> [Accessed April 19, 2018].
- Wilke, R. *et al.*, 2011. Spatial resolution and perception of patterns mediated by a subretinal 16-electrode array in patients blinded by hereditary retinal dystrophies. *Investigative Ophthalmology and Visual Science*, 52(8), pp.5995–6003.

Weber, E. H. (1846). Tastsinn und Gemeingefuehl. In *Rudolph Wagners Handwörterbuch der Physiologie*. [Reprinted (1905) in E. Hering (Ed.) *Ostwald's Klassiker der exakten Wissenschaften*, No. 149. Leipzig: W. Engelmann]

## Figure and Table Legends

### **Fig.1 : (a) Stimulation Protocol, Test and Control condition & comparisons:**

Electrical stimuli were presented over a range of voltage/duration combinations. Constant-voltage stimulus blocks consisted of 5x repetitions of 9 durations. Within each repetition, the durations were randomized. 5s separated pulses. Voltage blocks were presented from lowest to highest amplitude. Subsequent voltage blocks were separated by 150 sec or greater. A block of full-field flash stimulus (20 repetitions of 2s ON & 2s OFF) was interleaved between voltage blocks throughout the experiment. Voltage-duration combinations that exceeded safety limits were omitted (grey triangle). **(b)** The different test (Nearby-R) and control conditions (internal- Distant-NR and external - Visual -OR). **(c)** Flash response characterization using according to Carciari. *et al.* 2003. The top row shows spike rasters of a full-field flash stimulus (20 trails, 2s ON 2s OFF).  $A_1$  and  $A_2$  represent the relative (relative to the baseline) response amplitude for ON and OFF.  $Tp1$  and  $Tp2$  time to peak (latency) for ON and OFF.  $D1$  and  $D2$  (durations) for ON and OFF, after  $A_1$  where the response is still above  $A_1/e$ . **(d)** Visual response changes were evaluated for the first (red) to second (blue) and first(red) to (last) using the average PSTH. PSTH binned at 2 ms intervals for all responses. Smoothed histogram (Gaussian smoothing filter, sigma = 4 ms)

**Fig. 2: Evaluating multimodality:** Overall distribution of response parameters for ON and OFF responses for WT and rd10 retinas for the test (Nearby-R) and the control conditions (Distant-NR and Visual-OR). Responses measure were latency, duration, relative response amplitudes for computing the ON/OFF index.

**Fig. 3: Evaluating multimodality based on ON/OFF index:** Overall distribution of response parameters of ON, OFF and ON/OFF RGC types for WT and rd10 retinas for

the test (Nearby-R) and the control conditions (Distant-NR and Visual-OR). Responses measures were latency and duration.

**Fig. 4: Diversity of alternation of visual responses to electrical stimulation. (A-E)** .Rastergram is depicting response for all six visual blocks. 1,2 and 6 were evaluated for response changes. (Top) PSTH shows the average PSTH for first block. (Bottom) shows the average PSTH for the last block. PSTH binned at 2 ms intervals for all responses. Smoothed histogram (Gaussian smoothing filter, sigma = 4 ms).

**Fig 5.1: Box-whisker plot for response amplitude.** Box plots for ON (solid line) and OFF (dashed) responses shown for first (red), second (blue) and last (green) for WT (**a-c**) and rd10 (**d-f**) retinas for the test (Nearby-R, a,d) and control conditions (Distant-NR b,e and Visual-OR c, f).

**Fig 5.2: Box-whisker plot for response latency.** Box plots for ON (solid line) and OFF (dashed) responses shown for first (red), second (blue) and last (green) for WT (**a-c**) and rd10 (**d-f**) retinas for the test (Nearby-R, a,d) and control conditions (Distant-NR b,e and Visual-OR c, f).

**Fig 5.3: Box-whisker plot for response duration.** Box plots for ON (solid line) and OFF (dashed) responses shown for first (red), second (blue) and last (green) for WT (**a-c**) and rd10 (**d-f**) retinas for the test (Nearby-R, a,d) and control conditions (Distant-NR b,e and Visual-OR c, f).

**Fig 6: Changes in ON/OFF ratio.** Percentage bar is showing the relative weighting of ON, OFF and ON-OFF responses for first, second and last block, for WT (a-c) and rd10 retina (d-f) for all the three conditions (Nearby-R, Distant -NR and Visual -OR).

**Table 1:** Retinal ganglion cell (RGC) counts for WT and *rd10* for test and control conditions. “Distances” are recording distances relative to the stimulating electrode. For the definition of ‘responsive’ (see *Jalligampala et al. 2017, Methods- Data Analysis*).

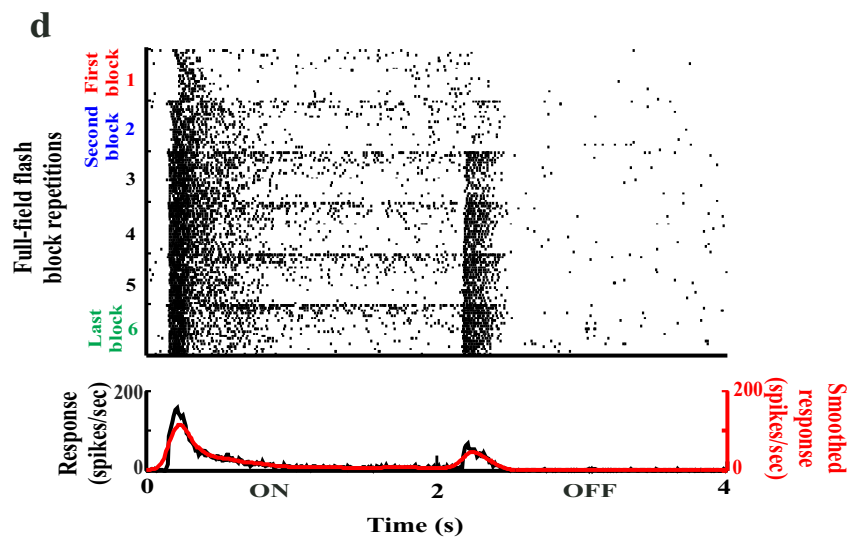
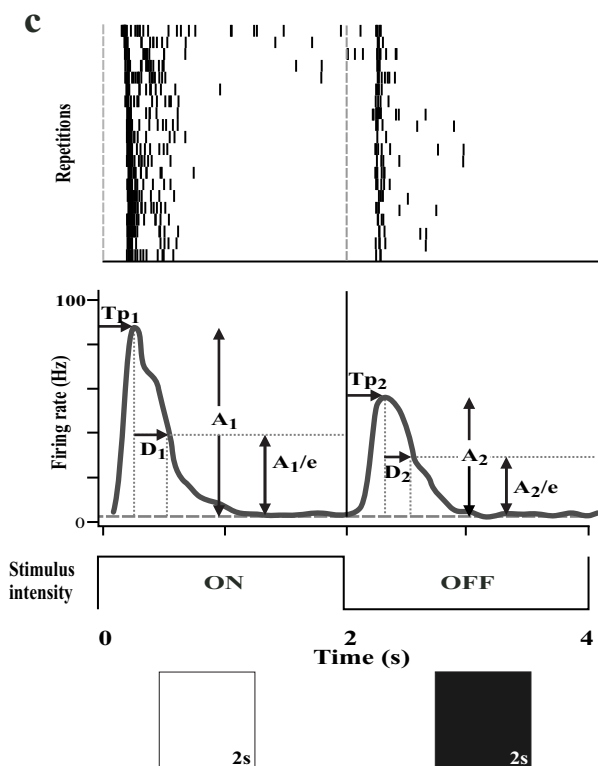
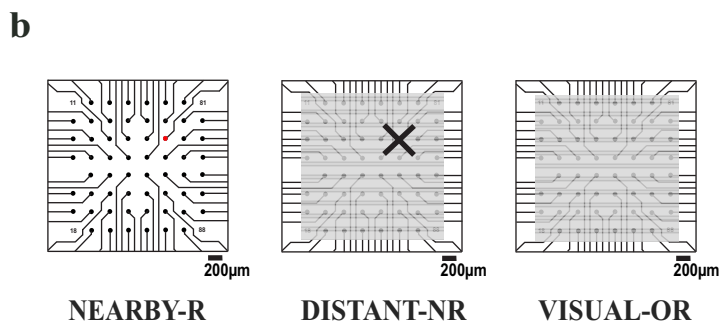
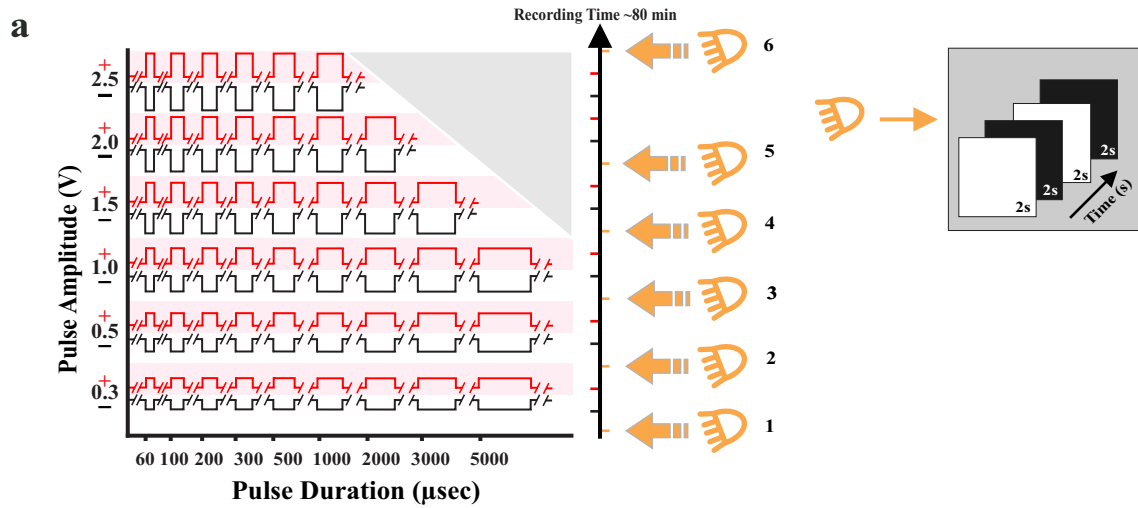
**Table 2 :** For the plots in Fig. 5 (5.1, 5.2, 5.3), the nonparametric Wilcoxon ranksum test (MATLAB,  $p < 0.05$ ) was used to determine significant changes. For each condition (near &

responsive, distant & non-responsive, and control) and each mouse strain (wt and rd10) we tested whether each visual response parameter differed between First vs. Second, First vs. Last and Second vs. Last flash stimulus blocks. For each of these tests, the quartiles of the First, Second and Last response parameter distributions are provided along with the p-value of the test. P-values for these tests are presented between the middle and right data blocks. Green boxes identify significant increase. Red boxes identify significant decreases. Bold p-values indicate significance. Red p-values indicate significance between test and control conditions.

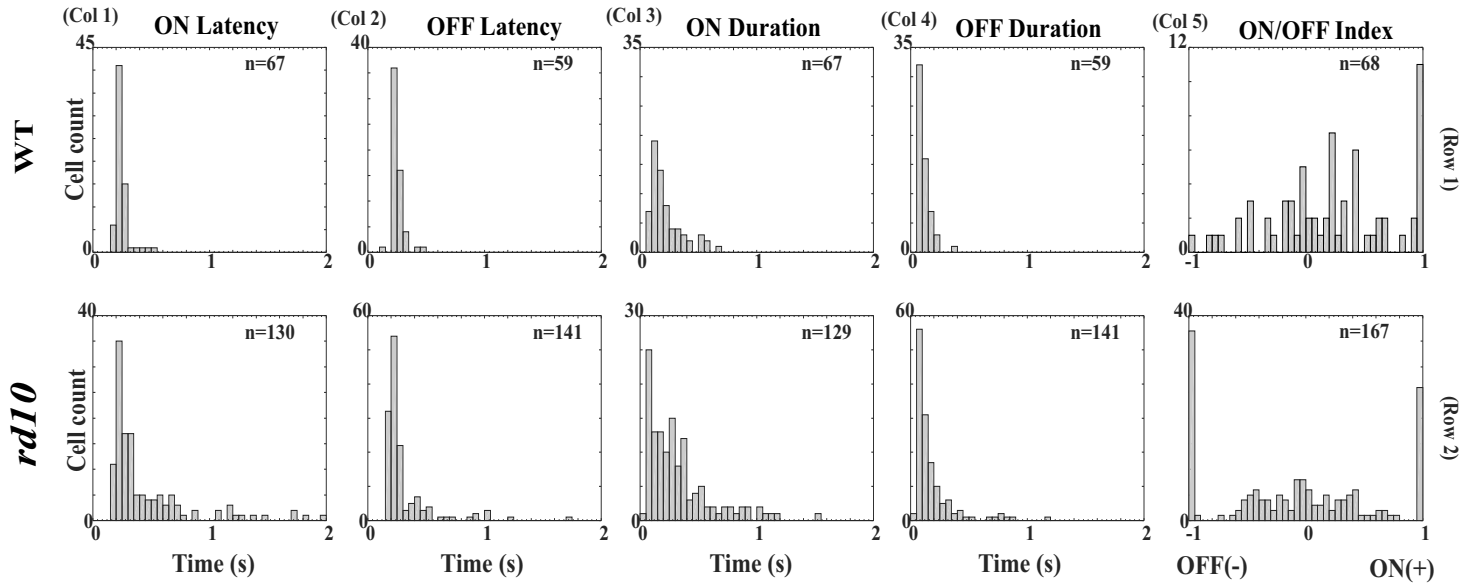
**Table 3 :** Cell counts for each of the box-whisker plot ( for Fig 5.1, 5.2 and 5.3).

**Table 4:** Cell counts for ON, OFF and ON-OFF and Total for evaluating change in ON/OFF ratio. shown in Fig. 6

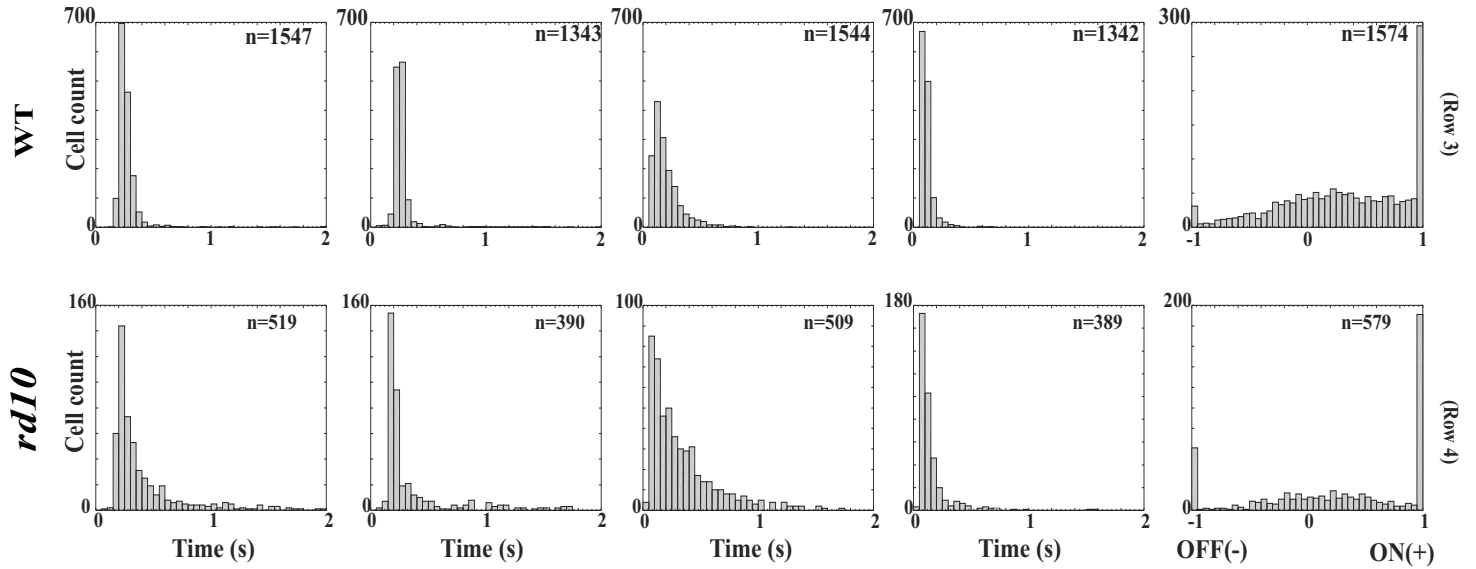




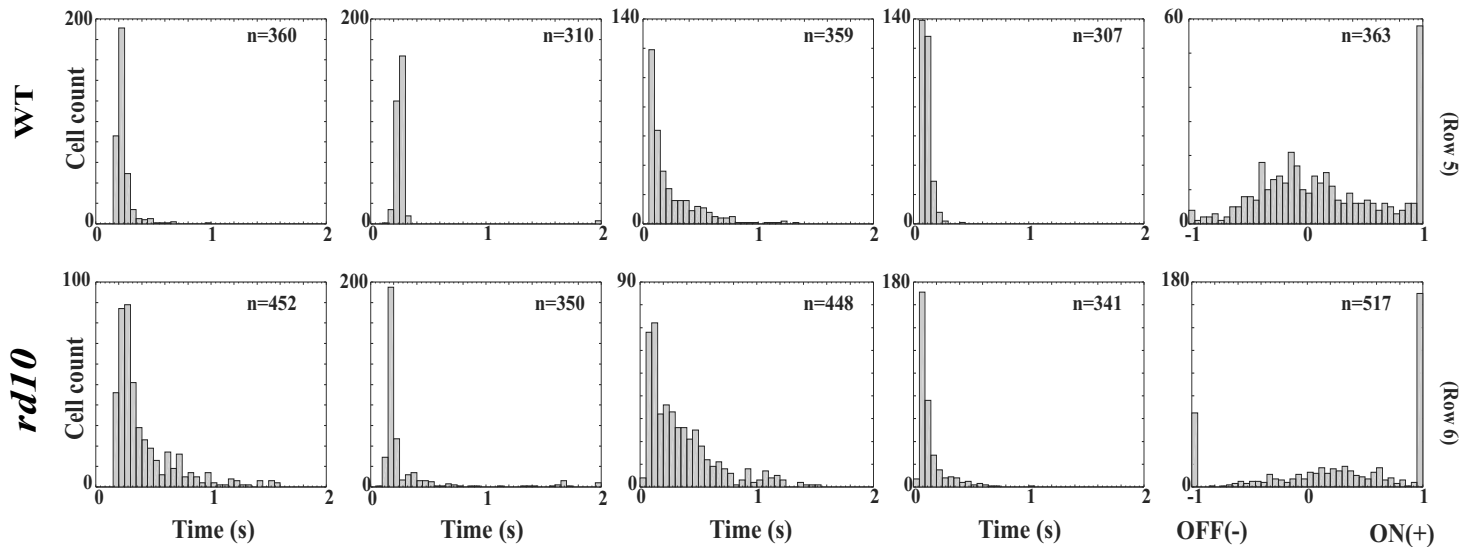
## NEARBY-R



## DISTANT-NR



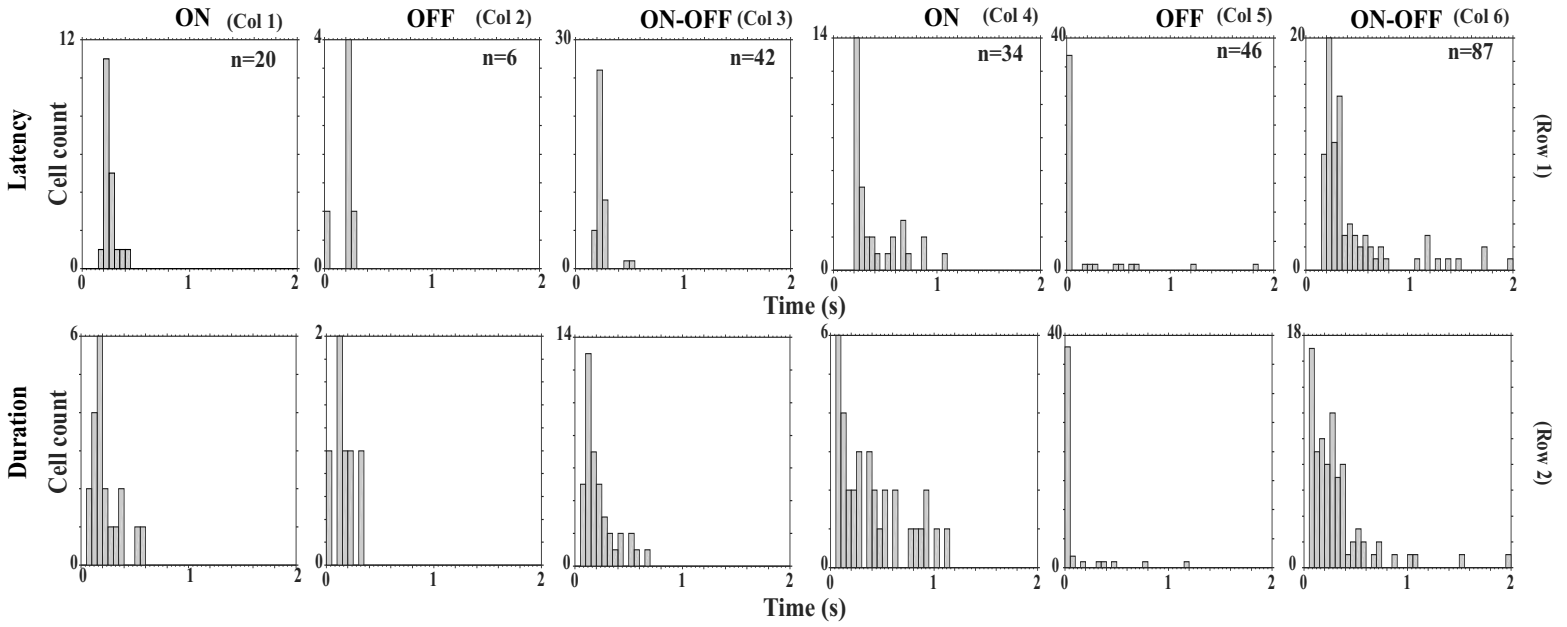
## VISUAL-OR



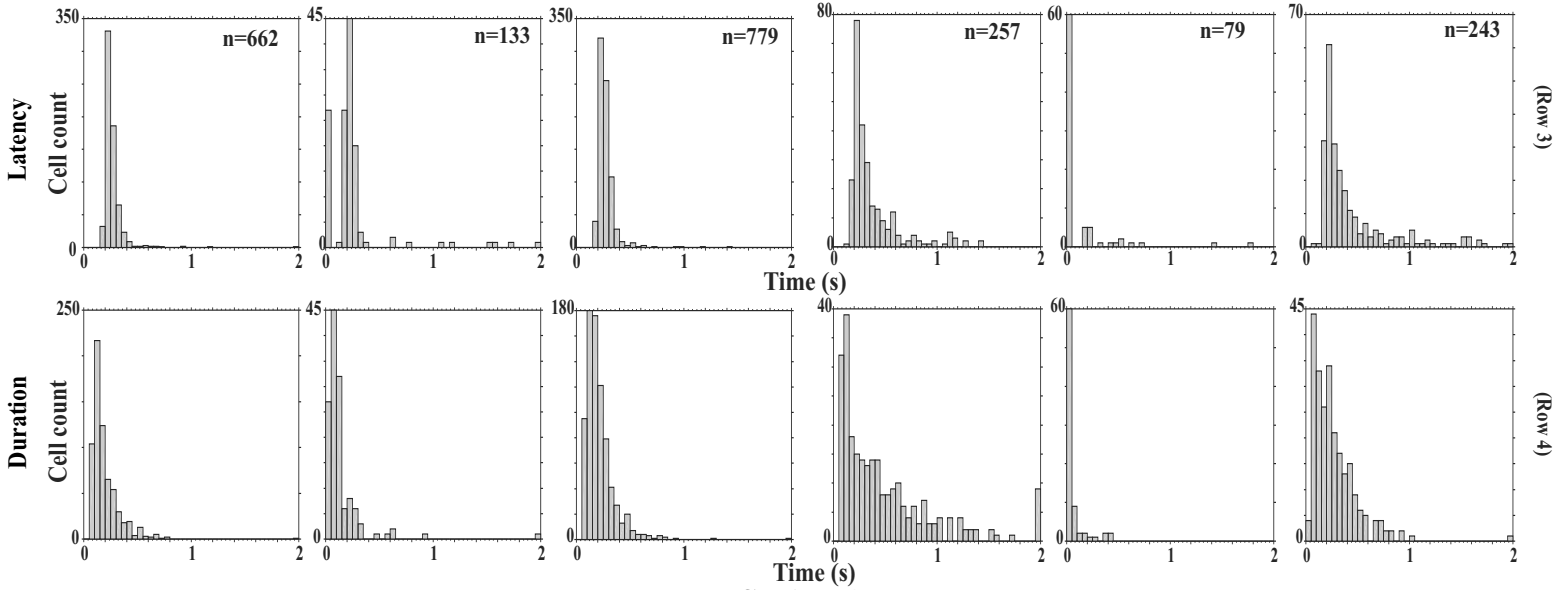
**WT**

***rd10***

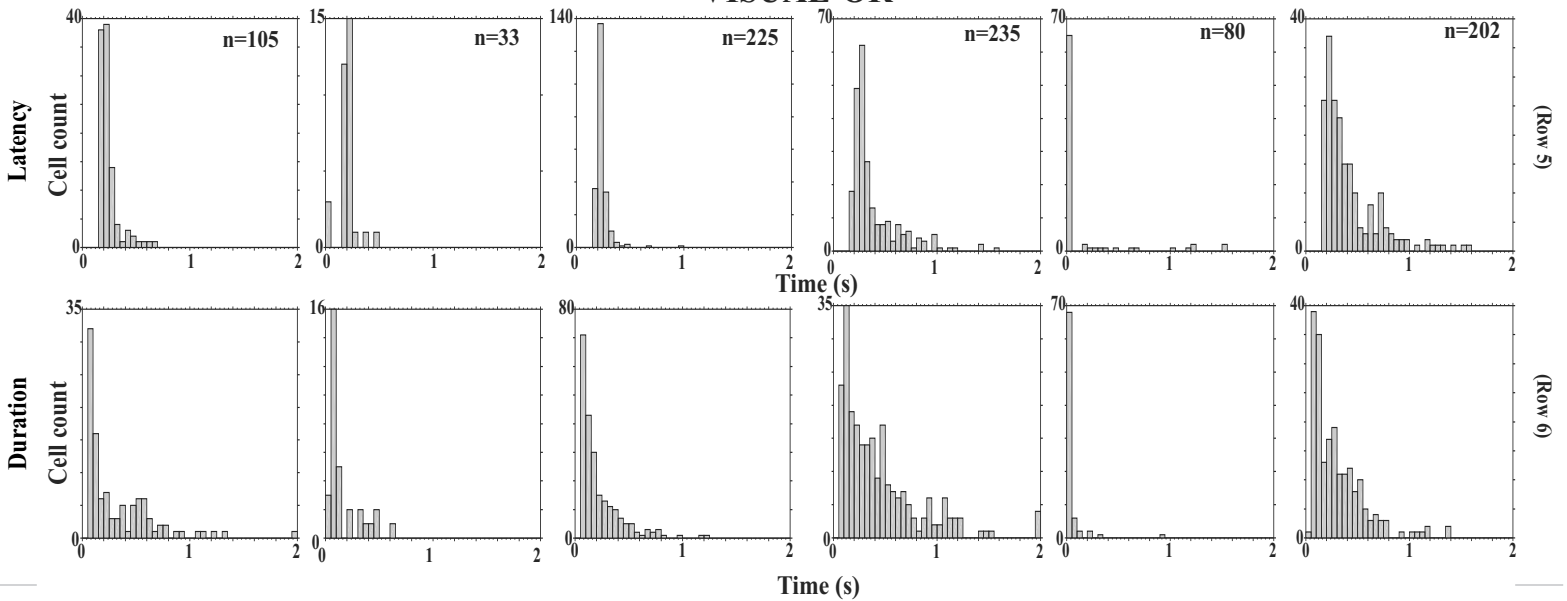
**NEARBY-R**

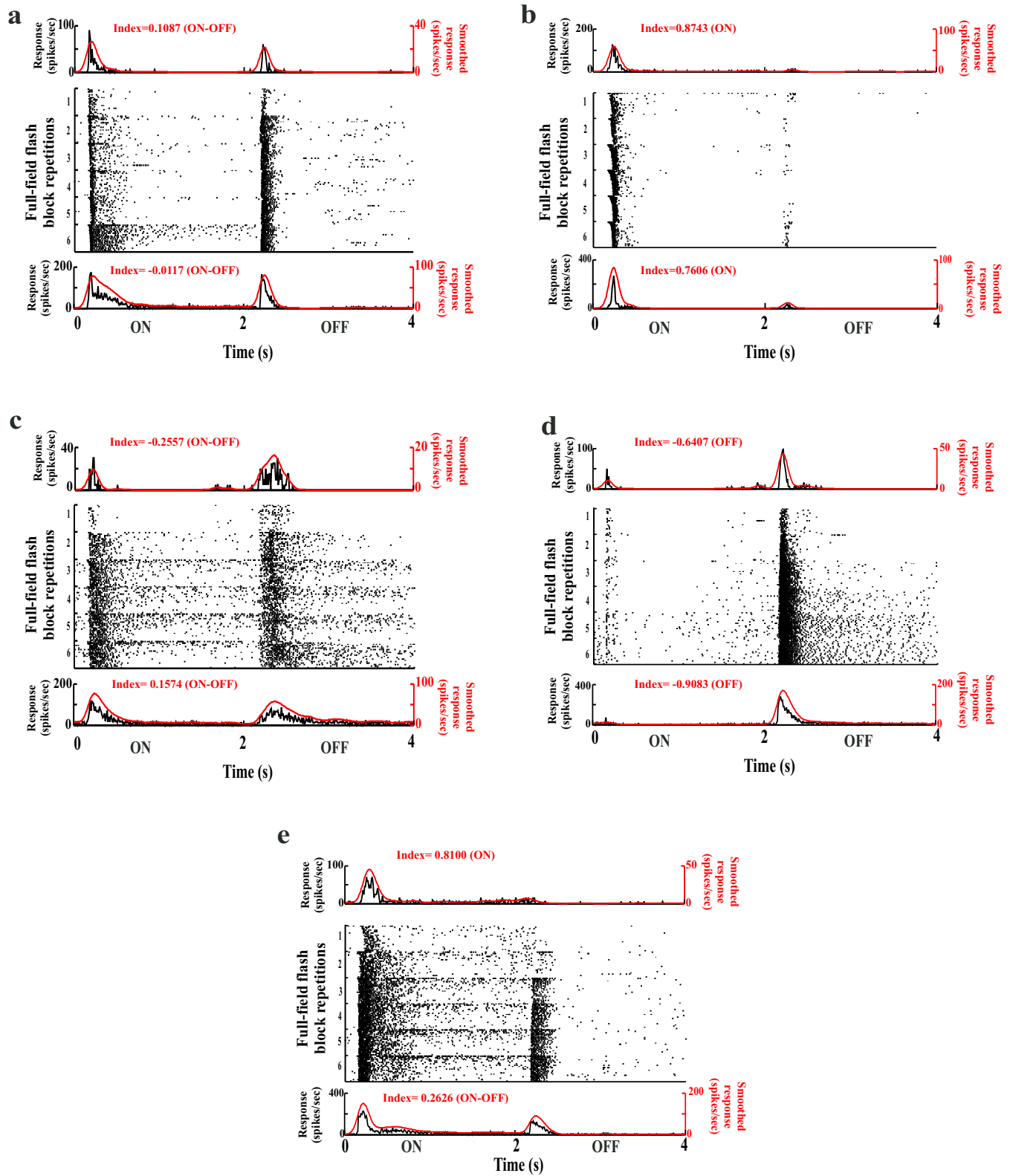


**DISTANT-NR**

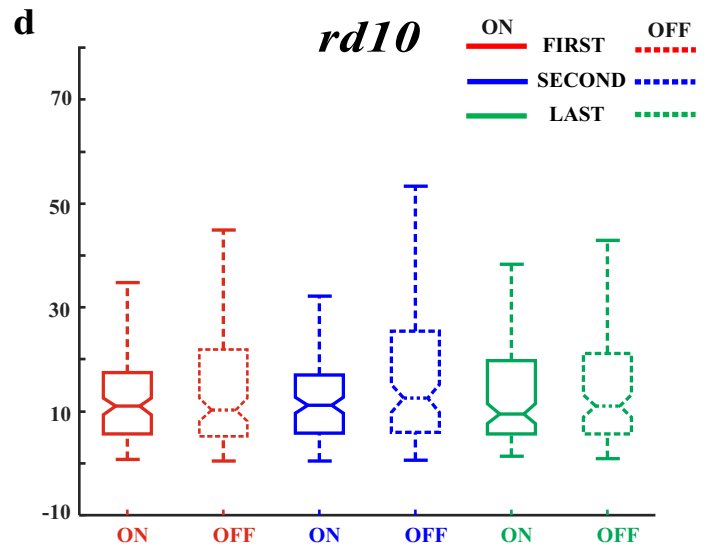
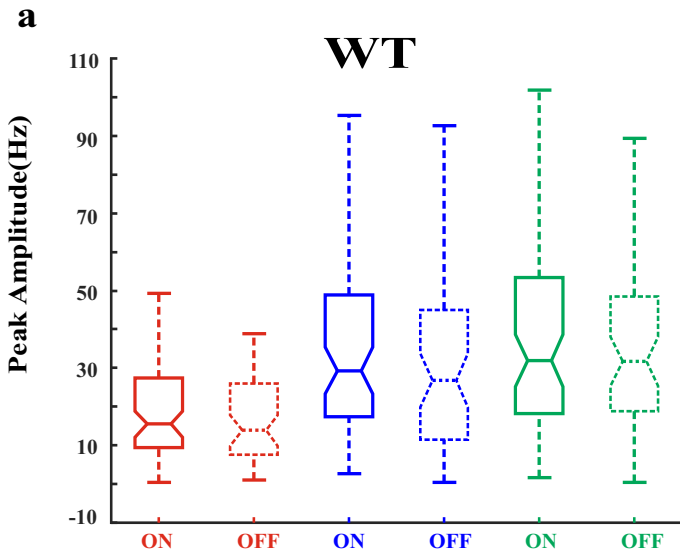


**VISUAL-OR**

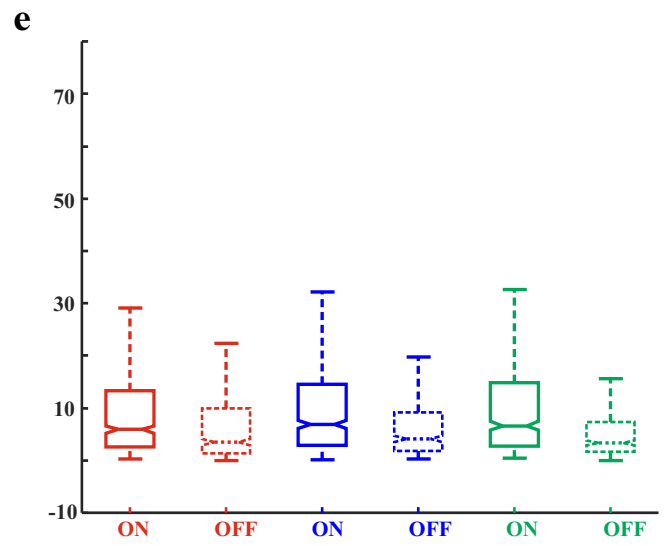
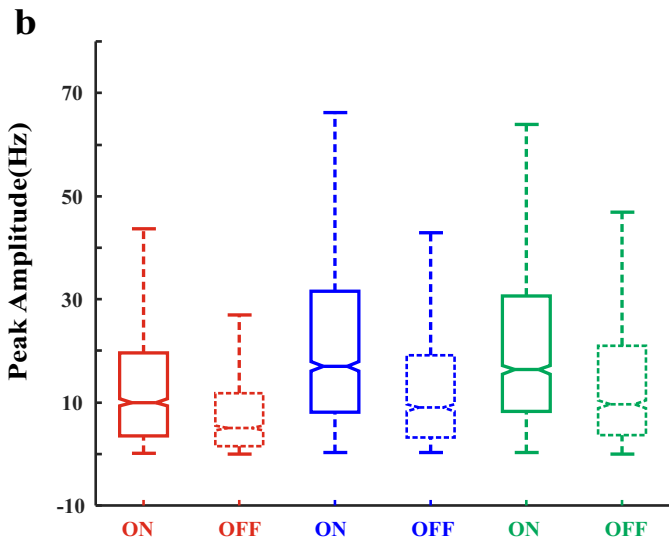




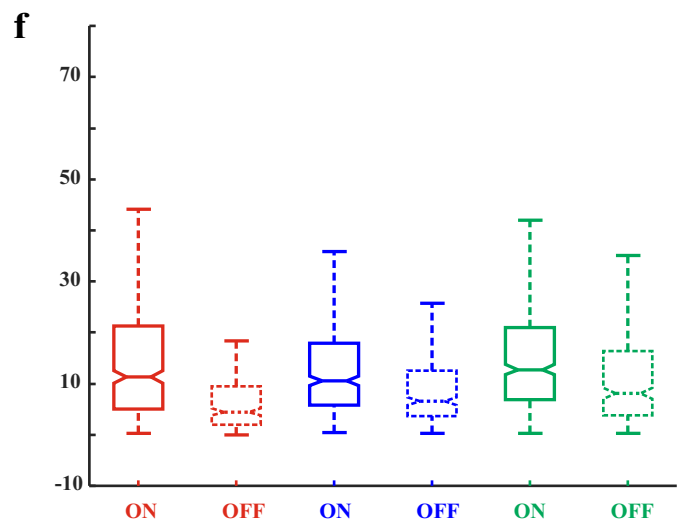
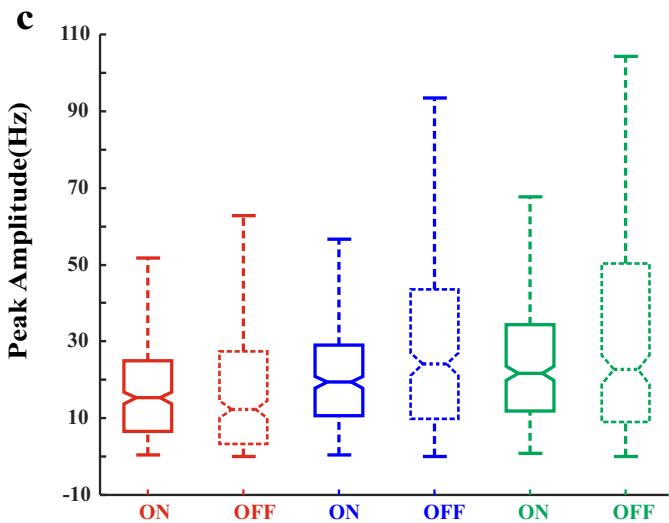
NEARBY-R

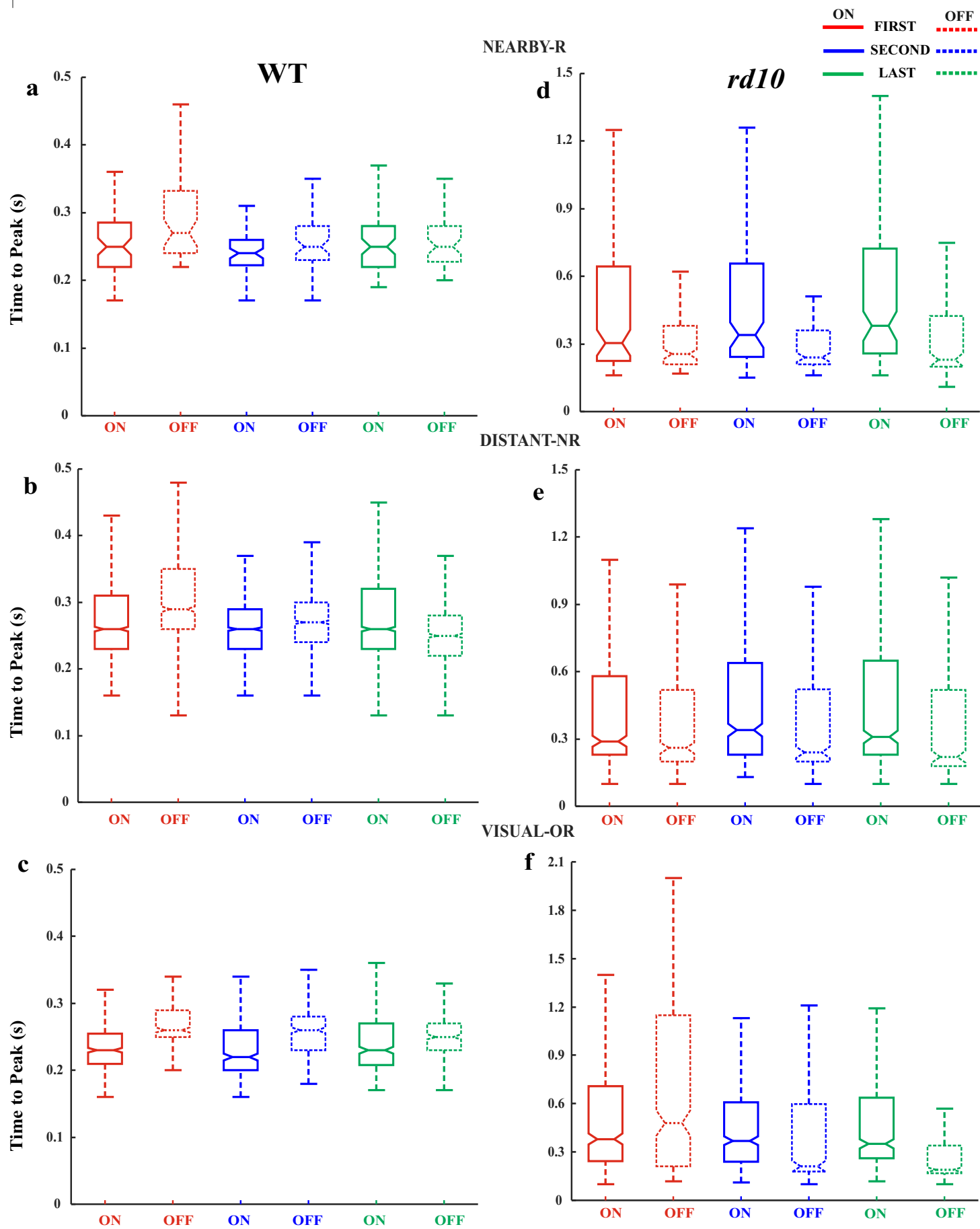


DISTANT-NR



VISUAL-OR







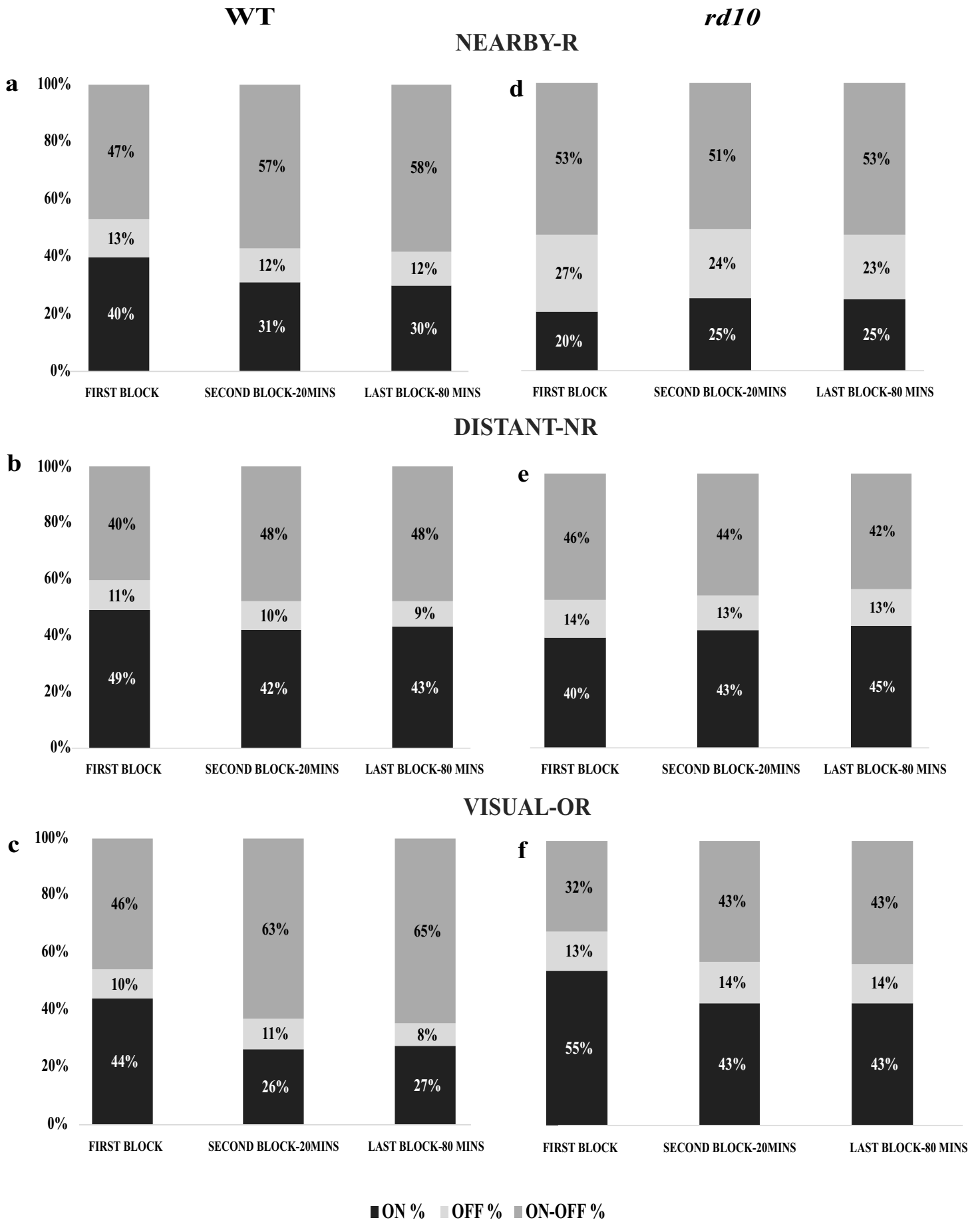




**Table 1****Test Condition (Nearby R)**

		<b>WT</b>	<b><i>rd10</i></b>
<b>All distances</b>	<b>Total</b>	<b>2078</b>	<b>1880</b>
	<b>Electrically responsive</b>	<b>354</b>	<b>1188</b>
	<b>Visually responsive</b>	<b>2076</b>	<b>1763</b>
<b>200-283 <math>\mu</math>m (nearby electrode distance)</b>	<b>Total</b>	<b>216</b>	<b>232</b>
	<b>Electrically responsive</b>	<b>68</b>	<b>174</b>
	<b>Visually responsive</b>	<b>68</b>	<b>167</b>

**Internal Control Condition (Distant NR)**

		<b>WT</b>	<b><i>rd10</i></b>
<b>All distances</b>	<b>Total</b>	<b>2078</b>	<b>1880</b>
	<b>Visually responsive</b>	<b>2076</b>	<b>1763</b>
<b>Non responsive &amp; &gt;300<math>\mu</math>m</b>	<b>Total</b>	<b>1576</b>	<b>632</b>
	<b>Visually responsive</b>	<b>1574</b>	<b>579</b>

**External Control Condition (VisualOR)**

		<b>WT</b>	<b><i>rd10</i></b>
<b>All distances</b>	<b>Total</b>	<b>366</b>	<b>573</b>
<b>All distances</b>	<b>Visually responsive</b>	<b>363</b>	<b>517</b>

Table 2

First Vs Last		TEST CONDITION						TEST VS INTERNAL		INTERNAL CONTROL CONDITION						TEST VS EXTERNAL		EXTERNAL CONTROL CONDITION																
		Distance 200-300 µm, Responsive(Near-by)						Nearby-R vs. Distant-NR		Distance > 300 µm, Non-responsive						Nearby-R vs. Visual-OR		Visual Only Control																
		WT			rd10			WT	rd10	WT			rd10			WT	rd10	WT			rd10													
		quartiles	0.25	0.5	0.75	0.25	0.5	0.75			0.25	0.5	0.75	0.25	0.5	0.75			0.25	0.5	0.75	0.25	0.5	0.75										
Amplitude (Hz)	ON	First	9.3431	15.4841	27.4666	5.6429	10.9961	17.4988			3.5161	9.9709	19.5954	2.597	5.9124	13.2933			6.4723	15.2725	24.9348	4.9872	11.3673	21.2146										
	Last	18.2528	31.8701	53.3581	5.6191	9.553	19.8047			8.3216	16.3089	30.5685	2.6942	6.5979	14.7771			11.8034	21.7521	34.413	6.8246	12.7532	20.9129											
	p-value		5.02E-06				0.7189					3.33E-40				0.1919					0.0032		0.3460		2.06E-08			0.0313						
Amplitude (Hz)	OFF	First	7.549	13.912	26.0128	5.1156	10.2896	21.9326			1.4897	5.0812	11.7408	1.3893	3.468	9.9291			3.3704	12.2762	27.4184	2.0415	4.4851	9.4341										
	Last	18.8978	31.685	48.4855	5.6929	11.0224	21.1205			3.6051	9.6971	21.0333	1.7064	3.3422	7.2785			8.9486	22.6461	50.364	3.7832	8.1316	16.3549											
	p-value		3.04E-05				0.6951					8.12E-07			0.0152					1.18E-29			0.8674			0.0251		2.83E-06		3.37E-08			5.90E-10	
Latency (sec)	ON	First	0.22	0.25	0.285	0.225	0.305	0.645			0.23	0.26	0.31	0.23	0.29	0.58			0.21	0.23	0.26	0.245	0.38	0.71										
	Last	0.22	0.25	0.28	0.2575	0.38	0.7225			0.22	0.26	0.32	0.23	0.31	0.65			0.21	0.23	0.27	0.26	0.35	0.6375											
	p-value		0.5678				0.0237					0.5353			0.3179					0.1688			1.13E-01			0.0516		0.2181		0.7669			0.4603	
Latency (sec)	OFF	First	0.24	0.27	0.3325	0.21	0.255	0.38			0.26	0.29	0.35	0.2	0.26	0.52			0.25	0.26	0.29	0.21	0.48	1.15										
	Last	0.2275	0.25	0.28	0.2	0.23	0.425			0.22	0.25	0.28	0.18	0.22	0.52			0.23	0.25	0.27	0.22	0.17	0.19	0.34										
	p-value		0.0012				0.2378					0.2981			0.0495					6.45E-79			2.78E-04			0.0137		2.42E-06		8.28E-07			8.39E-22	
Duration (sec)	ON	First	0.1	0.135	0.205	0.09	0.15	0.32			0.09	0.12	0.18	0.1	0.14	0.29			0.09	0.12	0.21	0.1	0.16	0.3525										
	Last	0.13	0.2	0.31	0.09	0.19	0.36			0.11	0.16	0.25	0.095	0.15	0.34			0.1	0.15	0.32	0.1	0.19	0.35											
	p-value		2.92E-04				0.6426					0.1583			0.7435					1.20E-28			0.5527			0.0885		0.9437		5.26E-05			0.4869	
Duration (sec)	OFF	First	0.09	0.1	0.12	0.09	0.12	0.19			0.08	0.095	0.12	0.08	0.1	0.17			0.08	0.09	0.11	0.09	0.12	0.185										
	Last	0.08	0.1	0.1225	0.08	0.11	0.1675			0.08	0.1	0.12	0.08	0.09	0.12			0.08	0.1	0.13	0.08	0.09	0.1325											
	p-value		0.5768				0.0691					0.3965			0.6564					0.0411			2.30E-03			0.2179		0.6474		4.50E-04			2.81E-06	

First Vs Second		Distance 200-300 µm, Responsive(Near-by)						Near vs. Distant		Distance > 300 µm, Non-responsive						Near vs. Visual only		Visual Only Control																
		WT			rd10			WT	rd10	WT			rd10			WT	rd10	WT			rd10													
		quartiles	0.25	0.5	0.75	0.25	0.5	0.75			0.25	0.5	0.75	0.25	0.5	0.75			0.25	0.5	0.75	0.25	0.5	0.75										
Amplitude (Hz)	ON	First	9.3431	15.4841	27.4666	5.6429	10.9961	17.4988			3.5161	9.9709	19.5954	2.597	5.9124	13.2933			6.4723	15.2725	24.9348	4.9872	11.3673	21.2146										
	Second	17.3452	29.3097	48.9727	5.7751	11.1358	16.9478			8.0905	16.9723	31.4854	2.8302	6.8679	14.6147			10.6987	19.3735	29.1273	5.8462	10.5321	17.9857											
	p-value		8.73E-05				0.9035					8.30E-03			0.1895					3.60E-42			0.0798			1.03E-04		0.3605		8.94E-05			0.9758	
Amplitude (Hz)	OFF	First	7.549	13.912	26.0128	5.1156	10.2896	21.9326			1.4897	5.0812	11.7408	1.3893	3.468	9.9291			3.3704	12.2762	27.4184	2.0415	4.4851	9.4341										
	Second	11.3932	26.853	44.9023	5.9759	12.5064	25.4325			3.1439	8.9588	19.1156	1.8444	4.0977	9.1503			9.9069	24.0762	43.6085	3.6157	6.623	12.4977											
	p-value		0.0039				0.1383					3.34E-04			0.8186					2.58E-23			0.0911			0.3180		0.3825		3.01E-08			1.66E-05	
Latency (sec)	ON	First	0.22	0.25	0.285	0.225	0.305	0.645			0.23	0.26	0.31	0.23	0.29	0.58			0.21	0.23	0.26	0.245	0.38	0.71										
	Second	0.2225	0.24	0.26	0.2425	0.34	0.6575			0.23	0.26	0.29	0.23	0.34	0.64			0.2	0.22	0.26	0.24	0.37	0.61											
	p-value		0.0857				0.3294					0.6276			0.3263					2.71E-06			0.0389			0.1410		0.4559		0.0867			0.1306	
Latency (sec)	OFF	First	0.24	0.27	0.3325	0.21	0.255	0.38			0.26	0.29	0.35	0.2	0.26	0.52			0.25	0.26	0.29	0.21	0.48	1.15										
	Second	0.23	0.25	0.28	0.21	0.24	0.36			0.24	0.27	0.3	0.2	0.24	0.5225			0.23	0.26	0.28	0.18	0.21	0.5975											
	p-value		0.0017				0.6334					0.9853			0.2745					1.26E-29			2.72E-01			7.85E-04		0.0015		0.0023			1.27E-09	
Duration (sec)	ON	First	0.1	0.135	0.205	0.09	0.15	0.32			0.09	0.12	0.18	0.1	0.14	0.29			0.09	0.12	0.21	0.1	0.16	0.3525										
	Second	0.11	0.14	0.2375	0.1	0.21	0.36			0.1	0.14	0.21	0.1	0.16	0.34			0.09	0.11	0.27	0.1	0.17	0.4											
	p-value		1.56E-01				0.2378					0.2906			0.3726					1.00E-12			0.146			0.8565		0.3712		1.44E-01			0.5970	
Duration (sec)	OFF	First	0.09	0.1	0.12	0.09	0.12	0.19			0.08	0.095	0.12	0.08	0.1	0.17			0.08	0.09	0.11	0.09	0.12	0.185										
	Second	0.08	0.09	0.11	0.08	0.12	0.2			0.08	0.1	0.12	0.08	0.1	0.14			0.09	0.1	0.13	0.08	0.1	0.17											
	p-value		0.0164				0.4345					0.0014			0.4258					0.0813			3.93E-01			4.27E-06		0.0424		2.78E-05			1.73E-02	

Second vs Last		Distance 200-300 µm, Responsive(Near-by)						Near vs. Distant		Distance > 300 µm, Non-responsive						Near vs. Visual only		Visual Only Control																
		WT			rd10			WT	rd10	WT			rd10			WT	rd10	WT			rd10													
		quartiles	0.25	0.5	0.75	0.25	0.5	0.75			0.25	0.5	0.75	0.25	0.5	0.75			0.25	0.5	0.75	0.25	0.5	0.75										
Amplitude (Hz)	ON	Second	17.3452	29.3097	48.9727	5.7751	11.1358	16.9478			8.0905	16.9723	31.4854	2.8302	6.8679	14.6147			10.6987	19.3735	29.1273	5.8462	10.5321	17.9857										
	Last	18.2528	31.8701	53.3581	5.6191	9.553	19.8047			8.3216	16.3089	30.5685	2.6942	6.5979	14.7771			11.8034	21.7521	34.413	6.8246	12.7532	20.9129											
	p-value		4.19E-01				0.8226					1.76E-01			0.8267					6.84E-01			0.6828			0.2959		0.0212		0.0366			0.0155	
Amplitude (Hz)	OFF	Second	11.3932	26.853	44.9023	5.9759	12.5064	25.4325			3.1439	8.9588	19.1156	1.8444	4.0977	9.1503			9.9069	24.0762	43.6085	3.6157	6.623	12.4977										
	Last	18.8978	31.685	48.4855	5.6929	11.0224	21.1205			3.6051	9.6971	21.0333	1.7064	3.3422	7.2785			8.9486	22.6461	50.364	3.7832	8.1316	16.3549											
	p-value		0.2217				0.2695					0.1201			9.33E-05					9.69E-02			0.0729			0.3814		3.55E-12		7.80E-01			0.0188	
Amplitude (Hz)	Second	0.2225	0.24	0.26	0.2425	0.34	0.6575			0.23	0.26	0.29	0.23	0.34	0.64			0.2	0.22	0.26	0.24	0.37	0.61											

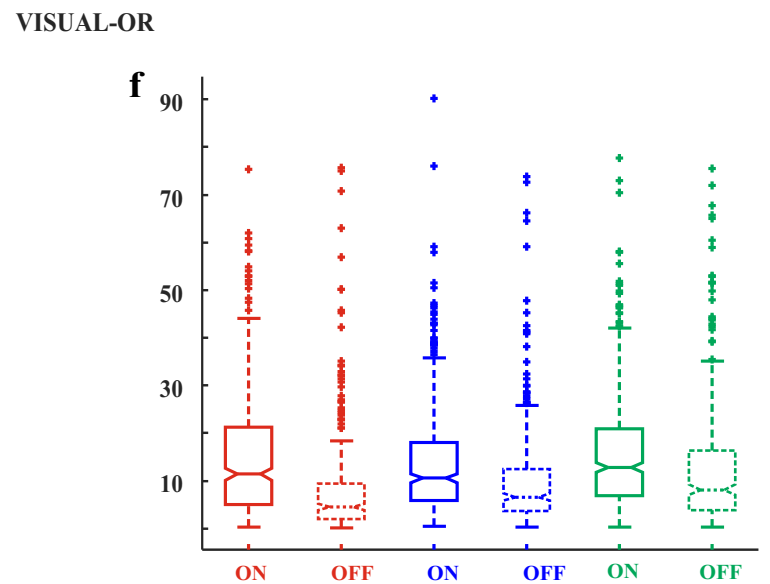
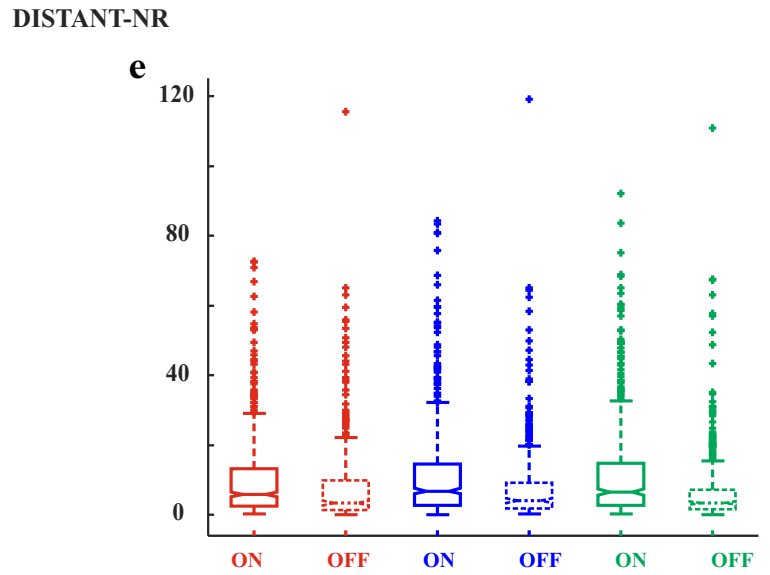
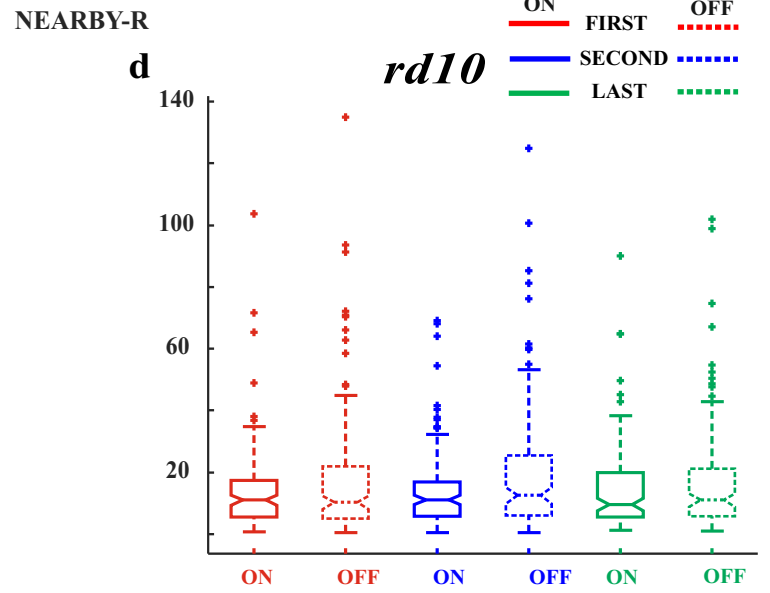
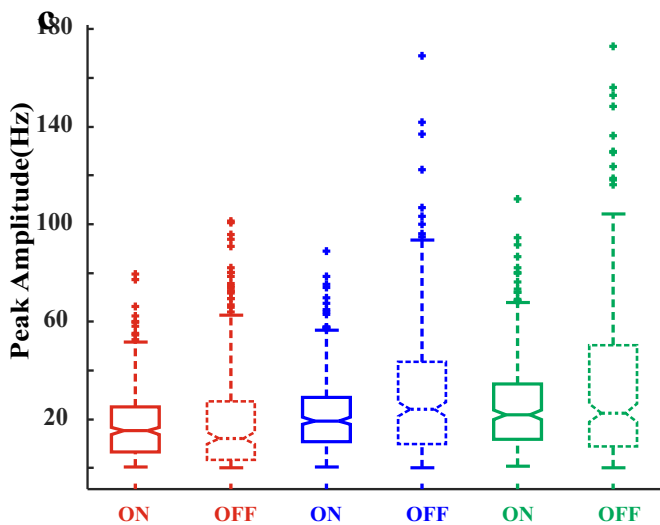
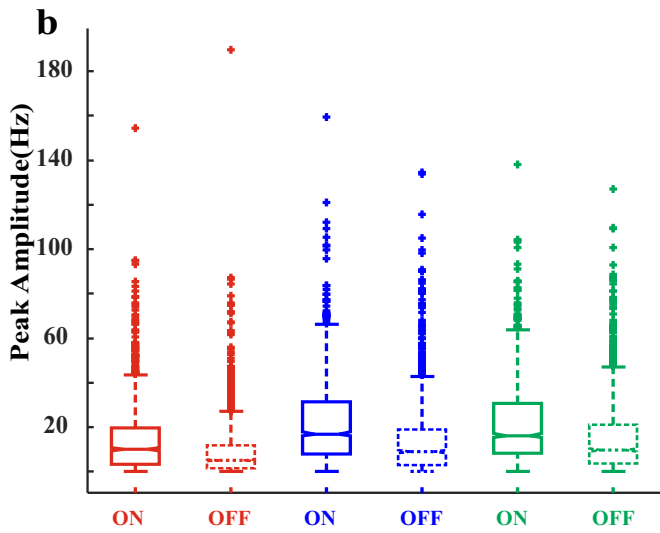
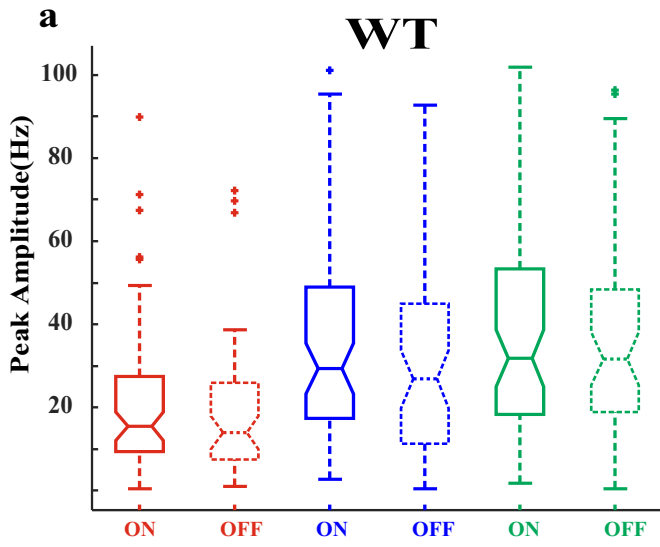
Latency (sec)	ON	Last	0.22	0.25	0.28	0.2575	0.38	0.7225			0.23	0.26	0.32	0.23	0.31	0.65			0.21	0.23	0.27	0.26	0.35	0.6375
		p-value	0.2419			0.1724			0.2636	0.035	0.0037			0.614			0.3640	0.2270	0.0989			0.4522		
	OFF	Second	0.23	0.25	0.28	0.21	0.24	0.36			0.24	0.27	0.3	0.2	0.24	0.5225			0.23	0.26	0.28	0.18	0.21	0.5975
	Last	0.2275	0.25	0.28	0.2	0.23	0.425			0.22	0.25	0.28	0.18	0.22	0.52			0.23	0.25	0.27	0.17	0.19	0.34	
	p-value	0.6038			0.3483			0.1404	0.1164	1.3479e-29			1.02E-02			0.1659	0.7593	0.0575			1.52E-04			
Duration (sec)	ON	Second	0.11	0.14	0.2375	0.1	0.21	0.36			0.1	0.14	0.21	0.1	0.16	0.34			0.09	0.11	0.27	0.1	0.17	0.4
	Last	0.13	0.2	0.31	0.09	0.19	0.36			0.11	0.16	0.25	0.095	0.15	0.34			0.1	0.15	0.32	0.1	0.19	0.35	
	p-value	1.34E-02			0.5471			0.0221	0.5745	2.81E-06			0.4079			0.0160	0.8883	9.20E-03			0.9893			
OFF	Second	0.08	0.09	0.11	0.08	0.12	0.2			0.08	0.1	0.12	0.08	0.1	0.14			0.09	0.1	0.13	0.08	0.1	0.17	
Last	0.08	0.1	0.1225	0.08	0.11	0.1675			0.08	0.1	0.12	0.08	0.09	0.12			0.09	0.1	0.13	0.08	0.09	0.1325		
p-value	0.0952			0.3558			0.0056	0.4092	0.7763			1.59E-02			9.34E-04	0.2803	5.16E-01			2.48E-02				

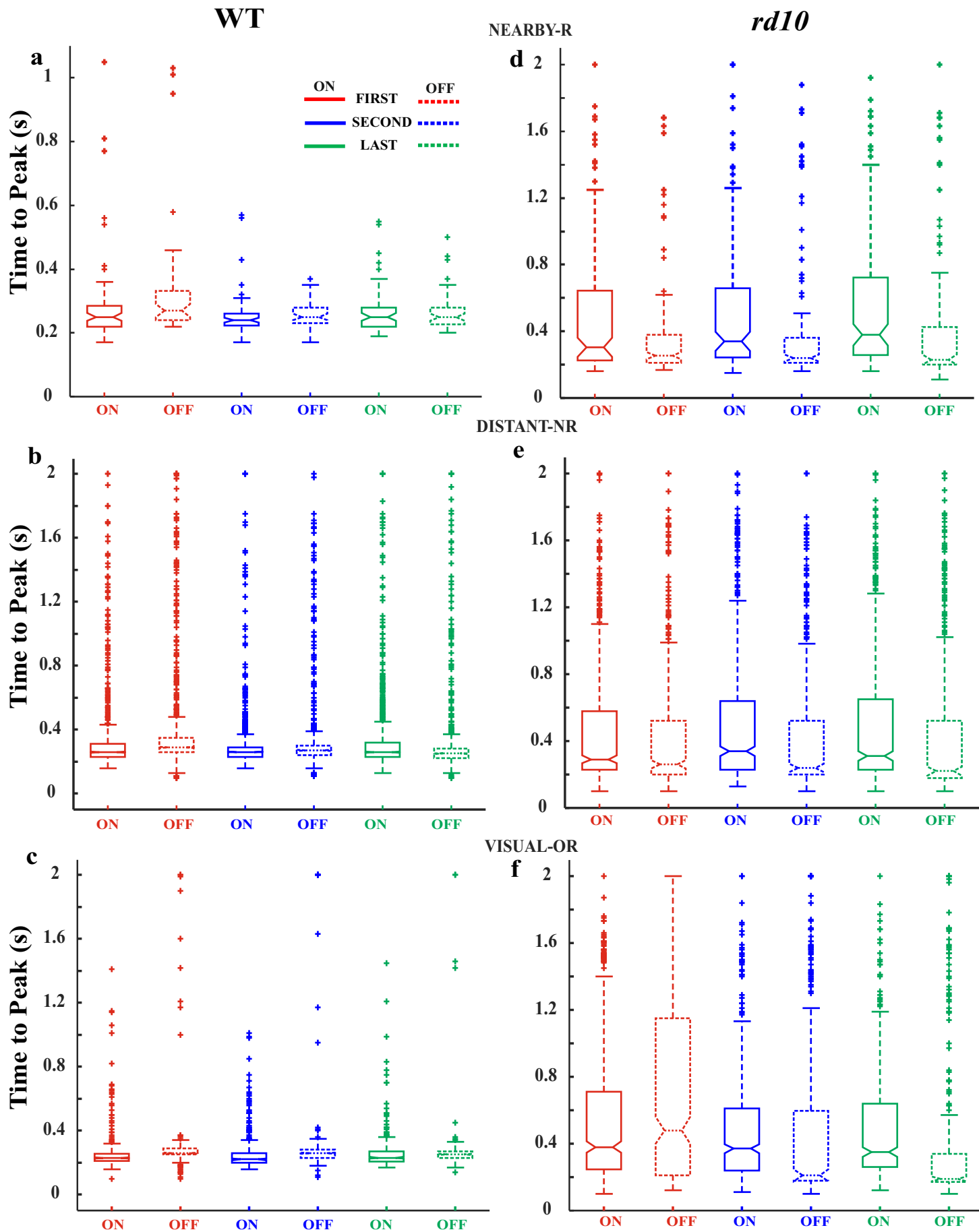
Table 3	WT (CELL COUNT)										rd10 (CELL COUNT)								
	NEARBY- (RESPONSIVE)										NEARBY- (RESPONSIVE)								
	AMPLITUDE			LATENCY			DURATION				AMPLITUDE			LATENCY			DURATION		
VISUAL TYPE	FIRST	SECOND	LAST	FIRST	SECOND	LAST	FIRST	SECOND	LAST	VISUAL TYPE	FIRST	SECOND	LAST	FIRST	SECOND	LAST	FIRST	SECOND	LAST
ON	68	67	66	68	67	66	68	67	66	ON	132	135	129	132	135	129	131	133	129
OFF	53	58	53	53	58	53	53	58	53	OFF	146	131	128	146	131	128	146	131	127
	DISTANT- (NON RESPONSIVE)										DISTANT- (NON RESPONSIVE)								
	AMPLITUDE			LATENCY			DURATION				AMPLITUDE			LATENCY			DURATION		
VISUAL TYPE	FIRST	SECOND	LAST	FIRST	SECOND	LAST	FIRST	SECOND	LAST	VISUAL TYPE	FIRST	SECOND	LAST	FIRST	SECOND	LAST	FIRST	SECOND	LAST
ON	1398	1527	1532	1398	1527	1532	1396	1523	1527	ON	531	529	529	531	529	529	526	523	520
OFF	1104	1317	1256	1104	1317	1256	1096	1315	1250	OFF	426	395	398	426	395	398	414	388	394
	VISUAL ONLY										VISUAL ONLY								
	AMPLITUDE			LATENCY			DURATION				AMPLITUDE			LATENCY			DURATION		
VISUAL TYPE	FIRST	SECOND	LAST	FIRST	SECOND	LAST	FIRST	SECOND	LAST	VISUAL TYPE	FIRST	SECOND	LAST	FIRST	SECOND	LAST	FIRST	SECOND	LAST
ON	356	354	357	356	354	357	355	354	356	ON	452	443	455	452	443	455	449	439	453
OFF	270	306	304	270	306	304	267	301	302	OFF	341	341	340	341	341	341	332	328	333

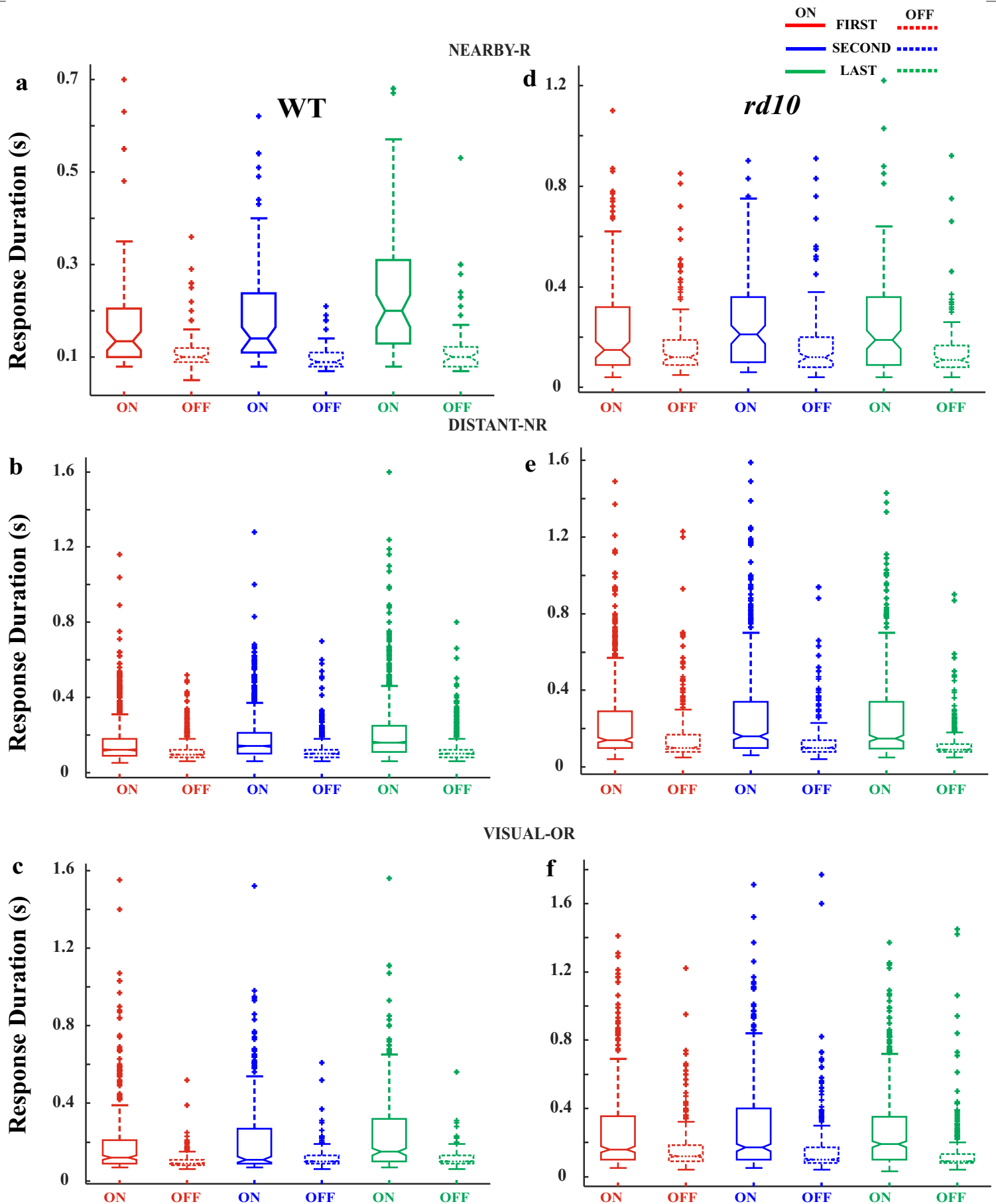
**Table 4**

**WT**

ELECTRICALLY RESPONSIVE (NEAR-BY)							TOTAL CELL COUNT
	ON	OFF	ON-OFF	ON %	OFF %	ON-OFF %	
FIRST BLOCK	27	9	32	40%	13%	47%	68
SECOND BLOCK-20MINS	21	8	39	31%	12%	57%	68
LAST BLOCK-80 MINS	20	8	39	30%	12%	58%	67
<b>DISTANT(NON-RESPONSIVE)</b>							
	ON	OFF	ON-OFF	ON %	OFF %	ON-OFF %	
FIRST BLOCK	709	153	585	49%	11%	40%	1447
SECOND BLOCK-20MINS	658	155	749	42%	10%	48%	1562
LAST BLOCK-80 MINS	672	142	745	43%	9%	48%	1559
<b>VISUAL ONLY</b>							
	ON	OFF	ON-OFF	ON %	OFF %	ON-OFF %	
FIRST BLOCK	157	37	164	44%	10%	46%	358
SECOND BLOCK-20MINS	94	38	226	26%	11%	63%	358
LAST BLOCK-80 MINS	99	29	234	27%	8%	65%	362
<b>rd10</b>							
ELECTRICALLY RESPONSIVE (NEAR-BY)							TOTAL CELL COUNT
	ON	OFF	ON-OFF	ON %	OFF %	ON-OFF %	
FIRST BLOCK	33	44	86	20%	27%	53%	163
SECOND BLOCK-20MINS	41	39	83	25%	24%	51%	163
LAST BLOCK-80 MINS	39	36	84	25%	23%	53%	159
<b>DISTANT (NON-RESPONSIVE)</b>							
	ON	OFF	ON-OFF	ON %	OFF %	ON-OFF %	
FIRST BLOCK	232	80	268	40%	14%	46%	580
SECOND BLOCK-20MINS	249	75	258	43%	13%	44%	582
LAST BLOCK-80 MINS	261	78	247	45%	13%	42%	586
<b>VISUAL ONLY</b>							
	ON	OFF	ON-OFF	ON %	OFF %	ON-OFF %	
FIRST BLOCK	280	69	164	55%	13%	32%	513
SECOND BLOCK-20MINS	219	73	216	43%	14%	43%	508
LAST BLOCK-80 MINS	220	69	220	43%	14%	43%	509









## **Appendix II- Chapter 4/ Publication 3**

# **TITLE: Spatiotemporal aspects of electrical desensitization in healthy mouse retinal ganglion cells (RGCs).**

**PREPARED FOR:** Experimental Eye Research

**AUTHORS:** Archana Jalligampala<sup>1-3\*ψ</sup>, Sudarshan Sekhar<sup>1-4ψ</sup>, Eberhart Zrenner<sup>1,2,4</sup>, Daniel L. Rathbun<sup>1,2,4\*</sup>

\*Corresponding Authors: Archana Jalligampala [archana.jalligampala09@gmail.com](mailto:archana.jalligampala09@gmail.com), Daniel L. Rathbun [daniel.rathbun@uni-tuebingen.de](mailto:daniel.rathbun@uni-tuebingen.de)

ψ Equal contributions

## **Affiliations:**

<sup>1</sup> Institute for Ophthalmic Research, Eberhard Karls University, D-72076 Tübingen, Germany

<sup>2</sup> Werner Reichardt Centre for Integrative Neuroscience [CIN], D-72076 Tübingen, Germany

<sup>3</sup> Graduate Training Center of Neuroscience/International Max Planck Research School, D-72074 Tübingen, Germany

<sup>4</sup> Bernstein Center for Computational Neuroscience Tübingen, D-72076 Tübingen, Germany

## **Funding & Acknowledgements:**

This study was supported by the Werner Reichardt Centre for Integrative Neuroscience [CIN] at the Eberhard-Karls University of Tübingen. The CIN is an Excellence Cluster funded by the Deutsche Forschungsgemeinschaft [DFG] within the framework of the Excellence Initiative [EXC307, including the senior professorship of Prof. Eberhart Zrenner and **PP 2011-07 & 2013-04** to DLR]. This study is also part of the research program of the Bernstein Center for Computational Neuroscience, Tuebingen, funded by the German Federal Ministry of Education and Research [BMBF, **01GQ1002 & 031A308**]. Additional funding was provided by the Tistou and Charlotte Kerstan Foundation [to AJ & DLR], the German Ophthalmology Society [DOG, to AJ], and PRO RETINA Germany foundation for prevention of blindness [to AJ].

The authors would especially like to thank Professor Thomas Euler and his laboratory for their guidance and support. We thank Mrs. Regina Ebenhoch for expert graphics support The

authors gratefully acknowledge the technical assistance of Kludija Masarini and Norman Rieger. In particular, DLR thanks Prof. Euler for his selfless mentorship, Dr. Tobias Breuninger for his work in setting up the optical pathway used in these experiments. Finally, we thank Professor Shelley Fried for many helpful discussions and his unwavering enthusiasm for this research.

**Competing Financial Interests:**

None

**Author Contributions:**

AJ , SS & DLR designed the experiments. AJ performed all the experiments. AJ & SS conducted the analysis. AJ prepared the draft of the manuscript. AJ, SS EZ & DLR provided critical feedback on the manuscript.

## Abstract:

*Objective:* Over the past two decades the field of retinal prostheses has achieved significant milestones by restoring visual percepts in patients suffering from retinitis pigmentosa (RP) and age-related macular degeneration (AMD). It has been demonstrated *invitro* that, repetitive electrical stimulation of the retinal network, results in a reduced sensitivity of the retinal neurons to respond to further stimulation. Such reduction in the RGC response is known as *desensitization*. This phenomenon is believed to contribute to visual percept fading often reported by human implant subjects. Although desensitization has been well characterized at fixed spatial locations ( $\tau$ , the time constant), little is known about how far in space desensitization extends ( $\lambda$ , space constant). Here we investigate the lesser-known spatial aspect of desensitization in the healthy mouse retinas.

*Approach:* We recorded the RGC responses to paired-pulse stimulation using micro-electrode array (MEA). By systematically varying the paired-pulses across different inter-electrode distance and different interpulse intervals we studied the spatiotemporal interaction of electrical desensitization.

*Main Results:* Spatiotemporal interaction of desensitization varies as a function of space and time. We identified that for the shortest inter-electrode distance (200  $\mu\text{m}$ ) the level of desensitization was maximum in comparison to other inter-electrode distance. For 200  $\mu\text{m}$  inter-electrode distance we saw a gradual decrease in responses for interpulse intervals from 1 s (1 Hz) to 100 ms (10 Hz), with maximum desensitization observed at 10 Hz. Interestingly, with further increase in frequencies, we observed an increase in RGC response.

*Significance:* Knowledge of these spatiotemporal interactions of electrical desensitization is essential for developing effective patterns of stimulation for the next generation retinal prostheses.

**Keywords:** retinal prosthesis, electrical stimulation, spatiotemporal interactions, MEA, spatial, desensitization

## Introduction:

Around four million people suffer from the blinding diseases of retinitis pigmentosa (RP) or age-related macular degeneration (AMD), with estimated worldwide prevalence rates of 1 in 4000 each for AMD and RP (Hamel, 2006; Hartong *et al.*, 2006; Mariotti S., 2012; Resnikoff and Foster, 2005). Currently, there is no cure for these diseases, but a few treatment strategies are being investigated. Such potential treatments include neuroprotection, photoreceptor restoration via stem cells, optogenetics, gene therapy and neuroprosthetic stimulation. Each of these modes of treatment has shown the potential for success in animal models (Bennett *et al.*, 2016; Nirenberg and Pandarinath, 2012; Schwartz *et al.*, 2015). However, prosthetic stimulation remains the only treatment to be approved for clinical use in human subjects (da Cruz *et al.*, 2013; Stingl *et al.*, 2017, 2015; Zrenner *et al.*, 2011).

The relative success of neuroprosthetic stimulation is possible because, while the retinal photoreceptors cease to transform incident light into neural signals and subsequently die, the other retinal neurons survive. This remaining retinal circuitry provides a substrate for sight restoration via prosthetic stimulation. Accordingly, it has now been demonstrated that humans blinded by retinitis pigmentosa can regain limited visual perception through the application of electrical pulses to the retina (Zrenner *et al.* 2011, Stingl *et al.* 2017, daCruz *et al.* 2013). However, as efforts to optimize artificial stimulation of the retina have proceeded, some practical impediments have been identified. Notable among these is the observation by human patients implanted with retinal prostheses that the visual percepts (phosphenes) evoked by an electrical pulse may fade with repeated stimulation (Zrenner *et al.* 2011, Stingl *et al.* 2015, Stingl *et al.* 2017). Furthermore, phosphenes fade more quickly with progressively shorter delays as the frequency of electrical stimulation is increased (e.g., pulses at 7 Hz fade after 7 seconds) (Freeman and Fried, 2011; Im and Fried, 2016; Jensen and Rizzo, 2007). For a retinal implant to provide optimal visual percepts, it is important that this limited temporal resolution is increased. Serendipitously, recent *in vitro* animal experiments have demonstrated that the spiking responses of retinal ganglion cells to electrical stimulation also decrease under repetitive stimulation in a frequency-dependent manner (Fried *et al.* 2006, Jensen & Rizzo 2007, Ryu *et al.* 2009, Freeman & Fried 2011). Because these retinal ganglion cells (RGCs) are the only neurons that carry visual information from the retina to

the brain, it is suspected that this desensitization of RGC responses may be partially responsible for the perceptual fading reported by human patients.

Although we are beginning to understand the frequency dependence and time course of desensitization (Im & Fried 2016, Freeman & Fried 2011, Jensen & Rizzo 2007) the distance to which desensitization extends across the retina remains unexplored. On the one hand, desensitization may extend only as far as the distance at which electrical stimulation can activate RGC action potentials (spikes). On the other hand, if desensitization is mediated by feedback in the retinal circuit, the area of desensitization could be significantly larger or smaller than that of electrical activation.

When the retina is electrically stimulated, two categories of spikes are recorded from RGCs (Fried *et al.* 2006). First are the ‘direct spikes’ which originate from direct electrical depolarization of the RGC membrane, and second is the ‘indirect spikes’ which are elicited through synaptic input to RGCs from neurons upstream of RGCs. The phenomenon of rapid desensitization is believed to be a property of indirect RGC spikes originating from stimulation of the retinal network (Freeman and Fried 2011, Im and Fried 2016). However, a recent study (D. Tsai *et al.*, 2011; David Tsai *et al.*, 2011) has shown that the ‘direct spikes’ can be desensitized at sufficiently high frequencies. Furthermore, Freeman and Fried (2011) were able to demonstrate that desensitization resulting from a 16 Hz pulse train consists of a fast component (time constant,  $\tau$ , = 176 msec), and a slow component ( $\tau$  = 14 seconds). However, because RGCs display many different spiking patterns in response to electrical stimulation, it remains unclear whether the two temporal components of desensitization are specific to certain types of RGCs or are universal. Indeed, it is believed that there may be upwards of 40 different functional RGC types whose unique visual response patterns are governed by a variety of different retinal sub-circuits (Baden *et al.*, 2016). These same circuits are likely to influence how each RGC type desensitizes in response to electrical stimulation. Further, how the spatial ( $\lambda$ ) and the temporal ( $\tau$ ) component of desensitization interact for different RGC types remains poorly understood. Therefore, a full understanding of the desensitization phenomenon will likely require accurate identification of the individual RGC types.

In light of these facts, the primary goals of the present study are as follows: (1) to determine the spatial extent of desensitization. By using paired-pulse stimulation and varying them across various inter-electrode distance and different interpulse intervals we can identify the spatial extent of desensitization. Further, we systematically investigate how such

parameters influence the spatiotemporal interaction of electrical desensitization. (2) In addition to exploring the spatial extent of desensitization, we validate the observations from previous studies for the temporal component of desensitization. (3) Based on the visual response to the full-field flash visual stimulus, we classify the cells into ON, OFF and ON-OFF RGC types (Carcieri *et al.*, 2003). Upon classifying the cells, we attempt to understand the spatial and temporal aspects of desensitization for these RGC types.

## Methods:

### Experimental Design

The data contained here represents the first-ever study to describe the spatial extent of electrical desensitization (space constant,  $\lambda$ ) of the retinal network in the healthy mouse retina. Apart from confirming the earlier observations of the temporal component of desensitization (time constant,  $\tau$ ), this study further explores the spatiotemporal interaction of desensitization. While most of the previous studies used rabbit and cat retinas (Cicione *et al.*, 2014; Freeman and Fried, 2011; Im and Fried, 2016; Jensen and Rizzo, 2007) to examine the aspects of desensitization, we used healthy mice retinas to explore the spatiotemporal interaction of desensitization. Our choice of mice was based on the easy access to the animal and suitable comparison to the diseased mice model of RP. For this study, our choice for healthy mice retina was to make comparisons to previous observations which investigated the temporal aspects in healthy retinas and to shed light on the spatial aspects of desensitization when the retinal circuit is intact and functional. Having a proper understanding of the healthy retina would help in developing suitable stimulation paradigms for degenerated retinas.

As a first step, we performed experiments to determine the **current threshold** for epiretinal network stimulation using microelectrode arrays (MEAs). While many previous studies (Boinagrov *et al.*, 2014; Goo *et al.*, 2011a; Jensen *et al.*, 2005; Ryu *et al.*, 2009b) have attempted to understand the stimulation thresholds of the retinal network to current stimulation, there still exists variability among research groups (and studies) while determining the appropriate current threshold (Jalligampala *et al.*, 2017). This means that the current threshold for one experimental setup might not be appropriate for another. Hence to account for this variability, we established the current threshold for our experimental setup. A total of 3 retinal tissues from 3 mice were used to determine the current threshold.

After determining the threshold, we sought out to investigate the **spatial and temporal aspects of desensitization** in the mouse retina to epiretinal network stimulation (current pulses). For determining the temporal aspects, we delivered trains of pulses to the retinal tissue via a single electrode of the MEA. Unlike, previous studies (Freeman and Fried, 2011; Jensen and Rizzo, 2007) which used the same cells (patch clamp recording) and same tissue to determine the threshold as well as the temporal aspects of desensitization, we used different mice (and different retinal tissues) to investigate the temporal component of desensitization. Our choice to use different mice/ different retinal tissue was based on the difference in our method for threshold determination (*refer to Data Analysis Threshold determination*) and the difference in experimental set up (patch clamp as opposed to our MEA recording). Further, it is known that the tissue property changes post electrical stimulation (hysteresis), hence to remove any stimulus-specific confound we used different retinal tissues. A total of 3 retinal tissue from 2 mice were used to examine the temporal component of desensitization.

Lastly, to determine the spatial extent and spatiotemporal interaction of desensitization, we delivered paired-pulse current stimuli (at two different electrodes of the MEA) over different inter-electrode distances. To examine, this, a total of 3 retinal tissue from 2 different mice were used. Thus, taken together, a total of 6 mice and 9 retinal tissues were used for this study. A detail of the number of RGCs for each condition and the stimulation protocol is described below. (*refer to Electrical stimulation and Results*).

## Animals

The animals were housed under standard white cyclic lighting, mimicking regular daily rhythms. They had free access to food and water. Adult wild-type (wt) C57Bl/6J (Jackson Laboratory, Bar Harbor, ME, USA) strains were used, with age ranging from post-natal day 60 to 120. The age range was chosen to make comparisons to the diseased model of RP (*rd10 mice, refer to Future Studies*), at a late stage of degeneration (complete loss of photoreceptors and heavy rewiring), which corresponds to the age at which the human subjects are currently being implanted. No gender specificity was considered for the study. All procedures were approved by the Tübingen University committee on animal protection (Einrichtung für Tierschutz, Tierärztlichen Dienst und Labortierkunde directed by Dr. Franz Iglauer) and performed in accordance with the Association for Research in Vision and



Ophthalmology (ARVO) statement for the use of animals in ophthalmic and visual research. All efforts were made to minimize the number of animals used and their suffering.

### **Retinal Preparation**

For retinal dissection, mice were anesthetized by CO<sub>2</sub> inhalation, checked for absence of withdrawal reflex to a pinch of the between-toe tissue, and then euthanized by cervical dislocation. Under normal room lighting, the eyes were removed to carbogenated (95% O<sub>2</sub> and 5% CO<sub>2</sub>) artificial cerebrospinal fluid (ACSF) solution containing the following (in mM): 125 NaCl, 2.5 KCl, 2 CaCl<sub>2</sub>, 1 MgCl<sub>2</sub>, 1.25 NaH<sub>2</sub>PO<sub>4</sub>, 26 NaHCO<sub>3</sub> and 20 Glucose, pH 7.4. For each eye, during the dissection process, performed under dim light conditions, the cornea, ora serrata, lens and vitreous body were removed, the retina was detached from the pigment epithelium, and the optic nerve was cut at the base of the retina. Special care was taken to remove all traces of vitreous material from the inner surface of the retina to optimize contact between the nerve fiber layer and recording electrodes. Retinas were maintained in carbogenated ACSF until needed. For recording, a retinal half was mounted with the ganglion cell layer down on a planar microelectrode array. Two miniature paintbrushes were used to orient and flatten the retinal half without risking damage to the microelectrode array (MEA) and the retina, and a dialysis membrane (CelluSep, Membrane Filtration Products Inc., Seguin, Texas, USA) mounted on a custom Teflon ring was lowered onto the retina to press it into closer contact with the MEA (Meister *et al.*, 1994). After securing the MEA under the preamplifier, the retina was continuously superfused with carbogenated ACSF (~6 ml/min) maintained at 33°C using both a heating plate and a heated perfusion cannula (HE-Inv-8 & PH01; Multi Channel Systems, Reutlingen, Germany). An adaptation time of >30 minutes was provided before recording the data.

### **Microelectrode array & Data Acquisition**

For recording the spiking responses from the RGCs, a planar MEA, containing 59 circular titanium nitride electrodes (diameter: 30µm, interelectrode spacing: 200µm; 60MEA200/30iR-ITO, Multi Channel Systems, Reutlingen, Germany) was used. The array was in an 8X8 rectilinear grid layout, with indium tin oxide (ITO) electrode tracks insulated by silicon nitride (Si<sub>3</sub>N<sub>4</sub>) on a glass substrate. Electrodes were absent from the four corners of the grid, and one electrode was substituted with a large reference electrode. The impedance of the electrodes in saline water were approximately 200-250 kΩ at 1 kHz (as measured with

the NanoZ impedance meter from MCS, Reutlingen, Germany). The MEA60 system (MCS, Reutlingen, Germany) was used for data acquisition including: the RS-232 interface, a 60 channel preamplifier with integrated filters and a blanking circuit (MEA 1060-Inv-BC) controlled by MEA\_Select software to reduce recording noise by grounding any defective electrodes and to assign electrical stimulation waveforms to the selected electrode. Data were collected using the MC\_Rack program on a personal computer running Windows 7 and fitted with MC\_Card data acquisition hardware and an analog input card to record stimulus trigger signals. The raw data were recorded at a rate of 50 kHz/channel with a filter bandwidth ranging from 1 Hz - 3 kHz and amplification gain of 1100.

### **Electrical Stimulation and recording**

Stimulus pulses were generated using a stimulus generator (STG 4008; Multi Channel Systems, Reutlingen, Germany). The stimuli were delivered from the ganglion cell side of the retina (epiretinal) via one of the 59 electrodes (in case of determining the spatial extent two electrodes were used, refer to *Spatial component of desensitization*) which was always an internal electrode to ensure a maximum number of nearby recording electrodes and chosen based on proximity to electrodes with robust neural signals (Jalligampala et al 2017). Although subretinal implants deliver electrical stimulation from the photoreceptor side of the retina to activate the retinal network, it is well established that the desired network stimulation can be achieved by stimulating from either side of the retina (Im & Fried 2015, Boinagrov *et al.* 2014, Jalligampala *et al.* 2017 and Sekhar *et al.* 2016). Therefore, to have easy access to the acute retinal tissue, the electrodes of the MEA were used for both stimulating and recording. Before and after electrical stimulation, spontaneous spikes from the RGCs were recorded for 2 min each as a control measure to monitor overall effects of electrical stimulation on the retinal circuitry.

**Threshold stimuli:** To determine the thresholds for activation of RGCs, the retina was stimulated with constant current stimuli (biphasic, cathodic first, rectangular pulses with no interphase gap). The current stimulus amplitudes (1, 2, 3, 4, 5, 7.5 and 10  $\mu\text{A}$  at 500  $\mu\text{s}$  per phase) were provided sequentially from lower to higher amplitudes. Within each amplitude block, there were a total of 30 trials and each biphasic pulse was separated from another by 5 s. Each stimulus block was separated from the next by a minimum of 120 s while recording spontaneous activity for 60 s of the 120 s. A single electrode from 59 electrodes was used to

deliver the current pulses, and the remaining 58 electrodes were used for recording. For a definition of the threshold refer to *Data Processing and Data Analysis, Threshold determination*. Once the threshold was obtained from the population, current amplitudes at 2.5 X threshold and 2 X duration per phase (i.e., 1000  $\mu$ s per phase) was used for investigating the temporal as well as spatial components of desensitization. Our selection of 2.5 X threshold and 2 X duration was to ensure that the stimulus delivered was high enough to account for the cell to cell threshold variability and could stimulate majority of retinal ganglion cells via epiretinal network stimulation.

**Temporal component of desensitization ( $\tau$ ):** Pulse train stimulation- To gauge the effect of multiple stimuli, pulse trains of ten biphasic current pulses (2.5 X threshold, 10  $\mu$ A ) were delivered via a single electrode to the retina at different frequencies (2, 4, 10, 16, 20, 25, 40, 62,5 Hz). The frequencies were provided in sequential order from the lower value to higher values (i.e., 2Hz to 62.5Hz) Within each frequency, the stimulus train (10 current pulses) was repeated five times with five seconds in between consecutive pulse trains (**Fig. 1a**).

**The spatial component of desensitization ( $\lambda$ ):** To examine the spatial extent and the spatial and temporal interaction of desensitization, the retina was stimulated with a paired-pulse paradigm consisting of a conditioning/priming pulse followed by a test pulse. To determine the space constant ( $\lambda$ ), the location of the electrode (inter-electrode distances) that delivers the conditioning pulse or “priming” pulse was varied with respect to the test pulse (which was always provided to a fixed electrode. The paired pulses were charge-balanced biphasic current pulses–10  $\mu$ A amplitude, with duration of 1000  $\mu$ s per phase). The paired-pulse stimulus set (interpulse intervals of 1000, 500, 100, 50, 25 ms) was presented for different inter-electrode distances (1000, 800, 600, 400, 200  $\mu$ m) in decreasing order, i.e., from the farthest (1000  $\mu$ m) to the nearest (200  $\mu$ m). Within a given distance the entire paired-pulse stimulus set was presented in decreasing order, i.e., from 1000 ms (longest) to 25 ms (shortest). Each interpulse interval was repeated ten times with two seconds in between consecutive paired-pulse before the next interpulse interval was presented. Due to large stimulation artifacts at the electrode delivering the test pulse, the responses from the neighboring 8 electrodes ( 7 recording and 1 recording as well as stimulating, for 200  $\mu$ m interelectrode distance) surrounding the test pulse were used for analysis (**Fig. 1b**). Note:

For plotting the normalized response of the RGC as a function of inter-electrode distance, the inter-electrode distances were calculated between the different conditioning pulse electrodes and the recording electrode recording the RGC spikes.

### **Visual Stimulation**

Visual stimuli were presented to the retina from below through the transparent MEA by a commercially available DLP-based projector (K10; Acer Inc., San Jose, California, USA). The image was focused and centered onto the plane of the retina directly over the MEA with a custom-built series of optical components and manual microdrive with 3 degrees of freedom. Visual stimuli were controlled with custom software. Each visual stimulus block consisted of a full-field (~3 x 4 millimeters) 'flash' stimulus, cycling 2 seconds ON( 40 klx) followed by 2 seconds OFF (20 lux), 20 times without pause (mean illuminance = 20 klx, 99.9% Michelson contrast, The brightness range was chosen covered a wide range of intensities occurring in the natural environment (Rodieck, 1998). A minimum of four visual stimulus blocks (in case of spatial desensitization there were 6 visual blocks) were interleaved before, after, and within each electrical stimulation experiment (for threshold and temporal desensitization) that spanned ~60-90 minutes of recording time, including the first and last flash blocks.

### **Data Processing & Data Analysis**

The stored raw data were processed using commercial spike sorting software (Offline Sorter, Plexon Inc., TX, USA). Raw voltage traces were first filtered (using low-cut, 12 point Bessel filter at 51 Hz to exclude line noise); then putative events were detected using a threshold crossing method (4 standard deviations below the mean of the amplitude histogram). These events were sorted into clusters with an automated routine (T-distribution Expectation Maximization) to assign noise events as well as spiking events from up to 5 sources recorded on each electrode to separate "units." Finally, as a quality control step, multiple sorting solutions were manually inspected to identify the best solution and to occasionally modify this solution to minimize Type I and Type II errors in the attribution of events to different sources. Only units with a distinct waveform, interspike interval lock-out period, which demonstrated a refractory period in their autocorrelogram and was stable during the entire course of the experiment, were considered and included in the analysis presented here. Time stamps assigned to the detection threshold crossing of these sorted spikes were collected with NeuroExplorer (PlexonInc, TX, USA) and exported to MATLAB for further analysis.

**Threshold determination:** The spiking response was integrated over the interval spanning 10 to 100 milliseconds (refer to **3.2 Diversity of RGC responses, Jalligampala et al. 2017**) after pulse onset and averaged across the 30 repetitions of the seven stimulus amplitudes. Likewise, a spontaneous rate, chosen to best characterize the baseline firing rate within the context of ongoing electrical stimulation, was calculated from the 1 s of recording time before each pulse and averaged across all 210 responses (30 repetitions for seven stimulus amplitudes). The threshold was defined as the average spontaneous rate + SD (standard deviation). The threshold current amplitude was defined as the lowest current whose response exceeded the threshold as defined above.

**Temporal component of desensitization ( $\tau$ ):** For a single RGC, for each frequency pulse train, the responses were normalized to the first pulse response. For frequencies, less than 10 Hz, an integration window of 10-100 ms was considered for counting the number of spikes. For higher frequencies, (> 10 Hz) the counting window began at 10 ms and lasted until the next pulse.

**Spatial component of desensitization ( $\lambda$ ), Normalization 1:** To quantify the spatial extent of desensitization the spiking responses of the “test” pulse was integrated over the interval spanning 10 to 100 milliseconds. The responses were normalized to the average response (10 repetitions) for the longest interpulse interval (1000 ms) and at the farthest distance (1mm) test pulse which is expected to show the least desensitization.

**Normalization 2:** As an alternate metric to quantify the spatial component of desensitization, for each inter-electrode distance the spiking responses of the test pulse (response window of 10-100 ms) were normalized to the average response of the test pulse at the longest interpulse interval for that distance (1000 ms for each distance). This normalization would allow us to quantify the spatial component of desensitization during ongoing electrical desensitization as opposed to normalization 1, which normalizes the responses to the least desensitized pulse. For all the statistical comparisons, the non-parametric Wilcoxon’s *rank sum* test (MATLAB; The Mathworks, Natick, MA) was used with a significance threshold of 0.05.

## Results:

### RGC response characteristics and variability

In accordance with previous studies((Boinagrov *et al.*, 2014; Goo *et al.*, 2011b; Ryu *et al.*, 2009a, 2009b)it was feasible to elicit electrically driven RGC spikes by epiretinal network stimulation using biphasic current pulses. In total, 434 single units of RGCs showing electrically driven spiking activities were identified from 3 different retinal patches. **Fig. 1a.** shows an example raw waveform of a single RGC responding to biphasic current stimulation. It was observed that the electrically driven RGC spikes were concentrated 10-50 ms post-stimulation as seen from the rastergram and poststimulus time histogram (PSTH) on **Fig. 2b** and **2c**. The spiking response was integrated 10 to 100 ms post-stimulation. As typical for our data, few spikes were observed within the first 10 ms post-stimulus ( **Fig. 2b** grey shaded area). These spikes resulted from the direct RGC stimulation and were obscured with stimulation artifacts (which often lasted for few milliseconds), thus excluded from our analysis. Similarly, a longer response window (>100 ms) would not be preferable as for mice retinas the overall spontaneous rates are higher in comparison to the chick or rabbit retinas. Therefore, a longer response window would lead to a larger contribution from the spontaneous rates leading to a decreased signal to noise ratio of the evaluating response. Additionally, the 10 to 100 ms latency range minimizes the spike activation via photoreceptors, as these spikes are lost during late-stage degeneration. Thus, our selection of 10-100ms integration window was to represent indirect RGC stimulation through the activation of presynaptic neurons- bipolar cells. The intensity of the RGC responses was measured by calculating the number of evoked spikes in the 10-100ms response integration window. **Fig. 2d** shows the firing rate of the RGC as a function of pulse amplitudes. For the example cell, it was seen that with an increase in amplitude the cell's firing rate increased monotonically.

Many RGCs (186/434) showed a steady monotonic increase of RGCs firing rate with increase in current amplitude (**Fig. 3a**). A cell had a monotonic response when the cell's firing rate increased linearly with increasing current amplitudes. For these cells, the correlation coefficient between the evoked RGC spikes and the pulse amplitudes were larger than 0.7. With further increase in amplitude the monotonic responses saturated and in some cases, there was a slight decrease in response for the highest current amplitudes. These cells, from

earlier studies, have been categorized as well-modulated RGCs (Ryu et al 2009). For some cells (29/434), the responses decreased with increasing current amplitudes and were referred as monotonically decreasing RGCs (**Fig. 3b**). In some cases (219/434) the RGC responses were uncorrelated with, increasing current amplitude (**Fig. 3c**). These RGCs were referred to as nonmonotonic RGCs or poorly-modulated RGCs. This suggests that the responses to electrical stimulation vary from cell to cell and that, while determining electrical thresholds, the variability of RGC monotonicity is an essential factor which needs to be considered. It was seen that the thresholds for stimulation were variable from one cell to another, **Fig. 3d** shows the average response pattern of the entire population (inclusive of all response patterns,  $n=434$ , mean+ SE). Further, **Fig. 3e** shows the average response pattern of the 186 well-modulated RGCs. It can be seen that for the firing rates for the well-modulated RGCs were comparatively higher in comparison to the firing rate of the entire population. On calculating the thresholds for the entire population ( $4.0 \pm 0.5 \mu\text{A}$ , charge density:  $0.64\text{mC}/\text{cm}^2$ ) and for the well-modulated RGCs ( $2 \pm 0.2 \mu\text{A}$ , charge density:  $0.311\text{mC}/\text{cm}^2$ ), there was a two-fold difference between the thresholds further emphasizing the need to acknowledge the RGC variability while establishing thresholds for optimal stimulation.

### **Temporal component of desensitization (time constant, $\tau$ )- Response to Pulse train stimulation**

To evaluate the desensitizing effect of multiple pulses on RGC responses via retinal network activation, pulse trains consisting of ten biphasic current pulses at  $2.5 \times$  threshold ( $10 \mu\text{A}$ ) and variable frequencies were applied to the retina (*Methods*). In general, the number of spikes in response to the tenth pulse were lower in comparison to the first pulse spiking response. Example cells demonstrating desensitization of the normalized RGC responses to pulse train stimulation at different frequencies are shown in **Fig. 4a(i-iii)**. In accordance, with a previous study (Freeman & Fried 2011), the amount of desensitization and the RGCs responses to pulse trains were variable. For a few cells, the level of desensitization was negligible at the tenth pulse (and at times facilitated **Fig. 4a(i)** for 2 Hz), whereas some cells had no response by the tenth pulse, reemphasizing the importance of considering ganglion cell variability when examining desensitization at the population level. Apart from cell-to-cell variability, within individual cells, there was variability of response to repetition of the same stimulus. Such response variability could be a prime factor in the large error bars for the different frequencies at different pulses ( **Fig. 4a(i-iii)**). , **Fig. 4b** shows the normalized

spiking response averaged across the entire population (n=155). For most frequencies (2, 4, 10, 16, 20, 25 Hz) although there was a clear trend of decreasing response with subsequent pulses and increasing frequencies the level of desensitization was modest in comparison to previous studies (Jensen & Rizzo 2007, Freeman & Fried 2011). This modest decrease (Ryu *et al.* 2009) could be attributed to the higher spontaneous rates in mice retina in comparison to rabbit retinas which could increase the overall noise level. However, for higher frequencies like 40 Hz, we observed a potentiating response to subsequent pulses (**Fig. 4b red**). On the same lines, a study from Jensen & Rizzo (2007) also found an interesting pattern of response to interleaved pulses, but differing from our observations, their overall RGC response decreased in comparison to the first pulse and alternated in amplitude between successive pulses in a 'sawtooth' fashion. Likewise, for 62.5 Hz we observed irregular responses to subsequent pulses. To evaluate the level of desensitization for the entire population, we made pairwise comparisons between pulse rates by comparing the normalized response of the second pulse with the tenth pulse (Jensen & Rizzo 2007). We observed that for frequencies of 16, 20 and 25 Hz the level of desensitization was significantly more in comparison to 2, 4, 10 and 40 Hz (**Table 1 (a)**).

Next, we attempted to classify the entire population into different cell types (purely ON, purely OFF, and ON-OFF) based on their visual responses. For our population majority of the cells were classified as purely ON (n=74) and ON-OFF (n=71). Only 10 cells were classified as purely OFF cells. As low cell count could lead to faulty statistical comparisons, the purely OFF cells were not represented in the figures or statistical tests. **Fig. 5a** shows the average normalized response of the ON visual response type population (n=74). In lines to the previous observation from the entire population, there was a clear trend of decreasing spiking activity with higher frequencies and subsequent pulses. However, for the ON cells, at 40Hz although the overall spiking response was higher, there was no potentiating response to subsequent pulses. Instead, there was a reduced response (of the tenth pulse) when compared to the first pulse. By multiple pairwise comparisons as described above, for 16, 20 and 25 Hz the level of desensitization was significantly higher in comparison to 2, 4, 10, 40 Hz. Additionally, at 62.5 Hz, the level of desensitization was significantly more in comparison to 2Hz. (**Table 1 (b)**) **Fig. 5b** shows the average normalized response of the ON-OFF visual response type population (n=71). Frequencies at 2, 4, 10, 16, 20 and 25 Hz showed a decreased response to the tenth pulse in comparison to the first pulse, However, for higher frequencies (40 and 62.5 Hz), especially for 40 Hz the facilitation was very pronounced. Multiple pairwise



comparisons between frequencies showed that at 40 Hz the responses were significantly potentiated (less desensitized) in comparison to 2, 4, 10, 20 and 25 Hz (which had a higher level of desensitization, **Table 1 (c)**). This could suggest that the components of the OFF pathway could potentially contribute to a potentiating mechanism in the retina when stimulated at 40 Hz.

Take together; these results indicate that across a population (1) the level of desensitization increases with increase in pulse rates (2) There exists a considerable variability in between cells and within a single cell in response to repetitive stimulation.

### **The Spatiotemporal interaction of electrical desensitization-**

#### **I. Determining the spatial extent (space constant, $\lambda$ ) (when normalized to the least desensitized pulse, Normalization 1)**

There remains an inadequate understanding of the RGC response arising from the retinal network when the electrical stimulus interval is varied simultaneously both in space and time. To explore this interaction, the retina was stimulated at different interpulse intervals while varying the interelectrode distances between the “priming/ conditioning” and the “test” pulse (*Methods*). The neighboring 8 electrodes around the test pulse were used to examine the interactions of space and time in desensitization. Example cells (**Fig. 6 a(ii)**) show normalized responses of RGCs as a function of the interpulse interval for various interelectrode distances. For the shortest inter-electrode distance (200  $\mu\text{m}$ ), the level of desensitization was most pronounced. For distances  $>200 \mu\text{m}$  the level of desensitization was comparatively less and for some distances (800-1000 $\mu\text{m}$ ) there was facilitation of response (Cicione *et al.*, 2014). In example cell, **Fig. 6 a(ii)** for 200  $\mu\text{m}$  the level of desensitization was maximum for 10 Hz (100 ms). With shorter interpulse intervals (50 ms and 25 ms) there was an increase in response. In example cell, **Fig. 6 a(i)** for 200 $\mu\text{m}$  the level of RGC response desensitization was maximum irrespective of the of the interpulse interval, suggesting a strong dependence on inter-electrode distance.

**Fig. 6 b(ii)** demonstrate desensitized RGC responses for the same example cells as a function of interelectrode distance for different interpulse intervals. As discussed above for most of the RGCs the shortest distance (200  $\mu\text{m}$ ) had the most pronounced desensitization. It should be noted that for the single cell examples the inter-electrode distances are actual distances between the conditioning pulse electrode and the recording electrode. However, for the

population plot, we binned the actual inter-electrode distances to the inter-electrode distances between the test pulse and conditioning pulse (i.e., for an inter-electrode distance of 283  $\mu\text{m}$  we binned it to the nearest distance, i.e., 200  $\mu\text{m}$ ). This was done after visualizing the distribution of cells at different inter-electrode distances and for a better representation of the response pattern. **Fig. 6 (c & d)** shows population plot for the normalized response as a function of interpulse interval and inter-electrode distance respectively (n=43). In line with the example cells, we observed that the level of desensitization in comparison to other inter-electrode distance was maximum for the shortest distance (200  $\mu\text{m}$ ) and at an interpulse interval of 100 ms (10 Hz). However, similar to temporal aspects of desensitization the desensitization was modest even for the shortest distance (200  $\mu\text{m}$ ). Multiple pairwise comparisons (**Table 2(a)**) showed that across all interpulse intervals the level of desensitization was maximum for the shortest distance (200  $\mu\text{m}$ ). However, there was a weak dependence on the interpulse intervals (**Table 2(b)**) suggesting that the spatial component of desensitization ( $\lambda$ ) is a crucial factor and needs to be considered while developing new stimulation paradigms. Although the population of RGCs showed this common trend, it should be noted that within this population of RGCs there exists a notable heterogeneity of responses (Jalligampala *et al.* 2017, Ryu *et al.* 2009, Im & Fried 2016). Therefore, as a next step, we categorized the population in ON (n=14), OFF (n=3) and ON-OFF (n=26) cells (Carcieri *et al.* 2003). As stated above the number of OFF cells were low in our dataset, hence were not represented in the figures. For ON-OFF cells (**Fig. 7a(i) & b(i)**) the trend for the shortest distance (200  $\mu\text{m}$ ) was similar to that of the population. For the ON cells (**Fig. 7a(ii) & b(ii)**) the level of desensitization was maximum at 100 ms (10 Hz) across all inter-electrode distances.

## II. **Determining the spatial extent (space constant, $\lambda$ ) during ongoing electrical desensitization( when normalized to the longest interpulse interval of each inter-electrode distance, Normalization 2).**

As an alternate metric for measuring the spatial limit during ongoing electrical desensitization, we normalized the RGC responses to the response to the longest interpulse interval (1000 ms) at each inter-electrode distance. It should be noted that the cells which did not have a response at the longest interpulse interval (1000 ms) were excluded from the analysis. Hence the total population count decreased from 43 cells to 30 cells.

In agreement to previous observations described above, the level of desensitization was maximum for the shortest distance (200  $\mu\text{m}$ ) in comparison to other inter-electrode distance (**Fig. 8a**). Further, for 200  $\mu\text{m}$  there was a decreasing trend of RGC responses for interpulse intervals from 1000 ms (1 Hz) to 100 ms (10 Hz). However, for 50 ms (20 Hz) and 25 ms (40 Hz), the responses tend to increase. This trend was consistent for ON-OFF cells (n=18, **Fig. 8b**), however for the ON cells (n=9, **Fig. 8c**) although this trend was existent, it was very weak. Due to low cell count for OFF cells (n=3) the data was not represented in the figure. Multiple pairwise comparisons for all cells (n=30) showed that for 100 ms (10 Hz) and 50 ms (20 Hz) the level of desensitization was maximum for the shortest distance (200  $\mu\text{m}$ ) in comparison to other inter-electrode distance (**Table 3(a)**). Due to low cell count for ON and ON-OFF cells no significant statistical trend was observed (Supplement S1). Interestingly, for 25 ms (40 Hz) there was no statistical difference between the shortest inter-electrode distance and other inter-electrode distance. This was in agreement with the facilitation observed at 40 Hz (temporal aspects of desensitization), suggesting there exist some potentiating mechanisms in the retina when stimulated at 40 Hz.

## Discussion

In this present study, we have investigated the spatial extent of electrical desensitization in the retinal network, using current-controlled pulses in adult healthy mice retinas. Further, we explored the interaction between the spatial and the temporal components of desensitization. Our main findings were as follows: (1) In agreement with our previous study (Jalligampala *et al.* 2017), there exists a heterogeneity of RGC responses to electrical stimulation. We could classify the RGC responses to monotonically increasing cells, monotonically decreasing cells and non-monotonic cells. Unlike our previous study (Jalligampala *et al.* 2017) where the percentage of monotonic cells were higher for the WT retinas, we saw a comparatively equal distribution for both monotonic and non-monotonic cells. This heterogeneity of RGC responses affected the threshold determination, thereby making it a crucial point to consider while determining optimal stimulation paradigms. (2) In accordance, to previous desensitization studies (Jensen & Rizzo 2007, Freeman & Fried 2011) that investigated the temporal component ( $\tau$ , the time constant) of desensitization, we observed that the level of desensitization decreased with subsequent pulses and increasing frequencies. However, the level of desensitization was modest in comparison to the previous

studies. Further, we observed that there was variability of responses to different pulse rates (for most cases suppressive and some frequencies like 40Hz a facilitatory response) from one cell to another and within a single cell further reiterating the fact that variability of responses is a critical component which needs to be accounted while determining stimulation parameters for electrical desensitization. (3) While investigating the less understood spatial component of desensitization ( $\lambda$ , space constant), we observed that for the shortest inter-electrode distance (200 $\mu$ m) between the “conditioning” and “test” pulse the level of desensitization was more pronounced in comparison to other inter-electrode distances. Further, while exploring the spatiotemporal interaction of electrical desensitization, we observed that there was a strong dependence on the spatial component and a rather weak dependence on the temporal component.

### **Acknowledging variability of RGC responses**

#### ***Cell to Cell Variability***

There is a growing body of work illuminating the diversity of RGC types found in the mammalian retina. While this variability is most evident in the morphology of RGCs (Seung and Sümbül, 2014; Sümbül *et al.*, 2014), it can also be seen at the physiological responses of the RGCs (Baden *et al.* 2016). This diversity in RGC population strongly suggests that the sensitivity and the response patterns of the RGC to various electrical stimulation could vary considerably. Recent studies have attempted to address this variability in responses to different electrical stimulation (Jensen & Rizzo 2007, Jensen *et al.* 2005, Im and Fried 2016, Jepson *et al.*, 2013). In this present study, we consider it highly likely that the variability of responses ( **Fig. 3 a-c**) and thresholds observed owe to the diversity of the RGC population. Coupling the cell type identification similar to that of Baden *et al.* 2016 with high density MEA-based electrical stimulation will shed how different RGC types differ in their responses to electrical stimulation. Further, such variability could potentially serve as a basis for selective stimulation of different visual pathways.

Another source of population variability could be the distance from the stimulating electrode that is assigned to each RGC based on the electrode on which it was recorded. For determining the threshold, we pooled the cells which were electrically responsive at all electrodes. Further, using a MEA although we know the location of the recording electrodes, we do not know the exact location of the cell with respect to the recording electrodes. It is well known from the previous literature ( Jalligampala *et al.* 2017, Ryu *et al.* 2009,

Eickenscheidt *et al.*, 2012; Stett *et al.*, 2007) that electrical responsiveness decreases with increasing distance. Therefore, the actual location of the RGCs from the stimulating electrode could potentially lead to variability in the effective stimulus strength, thereby affecting the optimal thresholds for stimulation.

### ***Single Cell Variability***

Apart from cell-to-cell variability, there existed high variability within an individual cell for repetitions of the same stimulus. This variability could be specific for mouse retina which has comparatively higher spontaneous rates in comparison to the rabbit retina which has a relatively low spontaneous rate. (Lee *et al.*, 2013, Im & Fried 2015, Im & Fried 2016]. Such response variability could play a vital role in the large error bars seen for our single cell examples.

### **Temporal component of desensitization**

#### ***RGC response decrease with increasing pulse rates***

In agreement with the previous studies (Jensen & Rizzo 2007 and Freeman & Fried 2011), the overall trend of decreasing spiking activity with increasing frequencies and subsequent pulses was observed for our dataset. However, this decrease was modest in comparison the previous studies from rabbit retinas. This modest decrease could be specific to mouse retina which has a relatively high spontaneous rate. A similar study performed in mouse retina (Ryu *et al.* 2009) also showed a modest level of desensitization further supporting our observation. Interestingly, for 40 Hz we observed an overall facilitatory response with subsequent pulses. There are different possibilities which could reason this facilitatory response. (1) Synchronization of the RGC responses with the stimulus through the resonance of the oscillating network of excitatory and inhibitory neurons could result in a modified response (Crapper and Noel 1963). If this holds true, then this mechanism could explain our observation and the observation seen in the Jensen and Rizzo 2007 study.

(2) Facilitatory responses at higher stimulation rates (like 40 Hz) could be a consequence of the charge storing properties of the neural membranes. Previous studies ( Freeman & Fried 2011), have shown that a time constant of >100 ms is required to dissipate the charge on the membrane. Therefore, at shorter interpulse intervals (like 25 ms) there could be a summation of the charge with increasing number of pulses resulting in the likelihood of a spiking event. (3) This facilitatory response could arise from cell-specific / pathway-specific stimulation. Recent studies (Ho *et al.*, 2018; Im and Fried, 2016) have shown that with increasing

frequencies (like 20 and 40Hz) the responses of ON cells exhibited a reset behavior in which a new stimulus suppressed responses to any previous stimuli and initiated its own responses that were highly similar to the response from a single stimulus in isolation. Another study using ERG (electroretinogram) recordings in human subjects (Gauvin *et al.*, 2017) showed that delivering shorter duration flashes initiated a facilitatory effect of the OFF ERG's which has a 40 Hz component. Although with our visual classification we did not observe an explicit reset behavior for ON cells, it could be seen that for 40 Hz the overall firing rates were higher. Interestingly, for ON-OFF cells the facilitation was rather prominent, suggesting that the OFF pathway could play a vital role in the facilitatory response.

Testing of all the above possibilities is currently beyond the scope of this present study and remains warranted for future investigations.

### ***Mechanisms for Temporal Desensitization***

Several mechanisms have been presented in the literature behind RGC desensitization including the role of the retinal network as well as amacrine cell inhibition (with GABA and glycine) (**Fig. 9**). However, it must be noted that the RGC desensitization persists in the absence of amacrine cell inhibition (Freeman & Fried 2011). Tsai *et al.* showed that with high-frequency stimulation there is a decline in the RGC voltage-gated sodium current (Tsai *et al.* 2011). Additionally, studies from Sanchez *et al.* have shown that the RGC exhibit spike rate adaptation which could be attributed to specific K<sup>+</sup> channels on the RGCs (slow K channels and Calcium-activated K channels), suggesting desensitization of direct spikes arising from RGC stimulation. Studies from Freeman and Fried and Jensen & Rizzo suggested that the mechanism of rapid desensitization occurs upstream of the spike generator further supporting the role of many potential synaptic mechanisms that are independent of amacrine cells inhibition. Such mechanisms include the depletion of the readily releasable pool (RRP) of synaptic vesicles, desensitization of the postsynaptic receptors (NMDA and AMPA/Kainate receptors). However, to explore the various mechanisms and to discern the precise mechanisms of desensitization will require further investigations.

### **Spatiotemporal interaction of desensitization**

***Spatial spread of electrical stimulation- a trade-off between spatial resolution and spatial extent of desensitization***

To improve the efficiency of the current retinal prosthetic devices, it is necessary to provide an artificially elicited vision which is not only temporally dynamic but also of high spatial resolution. In recent years, many studies have investigated various electrode configurations and stimulation paradigms that would increase the spatial resolution of the retinal implant. The ability to discern various spatial patterns across an electrode array depends partly on the number of stimulation sites on the array and partly on the spread of the electric current within the retina. To achieve a high spatial resolution, several hundred electrodes are needed to provide a useful perception. However, the current spread in the retina (when stimulated at a single electrode) can effectively reduce the number of stimulation channels thereby confining the spatial resolution (Gerhardt *et al.*, Lovell, Stett 2007, hossenizadeh 2017). One strategy that shows promising results in improving the spatial resolution of retinal prostheses is simultaneous stimulation of multiple electrodes. Interactions that occur when combinations of electrodes are stimulated simultaneously are capable of increasing the repertoire of visual percepts that can be elicited compared to conventional single-electrode stimulation. However, stimulating multiple electrodes simultaneously could lead to electrical crosstalk in between the electrodes of the array (Wilke *et al.* 2011). Numerous studies (Cicione *et al.*, 2012; Dumm *et al.*, 2014; Jepson *et al.*, 2013; Matteucci *et al.*, 2013) have investigated various strategies which could potentially reduce the effects of crosstalk. These strategies include current steering or current focussing by simultaneously stimulating multiple electrodes and appropriate choice of return electrode configuration (like bipolar, tripolar and hexagonal). Although these strategies help in crosstalk effects, they restrict the temporal resolution thereby resulting in fading of phosphenes. A recent study of cortical activity (Cicione *et al.* 2014) showed that a minimum spacing of 2.5-3 mm between the retinal electrodes (suprachoroidal implant array) is required to eliminate crosstalk and suppression of responses when stimulated with higher frequencies. Considering our proximity to the retina, an inter-electrode distance  $>200 \mu\text{m}$  could limit crosstalk and desensitization to a substantial extent. Therefore, for an efficient retinal implant, it is crucial to find the best trade-off between the acceptable spatial resolution and the spatial extent of desensitization.

### ***Effect of Interpulse interval***

In our study for the shortest inter-electrode distance (200  $\mu\text{m}$ ), we observed the maximum level of desensitization at an interpulse interval of 100 ms (10 Hz). Our results were in agreement with previous studies with human subjects (Zrenner *et al.* 2011, Stingl *et al.* 2017,

Stingl *et al.* 2015), which showed maximum phosphene fading for frequencies  $\sim 10$  Hz. However, interestingly in our data, we saw that for frequencies of 20 and 40 Hz the responses tend to increase (or show less desensitization effects). This effect was in agreement with our observation of temporal desensitization.

## Limitations

- 1) The current study was performed in adult healthy mouse retinas. However, for the applicability of the results found here to human clinical trials, it is necessary that these experiments need to be performed in late-stage degenerated retinas. Several differences between the healthy and degenerated retinas may alter the responses to repetitive stimulation. Although the photoreceptors are gone the inner retinal circuitry, which is the prime target for subretinal and suprachoroidal implants undergo several changes during the process of the degeneration (Gargini *et al.*, 2007; Menzler and Zeck, 2011; Stasheff, 2008). Therefore, further testing in the degenerated retina will be necessary to understand how such spatiotemporal interactions change during the process of the degeneration.
- 2) Due to large stimulus artifacts of the test pulse, we were unable to record any ganglion cell activity at the test pulse electrode. Therefore, we measured the activity in the surrounding 8 electrodes. However, the large inter-electrode distance (200-283  $\mu\text{m}$ ) could potentially result in a weak spatiotemporal interaction (as seen from our data with a modest level of desensitization at 200  $\mu\text{m}$ ). Therefore, a high-density MEA with closely spaced electrodes would help in a better approximation of the spatial extent of desensitization.

## Conclusions

### *Implications for Retinal Prosthesis*

It is well known from the previous literature that electrical desensitization plays a vital role in the fading of visual percepts also known as phosphenes observed by patients upon repetitive electrical stimulation of the retina (Cicione *et al.*, 2014; Freeman and Fried, 2011; Jensen and Rizzo, 2007). However, phosphene fading is rather complicated and varies from one subject to another. Upon repetitive stimulation, the phosphenes not only loses its brightness (temporal) but also patients report a marked change in size, shape and at times



color of the phosphenes (Perez-Fornos *et al.*, 2012). Therefore, understanding the spatiotemporal interaction of desensitization is crucial for understanding the fading of visual percepts. Our results along with previous other studies (Freeman & Fried 2011, Ciocine *et al.* 2014, Jensen & Rizzo 2007) raise the possibility that the desensitization we observe at the retinal level (RGC desensitization) could be contributing to the fading of visual percepts. However, our results do not preclude the possibility that alternative mechanisms like saccadic suppression (Bremmer *et al.*, 2009) and adaptation of neurons in the thalamus or visual cortex could contribute to the fading of phosphenes.

### ***Strategies to limit desensitization***

Apart from understanding the spatiotemporal interaction of desensitization, it is necessary to develop strategies which could potentially limit desensitization. Davuluri *et al.* showed that by using time-varying pulses (i.e., each pulse has a different duration and amplitude when compared to the preceding pulse while keeping the charge at threshold level) different population of neurons could be stimulated (due to different pulse width and amplitudes, (Davuluri and Weiland, 2014). By stimulating different population of neurons, the “electrical image” on the retina might continuously shift (like microsaccades) thereby helping in limiting electrical desensitization.

Derived from our study, one possible strategy to lower desensitization effect/perceptual fading would be to stimulate the retina at interleaving electrodes separated by distances >0.2mm, with varying interpulse intervals.

## **References**

- Baden, T., Berens, P., Franke, K., Román Rosón, M., Bethge, M., Euler, T., 2016. The functional diversity of retinal ganglion cells in the mouse. *Nature* 529, 345–350. doi:10.1038/nature16468
- Bennett, J., Wellman, J., Marshall, K.A., McCague, S., Ashtari, M., DiStefano-Pappas, J., Elci, O.U., Chung, D.C., Sun, J., Wright, J.F., Cross, D.R., Aravand, P., Cyckowski, L.L., Bennicelli, J.L., Mingozzi, F., Auricchio, A., Pierce, E.A., Ruggiero, J., Leroy, B.P., Simonelli, F., High, K.A., Maguire, A.M., 2016. Safety and durability of effect of contralateral-eye administration of AAV2 gene therapy in patients with childhood-

- onset blindness caused by RPE65 mutations: a follow-on phase 1 trial. *Lancet* (London, England) 388, 661–672. doi:10.1016/S0140-6736(16)30371-3
- Boinagrov, D., Pangratz-Fuehrer, S., Goetz, G., Palanker, D., 2014. Selectivity of direct and network-mediated stimulation of the retinal ganglion cells with epi-, sub- and intraretinal electrodes. *J. Neural Eng.* 11, 26008. doi:10.1088/1741-2560/11/2/026008
- Bremmer, F., Kubischik, M., Hoffmann, K.-P., Krekelberg, B., 2009. Neural dynamics of saccadic suppression. *J. Neurosci.* 29, 12374–83. doi:10.1523/JNEUROSCI.2908-09.2009
- Carcieri, S.M., Jacobs, A.L., Nirenberg, S., 2003. Classification of retinal ganglion cells: a statistical approach. *J. Neurophysiol.* 90, 1704–1713. doi:10.1152/jn.00127.2003
- Cicione, R., Fallon, J.B., Rathbone, G.D., Williams, C.E., Shivdasani, M.N., 2014. Spatiotemporal Interactions in the Visual Cortex Following Paired Electrical Stimulation of the Retina. *Invest. Ophthalmol. Vis. Sci.* 55, 7726–7738. doi:10.1167/iovs.14-14754
- Cicione, R., Shivdasani, M.N., Fallon, J.B., Luu, C.D., Allen, P.J., Rathbone, G.D., Shepherd, R.K., Williams, C.E., 2012. Visual cortex responses to suprachoroidal electrical stimulation of the retina: effects of electrode return configuration. *J. Neural Eng.* 9, 36009. doi:10.1088/1741-2560/9/3/036009
- da Cruz, L., Coley, B.F., Dorn, J., Merlini, F., Filley, E., Christopher, P., Chen, F.K., Wuyyuru, V., Sahel, J., Stanga, P., Humayun, M., Greenberg, R.J., Dagnelie, G., Argus II Study Group, for the A.I.S., 2013. The Argus II epiretinal prosthesis system allows letter and word reading and long-term function in patients with profound vision loss. *Br. J. Ophthalmol.* 97, 632–6. doi:10.1136/bjophthalmol-2012-301525
- Davuluri, N.S., Weiland, J.D., 2014. Time-varying pulse trains limit retinal desensitization caused by continuous electrical stimulation, in: 2014 36th Annual International Conference of the IEEE Engineering in Medicine and Biology Society. IEEE, pp. 414–417. doi:10.1109/EMBC.2014.6943616
- Dumm, G., Fallon, J.B., Williams, C.E., Shivdasani, M.N., 2014. Virtual electrodes by current steering in retinal prostheses. *Investig. Ophthalmol. Vis. Sci.* 55, 8077–8085. doi:10.1167/iovs.14-15391
- Eickenscheidt, M., Jenkner, M., Thewes, R., Fromherz, P., Zeck, G., 2012. Electrical stimulation of retinal neurons in epiretinal and subretinal configuration using a multicapacitor array. *J. Neurophysiol.* 107, 2742–2755. doi:10.1152/jn.00909.2011

- Freeman, D.K., Fried, S.I., 2011. Multiple components of ganglion cell desensitization in response to prosthetic stimulation. *J. Neural Eng.* 8, 16008. doi:10.1088/1741-2560/8/1/016008
- Fried, S.I., Hsueh, H.A., Werblin, F.S., 2006. A method for generating precise temporal patterns of retinal spiking using prosthetic stimulation. *J. Neurophysiol.* 95, 970–8. doi:10.1152/jn.00849.2005
- Gargini, C., Terzibasi, E., Mazzoni, F., Strettoi, E., 2007. Retinal organization in the retinal degeneration 10 (rd10) mutant mouse: A morphological and ERG study. *J. Comp. Neurol.* 500, 222–238. doi:10.1002/cne.21144
- Gauvin, M., Sustar, M., Little, J.M., Breceelj, J., Lina, J.-M., Lachapelle, P., 2017. Quantifying the ON and OFF Contributions to the Flash ERG with the Discrete Wavelet Transform. doi:10.1167/tvst.6.1.3
- Goo, Y.S., Ye, J.H., Lee, S., Nam, Y., Ryu, S.B., Kim, K.H., 2011a. Retinal ganglion cell responses to voltage and current stimulation in wild-type and rd1 mouse retinas. *J. Neural Eng.* 8, 35003. doi:10.1088/1741-2560/8/3/035003
- Goo, Y.S., Ye, J.H., Lee, S., Nam, Y., Ryu, S.B., Kim, K.H., 2011b. Retinal ganglion cell responses to voltage and current stimulation in wild-type and rd1 mouse retinas. *J. Neural Eng.* 8, 35003. doi:S1741-2560(11)78136-8 [pii]\r10.1088/1741-2560/8/3/035003
- Hamel, C., 2006. Retinitis pigmentosa. *Orphanet J. Rare Dis.* 1, 40. doi:10.1186/1750-1172-1-40
- Hartong, D.T., Berson, E.L., Dryja, T.P., 2006. Retinitis pigmentosa. *Lancet* 368, 1795–1809. doi:10.1016/S0140-6736(06)69740-7
- Ho, E., Lorach, H., Goetz, G., Laszlo, F., Lei, X., Kamins, T., Mariani, J.-C., Sher, A., Palanker, D., 2018. Temporal structure in spiking patterns of ganglion cells defines perceptual thresholds in rodents with subretinal prosthesis. *Sci. Rep.* 8, 3145. doi:10.1038/s41598-018-21447-1
- Im, M., Fried, S.I., 2016. Temporal properties of network-mediated responses to repetitive stimuli are dependent upon retinal ganglion cell type. *J. Neural Eng.* 13, 25002. doi:10.1088/1741-2560/13/2/025002
- Im, M., Fried, S.I., 2015. Indirect activation elicits strong correlations between light and electrical responses in ON but not OFF retinal ganglion cells. *J. Physiol.* 593, 3577–3596. doi:10.1113/JP270606
- Jalligampala, A., Sekhar, S., Zrenner, E., Rathbun, D.L., 2017. Optimal voltage stimulation

- parameters for network-mediated responses in wild type and rd10 mouse retinal ganglion cells. *J. Neural Eng.* 14. doi:10.1088/1741-2552/14/2/026004
- Jensen, R.J., Rizzo, J.F., 2007. Responses of ganglion cells to repetitive electrical stimulation of the retina. *J. Neural Eng.* 4, S1–S6. doi:10.1088/1741-2560/4/1/S01
- Jensen, R.J., Ziv, O.R., Rizzo, J.F., 2005. Thresholds for activation of rabbit retinal ganglion cells with relatively large, extracellular microelectrodes. *Investig. Ophthalmol. Vis. Sci.* 46, 1486–1496. doi:10.1167/iovs.04-1018
- Jepson, L.H., Hottowy, P., Mathieson, K., Gunning, D.E., Dabrowski, W., Litke, A.M., Chichilnisky, E.J., 2013. Focal electrical stimulation of major ganglion cell types in the primate retina for the design of visual prostheses. *J. Neurosci.* 33, 7194–7205. doi:10.1523/JNEUROSCI.4967-12.2013
- Lee, S.W., Eddington, D.K., Fried, S.I., 2013. Responses to pulsatile subretinal electric stimulation: effects of amplitude and duration. *J. Neurophysiol.* 109, 1954–68. doi:10.1152/jn.00293.2012
- Mariotti S., 2012. Global Data on Visual Impairments 2010. *World Heal. Organ.* 20.
- Matteucci, P.B., Chen, S.C., Tsai, D., Dodds, C.W.D., Dokos, S., Morley, J.W., Lovell, N.H., Suaning, G.J., 2013. Current steering in retinal stimulation via a quasimonopolar stimulation paradigm. *Investig. Ophthalmol. Vis. Sci.* 54, 4307–4320. doi:10.1167/iovs.13-11653
- Meister, M., Pine, J., Baylor, D.A., 1994. Multi-neuronal signals from the retina: acquisition and analysis. *J. Neurosci. Methods* 51, 95–106. doi:10.1016/0165-0270(94)90030-2
- Menzler, J., Zeck, G., 2011. Network Oscillations in Rod-Degenerated Mouse Retinas. *J. Neurosci.* 31, 2280–2291. doi:10.1523/JNEUROSCI.4238-10.2011
- Nirenberg, S., Pandarinath, C., 2012. Retinal prosthetic strategy with the capacity to restore normal vision. *Proc. Natl. Acad. Sci. U. S. A.* 109, 15012–7. doi:10.1073/pnas.1207035109
- Perez-Fornos, A., Sommerhalder, J., da Cruz, L., Sahel, J.A., Mohand-Said, S., Hafezi, F., Pelizzone, M., 2012. Temporal properties of visual perception on electrical stimulation of the retina. *Invest Ophthalmol Vis Sci* 53, 2720–2731. doi:10.1167/iovs.11-9344
- Resnikoff, S., Foster, A., 2005. The impact of Vision 2020 on global blindness. *Eye (Lond)*. 19, 1133–1135. doi:10.1038/sj.eye.6701973
- Rodieck, R.W., 1998. *The First Steps in Seeing*, First. ed. Sinauer Associates, Inc., Sunderland, Massachusetts.

- Ryu, S.B., Ye, J.H., Lee, J.S., Goo, Y.S., Kim, C.H., Kim, K.H., 2009a. Electrically-evoked neural activities of rd1 mice retinal ganglion cells by repetitive pulse stimulation. *Korean J. Physiol. Pharmacol.* 13, 443–448. doi:10.4196/kjpp.2009.13.6.443
- Ryu, S.B., Ye, J.H., Lee, J.S., Goo, Y.S., Kim, K.H., 2009b. Characterization of retinal ganglion cell activities evoked by temporally patterned electrical stimulation for the development of stimulus encoding strategies for retinal implants. *Brain Res.* 1275, 33–42. doi:10.1016/j.brainres.2009.03.064
- Schwartz, S.D., Hubschman, J.-P., Heilwell, G., Franco-Cardenas, V., Pan, C.K., Ostrick, R.M., Mickunas, E., Gay, R., Klimanskaya, I., Lanza, R., 2015. Embryonic stem cell trials for macular degeneration: a preliminary report. *Lancet* 379, 713–720. doi:10.1016/S0140-6736(12)60028-2
- Sekhar, S., Jalligampala, A., Zrenner, E., Rathbun, D.L., 2016. Tickling the retina: integration of subthreshold electrical pulses can activate retinal neurons. *J. Neural Eng.* 13, 46004. doi:10.1088/1741-2560/13/4/046004
- Seung, H.S., Sümbül, U., 2014. Neuronal cell types and connectivity: Lessons from the retina. *Neuron* 83, 1262–1272. doi:10.1016/j.neuron.2014.08.054
- Stasheff, S.F., 2008. Emergence of sustained spontaneous hyperactivity and temporary preservation of OFF responses in ganglion cells of the retinal degeneration (rd1) mouse. *J. Neurophysiol.* 99, 1408–1421. doi:10.1152/jn.00144.2007
- Stett, A., Mai, A., Herrmann, T., 2007. Retinal charge sensitivity and spatial discrimination obtainable by subretinal implants: key lessons learned from isolated chicken retina. *J. Neural Eng.* 4, S7–S16. doi:10.1088/1741-2560/4/1/S02
- Stingl, K., Bartz-Schmidt, K.U., Besch, D., Chee, C.K., Cottrill, C.L., Gekeler, F., Groppe, M., Jackson, T.L., MacLaren, R.E., Koitschev, A., Kusnyerik, A., Neffendorf, J., Nemeth, J., Naeem, M.A.N., Peters, T., Ramsden, J.D., Sachs, H., Simpson, A., Singh, M.S., Wilhelm, B., Wong, D., Zrenner, E., 2015. Subretinal Visual Implant Alpha IMS – Clinical trial interim report. *Vision Res.* 111, 149–160. doi:10.1016/J.VISRES.2015.03.001
- Stingl, K., Schippert, R., Bartz-Schmidt, K.U., Besch, D., Cottrill, C.L., Edwards, T.L., Gekeler, F., Greppmaier, U., Kiel, K., Koitschev, A., Kühlewein, L., MacLaren, R.E., Ramsden, J.D., Roider, J., Rothermel, A., Sachs, H., Schröder, G.S., Tode, J., Troelenberg, N., Zrenner, E., 2017. Interim Results of a Multicenter Trial with the New Electronic Subretinal Implant Alpha AMS in 15 Patients Blind from Inherited

- Retinal Degenerations. *Front. Neurosci.* 11, 445. doi:10.3389/fnins.2017.00445
- Sümbül, U., Song, S., McCulloch, K., Becker, M., Lin, B., Sanes, J.R., Masland, R.H., Seung, H.S., 2014. A genetic and computational approach to structurally classify neuronal types. *Nat. Commun.* 5, 3512. doi:10.1038/ncomms4512
- Tsai, D., Morley, J.W., Suaning, G.J., Lovell, N.H., 2011. Sodium channel inactivation reduces retinal ganglion cell responsiveness to repetitive prosthetic stimulation. 2011 5th Int. IEEE/EMBS Conf. Neural Eng. NER 2011 550–553. doi:10.1109/NER.2011.5910607
- Tsai, D., Morley, J.W., Suaning, G.J., Lovell, N.H., 2011. Frequency-dependent reduction of voltage-gated sodium current modulates retinal ganglion cell response rate to electrical stimulation. *J. Neural Eng.* 8, 66007. doi:10.1088/1741-2560/8/6/066007
- Zrenner, E., Bartz-Schmidt, K.U., Benav, H., Besch, D., Bruckmann, A., Gabel, V.-P., Gekeler, F., Greppmaier, U., Harscher, A., Kibbel, S., Koch, J., Kusnyerik, A., Peters, T., Stingl, K., Sachs, H., Stett, A., Szurman, P., Wilhelm, B., Wilke, R., 2011. Subretinal electronic chips allow blind patients to read letters and combine them to words. *Proc. Biol. Sci.* 278, 1489–97. doi:10.1098/rspb.2010.1747
- Crapper DR, Noell WK. Retinal excitation and inhibition from direct electrical stimulation. *J Neurophysiol.* 1963;26:924– 947.

## Figure and Table Legends:

**Fig. 1: (A) Schematic Temporal desensitization protocol.** To examine the effects of multiple stimulus pulses, trains of ten stimuli (2- 62.5Hz, each frequency repeated 5x with 5 s between each repeat) were also applied (Cathodic first biphasic 10 $\mu$ A, 1ms per phase).

**(B) Schematic representation of spatiotemporal desensitization protocol:** Cathodic first biphasic 10 $\mu$ A, 1ms per phase paired-pulses were delivered at **priming and test pulse**. For each inter-electrode distance ( 1mm to 0.2 mm), i.e. the distance between priming/conditioning pulse and test pulse (always fixed), the different interpulse intervals (arrow numbered 1.) were presented at two different electrodes from the highest to the lowest interpulse interval (1000 ms to 25 ms) with a stimulus amplitude of 10  $\mu$ A, repeated 10 times for each interval. After the entire cycle of interpulse intervals was completed for an interelectrode spacing, the priming pulse was moved to the next inter-electrode distance closer to the test pulse (arrow numbered 2.). The responses from the neighboring electrodes

(red) surrounding the test pulse electrode (open circle) were used for analysis as the responses from the test pulse electrode were masked by the stimulus artifact, although in some rare case, we were able to record responses from the test pulse electrode (open black). The priming pulse was represented by a solid black circle.

**Fig 2: Representative ganglion cell recording.** a) Digitized voltage trace of responses to biphasic current pulses. Stimulus artifacts indicated with black arrow and spikes in red. Zoom level 80 ms 20 $\mu$ V. b) Rastergram of all responses for this cell. The same spike train is shown in a) are identified with an arrow (3 $\mu$ A). c) Peristimulus time histogram binned at 2 ms intervals for all responses. Smoothed histogram (Gaussian smoothing filter, sigma = 4 ms) is overlaid. The grey bar covering b-c indicates the 10 ms excluded from the response. The yellow bar is the 90 ms of response integration. e) Response plotted as a function stimulus amplitude. Each point is an average of 30 trials. Error bar denotes Mean  $\pm$  S.E.

**Fig. 3: Ganglion Cell Variability.** Example cells are showing ganglion cell response variability to increasing current amplitude. **(A-C)** The stimulus-response curve for single cells showing monotonically increasing response, monotonically decrease response and non-monotonic response to current amplitudes. **(D)** Average behavior of all the RGCs. Mean  $\pm$ S.E. **(E)** Average behavior of well-modulated RGCs. Mean  $\pm$ S.E. Threshold defined as spontaneous rate+ SD.

**Fig. 4: Response to Repetitive Pulse Trains. A(I-III)** Example cells showing normalized spiking response (mean  $\pm$  SD) to trains of pulses delivered at different frequencies (low to high, see legend ). All cells are desensitized with increasing frequencies. Interestingly for 40 Hz, most cells exhibited abnormally high responses. **(B)** Population average pulse train responses show a clear trend of decreased spiking activity in response to higher frequencies as well as decreasing responses for subsequent pulses (Mean $\pm$  SE). For each frequency, the responses were normalized to the first pulse response. For higher frequencies like 40Hz and 62.5Hz, the response pattern may be unreliable due to very short integration windows. Error bars are not shown for clarity. Note: For frequencies less than 10 Hz, an integration window of 10-100 ms was considered for counting the number of spikes; for higher frequencies, the counting window began at 10 ms and lasted until the next pulse.

**Fig. 5. Response to Repetitive Pulse Trains (for RGC types):** Population responses from ON (A) and ON-OFF (B) cells (error bars mean $\pm$  SE). Due to a low number of OFF cells (n=10) in the entire cell population they were not plotted in the panel.

**Fig. 6: Spatial extent of desensitization. A (I-II)** Example cells are showing normalized spiking response as a function of the interpulse interval for different distances. All cells show desensitization (reduced responses) at the shortest distance and at shorter durations (0.1-0.025s). Responses were normalized to the response for 1 s intervals at 1 mm distance which is expected to show the least desensitization. **B(I-II)** For the same cells normalized spiking response as a function of inter-electrode distances for different interpulse intervals. **(C-D)** Show population plot of normalized response for both interpulse intervals and inter-electrode distances, respectively. Desensitization appears weak except at distances greater than 0.4 mm. The x axis is plotted in log scale. For all cells the shortest distance was statistically different in comparison to other inter-electrode distance across all interpulse intervals. (p<0.05 , Wilcoxon ranksum test)

**Fig. 7: Spatial extent of desensitization (for RGC types): A(I) B(I)** Population plot ON-OFF cells for both interpulse intervals and interelectrode distance respectively. **A(II) b(II)** Population plot of pure ON cells for both interpulse intervals and inter-electrode distance respectively. Error bars for single cells is SD. Error bars for population plot is Mean $\pm$  SE. X-axis plotted in log scale.

**Fig. 8: Alternate metric for spatiotemporal extent of desensitization.** To quantify the spatiotemporal aspects of desensitization during the course of electrical stimulation, we normalized the responses for each distance to the response at the longest time interval (1s). **(A)**Show population plot of all cells. The responses were desensitized for the shortest distance. However, for interpulse intervals (1s-0.1s), the cells show an increased desensitized responses. For shorter intervals (0.05-0.025s) there was an increasing trend, which could be attributed to either shorter interpulse intervals or some harmonics in the neural system. Note the “n” variation is due to the fact that cells which did not have a response at the longest duration were excluded from the analysis due to normalization. **(B)** Show population plot of ON-OFF cells which show a similar trend as mentioned above. **(C)** Show population plot of



pure ON cells. For distances ( $\leq 0.6\text{mm}$ ) the desensitization was maximum at 0.1s (10Hz). Error bars for single cells is SD. Error bars for population plot is Mean $\pm$  SE. For all cells, the interpulse intervals (0.05 and 0.1s) were statistically significant in comparison to other durations ( $p < 0.05$ , Wilcoxin Ranksum Test)

**Fig . 9: Possible Neural Mechanisms.** Desensitization occurring via retinal network could be accounted by mechanisms like receptor (NMDA, AMPA) desensitization, inactivation of calcium currents due to run down of the concentration gradient neurotransmitter depletion, inhibitory amacrine feedback, decline in sodium current and adaptation of spike rates in ganglion cells via slow activating channels like K and L-type VGCC (voltage gated calcium channels).

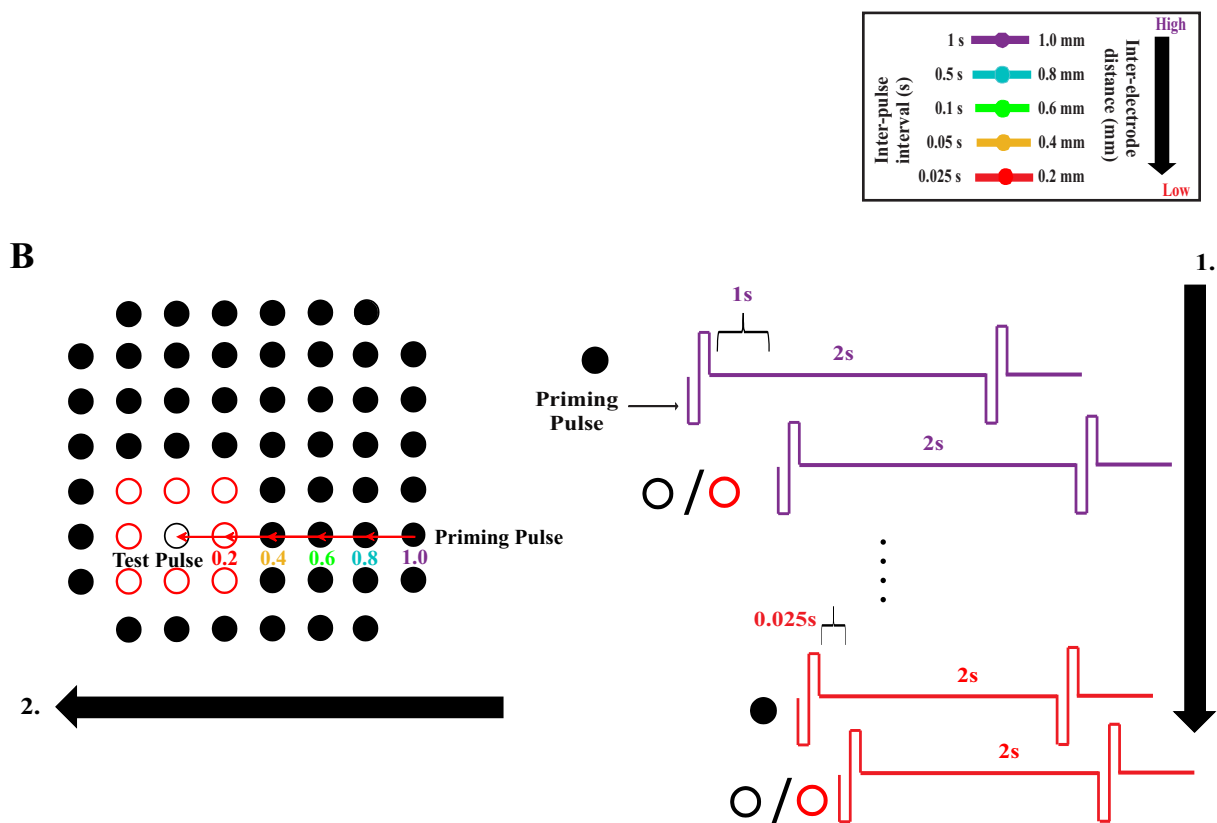
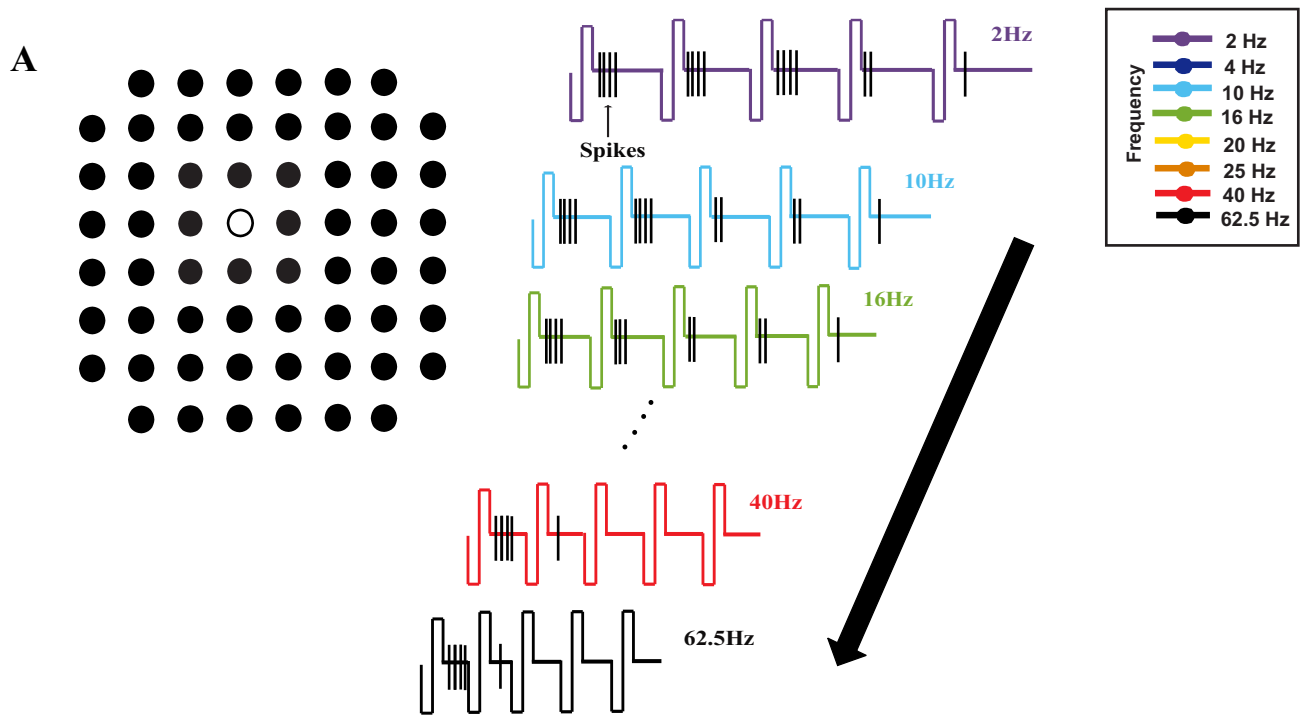
**Table 1: Pairwise comparisons between pulse rates. (A) All cells (B) ON cells (C) ON-OFF Cells.** For All cells and ON cells the 16, 20, 25 Hz was significantly more desensitized than 2, 4, 10 and 40 Hz. For OFF cells all the frequencies except 62.5Hz were significantly more desensitized than 40Hz. ( $p < 0.05$  Wilcoxon ranksum test.)

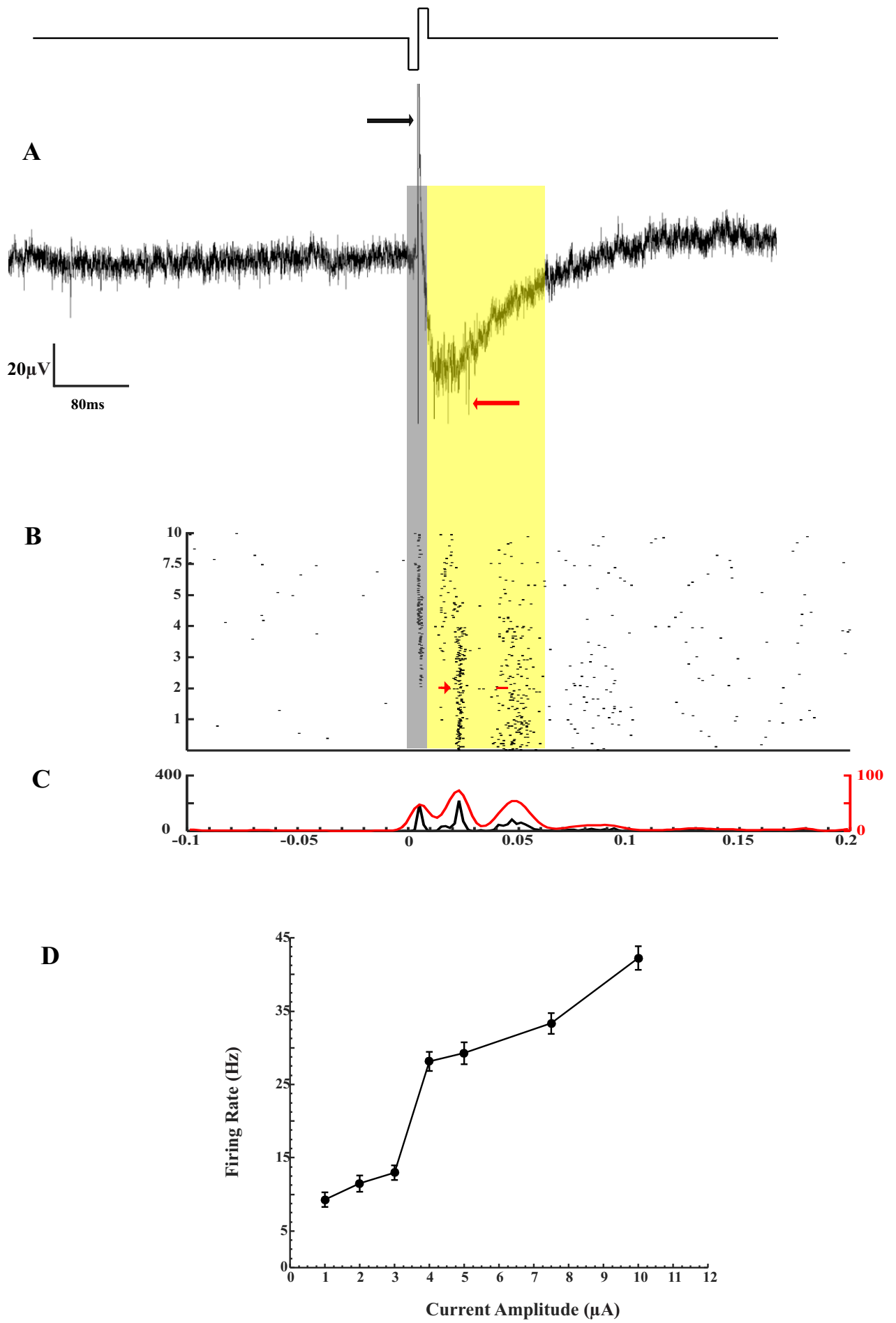
**Table 2: Pairwise comparisons for spatiotemporal interaction of desensitization. (Normalization 1) (A) Comparison between different inter-electrode distances at constant interpulse intervals. (B) Comparisons for different inter-pulse intervals at constant inter-electrode distances.** For the shortest distance the cells were more desensitized. ( $p < 0.05$  Wilcoxon ranksum test)

**Table 3: Pairwise comparisons for spatiotemporal interaction of desensitization. (Normalization 2) (A) Comparison between different inter-electrode distances at constant interpulse intervals.** For 0.05s and 0.1s the desensitization was maximum for 200  $\mu\text{m}$ . ( $p < 0.05$  Wilcoxon ranksum test)

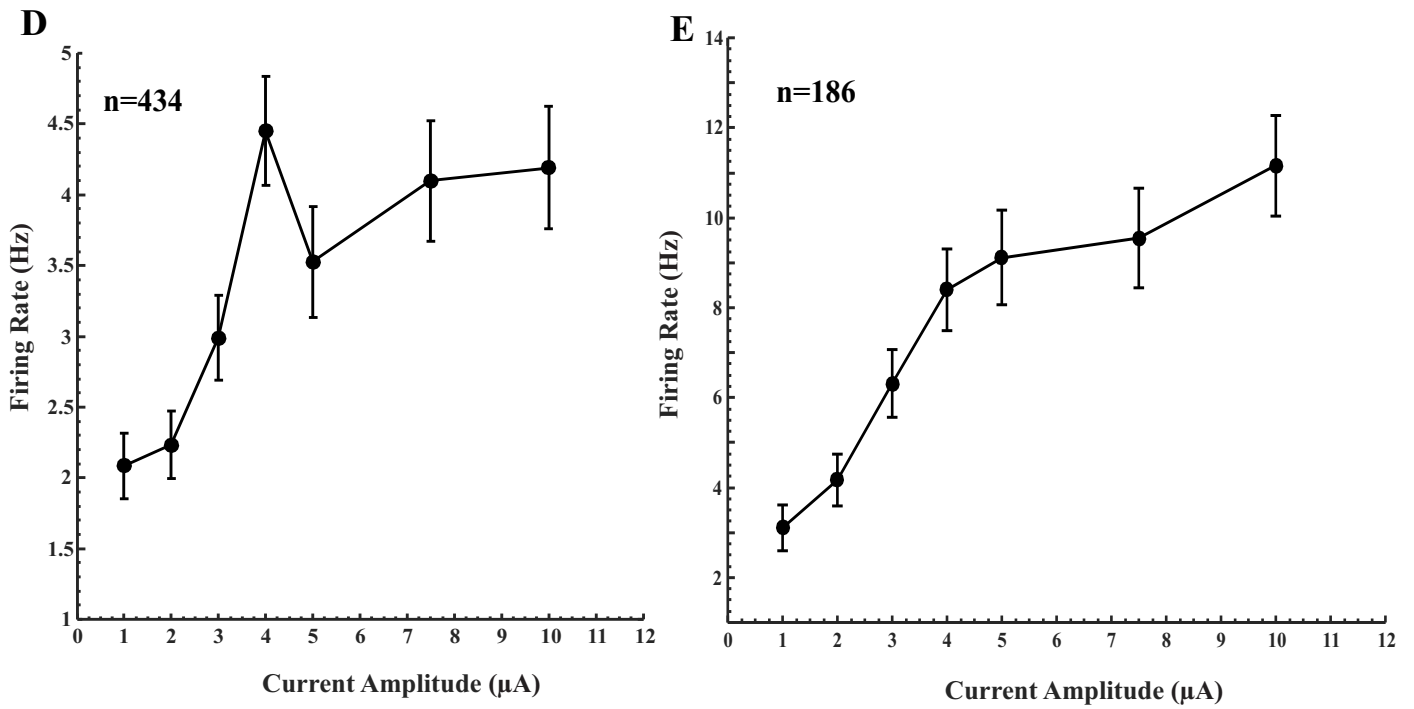
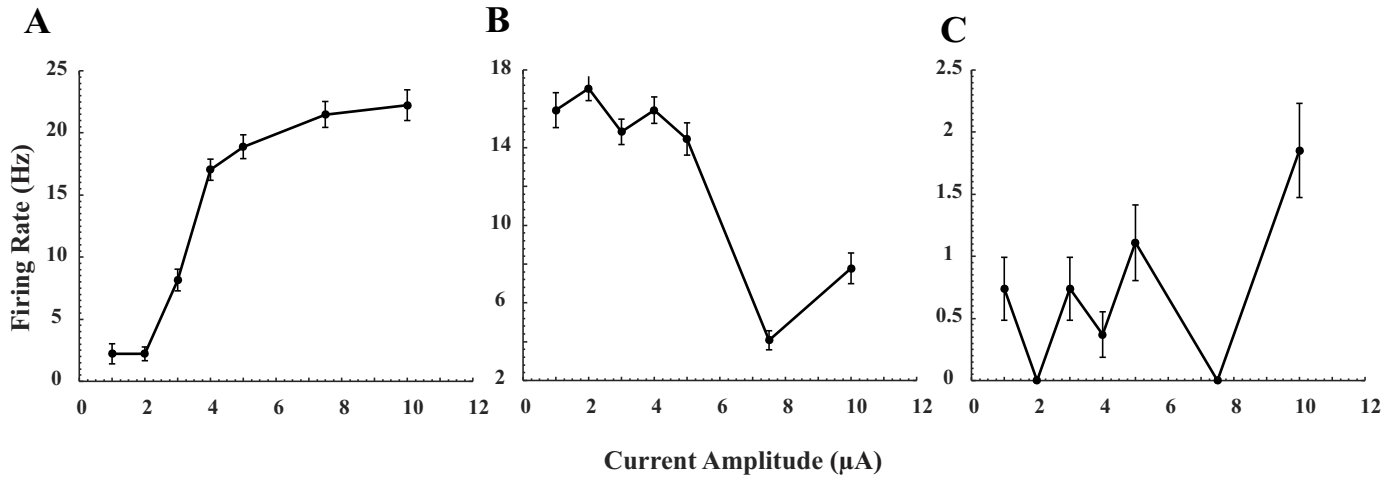
**S1: Pairwise comparisons for spatiotemporal interaction of desensitization. (Normalization 2)-RGC types (B) and (C).** Comparison between different inter-electrode

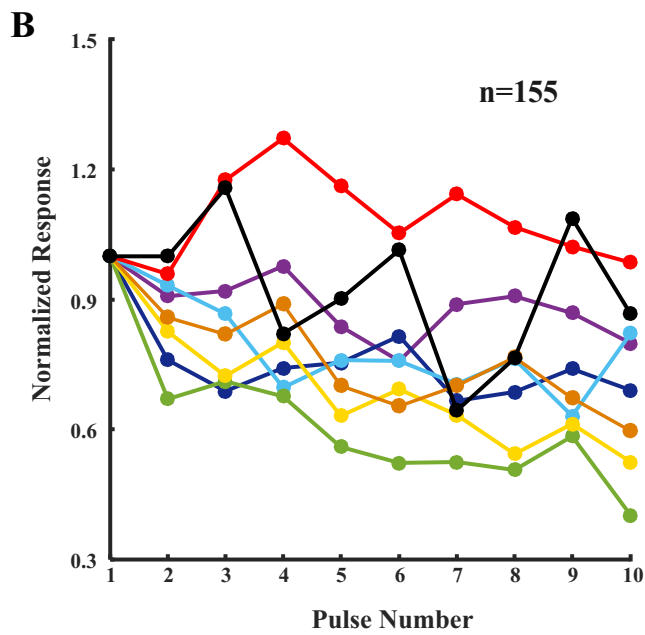
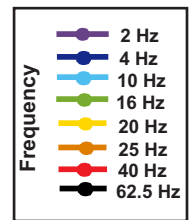
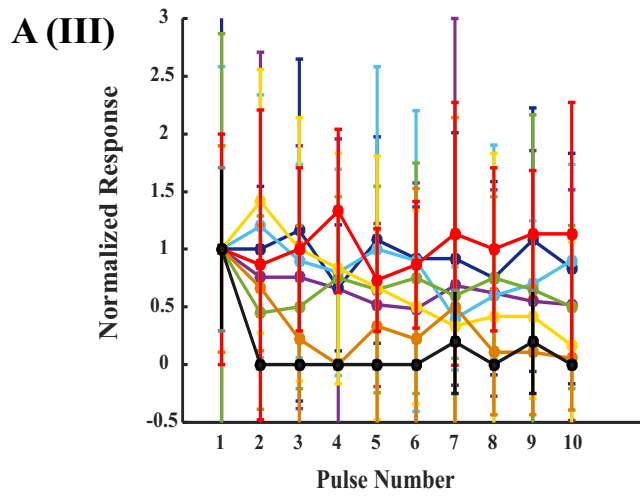
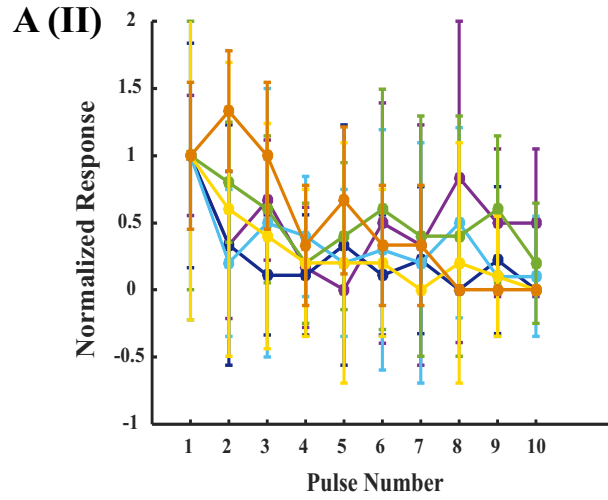
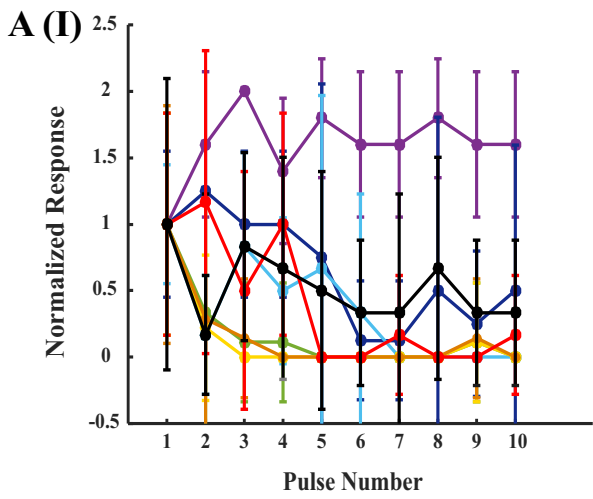
distances at constant interpulse intervals. There was no clear trend for desensitization. ( $p < 0.05$  Wilcoxon ranksum test) , probably due to low cell counts.

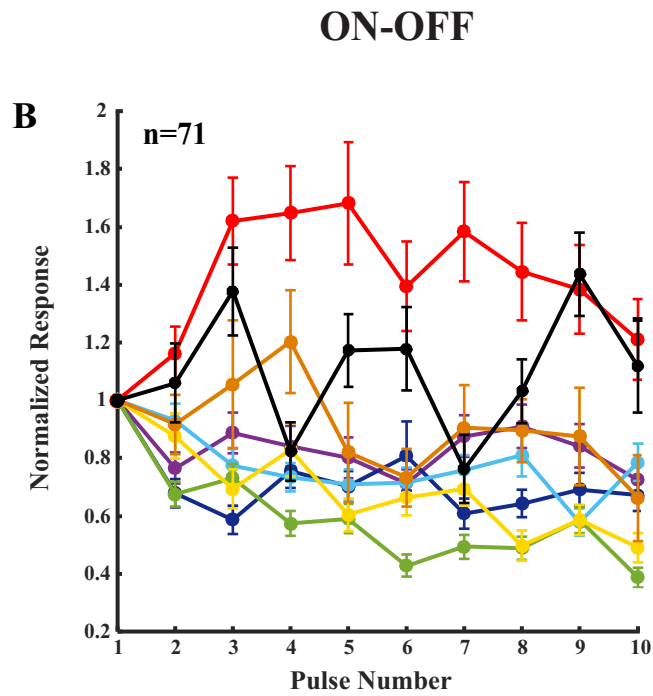
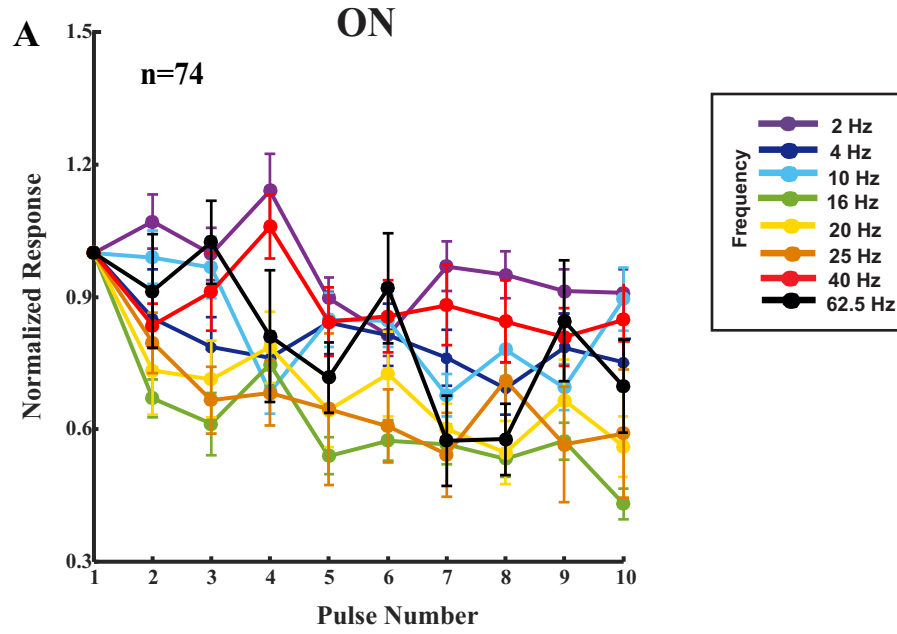


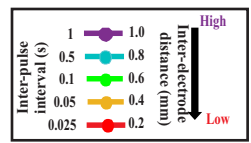


Jalligampala et al.  
Fig 2



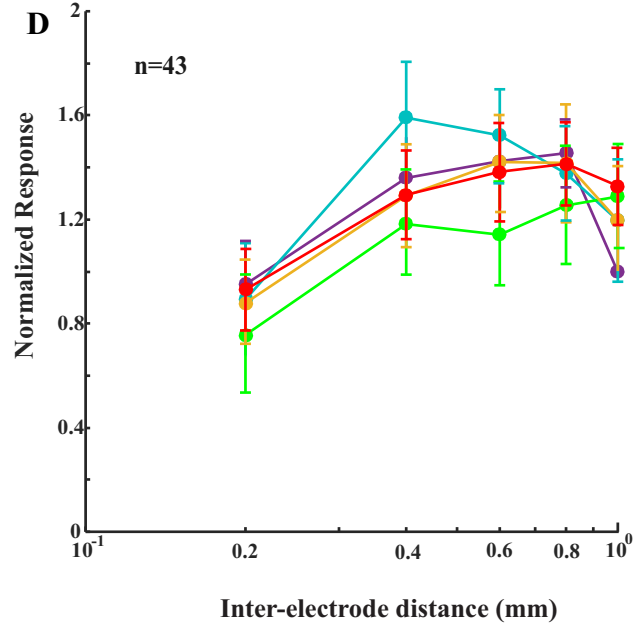
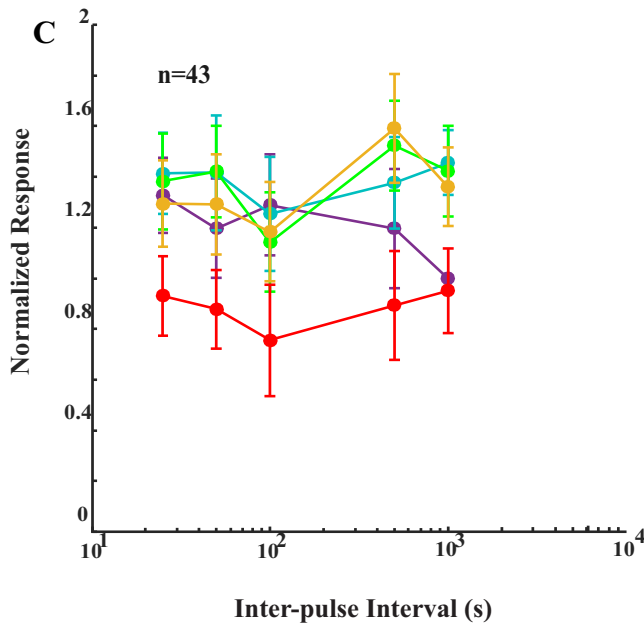
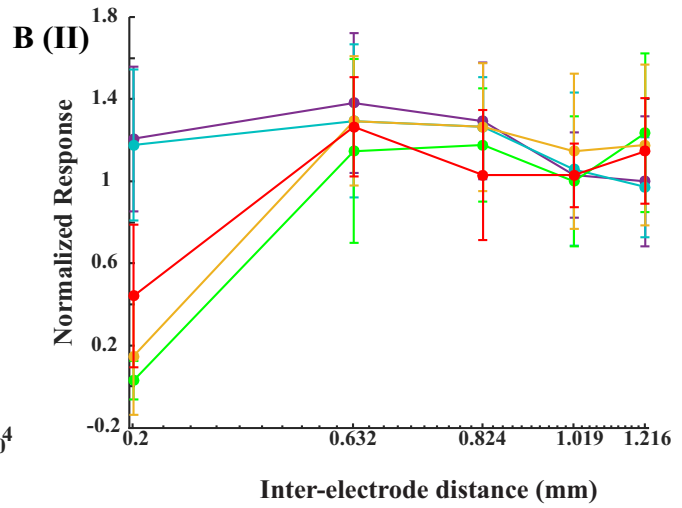
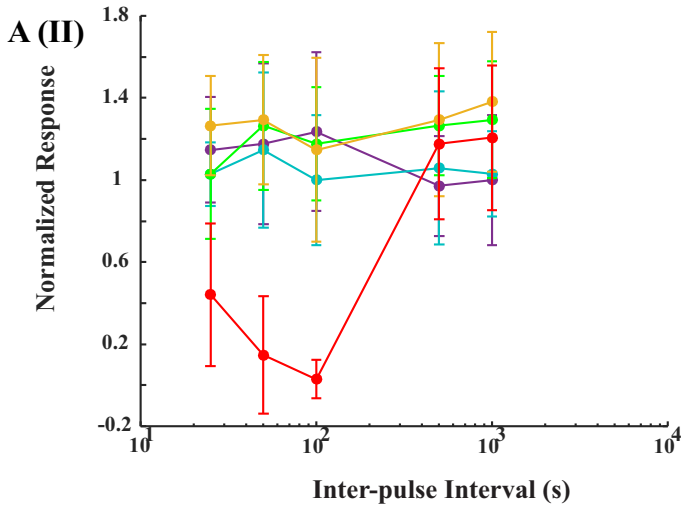
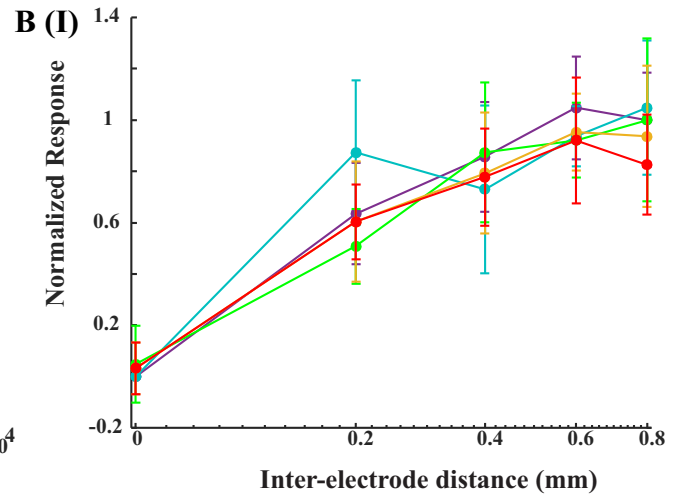
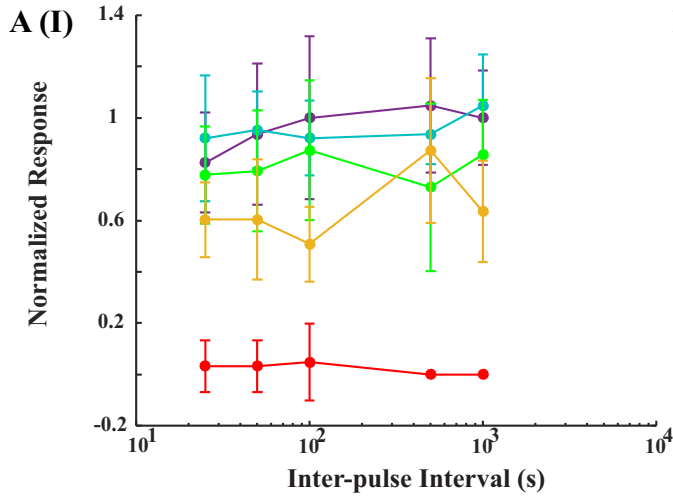




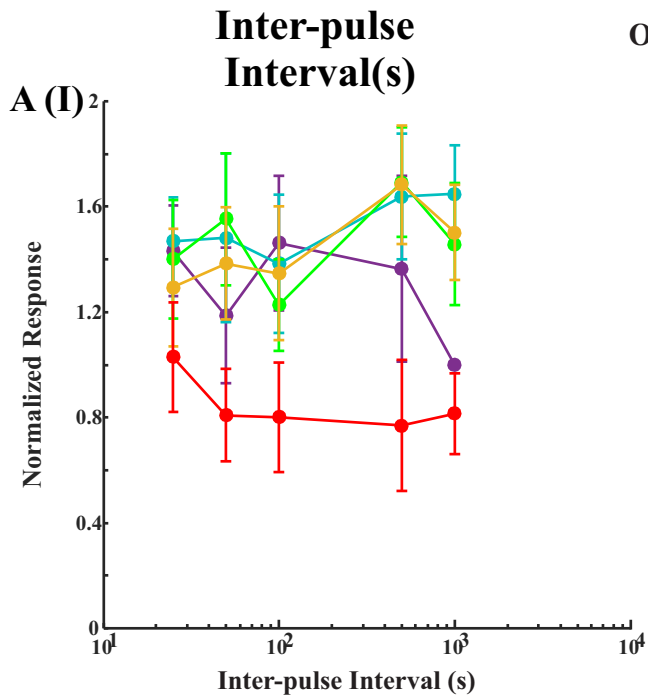
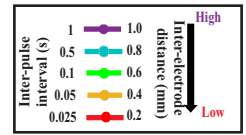


**Inter-pulse Interval(s)**

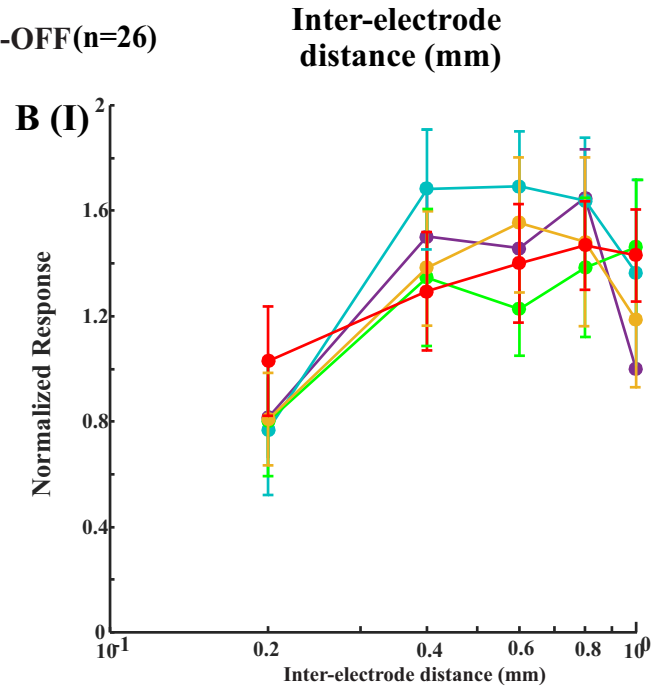
**Inter-electrode distance (mm)**



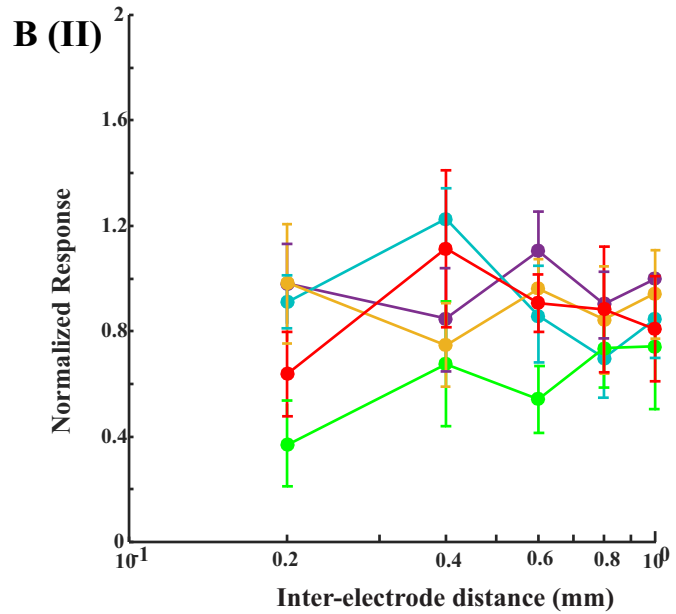
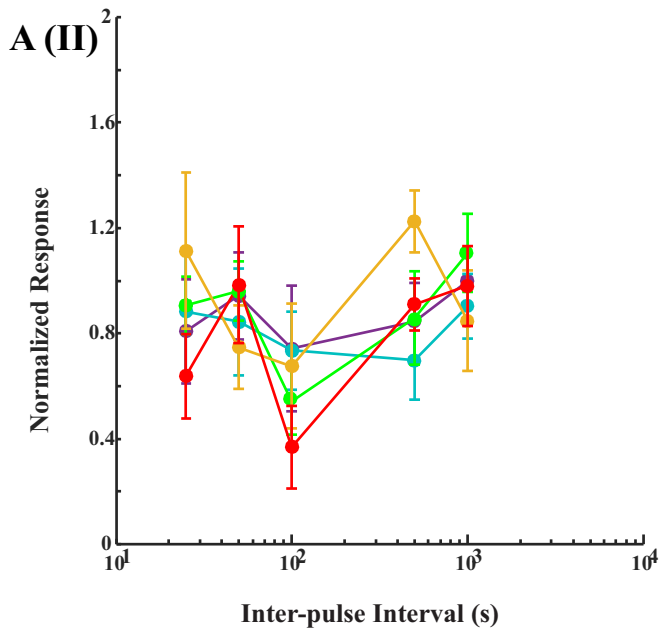


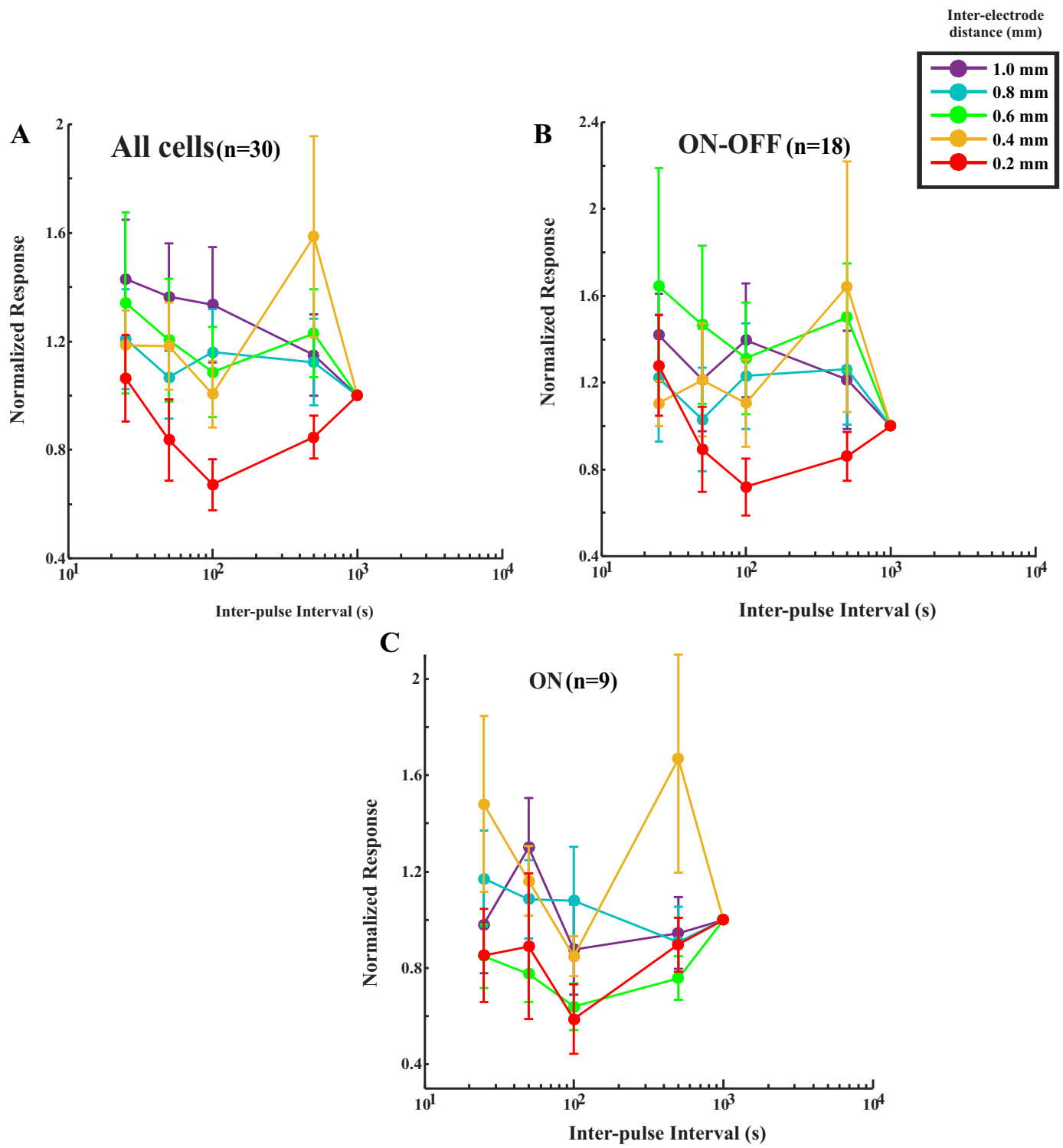


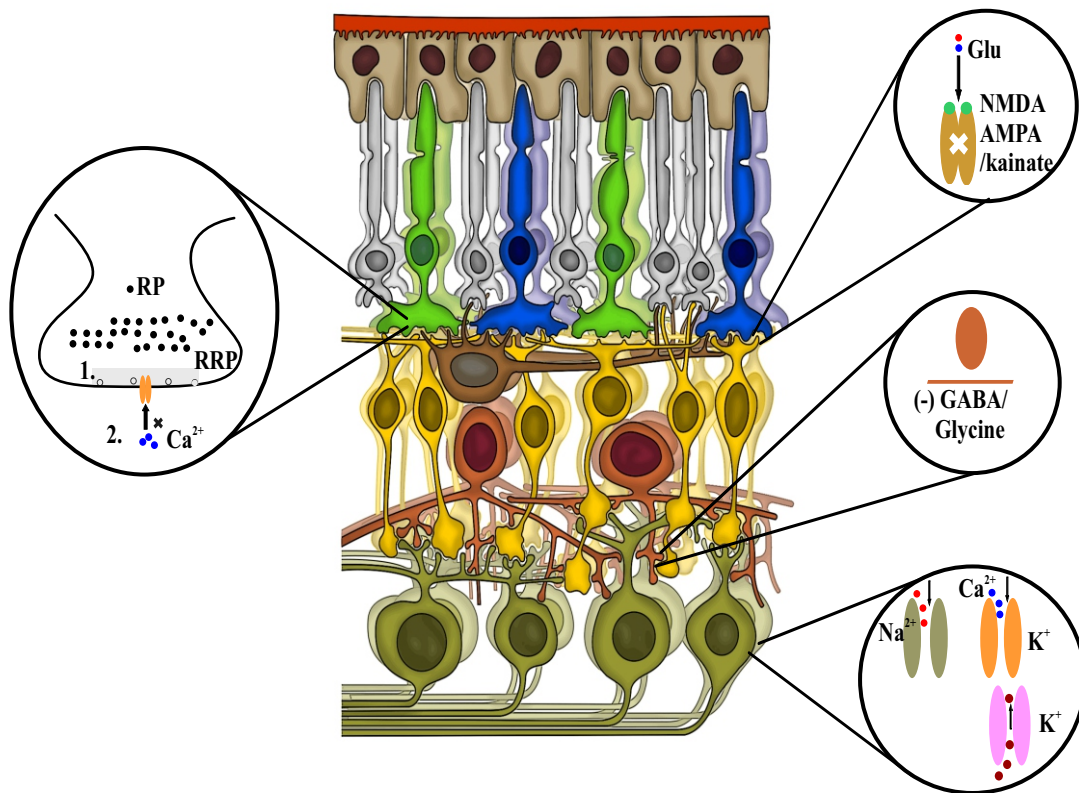
ON-OFF(n=26)



ON(n=14)







Jalligampala et al.  
Fig 9

**Table 1****A) All cells (n=155)**

Frequency(Hz)	2	4	10	16	20	25	40	62.5
2		0.5444	0.7646	<b>9.60E-04</b>	<b>0.0215</b>	<b>9.56E-04</b>	0.3037	0.349
4			0.4387	<b>0.0014</b>	<b>0.0215</b>	<b>7.81E-04</b>	0.0719	0.4423
10				<b>0.0027</b>	<b>0.0253</b>	<b>0.0019</b>	0.5	0.3187
16					0.6182	0.2708	<b>1.26E-04</b>	0.4629
20						0.1938	<b>0.0023</b>	0.7484
25							<b>3.37E-04</b>	0.3594
40								0.1159
62.5								

**B) ON Cells (n=74)**

Frequency(Hz)	2	4	10	16	20	25	40	62.5
2		0.2901	0.773	<b>1.81E-04</b>	<b>0.0019</b>	<b>1.22E-05</b>	0.445	<b>0.0217</b>
4			0.6344	<b>0.0056</b>	<b>0.0131</b>	<b>1.57E-04</b>	0.7729	0.075
10				<b>0.0126</b>	<b>0.0478</b>	<b>0.0019</b>	0.6752	0.081
16					0.9737	0.0928	<b>1.98E-02</b>	0.917
20						0.117	<b>0.0495</b>	0.7464
25							<b>3.10E-03</b>	0.5669
40								0.095
62.5								

**C) ON-OFF Cells (n=71)**

Frequency(Hz)	2	4	10	16	20	25	40	62.5
2		0.7932	0.5142	3.72E-01	0.8737	6.93E-01	<b>0.0333</b>	0.2762
4			0.661	0.1166	0.5042	0.35	<b>0.016</b>	0.3454
10				0.1135	0.3485	0.2691	<b>0.047</b>	0.4885
16					0.4463	0.8921	<b>1.40E-03</b>	0.1512
20						0.7187	<b>0.0115</b>	0.2597
25							<b>1.92E-02</b>	0.2487
40								0.6734
62.5								

Wilcoxon Ranksum Test,  $p < 0.05$ , pairwise comparisons comparing ratio of normalized response of 2nd pulse to 10th pulse across all frequencies for all cells and visually responsive cells.

Table 2

**A) All cells ( across interpulse interval ,n=43)**

Comparisons(Inter-electrode distance)	Interpulse interval				
	1000ms	500ms	100ms	50ms	25ms
1 mm vs 0.8 mm	0.0215	0.5366	0.822	0.4839	0.607
1 mm vs 0.6 mm	0.1901	0.2977	0.3056	0.3529	0.6313
1 mm vs 0.4 mm	0.5767	0.2612	0.2817	0.9483	0.5948
1 mm vs 0.2 mm	0.032	0.0288	1.97E-04	0.0155	0.008
0.8 mm vs 0.6 mm	0.8934	0.6163	0.4727	0.8055	0.8968
0.8 mm vs 0.4 mm	0.6192	0.5862	0.5278	0.6314	0.8288
0.8mm vs 0.2 mm	0.0166	0.0107	0.0018	0.0026	0.0123
0.6 mm vs 0.4 mm	0.7954	0.8764	0.9586	0.5252	0.9311
0.6 mm vs 0.2 mm	0.0456	0.003	0.0043	0.0031	0.0374
0.4 mm vs 0.2 mm	0.0605	0.0034	0.0018	0.0186	0.0202

**B) All cells (across inter-electrode distance)**

Comparisons(Inter-electrode distance)	Interelectrode distance				
	1mm	0.8mm	0.6mm	0.4mm	0.2mm
1 s vs 0.5 s	0.9673	0.8458	0.707	0.3876	0.5804
1 s vs 0.1 s	0.4916	0.3871	0.2116	0.3182	0.0657
1 s vs 0.05 s	0.8184	0.6909	0.8969	0.8323	0.3678
1 s vs 0.025 s	0.0353	0.675	0.8255	0.938	0.8283
0.5 s vs 0.1 s	0.839	0.4493	0.0895	0.0751	0.21
0.5 s vs 0.05 s	0.7921	0.7921	0.8256	0.2897	0.7433
0.5 s vs 0.025 s	0.3527	0.873	0.5196	0.419	0.7476
0.1 s vs 0.05 s	0.6562	0.6718	0.164	0.5195	0.4293
0.1 s vs 0.025 s	0.3992	0.6623	0.243	0.2855	0.1021
0.05 s vs 0.025 s	0.263	0.9724	0.7393	0.6844	0.4759

Wilcoxon Ranksum Test  $p < 0.05$ , for constant interpulse interval and constant inter-electrode distance

**Table 3****A) All cells (n=30)**

Interpulse interval

Comparisons(Inter-electrode distance)	Interpulse interval			
	500ms	100ms	50ms	25ms
1 mm vs 0.8 mm	0.9293	0.501	0.228	0.1276
1 mm vs 0.6 mm	0.4732	0.2901	0.363	<b>0.0369</b>
1 mm vs 0.4 mm	0.3476	0.3708	0.8533	0.2279
1 mm vs 0.2 mm	0.5005	<b>0.0058</b>	<b>0.0061</b>	0.0666
0.8 mm vs 0.6 mm	0.6733	0.5246	0.7281	0.4775
0.8 mm vs 0.4 mm	0.3628	0.7957	0.2902	0.5791
0.8mm vs 0.2 mm	0.441	<b>0.0175</b>	0.0592	0.3327
0.6 mm vs 0.4 mm	0.7004	0.7842	0.3591	0.2166
0.6 mm vs 0.2 mm	0.1824	0.0541	<b>0.0426</b>	0.6097
0.4 mm vs 0.2 mm	0.0998	<b>0.0225</b>	<b>0.0129</b>	0.1956

Wilcoxon Ranksum Test  $p < 0.05$ , for constant interpulse interval

# S1

## ON cells (n=9)

Comparisons(Inter-electrode distance)	Interpulse interval			
	500ms	100ms	50ms	25ms
1 mm vs 0.8 mm	0.7163	0.8629	0.4216	0.6833
1 mm vs 0.6 mm	0.0893	0.1891	0.0534	0.3511
1 mm vs 0.4 mm	0.6209	0.5318	0.7494	0.6209
1 mm vs 0.2 mm	0.665	0.2868	0.1422	0.4233
0.8 mm vs 0.6 mm	0.1978	<b>0.0295</b>	0.1177	0.1966
0.8 mm vs 0.4 mm	0.3994	0.1976	0.9177	0.7795
0.8mm vs 0.2 mm	0.8785	0.1189	0.2571	0.1825
0.6 mm vs 0.4 mm	<b>0.0152</b>	0.1541	0.0984	0.0932
0.6 mm vs 0.2 mm	0.4342	0.7794	0.8167	0.422
0.4 mm vs 0.2 mm	0.1303	0.1821	0.1359	0.0988

## ON-OFF cells (n=18)

Comparisons(Inter-electrode distance)	Interpulse interval			
	500ms	100ms	50ms	25ms
1 mm vs 0.8 mm	0.7159	0.4665	0.2887	<b>0.0289</b>
1 mm vs 0.6 mm	0.0998	0.8121	0.6691	0.0903
1 mm vs 0.4 mm	0.6924	0.8493	0.9117	0.1997
1 mm vs 0.2 mm	0.7877	<b>0.0423</b>	0.2052	0.3265
0.8 mm vs 0.6 mm	0.1541	0.6804	0.1136	0.9243
0.8 mm vs 0.4 mm	0.7636	0.6807	0.296	0.3422
0.8mm vs 0.2 mm	0.5361	0.1492	0.669	0.6692
0.6 mm vs 0.4 mm	0.342	0.9369	0.7756	0.486
0.6 mm vs 0.2 mm	<b>0.0492</b>	0.0608	0.0931	0.837
0.4 mm vs 0.2 mm	0.3827	0.0548	0.1831	0.9747

Wilcoxon Ranksum Test  $p < 0.05$ , for constant interpulse interval for different visual response types